The molecular basis of the Fischer Tropsch reaction

The Molecular Basis of the Fischer Tropsch Reaction

PROEFSCHRIFT

ter verkrijging van de graad van doctor
aan de Technische Universiteit Eindhoven,
op gezag van de Rector Magnificus,
prof.dr. R.A. van Santen,
voor een commissie aangewezen
door het College voor Promoties
in het openbaar te verdedigen
op woensdag 9 januari 2002 om 16.00 uur

door

Ionel Mugurel Ciobîcă

geboren te Arbore, Roemenië

Dit proefschrift is goedgekeurd door de promotoren:

prof.dr. R.A. van Santen
en
prof.dr. A.W. Kleyn

Copromotor:
prof.dr. G.J. Kramer

This is the official first page.

The Molecular Basis of the Fischer Tropsch Reaction

PROEFSCHRIFT

ter verkrijging van de graad van doctor
aan de Technische Universiteit Eindhoven,
op gezag van de Rector Magnificus,
prof. dr. R. A. van Santen,
voor een commissie aangewezen
door het College voor Promoties
in het openbaar te verdedigen
op woensdag 9 januari 2002 om 16.00 uur

door

Ionel Mugurel Ciobîcă

geboren te Arbore, Roemenië

This is the unofficial first page, as a complain that I am not allowed to insert space in between initials and in between titles.

The Molecular Basis of the Fischer Tropsch Reaction

Ionel Mugurel Ciobîcă

PhD thesis, TUE, 2002

părinților mei
le dedic această lucrare
precum și soției
pentru înțelegere și suport

Contents

List of Figures

List of Tables

List of publications

1. R. A. van Santen, F. Frechard, I. M. Ciobîcă and A. P. J. Jansen, Gas-Surface News, 25 (1999) 2–7 ("Numerical simulations applied to catalysis on metal surfaces")

2. I. M. Ciobîcă, F. Frechard, R. A. van Santen, A. W. Kleyn, and J. Hafner, Chem. Phys. Lett., 311 (1999) 185–192 ("A theoretical study of CH_x chemisorption on the Ru(0001) surface")

3. I. M. Ciobîcă, F. Frechard, R. A. van Santen, A. W. Kleyn, and J. Hafner, J. Phys. Chem. B, 104, (2000) 3364–3369 ("A DFT Study of Transition States for C–H Activation on the Ru(0001) Surface")

4. B. Riedmüller, I. M. Ciobîcă, F. Papageorgopoulos, B. Berenbak, R. A. van Santen, and A. W. Kleyn, J. Chem. Phys., 115, (2001) 5244-5251 ("CO Adsorption on Hydrogen Saturated Ru(0001)")

5. B. Riedmüller, I. M. Ciobîcă, F. Papageorgopoulos, B. Berenbak, R. A. van Santen, and A. W. Kleyn, Surf. Sci., 465, (2000) 347-360 ("The dynamic interaction of CO with Ru(0001) in the presence of adsorbed CO and hydrogen")

6. I. M. Ciobîcă, F. Frechard, A. P. J. Jansen, R. A. van Santen, Stud. Surf. Sci., 133, (2001) 221–228 ("From DFT Calculations to Dynamic Monte Carlo Simulations. The reactivity of CH_x on the Ru(0001) Surface")

7. I. M. Ciobîcă, F. Frechard, C. G. M. Hermse, A. P. J. Jansen and R. A. van Santen, Surface Chemistry and Catalysis, editors: A. F. Carley, P. R. Davies,

G. J. Hutchings and M. S. Spencer, Kluwer-Academic/Plenum 2002, ("Modeling heterogeneous catalytic reactions")

8. I. M. Ciobîcă, R. A. van Santen, J. Phys. Chem. B, ("A DFT Study of CH_x Chemisorption and C–H Activation on the $Ru(11\bar{2}0)$ Surface") submitted

9. I. M. Ciobîcă, F. Frechard, R. A. van Santen, Phys. Chem. Chem. Phys. ("A DFT study of C–C coupling on Ru(0001) surface"), submitted

10. I. M. Ciobîcă, G. J. Kramer, Q. Ge, M. Neurock, and R. A. van Santen, J. Catal., ("A Fischer-Tropsch mechanism on Ru(0001)"), submitted

11. I. M. Ciobîcă, A. W. Kleyn, R. A. van Santen, J. Phys. Chem. B, ("CO and H adsorption an coadsorption on Ruthenium surfaces"), submitted

12. I. M. Ciobîcă, R. A. van Santen, J. Phys. Chem. B, ("CO dissociation on Ru flat and stepped surfaces") submitted

13. I. M. Ciobîcă, F. Frechard, R. A. van Santen, ("CO dissociation on several transitional metal dense packed surfaces") in preparation

Chapter 1

General introduction

The work described in this thesis focuses on the reaction mechanism of the Fischer Tropsch synthesis reaction. In section 1.1, we will provide some background in this reaction. Then we will discuss the scope of the thesis and the questions it addresses.

§1.1 Fischer Tropsch synthesis

Fischer Tropsch synthesis became first used industrially in Germany in World War II. It converts synthesis gas obtained from the gasification of coal, to synthetic oil. The process has been much improved now, and is industrially used as an alternative route for the production and transportation of fuels and petrochemical feedstock.

Since the reserves of crude oil will vanish before the reserves of coal and natural gas, the liquefaction of those carbon sources via Fischer Tropsch synthesis had become attractive to many companies. Currently commercial operations of Fischer Tropsch plants are in South Africa – Sasol (90% of the global production) and Malaysia – Shell (10% of the global production). Exxon, Rentech, Syntroleum, Energy International, etc, have developed pilot plants.

The product of Fischer Tropsch synthesis, the so-called synthetic crude oil, can be used directly in the refineries. It contains mainly linear hydrocarbon chains, and no S or N containing compounds. By hydrocraking of the synthetic crude oil, the

heavy hydrocarbons are converted into gasoil and kerosene. Isomerization, catalytic reforming, alkylation, and oligomerization, can further increase the octane number.

§1.2 Aim and scope of the thesis

Catalysis is a discipline at the border of many other disciplines: chemical engineering, physical chemistry, solid-state physics, organic and inorganic chemistry. Therefore, an understanding of a catalytical process requires knowledge from a broad area of sciences.

Theoretical chemistry, or quantum chemistry starts to be of increasing use for a better understanding of chemical processes at the molecular level. Theoretical chemistry will not replace experiments; it is a tool, which can be used as a complementary technique together with experiments.

The aim of this thesis is to develop, to explain, and to understand the mechanism of Fischer Tropsch synthesis at the atomic scale. Many mechanisms have been proposed in the literature and are subject to considerable debate. We have been able to reject the CO insertion mechanism. Since the adsorbed CH fragment is the most stable C_1 species on the Ru(0001) surfaces, we have developed an alternative mechanism (for this surface) compared to the conventional one, which is based on CH_2 fragment.

Using CH as a building unit implies the introduction of a hydrogenation step in the catalytic cycle, as well as steps involving more unsaturated growing chains. The unsaturated nature of the growing chain has also been proposed recently by Maitlis, who assumes a double C=C bond to be present at the growing side of the chain. We will show, however, that on ruthenium, the π bond is cleaved and the last two carbon atoms of the growing chain bind to the surface. Two mechanistic paths will be proposed. This provides an explanation of some of the experimental kinetic data, without the introduction of two C_1 active species as proposed so far.

§1.3 Outline of this thesis

This short chapter (e.g. §1) summaries the aim and implications of this study.

In next chapter, we will discuss the literature available on methane activation and adsorbed CH_x reactivity towards C–C coupling. In addition, CO chemisorption, decomposition, and coadsorption with H on different transitional metal surfaces will be discussed.

In chapter 3, the methods and models used in the quantum calculations are detailed. A few aspects of DFT and the computational program VASP will be discussed. In addition, the different surfaces studied will be presented.

After these introductory chapters results will be given. In chapter 4, we discuss methane activation on the Ru(0001) surface (or the methanation of adsorbed CH_x species). The complete reaction path is presented for two adsorption overlayer symmetries, p(2×2) and p(3×3), corresponding to 25% and 11% coverage. Adsorbate interaction between adsorbed CH_x and adsorbed H is also analyzed.

Chapter 5 deals with C_2H_x species as well as the coadsorption of two CH_x species. These results are important for the understanding of initial chain growth in the Fischer Tropsch process.

Chapter 6 presents a similar study as chapter 4, but on a more open surface, Ru(11$\bar{2}$0). The complete path for methane activation (or the methanation of CH_x species) is presented for the 1×1 structure (50.0% coverage). The comparison with closed packed surface is often made.

In chapter 7 we present adsorption of carbon monoxide on the flat Ruthenium surface for three structures ($\sqrt{3} \times \sqrt{3}$)R30°, p(2×2) and p(3×3) corresponding to 33%, 25% and 11% coverage, as well as the adsorption of carbon monoxide on stepped surfaces. The relative stability of the two most important adsorption sites: atop and hcp, is discussed for all coverages. A compressed layer of atomic hydrogen adsorbed on Ru(0001) surface is presented next. Several structures are depicted and their difference is analyzed based on the energy difference and geometries. Coadsorption of CO and H follows next. Three ratios of CO:H are studied (1:1, 1:3, 1:4) for a 2×2

structure corresponding to a total coverage of 50%, 100% and 125%, respectively. In the last part of this large chapter, we discuss the dissociation of CO on flat and stepped Ruthenium surfaces. Several direct dissociation reaction paths for flat and stepped surfaces are analyzed as well as two indirect routes: the Boudouard reaction (CO disproportionation) for a stepped surface and the H-insertion route, for the flat surface.

Chapter 8 deals with Dynamic Monte Carlo simulations for methane activation and the hydrogenation of adsorbed atomic carbon for two different approximations: with and without lateral interaction. Results are compared with Mean Field Approximation. A method for implementing DFT results in a model suitable for DMC is proposed.

Chapter 9 of this thesis compares two mechanistic pathways for the Fischer Tropsch process on the Ru(0001) surface based on most of the results presented in this thesis. Some interconnections with other chapter are discussed in the general conclusion.

The thesis is preceded with a List of Figures, List of Tables, as well as a List of Papers published and submitted. At the end, after an Appendix, which presents in more details how one can search for TS, a short summary of the thesis is presented in English, Dutch, Romanian and French.

Chapter 2

Literature survey of CH$_4$ and CO chemisorption

This chapter summarizes recent papers dealing with relevant aspects of the topics included in this thesis.

§2.1   Methane and CH$_\mathrm{x}$

CH$_\mathrm{x}$ species have been observed experimentally on Ru(0001) by George et al. [1] using the HREELS technique by initial adsorption of CH$_2$N$_2$. At low temperature (80 K), only CH$_2$ is present on the surface. Upon warming up the surface to 180 K and a peak for CH$_3$ appears in the spectra. At 280 K, the HREELS spectrum indicates a combination of CH$_\mathrm{x}$, with x = 0-3. At 700 K, only C remains on the surface.

CH$_3$ was detected on the Ru(0001) surface by Zhou [2] using TPD, H/TPD, AES, and HREELS following dissociative adsorption of CH$_3$I. C$_\mathrm{x}$H$_\mathrm{y}$ species were reported to be formed on Ru/Al$_2$O$_3$ during the reaction of carbon monoxide with hydrogen by Ahlafi et al. [3] They used both mass and FTIR spectrometry in separate flow and reactor systems. The alkyl C$_\mathrm{x}$H$_\mathrm{y}$ species give a well-defined methane peak during the transient hydrogenation.

With the same techniques, Wu et al. [4,5] have observed CH, CCH$_2$, and CCH$_3$

as well as graphitic carbon on Ru(0001) and Ru(11$\bar{2}$0) exposed to methane at 5 Torr for 120 s. The apparent activation energy for methane dissociation is found to be around 36 kJ$\times$mol^{-1} on the Ru(0001) surface. In the same group, methane coupling at low temperature on Ru(0001) and Ru(11$\bar{2}$0) catalysts was investigated [6]. For the Ru(0001) surface a maximum yield of ethane and propane is observed at $T_{H_2} =$ 400 K, whereas for Ru(11$\bar{2}$0) no maximum was found. The same three species (CH, CCH$_2$, and CCH$_3$) were observed on both surfaces with HREELS like in previous experiments. Only on Ru(11$\bar{2}$0) surface ethylidyne was detected below $T_{CH_4} =$ 400 K.

Jachimowski et al. [7] reported trapping–mediated dissociative chemisorption of ethane and propane on Ru(0001) with activation energies for the C–H bond cleavages of 39 kJ$\times$mol^{-1} for ethane and of kJ$\times$mol^{-1} for propane.

Carstens et al. [8] looked at methane activation on silica supported Ru. Methane dissociates above 373 K, and the activation barrier is in between 25 and 29 kJ$\times$mol^{-1}. Three different carbonaceous species C_{α}, C_{β}, and C_{γ} are formed. On a carburized catalyst, C_{α} decreases monotonically, C_{β} passes through a maximum, and C_{γ} increases monotonically, with increasing carbon coverage. For the non-carburized catalyst, C_{α} remains constant while C_{β} and C_{γ} keep have the same behavior. The distribution of carbon between C_{β} and C_{α} changes with the carbonaceous deposit, such that C_{β} is converted to C_{α}. The activation barrier for this process is estimated to 92 kJ$\times$mol^{-1}. Hydrogenation of the carbonaceous deposit produce methane and small quantities of ethane and propane. The C$_2$ hydrocarbons have a maximum that coincides with the maximum in the surface coverage of C_{β}. One can speculate that C_{α} is CH$_3$, C_{β} is CH and C_{γ} is atomic carbon.

Guczi et al. [9] present a low temperature methane activation under non-oxidative conditions over supported Ru–Co bimetallic system. A method of deuterium uptake by the surface CH$_x$ species formed after CH$_4$ dissociation is used to determine the H content in adsorbed CH$_x$ species. On Ru–Co/SiO$_2$ and Ru–Co/NaY[II], the ratio CHD$_3$/CD$_4$ is larger than one, and decreases with the increase of the temperature. On Ru–Co/Al$_2$O$_3$, and Ru–Co/NaY[I] (O$_2$ treated) the same ratio is smaller than one, and increases with the increase of the temperature. The amount of CH$_3$D is

very small for all supports and CH$_2$D$_2$ is present in quantities usually smaller than CHD$_3$ and CD$_4$.

Methane conversion to higher hydrocarbons via a two-step, oxygen free route was explored for Ru/SiO$_2$ and Cu–Ru/SiO$_2$ catalysts at T$_{H_2}$ of 368 K by Koranne et al. [10] The high initial yield exhibited by the Ru/SiO$_2$ catalyst leads to a complete deactivation in few reaction cycles. For Cu–Ru/SiO$_2$, the methane conversion decreases with the Cu content, but it improves the net methane yield.

Yang and Whitten [11, 12] studied CH$_x$ on pure and substitutional Fe/Ni (111) using an embedded cluster technique. They found that CH$_2$ and CH species prefer hollow sites. A small barrier is present for the dissociation of CH$_2 \rightarrow$ CH + H, with the H atom going to a site close to the CH$_2$ fragment. The substitutional Fe/Ni(111) surface is more active for methane decomposition than Ni(111), a barrier of only 24 kJ$\times$mol^{-1} is reported for the activation of CH$_2$, compared to 70 kJ$\times$mol^{-1} for a clean Ni(111) surface.

Siegbahn and Panas studied CH$_x$ chemisorption on Ni(100) and Ni(111) using an ab initio cluster approach [13]. They found that CH$_x$ fragments have a similar stability on both Ni(100) and on Ni(111) surfaces. The vibrational C–H stretching frequencies computed for CH$_x$ on Ni(100) are in good agreement with experimental results.

Burghgraef et al. [14–17] studied methane activation on Co and Ni clusters using the Density Functional Theory (DFT). Methane decomposition steps are found to be endothermic, except the transformation of CH$_2 \longrightarrow$ CH + H. A barrier of approximately 100 kJ$\times$mol^{-1} was reported for the CH$_4$ activation on these clusters.

Kratzer et al. [18] studied methane dissociation on pure and on gold–alloyed Ni(111) surfaces using a periodic DFT approach. The rupture of the C–H bond occurs preferentially on a top Ni site, with a barrier of about 100 kJ$\times$mol^{-1}. The corresponding transition state has been taken from the cluster calculations of Burghgraef et al [14] with very similar energetic results.

Triguero et al. [19] investigated the chemisorption of CH$_x$ on Cu(100) using a cluster model with DFT method as well as with ab initio theory. The results are

similar for both methods if the core–valence correlation is taken into account. The four–fold hollow site is the preferred adsorption site for methine (–CH) at both levels, while the methyl radical adsorbs at the atop position. The case of methylene is less clear, a slight preference for the hollow site over the bridging site was found.

Paul and Sautet [20–22] studied the relative stability of CH_x species on Pd(111) with DFT slab calculations. The H, C and CH species are found to prefer the hollow sites. CH_2 adsorbs on a bridge site while CH_3 is located on the atop site. The con/-se/-cu/-tive methane decomposition steps are endothermic except for the transformation of $(CH_2)_{ad}$ to CH_{ad}.

Au et al and Liao et al. [23, 24] studied methane dissociation on Rh, Ni, Pd, Pt and Cu (111) metal surfaces with and without preadsorbed atomic oxygen, using DFT with clusters as models for the transition metal surfaces. For the overall decomposition of methane to C_{ad}, and H_{ad} the energy is found to become less exothermic in the order Ni < Pd $\simeq$ Pt while for Cu the overall dissociation reaction is endothermic. Chemisorbed atomic O on the unstable atop sites promotes methane dissociation on Ni, Pd, Pt and Cu, while atomic O on a hollow site promotes methane dissociation only on Cu.

Recent results from Au et al. [25] with the empirical Bond Order Conservation (BOC) technique show that the barriers for $CH_x \rightarrow CH_{x-1} + H$ are between 60 and 200 $kJ \times mol^{-1}$, on Ru, Os, Rh, Ir, Pd, Pt, Cu, Ag and Au clusters. For Ru the predictions for the barriers are 60, 85, 75 and 115 $kJ \times mol^{-1}$ for the CH_x (x = 4-1) decompositions respectively. The adsorption energies for CH_x and the geometries are reported as well. The influence of preadsorbed atomic oxygen and the C–C coupling is also discussed.

§2.2   C–C coupling

C_1H_x, and C_2H_y have been studied intensely because of their interest in Fischer Tropsch synthesis, methane activation and ethene reactivity over transitional metal surfaces [26–29]. Several theoretical studies based on ab initio calculations for the

C_2H_z chemisorption on transition metal surfaces have been recently published.

On the 2×2 Pt(111) surface Papoian et al. [30] studied the chemisorption of H, CH_3 and C_2H_5 species. Calculations are based on the DFT method, with a periodical metal slab representing the surface. While H has not any clear preference for an adsorption site, CH_3 and C_2H_5 favor atop sites for adsorption. The bridge and the three-fold sites have been found unfavorable.

Kua and al. [31, 32] studied the chemisorption of C_2H_z and CH_x also on the Pt(111) surface. Calculations are based on the cluster using a nonlocal B3LYP functional. Methyl has been found to prefer the atop site, methylene prefers the bridge site and CH and C prefer hollow sites. The CH species is the most stable from the CH_x series. Ethyl adsorbs atop, ethylidene on bridge sites, ethylene is most stable in the di-σ adsorption mode, vinyl in a tri-σ configuration, acetylene in a tetra-σ configuration, vinylidene on a hollow site. CCH and CC adsorb with the C–C bond tilted, one C is above a hollow site and the other atop. The most stable species from the C_2H_z series is ethylidyne on hollow sites, followed by acetylene, vinyl and di-σ ethylene whereas CCH and CC are the most unstable. For all CH_x and C_2H_x species, each C atom follows the classic octet rule with 4 σ bonds.

Watve et al. [33] studied also the stability of C_2H_z adspecies on Pt(111) as well as on Pt(211). Calculations are based on the cluster and slab approach. Again, it appears that carbon binds to sites that preserve the tetrahedral geometry and saturate the coordination of the carbon atoms in the adsorbed C_2H_z species. Transition States for C–C bond dissociation have also been presented. The easiest bonds to dissociate are for CH–CH_3 on Pt(111) and CH–CH_2 on Pt(211), while the most difficult appears to be with CH_2–CH_2 on both surfaces.

§**2.3   Carbon monoxide and hydrogen**

Adsorption of CO to metal surfaces has over the years become the prototype system for molecular chemisorption. A rather simple bonding model has in general been accepted [34–46]. It is known that on the late transition metals the energetic

difference between free and adsorbed CO (the heat of adsorption), is much smaller (≈ 100 kJ$\times$mol^{-1} or ≈ 1 eV) than the C–O dissociation energy (1084 kJ$\times$mol^{-1} or 11.23 eV [47]). This observation has led to the plausible assumption of a weak molecule surface interaction where the chemisorption process causes only a small modification of the molecular orbital structure of the free molecule. Consequently, the adsorbate electronic structure has been described as the free molecule, treated as a unit, interacting with the substrate states. In this interaction a crucial role is played by the CO frontier orbitals, namely the highest occupied molecular orbital (HOMO) 5σ and the lowest unoccupied molecular orbital (LUMO) $2\pi^*$. A dative bond between the CO 5σ and metal states of σ symmetry is formed, leading to charge donation into the metal, which is compensated by a backdonation into the CO $2\pi^*$. In this simple frontier orbital picture a synergetic π and σ bond is achieved, where the internal C–O bond is weakened due to the increased population of the antibonding CO $2\pi^*$ in the backdonation. This simplistic model has been challenged repeatedly; substantial mixing especially between the σ orbitals has been proposed [48–51] and the concept of a repulsive σ interaction has been discussed [52–56]. In spite of this criticism the frontier orbital description of the surface-chemical bond has been reinforced recently based on the interpretation of theoretical results indicating that the adsorption energetics can be described in terms of only the energy positions of the CO $2\pi^*$ level and the metal d-band [44, 46, 57].

The adsorption of carbon monoxide and the coadsorption with hydrogen on the close–packed Ru(0001) surface is particularly interesting because of its relevance to the Fischer–Tropsch synthesis and the methanation reaction [58]. While both CO and H$_2$ adsorption on the ruthenium surface has been studied quite extensively over the past decades, only little information is available for the hydrogen carbon monoxide coadsorption system on Ru(0001).

The saturation fractional coverage of dissociatively chemisorbed molecular hydrogen is one adatom per Ru(0001) unit cell [59]. While at low surface coverages hydrogen resides in the fcc–three-fold hollow sites, at saturation coverage hydrogen was found to occupy a site of slightly reduced symmetry. This is presumably due to

either a shift of the hydrogen adatom towards the bridge position or a reconstruction of the ruthenium surface [60].

The CO on Ru(0001) adsorption system has been widely studied [61, 62]. CO is known to adsorb non–dissociatively [61] in the upright position with the C end facing the surface [63]. Adsorption is non-activated and a precursor model including two intrinsic and one extrinsic precursor has been proposed [64] for a surface partially covered by CO. The adsorption energy varies with coverage from 160–175 kJ×mol^{-1} [65, 66] in the 0.33 to 0 ML coverage regime. The preferred site is the atop site for coverages up to 0.33 ML [62].

Molecular beam scattering experiments of NO or CO at Ru(0001)-H(1×1) yielded some quite remarkable observations. At first, the angular distributions of the scattered CO and NO in the energy region of thermal to 250 kJ×mol^{-1} are remarkably sharp. In fact, these are the sharpest angular distributions ever measured for molecular scattering at surfaces [67–72]. This strongly suggests that the hydrogen completely eliminates the binding potential of the Ru(0001) surface, turning it into a flat molecular mirror. However, measurements of the sticking coefficient do not confirm this. The sticking coefficient is non-zero for energies above 20 kJ×mol^{-1} and increases to values exceeding 0.1 [67–69]. This suggests that the unit cell can be divided into three regions: a reflection region, a sticking region with a transition region in between [70]. The presence of the coexistence of a chemisorbed CO species with a compressed and presumably quite flat H-region was already confirmed by our first calculations on this system [69]. The calculations indicated that CO adsorbed on Ru(0001)-H(1 × 1) is much less strongly bound (45 kJ×mol^{-1}) than CO and Hydrogen on the bare surface and that phase separation is likely, as has been observed [73, 74].

CO adsorption and dissociation on transition metals has also been investigated quite extensively on a theoretical basis applying various computational methods. Delbecq et al. investigated CO and NO adsorption on Pd(100), Pd(111), Pd$_3$Mn(100) and Pd$_3$Mn(111) using extended Hückel [75] and DFT [46, 76] methods. The bridge and the three-fold hollow sites are preferred for the CO adsorption on bare Pd surfaces. On the alloy surfaces, CO adsorption is weaker.

LDA calculations were carried out by Eichler et al. [77] to examine the CO adsorption behavior on the Rh(100) surface. The bridge position is the most stable adsorption site for CO at all coverages. The ratio between CO molecules adsorbed bridge and CO adsorbed atop is not constant with the coverage. The difference between the adsorption energies for bridge and atop position shows a minimum at half coverage. At high coverage, CO forms a pseudo–hexagonal overlayer with p4($\sqrt{2} \times \sqrt{2}$) periodicity.

Morikawa et al. reported DFT calculations on CO decomposition on Ni(111) and Pt(111), the LDA results are corrected with GGA [78]. The Pt surface is found less active in dissociation, in agreement with experimental results. A late Transition State presents a very long C–O bond (2.0 Å) with the C atom being adsorbed in a three-fold site while the O atom is in a bridge site.

Large scale DFT calculations are used by Hammer et al. to investigate the interaction of CO with stepped and reconstructed Pt surfaces [79]. The adsorption energy on the steps is 70 kJ×mol^{-1} higher than on the flat terraces. The differences become larger, up to 100 kJ×mol^{-1}, if the adsorption energies on kinks are compared.

A systematic study of the adsorption of CO on the Pt(100), Pt(110) and Pt(111) is presented by Curulla et al. using HF ab initio cluster models [80]. The geometries and vibrational frequencies are invariant with the cluster size, however the adsorption energies are very sensitive to the cluster size. The bonding interaction is dominated by the π–backdonation, although the σ–donation plays a significant role.

A database of DFT GGA calculations of the chemisorption energies of CO over hexagonal compact surfaces of Ni, Cu, Ru, Pd, Ag, Pt, Au and Cu$_3$Pt is provided by Hammer et al. [44]. The smallest adsorption energy is for Au(111) and Ag(111) while Ru(0001) gives the highest adsorption energy from this series.

CO coadsorption with atomic O on Ru(0001) has been studied by Stampfl et al. with DFT [81,82]. The oxidation rate of CO is enhanced at high coverages of atomic O because at these coverages the O–Ru bonds are weaker. At low coverage, both CO and atomic O are strongly bonded to the surface, so CO$_2$ cannot be formed. The O prefers the hcp adsorption site, while the CO prefers to adsorb atop unless high

coverage of atomic O. In this case, the CO has to overcome a barrier of 30 kJ×mol^{-1}
to adsorb in the hcp site for a 75% coverage of atomic O on Ru(0001). CO oxidation
on a (1×1)O phase can proceed via two channels, namely the Eley–Rideal and the
Langmuir–Hinshelwood mechanism from which the latter one dominates.

Wang et al. also reported a study of CO coadsorption with atomic O on Ru(0001)
focusing on the tilting of CO [83]. The DFT calculations have been performed with a
cluster model. The interaction between CO and O can be described as a field–induced
chemistry: the charged atomic oxygen creates a local electrostatic field along the CO
adsorption site, which modifies the metal–carbon and the C–O bonds, resulting in a
tilt of the molecule. Bonn et al. [84] studied CO coadsorption with O on Ru(0001).
Electron-mediated dessorption, oxidation and phonon mediated dessorption of CO
is induced with a short (femto seconds) laser CO pulse.

Peebles et al. [85] showed experimentally that the CO sticking probability drops
with increasing deuterium coverage, meaning that deuterium acts as a site blocker
for CO adsorption. There was no evidence for a chemical reaction between hydrogen
and CO at 100 K and no additional thermal dessorption states appear in the TPD. A
strong repulsive interaction between the deuterium atoms and carbon monoxide was
also found. Further evidences for this observation were provided by Mak et al. [86],
who determined the hydrogen diffusion coefficients as a function of preadsorbed CO
coverage (θ_{CO} = 0-0.2 ML) at T = 260 K with LITD. They found a hydrogen
exclusion radius that is in the order of the Van der Waals radius of the CO molecule.

However, even on a fully deuterium saturated surface, considerable amounts of
CO, up to 20% of the CO saturation coverage, could be adsorbed [85]. Since the D–
CO interaction is repulsive in the mixed overlayer and deuterium blocks adsorption
sites, an interesting question is, how a gas phase CO molecule adsorbs in the hydrogen
overlayer.

The coadsorption of CO and hydrogen on several transitional metal surfaces has
been reviewed by White et al. [73] with a conclusion that CO and hydrogen form
segregated rather than mixed structures on the close packed (fcc(111), hcp(0001))
surfaces. This is attributed to a strong repulsive H–CO interaction on the surface

that is the dominant lateral interaction in these coadsorbed systems.

Bibliography

[1] P. M. George, A. R. Averey, W. H. Weinberg, F. N. Tebbe, *J. Am. Chem. Soc.*, 105, (1983), 1394

[2] Y. Zhou, M. A. Henderson, W. Feng, J. White, *Surf. Sci.*, 224, (1989), 386

[3] H. Ahlafi, M. Nawdali, A. K. Bencheikh, D. Bianchi, *Bull. Soc. Chim. Belg.*, 106, (1997), 245

[4] M. -C. Wu and D. W. Goodman *J. Am. Chem. Soc*, 116, (1994), 1364

[5] M. -C. Wu and D. W. Goodman *Surf. Sci. Lett.*, 306, (1994), L529

[6] P. Lenz–Solomun, M. -C. Wu, D. W. Goodman, *Catal. Lett.*, 25, (1994), 75

[7] T. A. Jachimowski, W. H. Weinberg, *Surf. Sci.*, 372, (1997), 145

[8] J. N. Carstens, A. T. Bell, *J. Catal.*, 161, (1996), 423

[9] L. Guczi, K. V. Sarma, L. Borkó, *J. Catal.*, 167, (1997), 495

[10] M. M. Koranne, D. W. Goodman, *Methane and Alkane Conersion Chemistry* Plenum Press, New York, 1995, 49

[11] H. Yang and J. L. Whitten *Surf. Sci.*, 289, (1993), 30

[12] H. Yang and J. L. Whitten *J. Chem. Phys.*, 91, 1, (1989), 126

[13] P. E. M. Siegbahn and I. Panas *Surf. Sci.*, 240, (1990), 37

[14] H. Burghgraef, A. P. J. Jansen and R. A. van Santen, *Surf. Sci.*, 324, (1995), 345

[15] H. Burghgraef, A. P. J. Jansen and R. A. van Santen, *Faraday Discuss.*, 96, (1993), 337

[16] H. Burghgraef, A. P. J. Jansen and R. A. van Santen, *Surf. Sci.*, 344, (1995), 149

[17] H. Burghgraef, A. P. J. Jansen and R. A. van Santen, *J. Chem. Phys.*, 101, 12, (1994), 11012

[18] P. Kratzer, B. Hammer and J. K. Nørskov *J. Chem. Phys.*, 105, 13, (1996), 5595

[19] L. Triguero, U. Wahlgren, L. G. M. Pettersson and P. Siegbahn *Theor. Chim. Acta*, 94, (1996), 297

[20] J. -F. Paul and P. Sautet *J. Phys. Chem. B*, 102, (1998), 1578

[21] J. -F. Paul and P. Sautet 11th *International Congress on Catalysis – 40th Anniversary Studies in Surface Science and Catalysis* vol. 101, 1253–1261

[22] J. -F. Paul and P. Sautet *Symposium Advances and Applications of Computational Chemical Modeling to Heterogeneous Catalysis Presented Before the Division of Petroleum Chemistry, Inc. 213th National Meeting, American Chemical Society, San Francisco, CA* April 13–17, 1997

[23] C. -T. Au, M. -S. Liao and C. -F. Ng *Chem. Phys. Lett.*, 267, (1997), 44

[24] M. -S. Liao, C. -T. Au and C. -F. Ng *Chem. Phys. Lett.*, 272, (1997), 445

[25] C. -T. Au, C. -F. Ng and M. -S. Liao *J. Catal.*, 185, (1999), 12

[26] M. Araki and V. Ponec, *J. Catal.*, 44, (1976), 439

[27] P. Biloen and W. M. H. Sachtler *Adv. Catal.*, 30, (1981), 165

[28] R. A. van Santen, A. de Koster and T. Koerts *Catal. Lett.*, 7, (1990), 1

[29] J. P. Hindermann, G. J. Hutchings and A. Kiennemann *Catal. Rev. – Sci. Eng.*, 35, 2, (1993), 1

[30] G. Papoian, J. K. Nørskov, R. Hoffman, *J. Am. Chem. Soc.*, 122, (2000), 4129

[31] J. Kua, W. A. Goddard III, *J. Phys. Chem. B*, 102, (1998), 9492

[32] J. Kua, W. A. Goddard III, *J. Phys. Chem. B*, 103, (1999), 2318

[33] R. M. Watwe, R. D. Cortight, J. K. Nørskov, J. A. Dumesic, *J. Phys. Chem. B*, 104, (2000), 2299

[34] D. E. Eastman and K. Cashion, *Phys. Rev. Lett.*, 27, (1971), 1520

[35] C. L. Allyn, T. Gustafsson, and E. W. Plummer, *Solid State Commun.*, 24, (1977), 531

[36] C. L. Allyn, T. Gustafsson, and E. W. Plummer, *Chem. Phys. Lett.*, 47, (1997), 127

[37] C. L. Allyn, T. Gustafsson, and E. W. Plummer, *Solid State Commun.*, 28, (1978), 85

[38] T. Gustafsson and E. W. Plummer, in *Photoemission from Surfaces*, edited by B. Feuerbacher, B. Fitton, and R. Willis, Wiley, London, 1977

[39] S.-S. Sung and R. Hoffmann, *J. Am. Chem. Soc.*, 107, (1985), 578

[40] E. Wimmer, C. Fu, and A. Freeman, *Phys. Rev. Lett.*, 55, (1985), 2618

[41] B. Gumhalter, K. Wandelt, and P. Avouris, *Phys. Rev. B*, 37, (1988), 8048

[42] A. Nilsson and N. Mårtensson, *Phys. Rev. B*, 40, (1989), 10249

[43] *The Chemical Physics of Solid Surfaces and Heterogeneous Catalysis*, edited by D. A. King and D. P. Woodruff, Elsevier, Amsterdam, 1990, Vol. 3A

[44] B. Hammer, Y. Morikawa, and J. K. Nørskov, *Phys. Rev. Lett.*, 76, (1989), 2141

[45] F. Delbecq, *Surf. Sci.*, 389, (1997), L1131

[46] F. Delbecq and P. Sautet, *Phys. Rev. B*, 59, (1999), 5142

[47] I. Toyoshima, and G. A. Somorjai, *Catal. Rev. Sci. Eng.*, 19, (1997), 105,

[48] P. Hu, D. A. King, M.-H. Lee, and M. C. Payne, *Chem. Phys. Lett.*, 246, (1995), 73

[49] W. Wurth, *Vacuum*, 40, (1990), 3

[50] F. Greuter, D. Heskett, E. W. Plummer, and H.-J. Freund, *Phys. Rev. B*, 27, (1983), 7117

[51] A. Nilsson, P. Bennich, T. Wiell, N. Wassdahl, N. Mårtensson, J. Nordgren, O. Björneholm, and J. Stöhr, *Phys. Rev. B*, 51, (1995), 10244

[52] P. S. Bagus, C. J. Nelin, and C. W. Bauschlicher, *Phys. Rev. B*, 28, (1983), 5423

[53] P. S. Bagus, K. Hermann, and C. W. Bauschlicher, *J. Chem. Phys.*, 81, (1984), 1966

[54] P. S. Bagus and K. Hermann, *Phys. Rev. B*, 33, (1986), 2987

[55] K. Hermann, P. S. Bagus, and C. J. Nelin, *Phys. Rev. B*, 35, (1987), 9467

[56] G. te Velde and E. Baerends, *Chem. Phys.*, 177, (1993), 399

[57] M. Mavrikakis, B. Hammer, and J. K. Nørskov, *Phys. Rev. Lett.*, 81, (1998), 2819

[58] H. N. Storch, N. Golumbic, and R. B. Anderson, *The Fischer-Tropsch and related synthesis*, Whiley New York, 1951.

[59] Y. K. Sun and W. H. Weinberg, *Surf. Sci.* 214, (1989), L246

[60] H. Shi and K. Jacobi, *Surf. Sci.* 313, (1994), 289

[61] J. C. Fuggle, T. E. Madey, M. Steinkilberg, and D. Menzel, *Surf. Sci.*, 52, (1975), 521

[62] H. Pfnür, D. Menzel, F. M. Hoffmann, A. Ortega, and A. M. Bradshaw, *Surf. Sci.*, 93, (1980), 431

[63] J. C. Fuggle, T. E. Madey, M. Steinkilberg, and D. Menzel, *Chem. Phys.*, 11, (1975), 307

[64] H. Pfnür and D. Menzel, *J. Chem. Phys.*, 79, (1983), 2400

[65] H. Pfnür, P. Feulner, and D. Menzel, *Chem. Phys. Lett.*, 59, (1979), 481

[66] H. Pfnür, P. Feulner, and D. Menzel, *J. Chem. Phys.*, 79, 4613 (1983), 4613

[67] B. Berenbak, D. A. Butler, B. Riedmüller, D. C. Papageorgopoulos, S. Stolte, and A. W. Kleyn. *Surf. Sci.*, 414, (1998), 271

[68] B. Riedmüller, I. M. Ciobîcă, D. C. Papageorgopoulos, B. Berenbak, R. A. van Santen, and A. W. Kleyn. *Surf. Sci.*, 465, (2000), 347

[69] B. Riedmüller, I. M. Ciobîcă, F. Papageorgopoulos, B. Berenbak, R. A. van Santen, and A. W. Kleyn, *J. Chem. Phys.*, 115, (2001), 5244

[70] B. Berenbak, B. Riedmüller, C. T. Rettner, D. J. Auerbach, S. Stolte, and A. W. Kleyn. *Phys. Chem. Comm.*, 16, (2001), 1

[71] D. A. Butler, B. Berenbak, S. Stolte, and A. W. Kleyn. *Phys. Rev. Lett.*, 78, (1997), 4653

[72] B. Berenbak, B. Riedmüller, D. A. Butler, C. T. Rettner, D. J. Auerbach, S. Stolte, and A. W. Kleyn. *Phys. Chem. Chem. Phys.*, 2, (2000), 919

[73] J. M. White, and S. Akhter, *CRC Crit. Rev. Solid State Mater. Sci.*, 14, (1988), 130

[74] B. Riedmüller, D. C. Papageorgopoulos, B. Berenbak, R. A. van Santen, and A. W. Kleyn. *in preparation*

[75] F. Delbecq, B. Moraweck, and L. Vérité, *Surf. Sci.*, 396, (1998), 156

[76] F. Delbecq and P. Sautet, *Chem. Phys. Lett.*, 302, (1999), 91

[77] A. Eichler and J. Hafner, *J. Chem. Phys.*, 109, (1998), 5585

[78] Y. Morikawa, J. J. Mortensen, B. Hammer, and J. K. Nørskov, *Surf. Sci.*, 386, (1997), 67

[79] B. Hammer, O. H. Nielsen, and J. K. Nørskov, *Cat. Lett.*, 46, (1997), 31

[80] D. Curulla, Clotet A., and J. M. Ricart, *J. Phys. Chem. B*, 103, (1999), 5246

[81] C. Stampfl and M. Scheffler, *Phys. Rev. Lett.*, 78, (1997), 1500

[82] C. Stampfl and M. Scheffler, *Surf. Sci.*, 433-435, (1999), 119

[83] R. L. C Wang, Kreuzer H. J., and D. Menzel, *Z. Phys. Chem.*, 202, (1997), 205

[84] M. Bonn, S. Funk, C. Hess, D. N. Denzler, C. Stampfl, M. Scheffler, M. Wolf, and G. Ertl. *Science*, 285, (1999), 1042

[85] D. E. Peebles, J. A. Schreifels, and J. M. White, *Surf. Sci.*, 116, (1982), 117

[86] C. H. Mak, A. A. Deckert, and S. M. George, *J. Chem. Phys.*, 8, (1989), 5242

Chapter 3

Method and Model

In this chapter, I will describe, in a few pages, the method used for the quantum chemical calculations, as well as, the chemical models for the particular calculations I performed.

§3.1   Method

Density Functional Theory developed by Kohn, Hohenberg and Sham [1, 2] is widely used today and implemented in many programs performing quantum chemical calculations. A good introduction to DFT can be found in the book of Parr and Yang [4], also for a shorter presentation of DFT, one can have a look at the Nobel lecture of Walter Kohn [5].

The main advantage of DFT, compared to the traditional Hartree–Fock and post Hartree–Fock methods, is the relatively low computational cost for accurate results. Recent functionals allow to compute, relative energies within 20 kJ×mol^{-1} while post Hartree–Fock techniques can be more accurate but at a prohibitive cost: with DFT the effective scaling of the calculations is between n^2 and n^3 (n being the size of the system), while post HF are at least above n^4.

§3.1.1   Density Functional Theory

We can write the total hamiltonian for an N-electron system for the ground state:

$$\hat{H} = \hat{T} + \hat{V} + \hat{U} = \sum_{i=1}^{N} \left(-\frac{1}{2}\nabla_i^2 \right) + \sum_{i=1}^{N} v(\vec{r}_i) + \sum_{i<j}^{N} \frac{1}{r_{ij}} \tag{3.1}$$

where $\hat{H}$ is the hamiltonian, $\hat{T}$ is the operator for kinetic energy, $\hat{V}$ is the operator for potential energy, $\hat{U}$ is the operator for internal energy, $-\frac{1}{2}\nabla_i^2$ is the kinetic energy for the electron i in atomic units, $v(\vec{r}_i)$ is the potential energy of the electron i in atomic units and $\frac{1}{r_{ij}}$ is the interaction energy of two electrons i and j. The external potential $v(\vec{r})$ is a unique functional of the electronic density, $\rho(\vec{r})$, apart from a trivial constant.

The Kohn-Sham theorem postulates that there is a unique universal functional of the density, $F[\rho(\vec{r})]$, independent of the external potential $v(\vec{r})$, such that the expression $E[\rho(r)] = \int v(\vec{r})\rho(\vec{r})d\vec{r} + F[\rho(\vec{r})]$ has its *minimum* value at the correct ground state energy associated with $v(\vec{r})$, where $F[\rho(\vec{r})]$ is equal to $\langle\Psi|\,(\hat{T}+\hat{U})\,|\Psi\rangle$. Ψ is the wave function of the system.

Kohn-Sham does not introduce a way to treat exactly the kinetic energy of non-interacting particles, but a way of using Hohenberg-Kohn theorem knowing that one cannot get a good T(ρ). Therefore, the idea is to split T in two parts: T(ψ) (for non-interacting electrons) and one term in V$_{xc}$. The advantage of this is that it is working and the disadvantage is that it is an approximation, it is more complicated (because H(ρ) become H(ρ,ψ)).

The Kohn-Sham equations are exact in their treatment of the very non-local kinetic energy for non-interacting system and Hartree Coulomb energy, which are dominant parts of the total energy. The remaining exchange correlation functional, $E_{xc}[\rho(\vec{r})]$, tends to be local in character and is treated in an approximate fashion.

Kohn-Sham equations can be derived by minimizing the total energy functional with respect to the $\psi_i(\vec{r})$, the monoelectronic wave functions:

$$\left\{-\frac{1}{2}\nabla^2 + v_{eff}\right\}\psi_i(\vec{r}) = \epsilon_i\psi_i(\vec{r}) \tag{3.2}$$

where $v_{eff}(\vec{r}) = v(\vec{r}) + \int \frac{\rho(\vec{r})}{|\vec{r}-\vec{r'}|}d\vec{r} + v_{xc}(\vec{r})$ with $v_{xc}(\vec{r}) = \frac{\partial(\rho(\vec{r})\epsilon_{xc}(\rho))}{\partial\rho(\vec{r})}$.

Both, the exact charge density and exact form of the $E_{xc}(\rho)$ are not known. If $E_{xc}(\rho)$ is known, then the above equation leads to the exact solution in terms of self-consistent Hartree-like independent particle equations.

The $E_{xc}(\rho)$ is calculated by expansion for slowly varying density for the special case, namely homogeneous electron gas, where all the gradient terms disappear:

$$E_{xc}[\rho] = \int \epsilon_{xc}(\rho(\vec{r}))d\vec{r}, \tag{3.3}$$

where $\epsilon_{xc}(\rho(\vec{r}))$ is a function. So:

$$E^{LDA}[\rho] = T_s[\rho] + E_{ext}[\rho] + E_{coul} + E_{xc}[\rho] =$$

$$= T_s[\rho] + \int v(\vec{r})\rho(\vec{r})d\vec{r} + \frac{1}{2} \int \int \frac{\rho(\vec{r}\prime)\rho(\vec{r})}{|\vec{r} - \vec{r}\prime|} d\vec{r}\prime d\vec{r} + E_{xc}[\rho] \qquad (3.4)$$

where $T_s[\rho]$ can be express in terms of the eigenvalues of the Kohn-Sham orbitals, $E_{ext}[\rho]$ is the external potential energy, and E_{coul} is the Coulomb energy. Then we can obtain the expression of the total energy.

§3.1.2   VASP

The program VASP [6, 7] (Vienna *ab initio* Simulation Package), developed by the group of Prof. J. Hafner has been used extensively by us to obtain a fundamental understanding of reactions on metal surfaces. VASP applies DFT to periodical systems, using plane waves and ultrasoft pseudopotentials (US–PP) [8,9]. The US–PP reduces significantly the number of plane waves needed by relaxing the norm conservation constraint on the pseudo wavefunction.

The Kohn–Sham equations are solved self–consistently with an iterative matrix diagonalization combined with a Broyden mixing [10] method for the charge density. The combination of these two techniques makes the code very efficient, especially for transition metal systems that present a complex band structure around the Fermi level. The forces acting on the atoms are calculated and can be used to relax the geometry of the system.

The functional from the Generalized Gradient Approximation of Perdew and Wang [11] has been chosen because of its good description of chemical bond energies.

Most of the *algorithms* implemented in VASP use an iterative matrix-diagonalization scheme. They are based on the conjugate gradient scheme, or a residual minimization scheme - direct inversion in the iterative subspace (RMM-DIIS). Those algorithms are working in a following way: it calculate the electronic ground state for given geometry, calculate forces, and then, based on the forces a new geometry is predicted and those steps are repeated until a criterion is reached. This is usually when the differences in energies are less than 10^{-4} eV ($\approx$0.1 kJ$\times$mol^{-1}). A special algorithm is the quasi-Newton, where the energy criterion is ignored and only the forces are minimized. Transition States structures and energies are also possible to find using a different technique implemented in the VASP code. Frequencies are

not possible to be directly calculated with this code, but in the future, a subroutine will be available to do so.

Plane waves are used as basis set and ultra soft pseudopotentials are replacing the core part of atoms. This allows a significant decrease of computational time. The Hamiltonian is easy to be determined in peaces in direct and reciprocal space. Fast Fourier Transformations (FFT) are used to switch from direct to reciprocal space and opposite. This allows a decrease of number of planewaves, which allows a partial diagonalization.

For the *mixing of the charge density*, an efficient Broyden/Pulay mixing scheme is used for convergence in a self-consistent density functional calculation. The linear mix of the two (or more) previous charge densities can be made; this can give significant benefits [6, 12]. It is often important to mix in a small amount of the input charge densities, as well as performing the mixing.

For *partial occupancies*, (techniques to improve the convergences with respect to k-points sampling) different methods are used: linear tetrahedron method (good for bulk calculation), smearing methods like finite temperature approaches (good for convergence of metallic surfaces), or improved functional form: Methfessel and Paxton method, finite methods, like gaussian or fermi smearing (good for accurate calculation required for DOS diagram, etc.)

The number of $\boldsymbol{k}$–*points* sample in the irreducible part of the Brillouin zone is important for the accurate integration of the properties computed in reciprocal space. The $\mathbf{k}$–points sample is often calculated by the program using the Monkhorst–Pack [13] method using a given mesh.

Within the finite temperature approach, *forces* are defined as the derivative of the generalized free energy.

From computational point of view, everything is kept in memory. A lot of memory needed (from hundreds Mb to 2 Gb) and large bandwidth between memory and processor are needed. The code calls FFT (fast Fourier transformations) libraries as well as BLAS and LAPAK. The code is implemented on Cray C94, SP2, Origin SGI, T3E, Linux-PC's, etc. with a parallel version using mpi (message passing interface). See Table 3.1 for a computational review.

One can see the importance of FFT procedure, which uses the most of the computational time. Next, in time consuming, is the calculation of the nonlocal pseudopotentials and the BLAS subroutines (Basic Linear Algebra Subprograms).

time	(%)	cumulative time (%)		procedure	
5.7e+03s	(35.9)	5.7e+03s	(35.9)	`FPASSM`	FFT3D
2.1e+03s	(13.3)	7.9e+03s	(49.2)	`RPRO1`	non local pseudo
1.9e+03s	(12.0)	9.8e+03s	(61.3)	`RACC`	non local pseudo
1.9e+03s	(11.8)	1.2e+03s	(73.0)	`IPASSM`	FFT3D
1.1e+03s	(7.1)	1.3e+03s	(80.2)	`ZGEMV_MCV`	BLAS
1.1e+03s	(6.6)	1.4e+03s	(86.8)	`ZGEMM_MM`	BLAS

Table 3.1: A VASP job review.

§**3.1.3   Nudged Elastic Band**

The Nudged Elastic Band (NEB) Method developed by Jónsson et al. [14] is used to determine the Transition States. The main difference between NEB and elastic band (EB) method [15] is that on NEB the perpendicular component of the spring force (on the reactional path) and the parallel component of the true force (on the reactional path) are projected out. Both are chain–of–states methods. Two points in the configuration space (hyperspace containing all the degrees of freedom) are needed (initial and final state) and a linear interpolation can be made to produce the images along the elastic band. The program will run simultaneously each image and will communicate (the forces) at the end of each ionic cycle in order to compute the force acting on each image. For some more details about methods to get TS, see the Appendix 1.

The term "nudged" indicates that the projection of the parallel component of true force acting on the images and the perpendicular component of the spring force are canceled. A smooth switching function is introduced that gradually turns on the perpendicular component of the spring force where the path becomes kinky at large differences in the energies between images.

The results obtained with the NEB are refined with a quasi–Newton algorithm [12] implemented in VASP. This implies that the atoms are moved to minimize the forces. The total energy is not taken into account for minimization. In this way, the program is searching a stationary point. Only in the very few cases when the given initial geometry is close to the geometry of the TS it is possible to reach the TS directly with the quasi–Newton technique, so the NEB is still required.

In one case, we proceeded in an alternative way. We used a cluster model to

search for TS. The geometry was ported to the periodical model and we used the quasi–Newton algorithm to reach the saddle point.

§3.1.4 Dynamic Monte Carlo

Although kinetics plays such an important role in catalysis, its theory has for a long time mainly been restricted to the use of macroscopic deterministic rate equations. These implicitly assume a random distribution of adsorbates on the catalyst's surface. Effects of lateral interactions, reactant segregation, site blocking, and defects have only been described *ad hoc*. With the advent of Dynamic Monte–Carlo simulations (DMC simulations), also called Kinetic Monte–Carlo simulations, it has become possible to follow reaction systems on an atomic scale, and thus to study these effects properly.

Three parts can be distinguished in our DMC method; the model representing the catalyst and the adsorbates, the Master Equation (ME) that describes the evolution of the system, and the DMC algorithms to solve the ME. The ME and the DMC algorithms have been described extensively elsewhere [16–18]. The three parts contribute differently to making our DMC method useful. The model insures that it is easy to study a very broad range of systems and phenomena. The ME forms the link with other kinetic theories like macroscopic rate equations and reaction–diffusion equations. As the parameters in the ME can be calculated using *ab–initio* quantum chemical methods, very similar to normal rate constants, the ME allows us to talk about *ab–initio* kinetics. Finally, the DMC algorithms make our DMC method extremely efficient.

The mathematical model

For our model, we assume that adsorption takes place at well–defined sites. A grid of points represents these sites. We assume that these points form a regular grid, a lattice, although this is not strictly necessary. One can block this grid into unit cells and we admit the case with more than one grid point per unit cell. It is important to realize that the model does not contain any information on the distance between the sites, or which sites are nearest neighbors, next–nearest neighbors, etc. This kind of information is contained implicitly in the description of the reactions.

A label is attached to each grid point. The most common use of this label is that it specifies the adsorbate at the site or that the site is vacant. Because of reactions, this

implies that the labels will change during a simulation. Indeed, a simulation consists of nothing but changes of the labels according to reactions, and the determination of times when the reactions take place. The specification of a reaction consists of a set of grid points, labels attached to them corresponding to the adsorbates before the reaction has taken place (reactants), labels corresponding to the adsorbates after the reaction has taken place (products), and some rate constant. The set of grid points should be regarded as a representation for all sets of grid points where the reaction may occur. All these sets are related via translational symmetry and possibly (combinations with) rotations and reflections.

The use of labels need not be restricted to the specification of the adsorbate at a site. It may also tell something about the type of site. This usage of the label allows us to handle different sites reconstructions, defects, steps, etc.

The Master Equation

The Master Equation (ME) describes the evolution of the adlayer and the substrate

$$\frac{dP_\alpha}{dt} = \sum_\beta \left[W_{\alpha\beta} P_\beta - W_{\beta\alpha} P_\alpha \right], \qquad (3.5)$$

where α and β refer to the configuration of the adlayer, the P's are the probabilities of the configurations, t is time, and the W's are transition probabilities per unit time. These transition probabilities give the rates with which reactions change the occupations of the sites. They are very similar to reaction rate constants and we will use this term in the rest of this paper. $W_{\alpha\beta}$ corresponds to the reaction that changes β into α. A configuration could be regarded as the way the adsorbates are distributed over all sites in the system.

The ME has been used extensively in the statistical physics literature for the dynamics of all kinds of lattice–gas models. We would like to point out, however, that for reactions on surfaces this equation could be derived from first principles [18]. The derivation shows that the rate constants can be written as

$$W_{\alpha\beta} = \frac{k_B T}{h} \frac{Q^\ddagger}{Q} \exp\left[-\frac{E_{bar}}{k_B T} \right], \qquad (3.6)$$

with k_B the Boltzmann–constant, h Planck's constant, T temperature, and E_{bar} the energy barrier of the reaction that transforms configuration β into configuration α.

The partition function $Q^\ddagger$ and Q can be interpreted as the partition functions of

the transition state and the reactants, respectively, although there are some small, often negligible, differences [18]. This expression is, of course, familiar from Transition–State Theory (TST). Indeed, the derivation of the ME is very similar to Keck's derivation of the variational form of TST [19–21]. The important point is that the derivation of the ME from first principles makes an *ab–initio* approach to kinetics possible.

The Dynamic Monte Carlo algorithm

The DMC simulations produce a numerical solution to the ME. In fact, there are numerous DMC algorithms that might be used; a recent taxonomy of these algorithms contained no less than 48 [22]. Most of them are not efficient for any reaction system, however. For a general ME various algorithms have been given by Binder [23]. DMC algorithms for rate equations have even been given earlier by Gillespie [24, 25]. Our work has mainly focused on making these algorithms efficient for lattice–gas systems [16, 17, 22]. We will deal here only with the essential aspects, and we will point out the most important factors that determine the choice of the algorithm. All DMC algorithms generate an ordered list of times at which a reaction takes place, and for each time in that list the reaction that occurs at that time. A DMC simulation starts with a chosen initial configuration. The list is traversed and changes are made to the configuration corresponding to the occurring reactions.

The conceptually simplest is the First–Reaction Method (FRM) [16, 17, 23–25]. It can be applied to any system, but it may not be the most efficient method [22]. For each configuration that occurs a list of all possible reactions is computed, and for each reaction a time of occurrence is generated. If the rate constant is time independent and the current time is t, then the reaction $\beta \rightarrow \alpha$ will occur at time $t + \Delta t$ with $\Delta t = -(\ln r)/W_{\alpha\beta}$, where r is a random deviate of the unit interval [26]. The list of all reactions is ordered according to time of occurrence, and the configuration is changed corresponding to the first reaction in the list. This leads to a new configuration and a new time, and then the whole procedure is repeated. As the list of reactions does not have to be regenerated entirely after each configuration change, FRM is not as inefficient as it may seem. However, computer time per reaction does depend logarithmically on the number of sites in the system. This is because the list of reactions is implemented as a priority queue. Operations on it scale logarithmically with its size, [27] and the number of reactions, which is its size, is proportional to

the size of the system. It can be shown that FRM generates configurations with probabilities that are solutions of the ME.

Lateral interactions

Simulations with lateral interactions are significantly slower than simulations without lateral interactions. This is because a new reaction time has to be computed when the occupation of a site involved in the reaction changes. With lateral interactions this has to be done even each time that a change occurs in the neighborhood contributing to the activation energy. This is simply an effect of having to use the enlarged interaction region. Because the rate of a reaction varies significantly depending on the neighborhood, we use FRM as the simulation method. Other methods are less efficient in this case.

§3.2 Model

Next, the computational model is discussed.

§3.2.1 Bulk

The very first calculations concerning Ru were, obviously, for bulk structures. Ru is an hcp metal. Because of that the unit cell cannot contain just one atom, the minimum is two. Calculations for the fcc structure of the metallic Ru were also performed. The Ru fcc bulk is with 8.65 kJ×mol^{-1} per atom less stable than the Ru hcp bulk. The metal-metal distance optimized with these bulk calculations was 2.70 Å, which is similar with the experimental value (2.70 Å).

§3.2.2 Bare surface

For the (0001) surface, we did calculations for several numbers of layers in the metal slab. This is the closest packed surface. The other surfaces, more open are $(11\bar{2}0)$, $(10\bar{1}0)$, etc.

Close packed surface

Supercells with 3 to 12 slab layers for Ru(0001) surface were calculated for the p(1×1) structure. The absolute energy of the slabs, per atom, changes dramatically

by adding or removing a slab layer, especially for small number of layers, see Figure 3.1. (2×2), (3×3) and $(\sqrt{3} \times \sqrt{3})$ R 30° are the most used structures in this study. They correspond to coverages of 25.0%, 11.1% and 33.3%. In Table 3.2, one can see the test we did in order to come out with a good model for the Ru(0001) surface. The model was tested using adsorbates, since this would be the task of it, to be a good model for the adsorption.
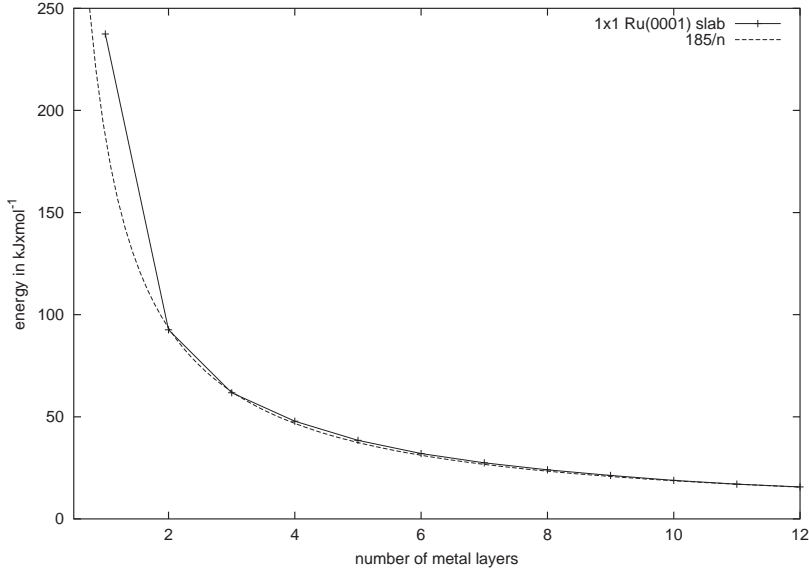
Figure 3.1: The absolute energy of the (1×1) Ru(0001) slabs (per atom) with respect to bulk Ruthenium atoms.

The k–points sampling is very important. Calculations have to be done in order to find a minimum mesh, which gives a similar energy with any larger mesh. The k–points sampling was generated following the Monkhorst–Pack [13] procedure with a $5 \times 5 \times 1$ mesh for the 2×2 supercell and $3 \times 3 \times 1$ for the 3×3 supercell. For the 2×2 supercell the use of this mesh gives 5 to 25 irreducible k–points sample (in the irreducible Brillouin zone) and for the 3×3 supercell the use of this mesh gives 3 to 13 irreducible k–points. Increasing the mesh to $7 \times 7 \times 1$ for the CH_2 adsorbed hcp will give a difference of 0.6 kJ×mol^{-1} and for the C adsorbed hcp the difference is 4.3 kJ×mol^{-1}, see Table 3.2.

The supercells are separated in z direction by vacuum layers. This can be important for large adsorbates. In Figure 3.2, one can see CH_2 adsorbed in hcp site in a system with 5 or 7 vacuum layers.

Propriety	System	Reference	Energy difference (kJ×mol^{-1})
k–points	CH$_2$ hcp	7×7×1/**5 × 5 × 1**	0.6
sampling	CH hcp	7×7×1/**5 × 5 × 1**	4.3
vacuum	CH$_3$ atop	7/**5**	−0.3
layers	CH$_4$ fcc	7/**5**	−2.6
slab layers	CH$_2$ hcp	6/**4**	−0.6
coverage	CH$_2$ hcp	1×1/**2 × 2**	−136.0
	CH$_2$ hcp	3×3/**2 × 2**	11.3
	CH hcp	3×3/**2 × 2**	21.8
	C hcp	3×3/**2 × 2**	39.7
slab	CH$_2$ hcp	no/**yes**	−7.8
optimization	C hcp	no/**yes**	−13.6
symmetry	CH$_2$ hcp	no/**yes**	0.0
one/two	CH$_2$ hcp	5 layers vacuum	6.2
sides	CH$_2$ hcp	4 layers vacuum	7.0
energy	C	300 eV	
cut–off	O	400 eV	
	Ru	205 eV (bulk)	
	Ru	300 eV (slab)	
spin	Ru slab	yes/**no**	0.0
	Co slab	yes/**no**	407.8
	C on Co	yes/**no**	168.9

Table 3.2: The test for the Ru(0001) surface model. The energy difference for the tested propriety against the model. Behind / are the standard values what we used.

The number of slab layers is also important. From the tests we performed, we conclude that 4 layers are good enough to describe the system. See Figure 3.3 for the difference between 4 and 6 slab layers. (The odd number of layers was carefully avoided because of the symmetry reason. Since ruthenium is an hcp metal, a slab with an odd number of layers will not have an inversion center, while a slab with an even number of layers will do. The cause is the missing "C" layer: fcc metals:
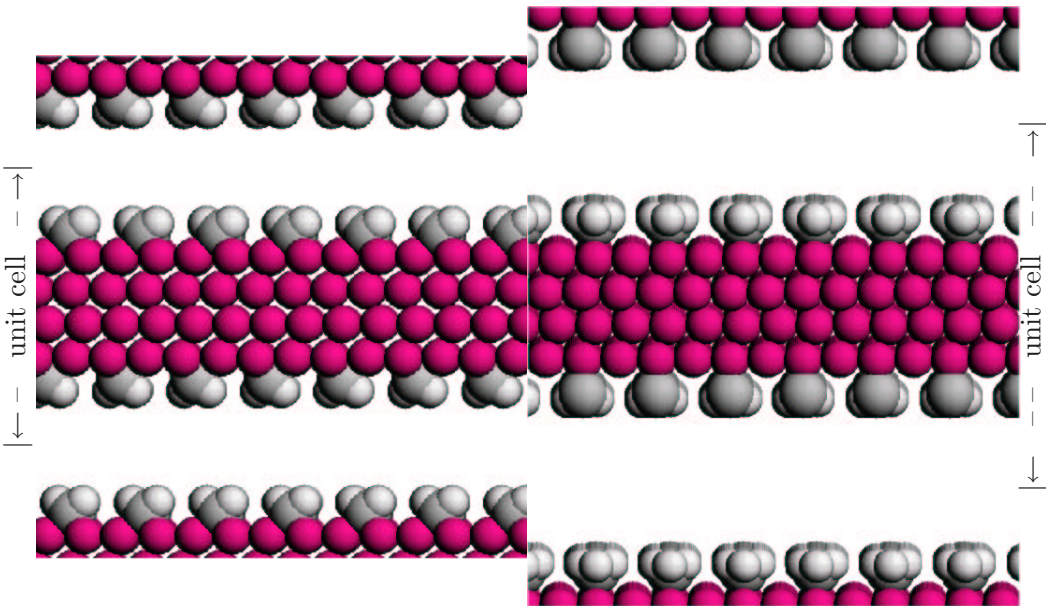
Figure 3.2: Side view of a slab with 5 and 7 vacuum layers.
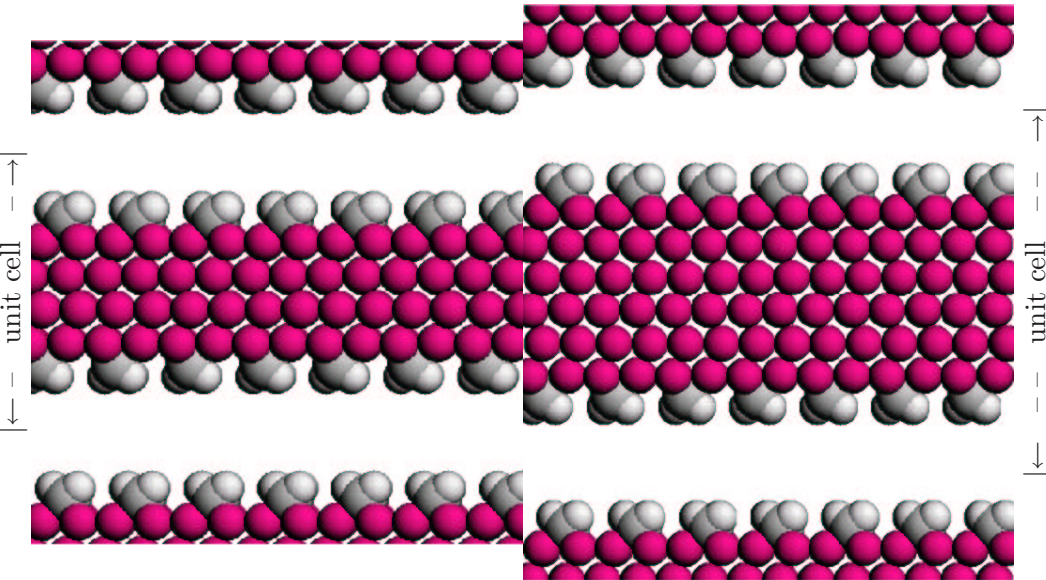
Figure 3.3: Side view of a slab with 4 and 6 metal layers.

ABCABC. . . , hcp metals: ABABAB. . .)

The coverage is also important, large differences are expected for adsorption en-

ergies. For most of the calculation performed, we choose a 2×2 structure (25.0%
coverage) and for few important structures, we performed calculations in 3×3 struc-
tures (11.1% coverage). See Figure 3.4 for a 2×2 and 3×3 structure.
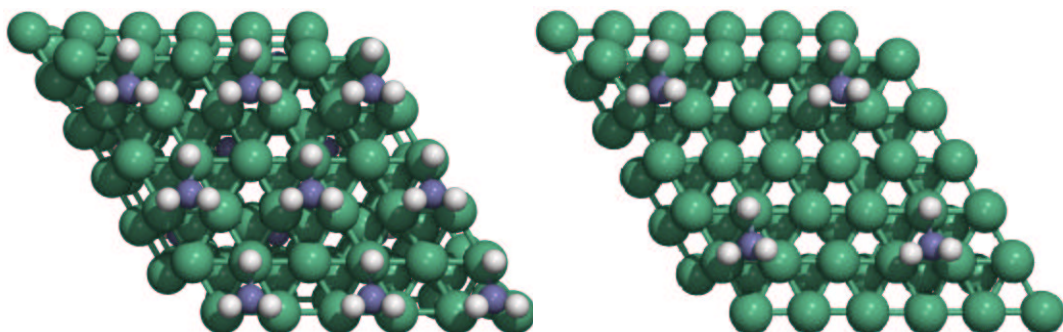
Figure 3.4: Top view of a 2×2 structure and a 3×3 structure.

We performed slab optimization of the system as well as optimization of the
adsorbates. Full optimization of the system can be important for species that strongly
adsorb because of the important distortion it produce in the metal slab.

Full use of the symmetry is made; this speed up calculation, by reducing the
degree of freedom. Adsorption on both sites with an inversion center is necessary, in
our opinion, to avoid artificial dipole–dipole interactions, see Figure 3.5.
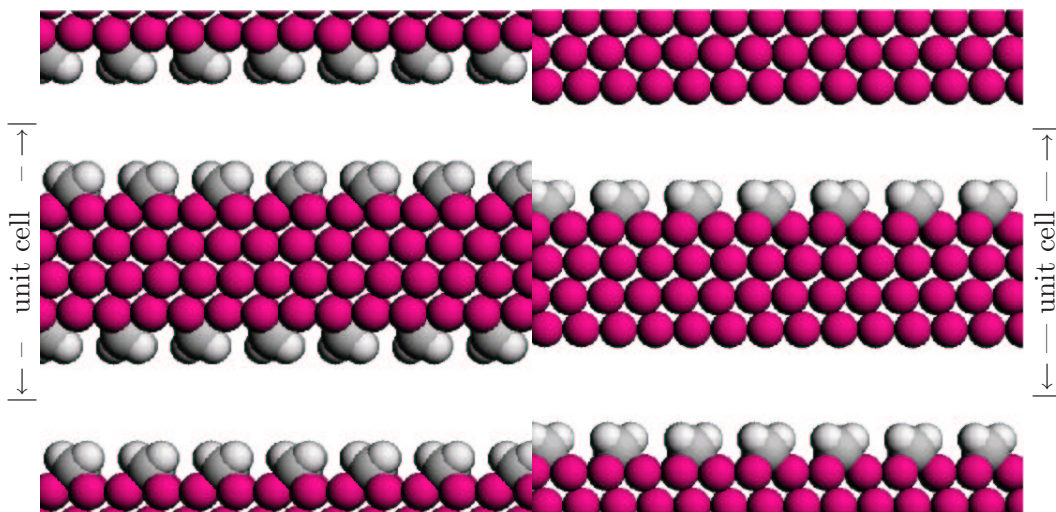
Figure 3.5: Side view of a slab with adsorbates on both sides and a slab with adsor-
bates on one side only.

The energy cut–off for the calculation is used according with the elements presented in the system. The Ru, and H pseudopotentials are converged with an energy cut–off for the plane–wave basis set (E_c) of 200 eV while for the C, and O pseudopotential it is 300 eV, and 400 eV respectively. Consequently, all the calculations were performed with an E_c of 300 eV for CH_x on Ru surfaces and 400 eV for CO on Ru surfaces.

A test of spin calculation was performed. For Ru the difference in energy and geometries for a spin polarized calculation and a non-spin polarized calculation is null. For Co (Fe and Ni) the difference is very large, which can be reduced by adsorbates, but it will not vanish.

More open surfaces
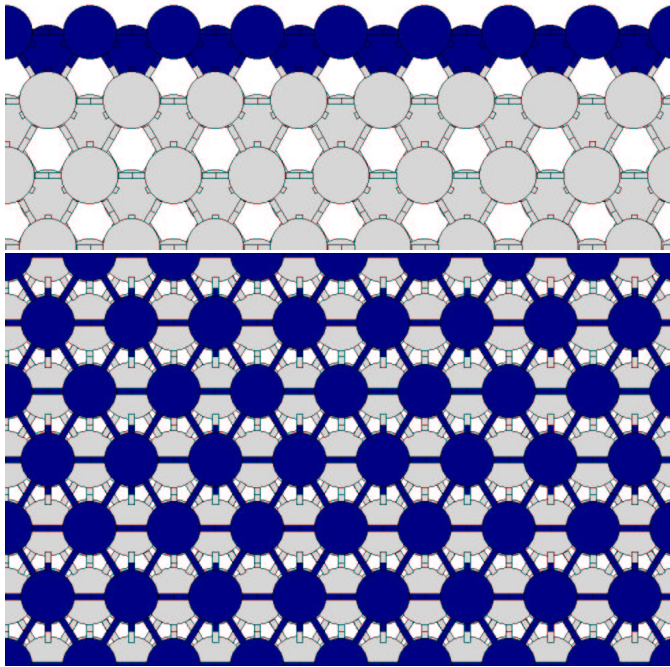
Figure 3.6: Side and top view of the $(10\bar{1}0)$ surface. The first layer is made darker. One can notice that each layer is formed by atoms not in the same plan.

Metals with a hexagonal compact package (hcp) structure have a unit cell, which is not a Bravais lattice. To make it easier to deal with the surface indices, 4 indices

are used. In the case of a surface of an fcc metal, the three indices can be switched: $(100) \equiv (010) \equiv (001)$.

In the case of a surface of an hcp metal, the set of three indices is more confusing when one want to switch the indices: $(110) \equiv (\bar{2}10) \equiv (1\bar{2}0)$. So the convention was to use an extra index, in the third position, which is redundant (the sum of the first three indices has to be zero), but in this way the equivalent surfaces are clearly seen: $(11\bar{2}0) \equiv (\bar{2}110) \equiv (1\bar{2}10)$.

A few test were done for the $(10\bar{1}0)$ surface, (see Figure 3.6). Methyl adsorbed on one of the hollow sites on this surface has adsorption energy with 10 kJ×mol^{-1} higher than methyl adsorbed on fcc sites on the Ru(0001) surface. $(11\bar{2}0)$ was chosen to be investigated further.
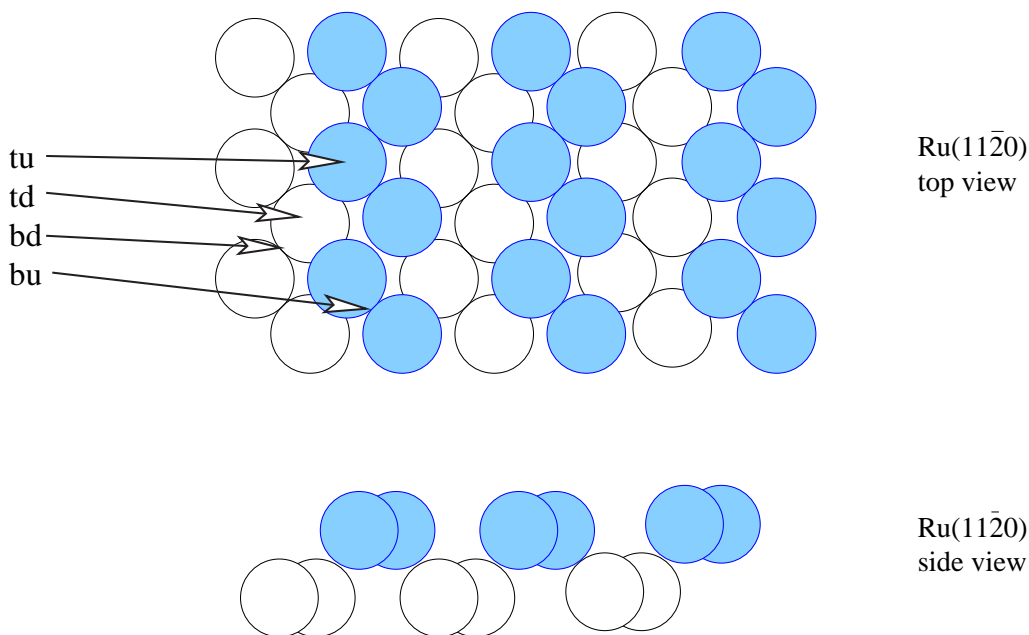
Figure 3.7: Side and top view of $(11\bar{2}0)$ surface. The white atoms are on the second layer. The adsorption sites are shown.

The $(11\bar{2}0)$ surface is a more open surface that $(10\bar{1}0)$. In Figure 3.7, one can see a side and top view of a such surface. The surface model consists of a super cell with a slab of 8 metal layers and 10 layers of vacuum between the surfaces. This may seems a lot, but it is similar to what we used for the Ru(0001) surface before. This surface is more open (see also Figure 3.8), the first two layers are both exposed

to the vacuum. The atoms on the first layer have 7 neighbors and the atoms from the second layer have 11 neighbors. (For the (0001) surface, each atom from the first layer has 9 neighbors.)
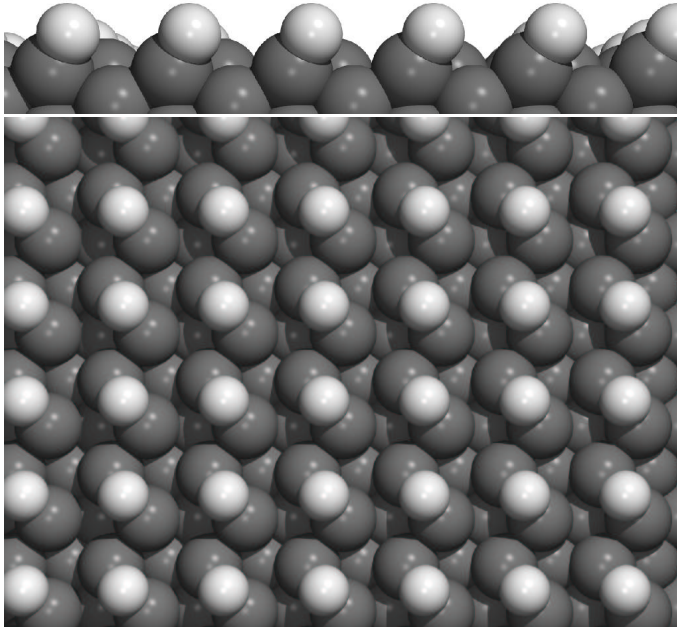
Figure 3.8: Side and top view of $(11\bar{2}0)$ surface with adsorbed H atoms on bridge sites, in a 1×1 structure at 50% coverage.

Adsorption on both sides with an inversion center avoids the generation of dipole–dipole interactions between the cells. Cells with 1×1 structures are considered (50% coverage) (see Figure 3.8).

The geometries of the surface and of the adsorbates are fully optimized. Intermediates have been studied on the four different sites for H atom and CH_x (x=1–3) species: atop up (tu), atop down (td), bridge up (bu) and bridge down (bd), see Figure 3.7. The atop up adsorption mode and bridge up adsorption mode involve only atoms from the first metal row, which are the ones more unsaturated. The atop down adsorption mode and bridge down adsorption mode involve not only atoms from the second row, but also from the first row. The atop down adsorption mode is in fact a five-fold coordinated site (one atom from the second row and four atoms from the first row), the adatom being at more or less the same height as the metal atoms from the first layer. The bridge down adsorption mode is a four-fold adsorption mode (two

atoms from the second layer (short bridge) and two atoms from the first row (long bridge)), the adatom being also more or less at the same height as the metal atoms from the first layer.

§**3.2.3   Stepped surfaces**

The steps issue is a hot topic in catalysis. Many people are convinced that catalytic processes take place at defects sites on surfaces and steps are one of most common local defects.
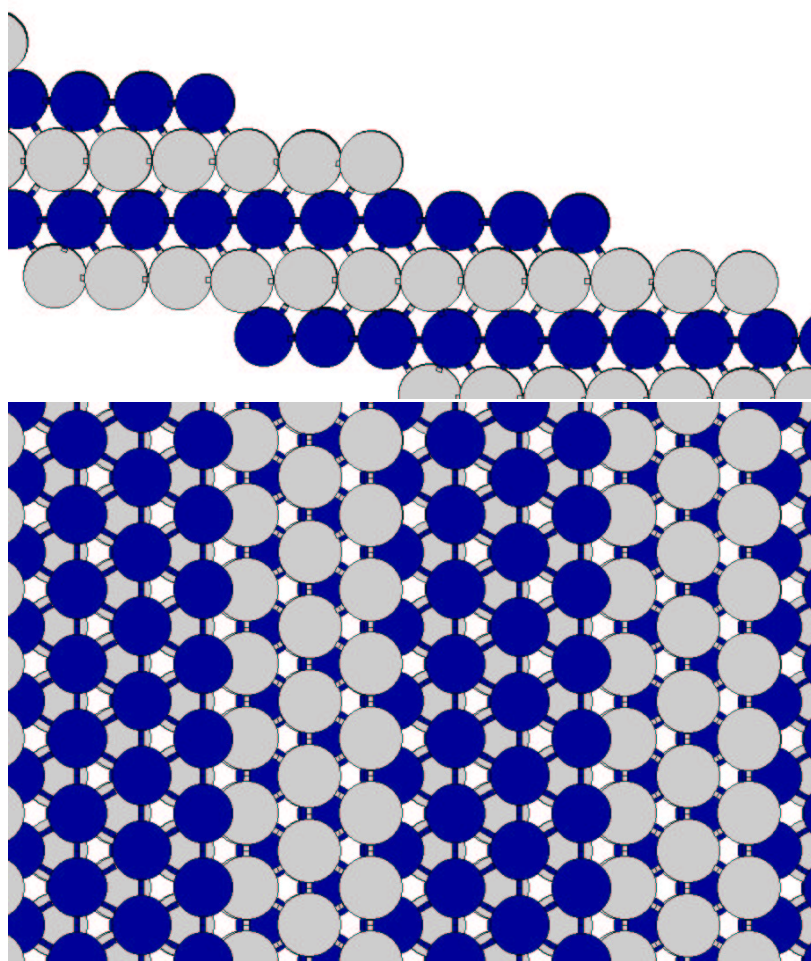
Figure 3.9: Top and side view of the stepped Ru surface with 3+4 atom wide rows on the terraces.

Stepped surfaces are not easy to model. For fcc metals, the easiest way is to consider a small supercell with just few atoms on the terrace. For the (111) hexagonal terraces, two steps are possible: the (111)-like or the (100)-like. In the case of hcp metals, the two different steps are present on the same (0001) hexagonal stepped surface (Figure 3.9) and these cannot be separated. This leads to a supercell with double size, compared with fcc metals. One solution to reduce the size of the supercell is to remove all the atoms from one terrace, and to have a double step.

If for fcc metals, steps are easier to represent, hcp metals are not that easy. There is no documentation about how to assign Miller indices to a stepped hcp surface. I did few attempts to do that.

We considered a few stepped surfaces, where the numbers of atoms on the terraces are 3+2, 3+3, 3+4, 3+5 and 3+6 (or 3+n in general). The $\vec{x}$ and $\vec{y}$ vectors are $(2, 0, 0)$ and $(\frac{(n+2)}{2}, \frac{(n+2)}{2}\sqrt{3}, \frac{2}{3}\sqrt{6})$, where n is here the atoms on the second terrace. The $\vec{z}$ vector is perpendicular on the terrace, rather than on the macroscopic surface. The direct product of the $\vec{x}$ and $\vec{y}$ vectors will give the plane indices for the surface. This is $(1, 0, \bar{1}, \frac{3(n+2)}{4\sqrt{2}})$ for the stepped surface with 3+n atoms on the terraces. Most of the people will expect here integers, but, I repeat, hcp metals do not have a Bravais lattice. The indices are the same for stepped surfaces with 2+3 and 3+2 atoms on the terraces. Generalization is possible here, stepped surfaces for hcp metals with $n + m$ atoms on the terraces have the same indices like stepped surfaces for hcp metals with $m + n$ atoms on the terraces. This is true since only the sum of n and m is used in the formula. To make it general, the plan indices are $(1, 0, \bar{1}, \frac{3(k-1)}{4\sqrt{2}})$ for k the total number of metal atoms in both terraces (or $k - 1$ is the number of atoms in the supercell in the direction perpendicular to the step).

§3.2.4   Comparison for different surfaces

In Table 3.3, one can see the adsorption energy of methyl radical on different Ruthenium surfaces. The adsorption energy varies with the coverage and with the adsorption site. We noticed a slightly preference for the adsorption on the edge of the step or on the more open surface.

§3.2.5   Physisorption on the Ru(0001) surface

In Figure 3.10, one can see the interaction potential between Ar and Ru(0001) surface. These kinds of studies are useful for comparison with similar data from
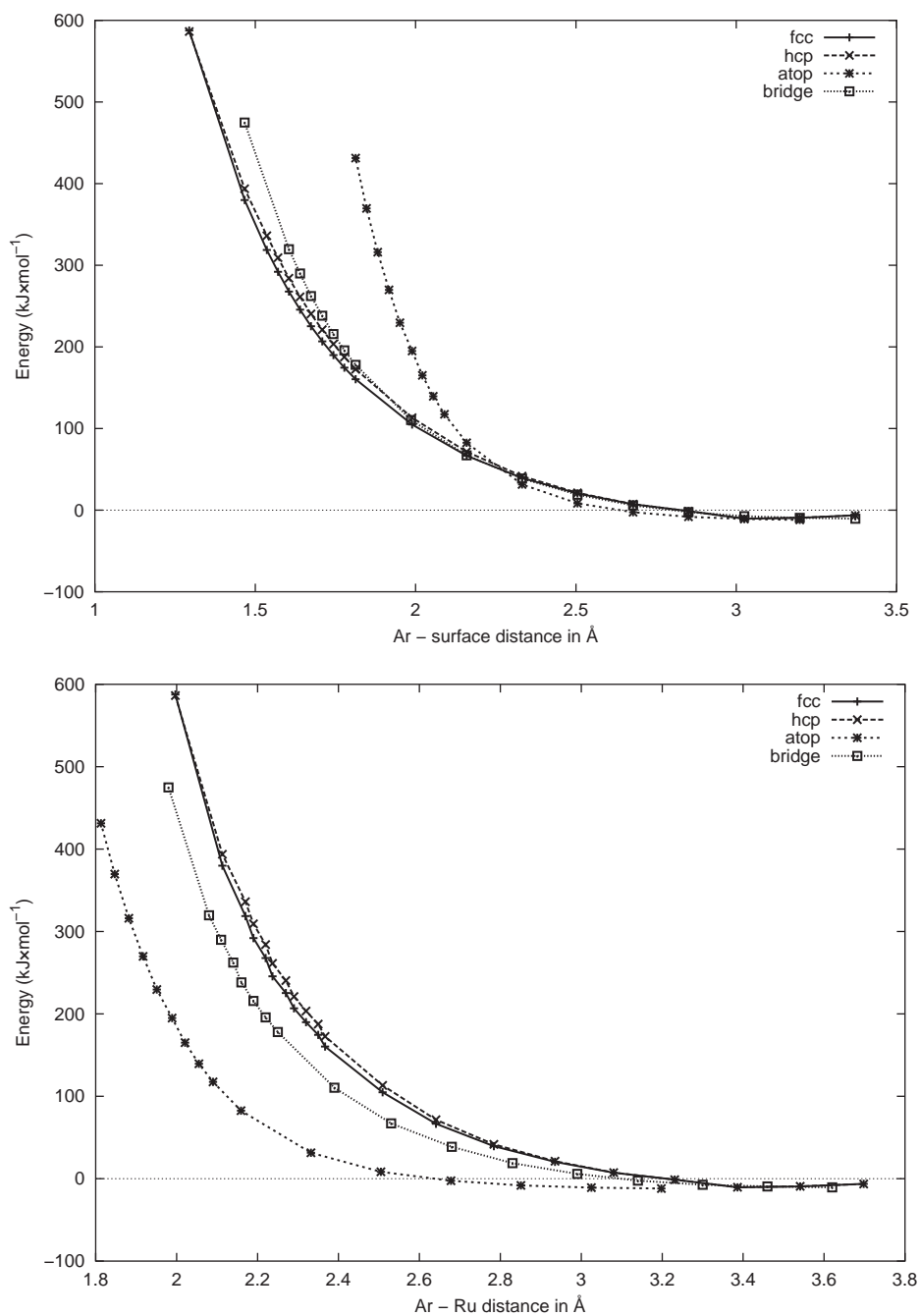
Figure 3.10: Potential energy for Ar approaching the Ru(0001) surface.

Surface	Site	Structure	Coverage	Adsorption Energy in kJ×mol^{-1}
hcp 0001	fcc	2×2	25.0%	-199
hcp 0001	fcc	3×3	11.1%	-210
fcc 111	fcc	2×2	25.0%	-208
fcc steps	bridge	$2 \times \frac{7}{3}$	25.0%	-224
hcp steps	fcc	2×5	20.0%	-207
hcp steps	fcc	2×4	16.7%	-208
hcp steps	fcc	2×3	25.0%	-193
hcp $10\bar{1}0$	hollow	2×2	25.0%	-209
hcp $11\bar{2}0$	bridge	1×1	50.0%	-221

Table 3.3: Adsorption energies for the CH_3 radical on several Ru surfaces, with respect to the bare surface and gas phase $\cdot CH_3$.

different systems (like CO on Ru(0001), for instance [28]).

The DFT based programs cannot reproduce physisorption, and any weak interactions (van der Waals, H bonds, etc.) This study of Ar physisorption was useful for its repulsion part, only the attractive part of the potential is actually weak.

Bibliography

[1] P. Hohenberg and W. Kohn, Phys. Rev. 136B 864 (1965).

[2] W. Kohn and L. J. Sham, Phys. Rev. 140A 1133 (1965)

[3] Parr R. G. and Yang W. *Density–Functional Theory of Atoms and Molecules* Oxford University Press, New York, (1989)

[4] R. G. Parr and W. Yang *Density–Functional Theory of Atoms and Molecules* Oxford University Press, New York, (1989)

[5] W. Kohn, *Rev. Mod. Phys.*, 71, 1253, (1999).

[6] Kresse, G.; Furthmüller, J., *Comp. Mat. Sci.*, 6, 15, (1996)

[7] Kresse, G.; Furthmüller, J., *Phys. Rev. B*, 54, 169, (1996)

[8] Vanderbilt, D., *Phys. Rev. B*, 41, 7892, (1990)

[9] Kresse, G.; Hafner, J., *J. Phys.: Condens. Matter*, 6, 8245, (1994)

[10] D. D. Jonsson, *Phys. Rev. B*, 38, 393, (1980)

[11] Perdew J. P., *Electronic Structure of Solids '91* Akademie Verlag, Berlin, 1991

[12] P. Pulay, *Chem. Phys. Lett.*, 73, 393, (1980)

[13] H. J. Monkhorst J .D. Pack, *Phys. Rev. B*, 13, 5188, (1976)

[14] Jónsson, H.; Mills, G.; Jacobsen, W., *Enrico Fermi Summer School (Lenci '97) proceedings*, 1997

[15] Pratt, L. R., *J. Chem. Phys.*, 85, 5045, (1986)

[16] A. P. J. Jansen, *Comput. Phys. Comm.*, 86, 1, (1995)

[17] J. J. Lukkien, J. P. L. Segers, P. A. J. Hilbers, R. J. Gelten and A. P. J. Jansen, *Phys. Rev. E*, 58, 2598, (1998).

[18] R. J. Gelten, R. A. van Santen and A. P. J. Jansen, *Dynamic Monte Carlo Simulations of Oscillatory Heterogeneous Catalytic Reactions* in *Molecular Dynamics: From Classical to Quantum Methods*, Elsevier Amsterdam, 1999

[19] J. C. Keck, *J. Chem. Phys.*, 32, 1035, (1960)

[20] J. C. Keck, *Discuss. Faraday Soc.*, 33, 173, (1962)

[21] J. C. Keck, *Adv. Chem. Phys.*, 13, 85, (1967)

[22] J. P. L. Segers, *Algorithms for the Simulation of Surface Processes*, Ph.D. thesis, Eindhoven University of Technology, 1999

[23] K. Binder, *Monte Carlo Methods in Statistical Physics*, Springer Berlin, 1986

[24] D. T. Gillespie, *J. Comput. Phys.*, 22, 403, (1976)

[25] D. T. Gillespie, *J. Phys. Chem.*, 81, 2340, (1977)

[26] W. H. Press, A. Teukolsky, W. T. Vetterling and B. P. Flannery, *Numerical Recipes in C: The Art of Scientific Computing*, Cambride University Press, 1992

[27] D. E. Knuth, *The Art of Computer Programming, Volume 3: Sorting and Searching*, Addison-Wesley, 1973

[28] B. Riedmüller, I. M. Ciobîcă, D. C. Papageorgopoulos, B. Berenbak, R. A. van Santen, A. W. Kleyn, *Surf. Sci.*, 465, 347, (2000)

Chapter 4

Methane activation on the Ru(0001) surface

The thermodynamics of methane decomposition on the Ruthenium (0001) surface has been investigated with ab initio periodic calculations for coverages of 25% and 11%. All surface intermediates are more stable than the gas phase methane although the last step of the decomposition path: CH $\rightarrow$ C + H, is highly endothermic. Amongst all of the surface species, CH appears to be the most stable, in agreement with experiments. All of the surface species (CH_x, (x = 3, 0) and H) adsorb on three-fold sites. Short-range lateral interactions between CH_x, (x = 3, 0) and H are also considered and are found to be mostly repulsive. The Transition States of the elementary reactions have been also investigated with the Nudged Elastic Band Method (NEB) [1] for 25% coverage. The calculated barriers are 85 kJ$\times$mol^{-1} for methane decomposition, 49 kJ$\times$mol^{-1} for methyl decomposition, 16 kJ$\times$mol^{-1} for methylene decomposition respectively. The decomposition of CH_{ads} requires the highest activation energy from the series with 108 kJ$\times$mol^{-1}.

A discussion concerning chemical bonding aspects of the transition states structures is presented.

§4.1   Introduction

The reactivity of methane on metal surfaces is a catalytically important reaction. The sequential dehydrogenation of methane or the sequential hydrogenations of carbon are essential parts of the Fischer–Tropsch mechanism. Many theoretical

and experimental studies have been conducted for CH_x species adsorbed on metal surfaces.

The cleavage of a C–H bond in methane is key to transforming natural gas into industrial useful products such as hydrogen and carbon monoxide. Adsorbed CH_x fragments formed upon CH bond cleavage are believed to be important in several catalytic processes occurring on transition metal surfaces. In the Fischer–Tropsch synthesis, methanation from CO and H_2 as well as carbon–carbon bond formation has been proposed to proceed via intermediate CH_x fragments [2–5].

The results to be presented here concern the chemisorption of CH_x intermediates on Ru(0001), as well as the Transition States of $CH_x \rightarrow CH_{x-1} + H$, x = 4-1, on the same surface, that were calculated using the Density Functional Theory method and the Nudged Elastic Band method. First, the relative stabilities of all of the species on the different sites present on the surface will be discussed at the 25% coverage level and the most stable sites are calculated for a lower coverage of 11.1%. Secondly, the consequences of lateral interactions between CH_x species and a coadsorbed H atom at 25.0% coverage are discussed. Third, the Transition States are presented.

Also an old idea of Frennet [6], that preadsorbed H can activate methane, has been explored for the reaction: $CH_4 + H_{ads} \rightarrow CH_{3ads} + H_2$.

§4.2 CH_x on Ru(0001) surface

The energies of the CH_x (x = 3-1) species adsorbed in different sites (fcc, hcp, bridge and atop at 25% coverage) are presented on the Figure 4.1. The subsurface C and H atoms are not stable, (only the energies for the octahedral sites are shown in Figure 4.1). Energies are given with respect to the most stable adsorption site, for each species. Absolute values relative to the CH_x in gas phase and the bare metal surface (also optimized) for the most stable adsorption modes are given in Table 4.1. The energies include structural changes due to the adsorption, as well as the lateral interactions between adsorbed species.

One observes that all of the surface species prefer the three-fold sites, the fcc site for H and for CH_3 and the hcp site for the others. The atop site is the most destabilizing position for all species. The bridge site energies for H, CH_3, and CH_2 are close to the interaction energy of the three-fold sites. This suggests that those species can easily diffuse over the surface.

The main information from the Figure 4.1 is the pronounced preference for the
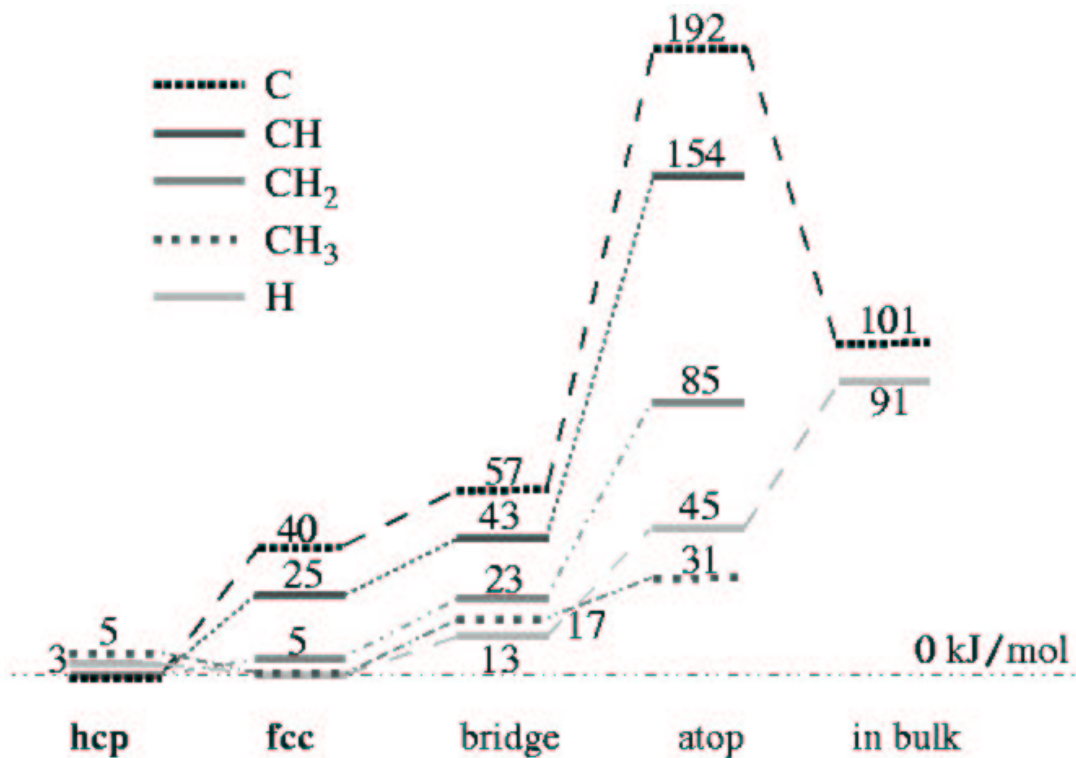
Figure 4.1: Relative energies diagram for CH$_x$ (x = 1, 2, 3), C and H adsorption on Ru(0001)

species	CH$_3$	CH$_2$	CH	C	H
adsorption site	fcc	hcp	hcp	hcp	fcc
energy (kJ×mol^{-1})	−198.8	−409.5	−641.96	−688.34	−53.5

Table 4.1: The binding energies of CH$_x$, C and H in their most stable sites (the zero level in Figure 4.1) relatively to the energy of the corresponding CH$_x$ in gas phase and the bare metal surface. For H, the reference is the dihydrogen molecule in the gas phase.

three-fold sites. This trend is expected for the C and H atoms but not for the CH$_x$ (x = 3, 2) species. This is significantly different from the results of other metals, Pd is an example [7–9], but also Pt [10–12], or Ni [13–20].

In the case of CH_2, two different geometries close in energies are possible in the three-fold sites: one with both hydrogen atoms equivalent, the C atom more or less located in the middle of the three-fold site and closer to one Ru atom by around 0.1 Å and the other one consists in one C–H bond almost parallel to the surface, pointing to a Ru atom and the other one C–H pointing outward o of the surface, the C atom is also near the middle of the three-fold site but closer to two Ru atoms by around 0.1Å. The C–H bond parallel to the surface is slightly longer (1.19 Å compared to 1.10 Å) and the distance Ru–H is 1.9 Å ($\approx$2.25 Å for the symmetric geometry), similar to the distances found for a single H atom in a three-fold site. In both geometries, H–C–H plane is perpendicular to the surface. The partial DOS diagrams show little differences for the two H, so the activation of this C–H bond is fairly small. These less symmetrical configurations of CH_2 are more stable by around 7 kJ×mol^{-1}.

The C–H bond lengths are around 1.1 Å for all intermediates CH_x. The Ru–C distances are in the 1.7 to 2.2 Å range. The larger the number of H atoms bonded to C and the number of Ru atoms coordinated to C, the longer the Ru–C bond. The angles Ru–C–Ru vary between 72° and 100° and the angles H–C–H between 113° and 106°, exception for the CH_2 tilted which have 99° in hcp site and 101° in fcc site.

Physisorption of CH_4 has been studied for the 2 × 2 structure with three different orientations (one, two or three H atoms pointing towards the surface) on the four different bonding sites. The potential energy surface appears to be rather flat and however, the adsorption energies are very small, DFT is not very accurate in describing weak interactions like Van der Waals. In only in two configurations, the adsorption energies are negative: in the case that one H atom points to an fcc site (E=−0.7 kJ×mol^{-1}) and with three H atoms point to a bridge site (E=−0.2 kJ×mol^{-1}). All other possibilities give positive adsorption energies (within 3 kJ×mol^{-1}), which are local minima. For the situation when the methane is pointing with 1 H to an fcc site, a 3 × 3 calculation gives an adsorption energy of −3.0 kJ×mol^{-1}. The major influence on the methane physisorption seems to be the lateral repulsion between the methane molecules. DFT calculations cannot be that reliable for these values of the physisorption energy.

The electronic factors that control the chemisorption can be analyzed with the help of projected density of states (PDOS). The PDOS are obtained by projecting the wavefunction onto the s, p, or d spherical harmonics, within the limit of a sphere centered on the atom in consideration.

With the help of the PDOS one can analyze the electronic factors which stabilize CH$_{3ad}$ in the fcc site rather than on an atop site and the relative stability of the CH$_{ad}$ fragment versus that of the C$_{ad}$ and H$_{ad}$ atoms. Assuming if the potential should be zero in the middle of the vacuum of the supercell, the Fermi level was shifted relatively to that calculated value. The new Fermi level is the work function of the system, with opposite sign.

Figure 4.2.A shows the PDOS of C 2p$_z$ atomic orbital for (CH$_3$)$_{ad}$ adsorbed on the fcc site and on atop site on the Ru(0001) surface. The 2p$_z$ orbital is more stabilized by around -2 eV for the fcc site compared to the top site. It strongly interacts with the bottom of the d metal valence electron band (the bonding components is in phase). The fcc site is preferred also because the interaction with three surface Ru atoms instead of one, this leads to a better stabilization of the surface. For the atop site the C 2p$_x$ atomic orbital interacts with the higher energy d$_{3z^2-2r^2}$ metal orbital. (The other projections for (CH$_3$)$_{ad}$ are not that much different for both sites.) As the metal d valence electron band is not completely filled, the antibonding levels are pushed up above the Fermi level, lowering the Pauli repulsions and favoring the highly coordinated sites.

Figure 4.2.B presents the PDOS of the C 2p$_x$ atomic orbital for CH$_{ad}$ and C$_{ad}$. Most of the C 2p$_x$ density of states for CH$_{ad}$ is contained in the sharp peak around -11 eV, which corresponds to the CH bond. For C$_{ad}$ the main part of the levels is at -11 eV. A comparison of the PDOS of the H s atomic orbital for CH$_{ad}$ and H$_{ad}$ (not shown) indicate a better stabilization of H in CH$_{ad}$. The C–H bond is stronger than the H–Ru bonds and it stabilizes the p$_z$ orbital of C in CH$_{ad}$ compared to that of C$_{ad}$.

We also performed some calculations to analyze the effect of lateral interactions. A CH$_x$ species (x = 0-3) was placed in the same unit cell in its most favorable site together with an H atom. For the 2 × 2 structure, there can be three different situations. H$_{ad}$ and (CH$_x$)$_{ad}$ can be close to each other, sharing two Ru atoms (the "close" situation). In this situation they are in the two different kinds of three-fold sites: (CH$_3$)$_{ad}$ fcc + H$_{ad}$ hcp, (CH$_2$)$_{ad}$ hcp + H$_{ad}$ fcc, CH$_{ad}$ hcp + H$_{ad}$ fcc and C$_{ad}$ hcp + H$_{ad}$ fcc. The second situation occurs when they are far from each other. The occupied sites are on opposite sides of a shared Ru atom. In this configuration, (CH$_x$)$_{ad}$ and H$_{ad}$ are again in different kinds of three-fold sites. We will refer to this situation as "far". The last situation arises when both species are on the same kind of site. They share one Ru atom but they are not opposite from each other. We will
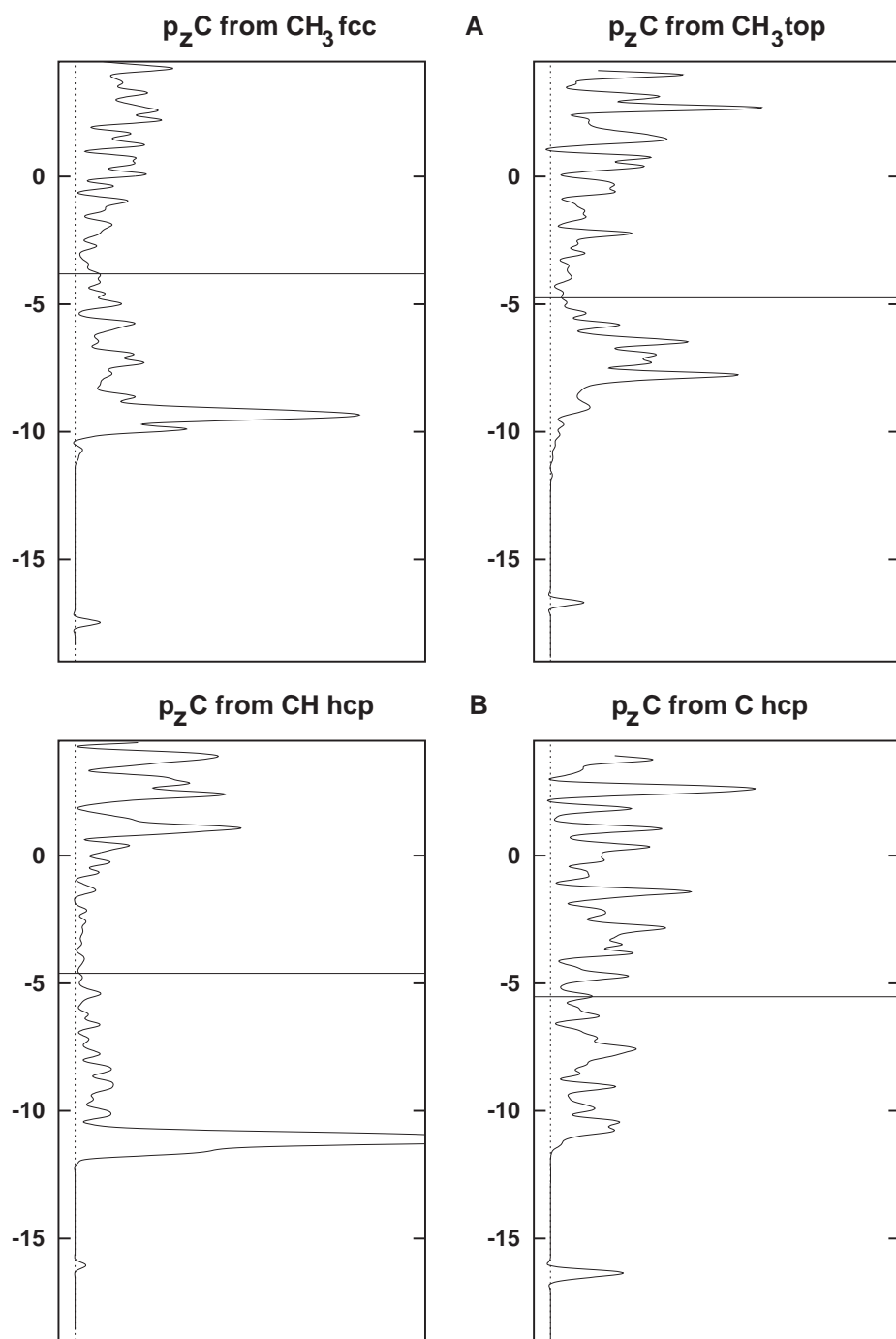
Figure 4.2: Projected density of states on the C p_z orbital in arbitrary units. A: C p_z orbital from CH_3 fcc and atop. B: C p_z orbital from CH hcp and C hcp.

refer to this situation with the word "same".

We have constructed the diagram in Figure 4.3 by adding the adsorption energy of the remaining H atoms from a 2×2 structure. These three situations ("far", "same" and "close" coadsorption sites) are illustrated in Figure 4.4 for the generic case of "X" and "o".
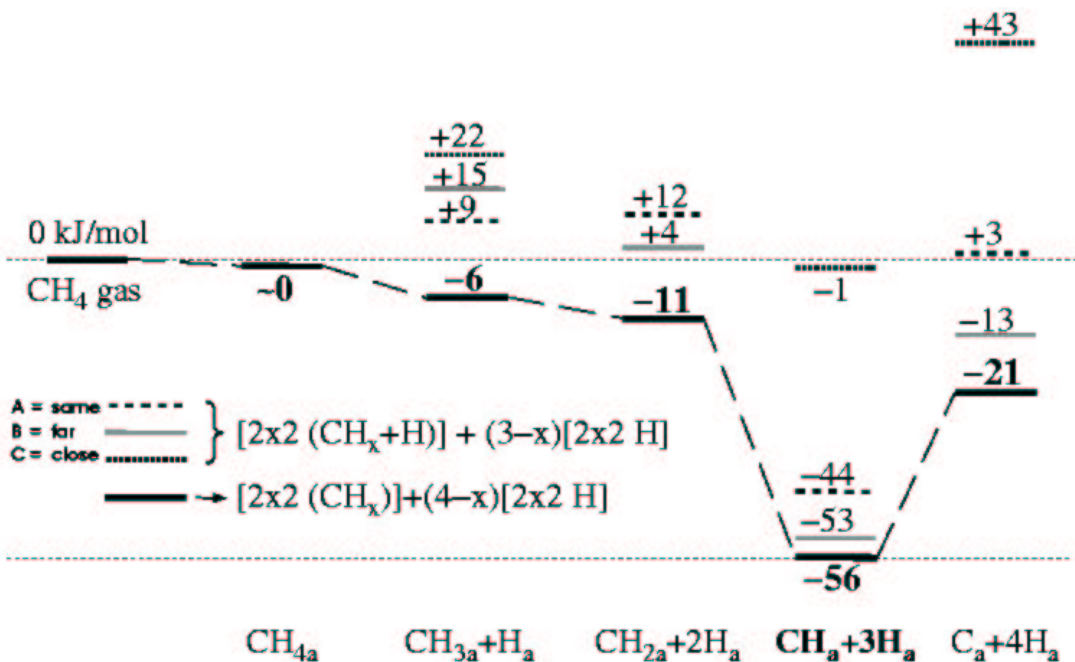
Figure 4.3: The path for methane decomposition on Ru(0001) in 2×2 structure with the lateral interaction between CH$_x$ and H.
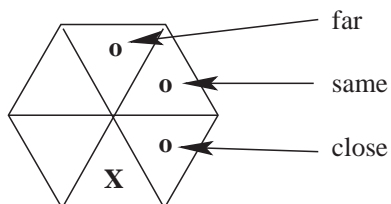
Figure 4.4: Three different situations for "X" and "o" in the same 2×2 supercell.

From the study of the lateral interactions it is found that the most favorable situation occurs when the CH$_x$ and the H are not adsorbed close. There are small

differences between the "same" and the "far" positions. These two results could be the direct products from the decomposition of CH_{x+1} on the surface. The "close" situation is not favorable as we can see from the large repulsion between CH_x and H. In the case of CH_3 the repulsions force the H to move almost in an atop site. For CH_2 (tilted) + H, because the CH_2 is tilted, the "close" configurations are not stable, the H atom goes to the adjacent hcp site. The main levels correspond to the most stable configuration when the H atoms can move away from the CH_x, an easy process as the transition state for the diffusion between two three-fold sites is about 13 kJ×mol^{-1}. It should be noticed that the "close" configurations for the CH and C species are metastable even if they are very high in energy.

The energy diagram is given for both coverages in Figure 4.5. Most of the elementary dissociation steps of adsorbed CH_x are exothermic, only the last elementary reaction step $CH_{ad} \rightarrow C_{ad} + H_{ad}$ is endothermic. For 11.1% coverage, the gains for the adsorption energies are large for CH and C, moderate for CH_3 and CH_2 and small for CH_4 and H. Repulsive interactions are mediated via the surface and increase with the coverage and the strength of the adsorbate–surface bonding. Therefore the exothermicity of the elementary reaction $(CH_{x+1})_{ad} \rightarrow (CH_x)_{ad} + H_{ad}$ (x = 3-1) increases by decreasing the coverage because the $(CH_x)_{ad}$ are more stabilized than the $(CH_{x+1})_{ad}$.

Adsorbed CH appears to be the most stable intermediate from the CH_x series. The sp hybridized C–H bond of CH_{ad} is stronger than that of H adsorbed on the surface. The repulsions due to the increasing coverage seem to come essentially from interactions through the surface and not from direct adsorbate–adsorbate interaction. Indeed, the differences are more important for the smaller species, which are also more strongly bonded to the surface.

Our calculations agree with the work of Au [21] for the adsorption energies for CH_x, (x = 0, 4) and H (see Table 4.1), as well as for the geometries. If we compare our results for methane decomposition with the results of Paul and Sautet [7–9] we note that on Ru the methane decomposition is an exothermic process whereas on Pd the same process is endothermic. In this sense Ru can be characterized as a more reactive metal than Pd. Reactivity appears to relate to the relative distribution of the valence electrons over the bonding and antibonding adsorbate–surface orbital fragments [23], the lower filling of the d band for Ru enhances the bonding nature.
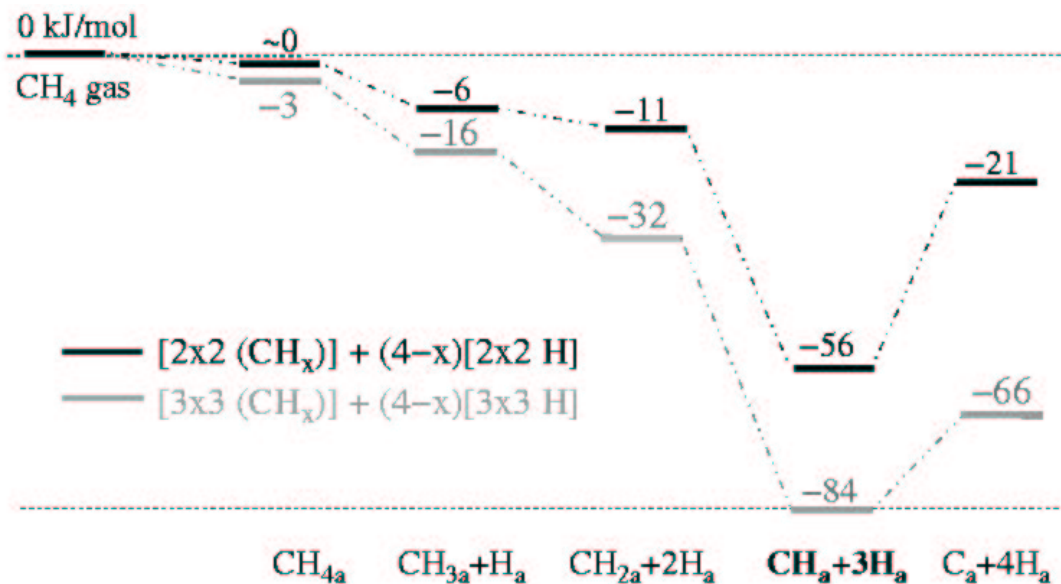
Figure 4.5: The path for methane decomposition on Ru(0001) in 2×2 and 3×3 structure (25% and 11% coverage).

§4.3 Barriers for the elementary reactions of methane activation on the Ru(0001) surface

The energies involved in the elementary reactions $CH_{(x)ads} \rightarrow CH_{(x-1)ads} + H_{ads}$, with x = 4-1, are presented in the Figure 4.6. The reference energy is the energy of the methane in gas phase. The plain lines represent the energy of the $CH_{(x)ads}$ at 25% coverage, to which the energy of (4−x) H_{ads} atoms at 25% coverage has been added. Thus, there is no interaction between the $CH_{(x)ads}$ and (4-x) adsorbed hydrogen atoms. The other two values represent the energy of $CH_{(x)ads}$ in interaction with one adsorbed H atom in the same 2×2 cell, to which we added as well the energy of 3-x H_{ads}'s. Therefore, this energy values take into account the interaction energy between $CH_{(x)ads}$ and *one* H atom in a 2×2 cell.

The reaction path for each of these elementary reactions is discussed below.
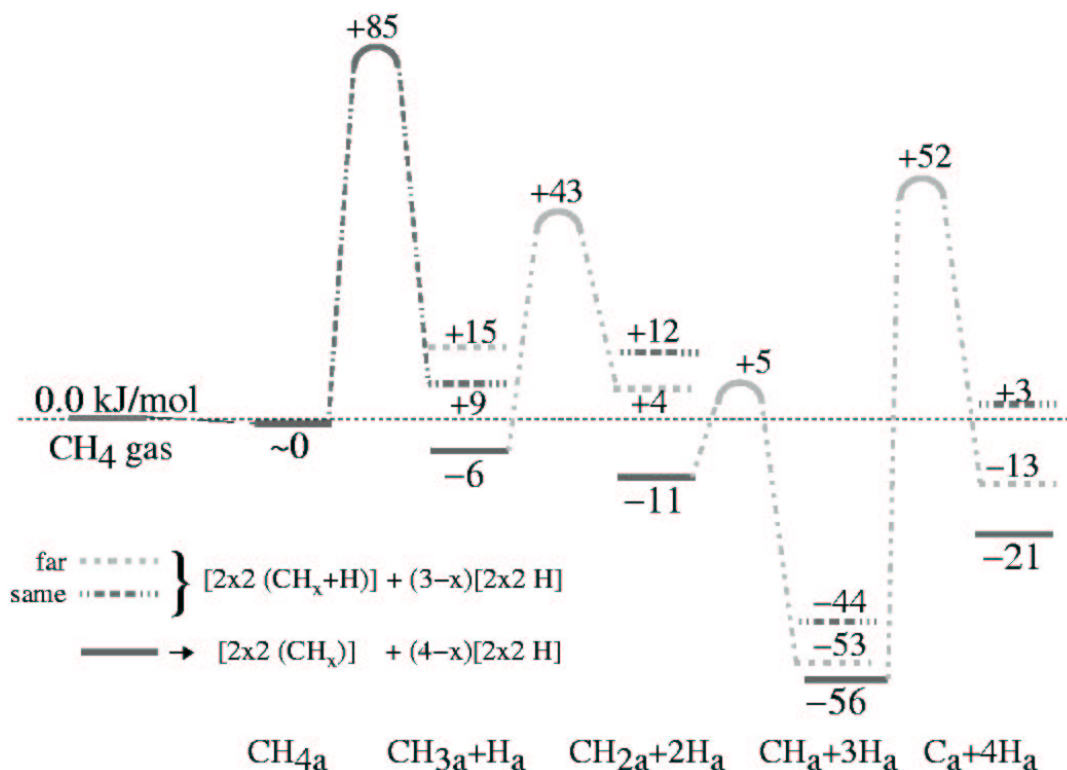
Figure 4.6: The complete diagram for methane decomposition. The energies are in kJ×mol^{-1}. The zero level is the energy of gas phase methane.

§4.3.1 $CH_{4ads} \rightarrow CH_{3ads} + H_{ads}$

The starting geometry for the determination of the transition state in this reaction was taken from Burghgraef [16]. The initial configuration of methane was physisorbed on atop site with 1 H pointing down. The final configuration was methyl adsorbed in a fcc site and one hydrogen atom adsorbed in a neighboring fcc site. However, along the reaction path we discover that the methane molecule first turns in order to point down with two H atoms, this geometry being more favorable for methane decomposition. The geometry of the transition state can be seen in Figure 4.7. The barrier for this reaction is about 85 kJ×mol^{-1} with respect to physisorbed methane.

We have also tested the hypothesis of the formation of subsurface H, which could result from methane decomposition. But this situation (e.g. a subsurface H atom below a methyl group on the surface), is around 110 kJ×mol^{-1} less stable than the case with both adsorbates on the surface. We predicted a difference of 91 kJ×mol^{-1}
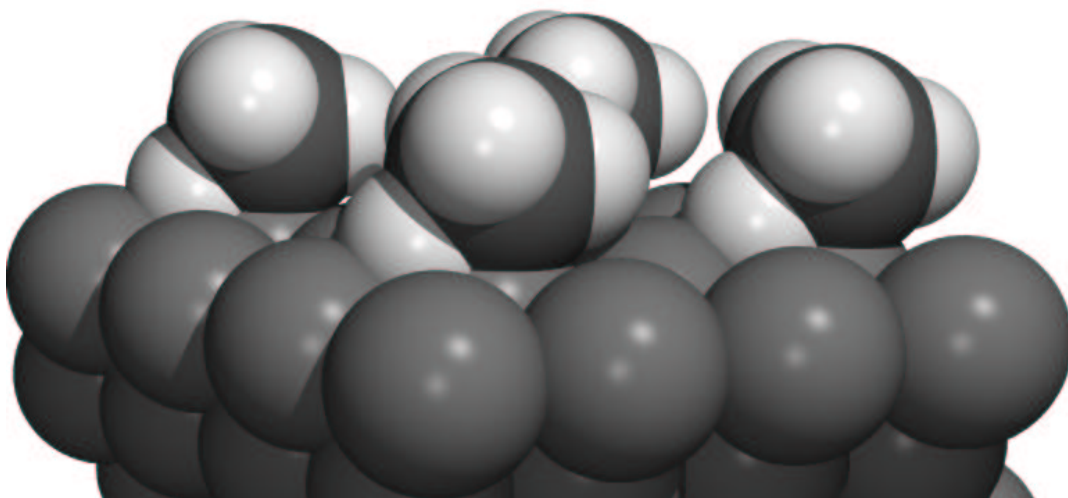
Figure 4.7: The TS for $CH_4 \rightarrow CH_3 + H$. Initial CH_4 is physisorbed with 1 H pointing to atop site and finally CH_3 is adsorbed in a fcc site as well as the H atom.

for the H externally adsorbed in a fcc site and H subsurface in an octahedral site [24]. The tetrahedral subsurface sites are even less favorable.

In the transition state, the C–Ru distance is 2.28 Å and the H–Ru distances are 1.69 Å and 2.19 Å for the activated H and 2.61 Å, 2.95 Å and 2.92 Å for the other three H atoms. The H–C–Ru angle is 48° and the activated H points to a bridge site. The H–C–Ru angles for the other three H atoms are 95°, 115°, and 118°. The C–H bonds are 1.57 Å for the activated H and 1.10 Å for the other three H atoms. There are six H–C–H angles, three involving the activated H atom (142°, 90°, and 94°), and three not involving the activated H atom (111°, 109° and 109°). Considering that activated H pointing to a three-fold site, the corresponding transition state energy is found to be considerably higher.

The Transition State energy found for methane activation is in agreement with the results of Au et al. [21] for methane on Ru surface while Jachimowski et al. [25] for ethane activation on Ru(0001) and Carstens et al. [26] for methane activation reported a much smaller activation energy for supported Ru particles. The disagree-

ment can be due to the presence of steps. For different metals (Ni, Co), Burghgraef et al. [16] and Kratzer et al. [20] et al. calculated a higher activation energy. The geometry of the transition state remains very close to that from Burghgraef et al. [16]

§4.3.2 $CH_{3ads} \rightarrow CH_{2ads} + H_{ads}$

The initial configuration for this elementary reaction is CH_3 adsorbed in an hcp site and the final configurations is CH_2 adsorbed in an hcp site and the H atom adsorbed in a fcc site. A similar path with the H atom ending in an hcp site was investigated. The second path is in fact the first path followed by a jump of the H atom from the hcp to the fcc site. The barrier for this reaction is 49 kJ×mol^{-1} with respect to CH_3 adsorbed. This transition state have a substantial higher activation energy than the one predicted by Au et al. [21] using the approximate BOC formula. The activation energy of methyl compared with methane is smaller. This is not surprising at all, because the methyl group is already adsorbed on the surface, while methane is in a very weak physisorbed state, quit far from the surface.

The geometry of the transition state can be seen in Figure 4.8. Again, one of the C–H bond is elongated. The C–Ru distances are 2.19 Å, 2.19 Å, and 2.11 Å, the H–Ru distances are 1.66 Å for activated H atom and 2.29 Å for the others. The H–C–Ru angle is 50° for the activated H and 81° for the other two H atoms. The C–H bond is 1.70 Å for activated H and 1.11 Å for the others. The H–C–H angle is 97° if it involves the activated H atom and 106° if not.

§4.3.3 $CH_{2ads} \rightarrow CH_{ads} + H_{ads}$

Two different reaction paths have been considered. The initial configuration was CH_2 adsorbed in an hcp site for both reactions and the final configurations were CH adsorbed in an hcp site and the H atom adsorbed in a neighboring three-fold site. The two alternative options are that H atom finishes in a fcc or in an hcp site. The final configurations have been called "same" and "far" as in our previous article [24], see also Figure 4.4 and the explanations before it. The barrier for this reaction is 16 kJ×mol^{-1}, with respect to CH_2 adsorbed hcp. The activation energy for this elementary reaction is very low if compared to the prediction of Au.

The activation of a C–H bond from methylene is very easy. This is partially because the CH_2 group is already adsorbed in a non-symmetrical way, with a slightly longer C–H bond (1.19 Å with respect to 1.10 Å for the other C–H bond), parallel
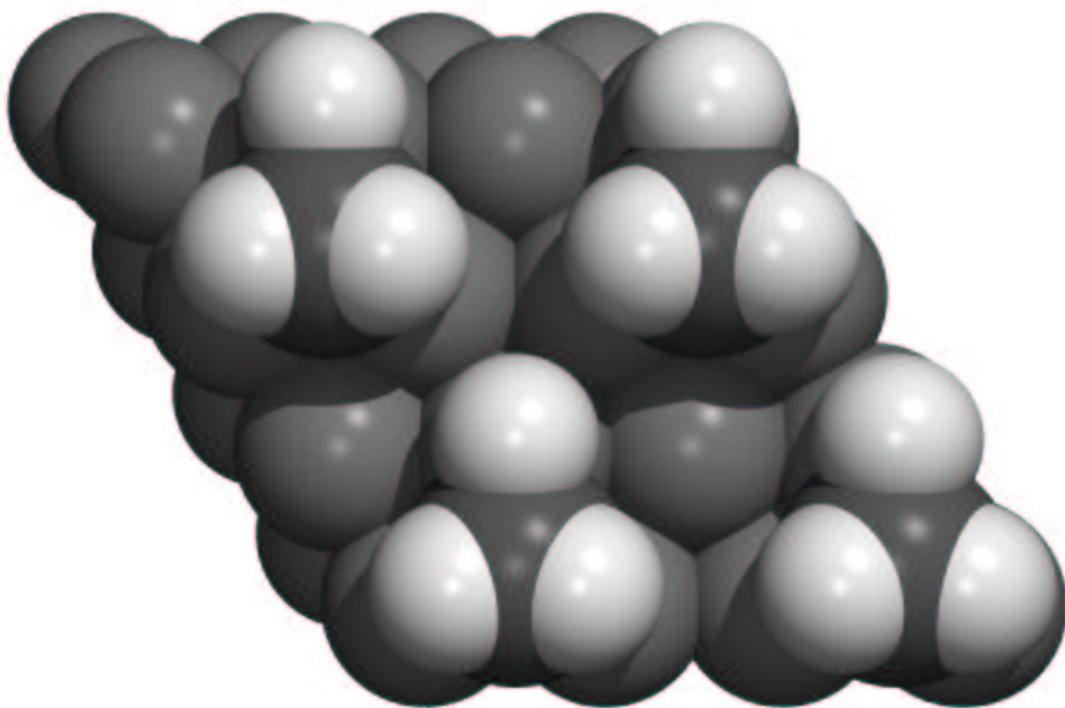
Figure 4.8: The TS for $CH_3 \rightarrow CH_2 + H$. Initial CH_3 is adsorbed in an hcp site and final CH_2 is adsorbed in an hcp site and H in fcc site.

to the surface and directed towards a Ru atom.

The geometry of the transition state can be seen in Figure 4.9. The C–Ru distances are 2.08 Å, 2.06 Å, and 2.06 Å. The H–Ru distances are 1.66 Å for the activated H atom and 2.81 Å for the other. The H–C–Ru angle is 52° for the activated H and 123° for the others H atoms. The C–H bonds are 1.58 Å and 1.10 Å respectively. The H–C–H angle is 88°.

§4.3.4 $CH_{ads} \rightarrow C_{ads} + H_{ads}$

Also, two different reaction paths have been considered. The initial configuration was CH adsorbed in an hcp site for both reactions and the final configurations were
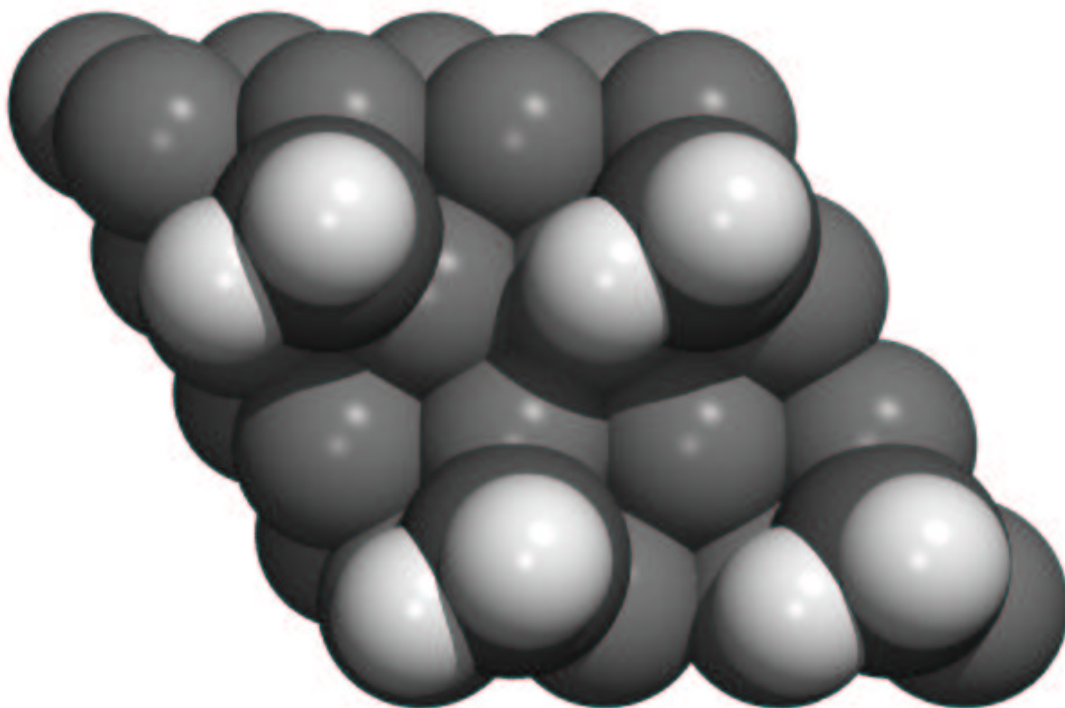
Figure 4.9: The TS for $CH_2 \rightarrow CH + H$. Initial CH_2 is adsorbed in an hcp site, as well as final CH and H is in a fcc site.

C atom adsorbed in an hcp site and the H atom adsorbed in a neighboring three-fold site, which can be fcc or hcp. The first choice, with the H atom in a fcc site, is a reaction where the H atom is passing over the top of a Ru atom and it arrives in the fcc site opposite to the hcp site where the C atom is located. The second choice, with the H atom in an hcp site, is a reaction where the H atom is passing also over the top of a Ru atom and it arrives in the hcp site close to the hcp site where the C is sitting. We observed from our results that the second variant can in fact be decomposed in two steps: the first variant followed by a diffusion of the H atom from the fcc site to the hcp one. The barriers for those two reactions are the same: 108 kJ×mol^{-1}, with respect to CH adsorbed hcp, in very good agreement with the result of Au et al. [21].

For the last Transition State from the methane decomposition path, we have the

largest barrier. This can be explain by the fact that the reaction is endothermic, and for the activation on a flat surface more energy is needed to tilt the C–H bond which is perpendicular to the surface than for C–H bond from methyl or methylene which have already an inclination. The geometry of the transition state can be seen in Figure 4.10. The C–Ru distances are 1.95 Å, 1.95 Å, and 1.98 Å. The H–Ru distance is 1.67 Å. The H–C–Ru angle is 54° and the C–H bonds are 1.69 Å.
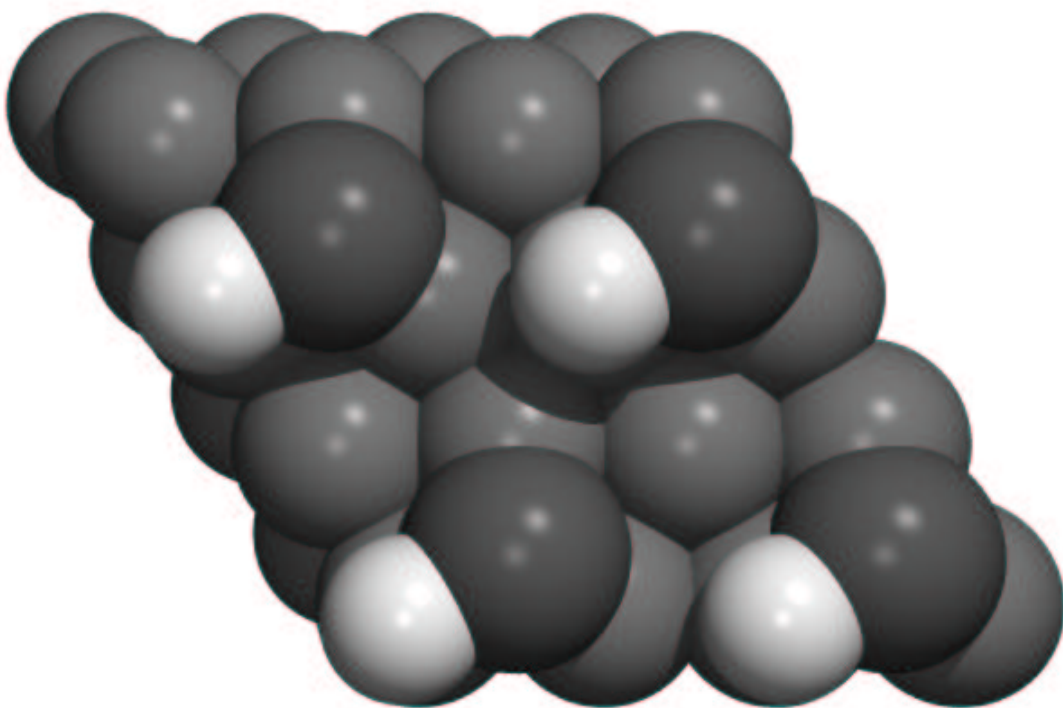
Figure 4.10: The TS for CH → C + H. Initial CH and final C are adsorbed in hcp sites and the H in a fcc site.

§4.3.5 $CH_4 + H_{ads} \rightarrow CH_{3ads} + H_2$

We analyzed this elementary reaction step in order to see if preadsorbed H on the surface activates methane. The initial configuration was with a H atom adsorbed

in a fcc site and the methane molecule physisorbed on a nearby top site, with three H atoms pointing down, one of them being above the adsorbed H on the surface. In those calculations we used 7 vacuum layers instead of 5 in order the avoid the interactions between the desorbing dihydrogen molecules in neighboring cells.

The proposal that a species "CH_5" can exist on a surface, (like an analog of the "CH_5^+" in solid acids) in order to explain a direct mechanism for D_2 + CH_4 exchange, appears to be unlikely as those species are highly unstable. The barrier we got is about 400 kJ×mol^{-1}.

The reaction starts by the approach of methane to the surface in the same way as without the preadsorbed H on the surface. One H atom from methane is activated, but because the three-fold site where it should go is already occupied, preadsorbed H is pushed to the next three-fold site. Around the transition state, the preadsorbed H atom reaches a bridge position, and will not continue its diffusion path, but will react with the activated H, to form the H_2 molecule. The remaining CH_3 is in atop position around the transition state and while the H_2 molecule is formed, it starts to migrate to a three-fold site.

§4.3.6   Transition States at lower coverage

Previously reported Transition States (TS) [22] were calculated in 2×2 structures, which imply important lateral interactions. New calculations were performed in 3×3 supercells, in order to have the barriers without the lateral interaction. The geometries of the TS found for the 2×2 supercells were the initial guess and the TS were located by minimizing only the forces.

The barriers calculated at 0.11 ML coverage differ from those obtained at 0.25 ML coverage. For the reactions CH_{x-1} + H $\rightarrow$ CH_x (x = 1, 2, 3, 4), the general trend is an increase of the barrier at low coverages compared with high coverage. This can be explained by the fact that the more H atoms are in a CH_x species the weaker the lateral interactions become. Therefore, if the species in the left–hand–side of the chemical equation have more repulsive interactions with the neighboring species than the species from the right–hand–side of the chemical equation the barrier will go up. (If the reactant is more destabillized than the product, the barrier will increase.) For the opposite reactions $CH_x \rightarrow CH_{x-1}$ + H (x = 1, 2, 3, 4), there is not a general trend. In the case of CH and CH_4 decomposition, the barriers decrease at lower coverage. In the case of CH_2 and CH_3 dissociation, no significant modification of the barriers

is found. The decrease of the barriers can be explained in a similar way as for the dehydrogenation reactions. The small change of the barrier for CH_2 and CH_3 can be due to the similar repulsive interactions with the neighboring species for both the products and the reactants. See Table 4.2 for values.

reaction vs. coverage	2×2	3×3	
$CH_4 \rightarrow CH_3 + H$	86	79	79
$CH_3 \rightarrow CH_2 + H$	49	51	52
$CH_2 \rightarrow CH + H$	16	16	* 22
$CH \rightarrow C + H$	112	100	101
$C + H \rightarrow CH$	69	87	88
$CH + H \rightarrow CH_2$	58	74	⋆ 68
$CH_2 + H \rightarrow CH_3$	54	61	58
$CH_3 + H \rightarrow CH_4$	91	98	97

Table 4.2: The energy barriers (TS) in $kJ \times mol^{-1}$ for the elementary reactions for methane dehydrogenation and C hydrogenation on the Ru(0001) surface, calculated at 0.25 ML and 0.11 ML coverages, 2×2 and 3×3 supercells respectively. The third column represents the TS calculated for 3×3 with a Brønsted–Polanyi formula (see equation 8.3, chapter 8) where we consider the final state the CH_x and the H already diffused away.

* CH_2 decomposition gives the correct result if we consider an early TS.

⋆ CH hydrogenation gives the correct result if we consider a late TS.

In the case of $CH_3 \rightarrow CH_2 + H$ reaction, due to the fact that CH_3 and CH_2 prefer different three-fold hollow sites for adsorption, two different reactions were considered: $CH_{3(hcp)} \rightarrow CH_{2(hcp)} + H_{(fcc)}$ and $CH_{4(fcc)} \rightarrow CH_{2(fcc)} + H_{(hcp)}$ (`fcc` is the three-fold site without a Ru atom below, in the second layer and `hcp` is the three-fold site with a Ru atom below, in the second layer). The barriers were computed for each reaction in 2×2 and 3×3 supercells. For the 2×2 supercell, there is no large difference for the activation energy, only 7 $kJ \times mol^{-1}$. With the 3×3 supercell appears a more important decrease for the reaction barrier if the CH_x species are in hcp sites. The difference becomes 14 $kJ \times mol^{-1}$ (see Table 4.3).

Since the H atom, CH_3 and the CH_2 present a small difference for fcc and hcp adsorption energies (respectively 3, 5 and -5 $kJ \times mol^{-1}$) it was difficult to conclude

reaction vs. coverage	2×2	3×3
$CH_{3(hcp)} \rightarrow CH_{2(hcp)} + H_{(fcc)}$	49	47
$CH_{3(fcc)} \rightarrow CH_{2(fcc)} + H_{(hcp)}$	56	61

Table 4.3: The energy barriers (TS) in kJ×mol^{-1} for the elementary reaction of methyl decomposition to methylene and hydrogen on Ru(0001) surface, calculated at 0.25 ML and 0.11 ML coverages (2×2 and 3×3 supercells respectively) for the two different three-fold sites.

which reaction will have the smaller barrier without performing the calculations.

§4.4   Discussion

DFT calculations, using the NEB Method and quasi–Newton algorithm to determine the Transition State for the elementary decomposition steps of methane on the most dense surface of Ru give the following results: the decomposition of CH_{2ads} to CH_{ads} and H_{ads} is the easiest with a barrier of 16 kJ×mol^{-1}. The most difficult reaction step is the decomposition of CH_{ads} in C_{ads} and H_{ads}, the barrier found is more than 100 kJ×mol^{-1}. For the cleavage of a C–H bond in CH_4 and adsorbed CH_3 the barriers are respectively 85 kJ×mol^{-1} and 49 kJ×mol^{-1}.

The Transition States have C–Ru distances in between 1.9 and 2.3 Å. The distances between the activated H, and the Ru atom are 1.66 Å, they are sitting atop, except for CH_4 with a slightly longer H–Ru distance, and the H atom is sitting bridge. The activated C–H bonds are in between 1.57 and 1.7 Å. The H–C–Ru angle is 48° for the activated H atom and larger for the other H atoms.

If we compare the values found for the transition state barrier energies, one notes that the activation barrier decreases with the number of H atoms bonded to the C atoms for the decomposition of CH_4 to CH_2, with the exception of the last step, the CH decomposition that has the higher activation energy. We expect that the last barrier should change if computed with a larger unit cell size (lower coverage). The C atom is very strongly bonded to the surface and it affects the metal surface to the second or even third order Ru neighbors. For instance, the difference in energy of adsorption for C adsorbed in an hcp site in 2×2 versus 3×3 is about 56 kJ×mol^{-1} [24]. The consequence of such lateral interactions to transition states will be the subject

of a later chapter.

If we compare our results with those from Au et al. [21], we find good agreement for the transition state barrier for methane and CH_{ads} decomposition. We predict 85 kJ×mol^{-1} while Au et al. [21] reports 60 kJ×mol^{-1} for methane activation and in the case of CH_{ads} we find 108 kJ×mol^{-1} and Au et al. [21] gives 115 kJ×mol^{-1}. However, in the case of CH_2 and CH_3 the agreement is not so good. We predict 49 kJ×mol^{-1} and 16 kJ×mol^{-1} for CH_3 and CH_2 decomposition, while Au et al. [21] gets 85 kJ×mol^{-1} and 75 kJ×mol^{-1} respectively. In the case of CH_3, we studied the methyl adsorbed in an hcp site, which is a few kJ×mol^{-1} less stable than the other three-fold site (fcc), but this does not justify the differences. In the case of CH_2, the BOC formula (used bu Au et al.) seems to fail. If we compare the adsorption energies and the heights above the Ru surface for CH_x, we have a good agreement between our results and those from Au et al. [21] on the Ru(3,7) cluster.

In comparison to other metals with a higher d–valence electron occupation, such as Co, Pd or Ni, Ru appears to be much more reactive. The transition state energies for CH_x activation are smaller than on different metals for CH_4, CH_3, and CH_2 activation, but are quite high for CH.

The partial DOS diagrams (not shown) for the activated H atom, in the Transition States, are very similar and only the main outlines will be mentioned. A small mixture of the H_s atomic orbital with C_s atomic orbital, 3-4 times less than for a non-activated H atom, is found at $\approx -15, -16$ eV below the Fermi Level (FL). Around $-12, -10$ eV below FL, an intense peak occurs for the interaction of H_s atomic orbital with Ru: $d_{3z^2-r^2}$ and the C_p atomic orbital oriented in the direction of the reaction path of the H atom. Up to the FL, the contribution is rather small (interaction between H_s and the other d orbitals of Ru atom) and above the FL, a broad set of peaks for the antibondings σ^*_{C-H}. For the methane, the lower peak is due to the interaction of H_s with just a very small amount of Ru: $d_{3z^2-r^2}$ from the Ru below the methane but especially with the d_{xz}, d_{xy} orbitals from the two neighboring Ru atoms forming the bridge site. Therefore, this peak is a bit larger than for the other activated H atoms.

In the partial DOS diagram for the $d_{3z^2-r^2}$ orbital of Ru that interacts with H an extra peak appears due to the interaction with the s atomic orbital of H and the p atomic orbitals of the C atom in the direction of reaction path.

From these data, one can conclude that in the Transition State for methane, the interaction occurs in between the sp^3 hybrid orbital of the C atom from where the H is removed and the $d_{3z^2-r^2}$ orbital of the Ru atom. For the methane, the d_{xz}, d_{xy}

orbitals of the neighboring Ru atoms, part of the bridge site, play the main role.

The activation of the CH bond is mainly through the bonding part σ_{C-H} molecular orbital, since the antibonding σ^*_{C-H} molecular orbital is still above the FL.

The height of the activation barrier can be related to changes of the geometry of the adsorbed CH_x. As we just said, for CH_x (x = 3-1) the activation and breaking of the CH bond is made with this CH bond on top of a Ru atom via interactions between the σ_{C-H} and the $d_{3z^2-r^2}$ orbital of Ru. The participation of the $Ru_{s,p}$ orbitals are limited. The other d orbitals interact weakly because of the symmetry of the σ_{C-H}. The height of the activation barrier can be related to changes of the geometry of the adsorbed CH_x. The distortion of CH_x necessary to go from the intermediate to the TS will control this energy barrier.

If we consider the increasing barrier heights for CH_x (x = 1-3) one see that the CH_{2ads} has already a CH bond pointing in a direction of a Ru atom and that only small modifications of the geometry are needed in order to reach the TS. With CH_{3ads}, a limited tilting of a CH bond over a metal atom is necessary. The most unfavorable case occurs with CH_{ads} where the $C_{p_x\text{-}p_y}$ orbitals are involved in the bonding with the surface while the C_{p_z} orbital is associated to the CH bond.

If this CH bond is bent over a Ru atom then two phenomena explain the strong destabilization of the TS compared to the intermediate: first the σ_{C-H} is weakened as the overlap between H_s and C_{p_z} decreases, moreover no significant compensations are possible with C_{p_x} or C_{p_y} which are strongly involved in the C–surface bond. Secondly, as the H_s–C_{p_z} overlap decreases, C_{p_z} starts to interact with the $d_{3z^2-r^2}$ and d_{xz}, d_{yz} orbitals of Ru in a π like interaction (C and Ru are not in the same plane so the overlap with $d_{3z^2-r^2}$ is non-null) which is not strong enough for pushing up the π^* levels above the Fermi level. Consequently, the combined weakening of the CH bond and increase of the C_{p_z}–$Ru_{d_{3z^2-r^2}}$ repulsions lead to the highest activation barrier.

The dissociation of methane is different, but, can be related to the behavior of CH_x (x = 1-3). The TS does not have the activated CH bond on top of a metal atom but in an intermediate position in between the top and bridge sites. The methane molecule is not strongly bonded to the surface as the other species so, additionally to the distortion, displacement, and reorientation are easily possible. An activated CH bond on top of metal atom would lead either to the situation that methane has to be close to the surface with strong steric repulsions or at larger distance from the surface but with bigger distortion of the methane geometry. The current TS

is a compromise for getting the better activation of the CH bond and the lesser distortions and repulsions.

All the TS at lower coverage present similar geometries with the one at higher coverage, the main differences are in the energies.

§4.5 Conclusions

The preferred adsorption sites for H, C and CH_x (x = 1, 2, 3) on Ru(0001) are the three-fold sites (fcc or hcp). A comparison of the site position energies for an adsorbed species provides an estimate of activation energy for diffusion. These activation energies are of the order of $13-17$ kJ$\times$mol^{-1} for H and CH_3, 23 kJ$\times$mol^{-1} for CH_2 and $43-57$ kJ$\times$mol^{-1} for CH and C for the transition between the hcp and the fcc site. Hence, H, CH_3, and CH_2 should diffuse easily at room temperature while it will be more difficult for C and CH. Under Fischer–Tropsch conditions, all of the intermediates should be mobile.

CH is found to be the most stable species of the CH_x series on Ru(0001) in good agreement with the experimental results from Wu and Goodman [28,29]. They identified four surface species: CH_{ad}, $(CCH_2)_{ad}$, $(CCH_3)_{ad}$ and graphitic carbonaceous compounds on Ru(0001).

As compared with other metals with a higher d–valence electron occupation, such as Pd, Ru appears to be much more reactive. The CH cleavage energy is exothermic for all species, except for CH_{ad}.

The smallest activation energy is found for CH_2 in disagreement with previous BOC results from Au et al. [21]. However, the highest activation energy for CH decomposition is in good agreement with Au et al. [21]. For CH_3 our activation energy is much smaller than the predictions of Au et al. [21], but in the case of CH_4, we have a reasonable agreement with Au et al. [21] and disparity with experimental results of Jachimowski et al. [25] and Wu et al. [29]. A possible explanation for the disagreement between experiment and calculation, is the presence of steps on the Ru(0001) surface in the experiments. Such a case has been met before in theoretical study of the dissociation of N_2 on Ru(0001). Here the much lower barrier found in the experiment could be shown to actually be due to surface steps. [31] Very recent results from Luntz [32] with laser assisted associative dessorption of CH_4 from Ru(0001) indicate a minimal barrier height for CH_4 dissociation of 100 kJ$\times$mol^{-1}.

In the case of methane, the activated H atom is in a nonsymmetrical bridge

position while for the decomposition of methyl, methylene, and methine the activated H atom is atop a Ru atom. The activation energies depend on the easiness to bring a CH bond on top of a metal atom from the stable adsorbed geometry.

The calculated geometries of Transitions States are close to those reported previously on different metal surfaces.

From the analysis of partial DOS diagrams we can conclude that for the methane decomposition the sp^3 hybrid of C atom and the s orbital of H atom interact mainly with the $d_{3z^2-r^2}$ orbital of the first Ru atom and with the d_{xz}, d_{xy} orbital of the second Ru atom. In all other cases the main interactions is only in between the σ_{C-H} and the $d_{3z^2-r^2}$ orbital of the Ru atom.

Comparing with other metals with more d electrons, Ru is more reactive. The calculated activation energies for methane decomposition found on Ni or Co by Burghgraef et al. [16] or Kratzer et al. [20] are significantly higher than our results on Ru(0001).

Bibliography

[1] Jónsson, H.; Mills, G.; Jacobsen, W., *Enrico Fermi Summer School (Lenci '97) proceedings*, 1997

[2] M. Araki and V. Ponec, *J. Catal.* 44, (1976), 439

[3] P. Biloen and W. M. H. Sachtler, *Adv. Catal.*, 30, (1981), 165

[4] R. A. van Santen, A. de Koster and T. Koerts *Catal. Lett.*, 7, (1990), 1

[5] J. P. Hindermann, G. J. Hutchings and A. Kiennemann, *Catal. Rev. – Sci. Eng.*, 35, 2, (1993), 1

[6] A. Frennet, *Cat. Rev. – Sci. Eng.*, 10, (1974), 37

[7] J. -F. Paul and P. Sautet *J. Phys. Chem. B*, 102, (1998), 1578

[8] J. -F. Paul and P. Sautet *11th International Congress on Catalysis – 40th Anniversary Studies in Surface Science and Catalysis* 101, 1253

[9] J. -F. Paul and P. Sautet *Symposium Advances and Applications of Computational Chemical Modeling to Heterogeneous Catalysis Presented Before the Di-*

vision of Petroleum Chemistry, Inc. 213th National Meeting, American Chemical Society, San Francisco, CA, April 13–17, 1997

[10] J. Kua, W. A. Goddard III, *J. Phys. Chem. B*, 102, (1998), 9492

[11] J. Kua, W. A. Goddard III, *J. Phys. Chem. B*, 103, (1999), 2318

[12] R. M. Watwe, R. D. Cortight, J. K. Nørskov, J. A. Dumesic, *J. Phys. Chem. B*, 104, (2000), 2299

[13] H. Yang and J. L. Whitten *Surf. Sci.*, 289, (1993), 30

[14] H. Yang and J. L. Whitten *J. Chem. Phys.*, 91, 1, (1989), 126

[15] P. E. M. Siegbahn and I. Panas *Surf. Sci.*, 240, (1990), 37

[16] H. Burghgraef, A. P. J. Jansen and R. A. van Santen, *Surf. Sci.*, 324, (1995), 345

[17] H. Burghgraef, A. P. J. Jansen and R. A. van Santen, *Faraday Discuss.*, 96, (1993), 337

[18] H. Burghgraef, A. P. J. Jansen and R. A. van Santen, *Surf. Sci.*, 344, (1995), 149

[19] H. Burghgraef, A. P. J. Jansen and R. A. van Santen, *J. Chem. Phys.*, 101, 12, (1994), 11012

[20] P. Kratzer, B. Hammer and J. K. Nørskov *J. Chem. Phys.*, 105, 13, (1996), 5595

[21] C. -T. Au, C. -F. Ng and M. -S. Liao, *J. Catal.*, 185, (1999), 12

[22] I. M. Ciobîcă, F. Frechard, A. W. Kleyn, J. Hafner, R. A. van Santen, *J. Phys. Chem. B*, 104, (2000), 3364

[23] R. A. van Santen and M. Neurock, *Catal. Rev. – Sci. Eng.*, 37, 4, (1995), 557

[24] I. M. Ciobîcă, F. Frechard, R. A. van Santen, A. W. Kleyn, J. Hafner, *J. Chem. Phys. Lett.*, 311, (1999), 185

[25] T. A. Jachimowski, W. H. Weinberg, *Surf. Sci.*, 372, (1997), 145

[26] J. N. Carstens, A. T. Bell, *J. Catal.*, 161, (1996), 423

[27] L. Triguero, U. Wahlgren, L. G. M. Pettersson and P. Siegbahn, *Theor. Chim. Acta*, 94, (1996), 297

[28] M. -C. Wu and D. W. Goodman, *J. Am. Chem. Soc.*, 116, (1994), 1364

[29] M. -C. Wu and D. W. Goodman, *Surf. Sci. Lett.*, 306, (1994), L529

[30] P. Lenz–Solomun, M. -C. Wu, D. W. Goodman, *Catal. Lett.*, 25, (1994), 75

[31] S. Dahl, A. Logadottir, R. C. Egeberg, J. H. Larsen, I. Chorkendorff, E. Törnqvist, J. K. Nørskov, *Phys. Rev. Lett.*, 83, 9, (1999), 1814

[32] A. C. Luntz, *personal communication*

Chapter 5

C_2 adsorption and C_1 coadsorption on Ru(0001)

The relative energies of adsorbed C_2H_z (z = 0-6) species as well as the interaction energies between the adsorbed single C-atom CH_x and CH_y (x, y = 0-3) species on the Ruthenium (0001) surface have been computed with ab initio periodic calculations for 25% coverage. The surface intermediates are more stable than gas phase methane or ethane. Of all the surface species, CCH_2 appears to be the most stable, in agreement with reported experiments. The more stable surface species C_2H_z (z = 0-4) adsorb on three-fold sites, excepted ethyl, which prefers the bridge sites. Short-range lateral interactions between CH_x and CH_y (x, y = 0-3) species are also considered and are found to be repulsive.

§5.1 Introduction

The cleavage or formation of a C–C bond is a key reaction step for many catalytic processes in the petrochemical industry. Adsorbed CH_x (x = 0-3) and C_2H_z (z = 0-5) fragments formed on a catalytically reactive surface are believed to be important in several processes catalyzed by transition metals. First, we will be going to discuss the adsorbed C_2H_z (z = 6-0) species. Then the interaction between two adsorbed CH_x (x = 0-3) species, which share a metal atom, will be analyzed. Only the noticeable changes for the geometries (essentially bond lengths) of the adsorbed species will be presented. The calculated reference molecular parameters in the gas phase, in a 10 Å×10 Å×10 Å cell, are ethane (C–C = 1.53 Å, C–H = 1.10 Å), ethylene (C–C =

1.33 Å, C–H = 1.10 Å) and acetylene (C–C = 1.20 Å, C–H = 1.07 Å).

§5.2 (2×2) C$_2$H$_z$ species on Ru(0001) surface (z = 6-0)

Since we know~\cite{Ionel-1} that all CH$_x$ species adsorb on a hollow three-fold site on Ru(0001), those were the first initial positions for the calculation of the adsorption energies. However, in some cases we were forced to reconsider this approach.

§5.2.1   CH$_3$CH$_3$

Ethane, like methane, is not a reactive molecule as it physisorbes only on metal surfaces. Current pure DFT functionals are not able to describe accurately such weakly bound systems, like Van der Waals interactions. Therefore, for the physisorption of ethane according to VASP we get a gas phase ethane molecule repelled by the bare metal surface albeit that the repulsion is small (see Figure 5.1). Any attempt to put the molecule closer to the surface failed.

§5.2.2   CH$_2$CH$_3$

Adsorbed ethyl is a special case as it is the only species, which prefers a bridge site rather than a hollow three-fold sites although the difference in energy is quite small. The adsorption energy for the bridged symmetric ethyl is -153 kJ$\times$mol^{-1} and -158 kJ$\times$mol^{-1} for the bridged nonsymmetrical ethyl, see Figure 5.1, second column, the dashed lines. The nonsymmetrical bridged ethyl has one H atom from the CH$_2$ group activated with C–H = 1.15 Å and Ru–H = 1.99 Å. The Ru–C bonds are 2.47 (the Ru atom is also bound to H) and 2.19 Å. The H atom from CH$_3$ closest to the surface is only 2.46 Å away from a Ru atom but the corresponding C–H bond is not significantly disturbed. See Figure 5.2. The bridged symmetric ethyl has both H atoms from the CH$_2$ group activated with distances to the carbon of 1.14 Å and 2.05 Å to the metal atom. See Figure 5.2.

The Ru–C bonds are 2.48 and 2.19 Å for the symmetric adsorption mode and 2.48, 2.48, and 2.20 Å for the asymmetric one. Those results are different from those of Kua and Watwe on Pt(111), where ethyl prefers atop sites while on Ru the two most stable geometries show one Ru–C bond significantly shorter by 0.28 Å. The shift of adsorbed ethyl from atop for Pt(111) to the two fold site for Ru(0001) agrees
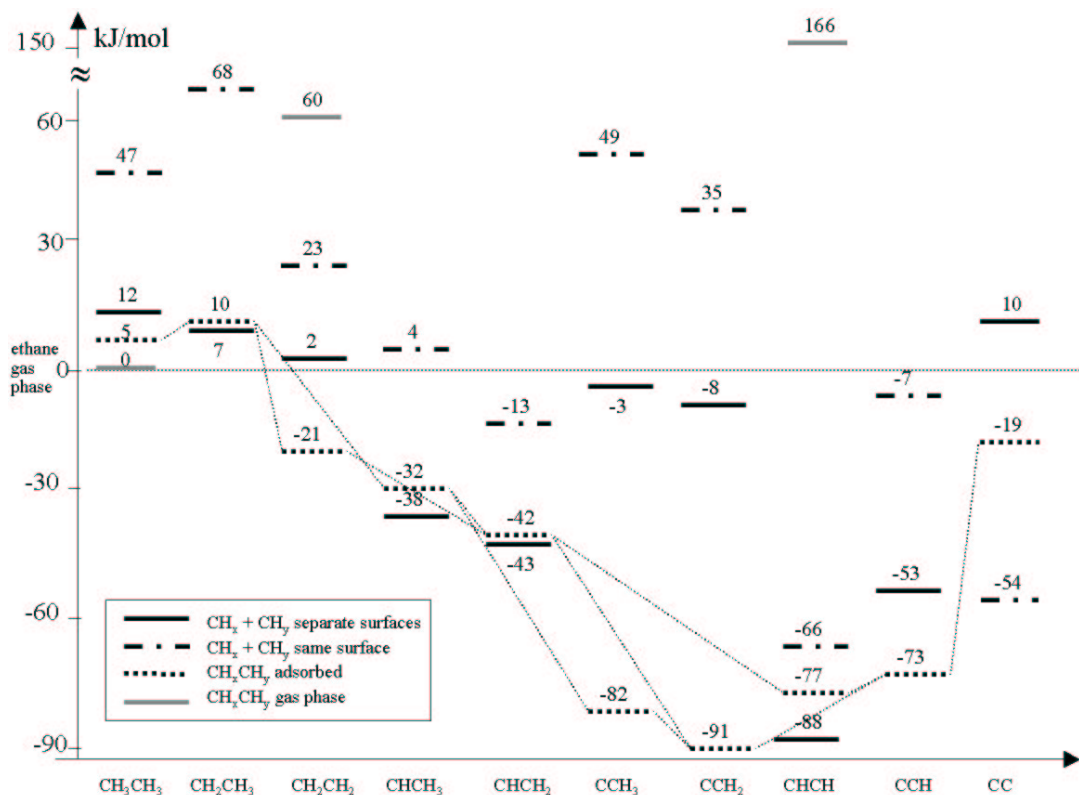
Figure 5.1: Adsorption energies of C_2H_z (z = 6-0), (in dashed lines) CH_x + CH_y (x, y = 3-0) with interactions (dashed lines, line-dot-line style) and without interactions (plain lines) on the Ru(0001) surface, in kJ×mol⁻¹. The reference line is the Ruthenium (0001) bare surface and gas phase ethane. Only the most stable configurations are shown in this diagram.

with earlier predictions that a decreasing occupation of the metal d orbitals tends to favor two fold or three-fold sites by reducing the Pauli repulsion [5].

§5.2.3 CHCH₃

Ethylidene adsorbs preferentially on hollow sites, as expected for Ru. The adsorption energy for the hcp site is -388 kJ×mol⁻¹, while for the fcc site is -369 kJ×mol⁻¹ with respect to bare Ru surface and gas phase ethylidene. The same adsorption energies are -25 and -6 kJ×mol⁻¹ with respect to a methyl species adsorbed in a fcc
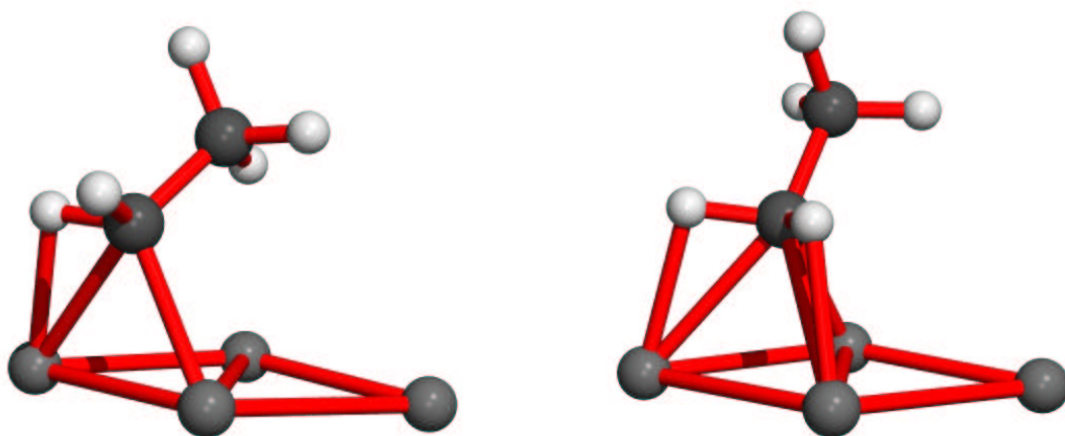
Figure 5.2: Asymmetric and symmetric adsorbed ethyl on the bridge site. The H atoms doesn't have a bond with the surface. It is just a way to show which H atoms are activated.

site and CH in an hcp site (see Figure 5.1, fourth column, the dashed lines). Kua and Watwe found a bridge site for the adsorption on Pt(111).

The geometries of adsorbed CH$_3$CH are very similar, the C–Ru bond lengths are 2.22 (2.25), 2.10 (2.10) and 2.09 (2.10) Å for the hcp (fcc) site.

The C–H bond of the CH group is activated because the carbon interacts with 3 Ru atoms and therefore it brings the H atom close to a Ru atom with Ru–H distances of 1.78 Å (hcp) and 1.84 Å (fcc). The resulting C–H bond length is 1.23 (1.21) Å for the hcp (fcc) site, see Figure 5.3.

§5.2.4   CCH$_3$

From the C$_2$H$_z$ species, ethylidyne is one of the most stable on the Ru(0001) surface like on Pt where ethylidyne is known to be a poison [2–4]. With respect to the bare Ru surface and ethylidyne in gas phase it adsorbs on hollow sites with the following adsorption energies: -558 kJ×mol^{-1} for the hcp site and -537 kJ×mol^{-1} for the fcc site. With respect to CH$_3$ adsorbed in a fcc site and adsorbed C in hcp site, the same adsorption energies become -79 kJ×mol^{-1}, respectively -58 kJ×mol^{-1} (see Figure 5.1, fifth column, the dashed lines).

The geometry of this species is symmetric with the C atom above the triangle
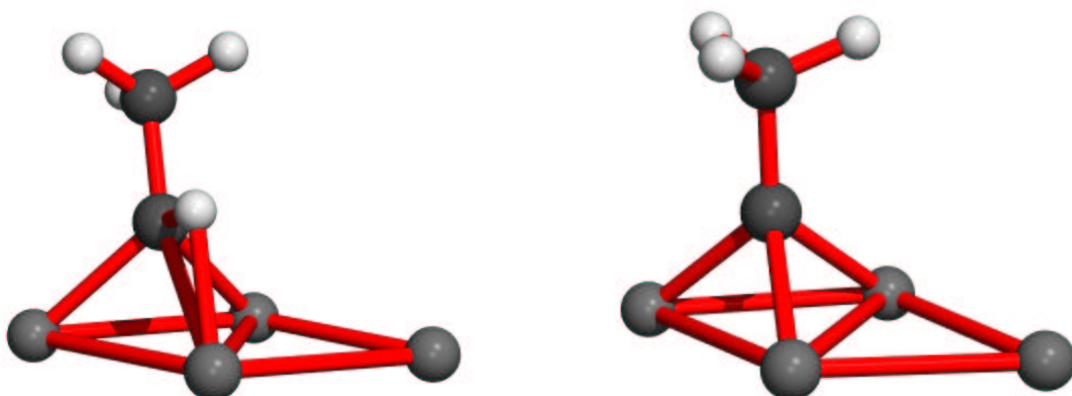
Figure 5.3: Adsorbed ethylidene and ethylidyne on the hcp site.

formed by the three Ru atoms forming the three-fold hollow site. The CH_3 group is on top of the C atom.

The geometries of CH_3C shows C–C bonds slightly shorter than for ethane with 1.50 Å (hcp) and 1.49 Å (fcc). The C–Ru bond lengths are 2.05 Å for CH_3C hcp and 2.06, 2.06, 2.03 Å for CH_3C fcc respectively (for the fcc site the bonds are not equal because the cell does not have tertiary axe), see Figure 5.3.

§5.2.5 CH_2CH_2

Ethylene is known to adsorb in two ways, the di-σ adsorption mode and the π adsorption mode. The di-σ adsorption mode has the ethylene bridging two metal atoms while the π adsorption mode has the center of ethylene above atop site. Besides those two classical adsorption modes, we found an other one with the center of mass above an hcp site, with one CH_2 in a tilted hcp configuration and the other CH_2 group in a tilted top site.

With respect to the bare metal surface and gas phase ethylene the adsorption energies are −81 kJ×mol⁻¹ for the π, −53 kJ×mol⁻¹ for di-σ and −80 kJ×mol⁻¹ for the asymmetric adsorption mode. The same adsorption energies calculated with respect to two adsorbed CH_2 groups are −23, +4.6 and −22 kJ×mol⁻¹ (see Figure 5.1, third column, the dashed lines) respectively. Kua and Watwe found that on Pt(111) ethylene prefers the di-σ adsorption mode, rather than the π one.

The fact that the π adsorption mode is favorable on Ru(0001) is in good agree-

ment with earlier results which claimed that di-σ adsorption mode is becoming less stable when there are less d-electrons available in the metal, so the π adsorption mode is the preferred one [6].

The C–C bond lengths are 1.47 Å for the di-σ, 1.43 Å for the π and 1.44 Å for the asymmetric adsorption mode. These values are in between those met for ethane (1.53 Å) and ethylene (1.33 Å) in the gas phase; moreover, the adsorbates are not planar anymore indicating that the carbon atoms are not longer sp^2. The dihedral angles formed by H–C–C–H with the H atoms on the same carbon, are 132° for the di-σ, 146° and 147° for π and 144° and 136° for the asymmetric geometry (the Ru–C–C plane is slightly tilted with 9.8°).

The C–Ru bond lengths are 2.21 and 2.20 Å for π, while for di-σ we have a bond of 2.20 Å and two longer bonds of 2.96 and 3.07 Å for each CH$_2$. The asymmetric adsorption mode has one C–Ru bond of 2.16 Å for one CH$_2$ group, while the other CH$_2$ group has three bonds of 2.58, 2.58 and 2.21 Å. See Figure 5.4 for the π adsorption mode, the di-σ adsorption mode and for the asymmetric adsorption mode.
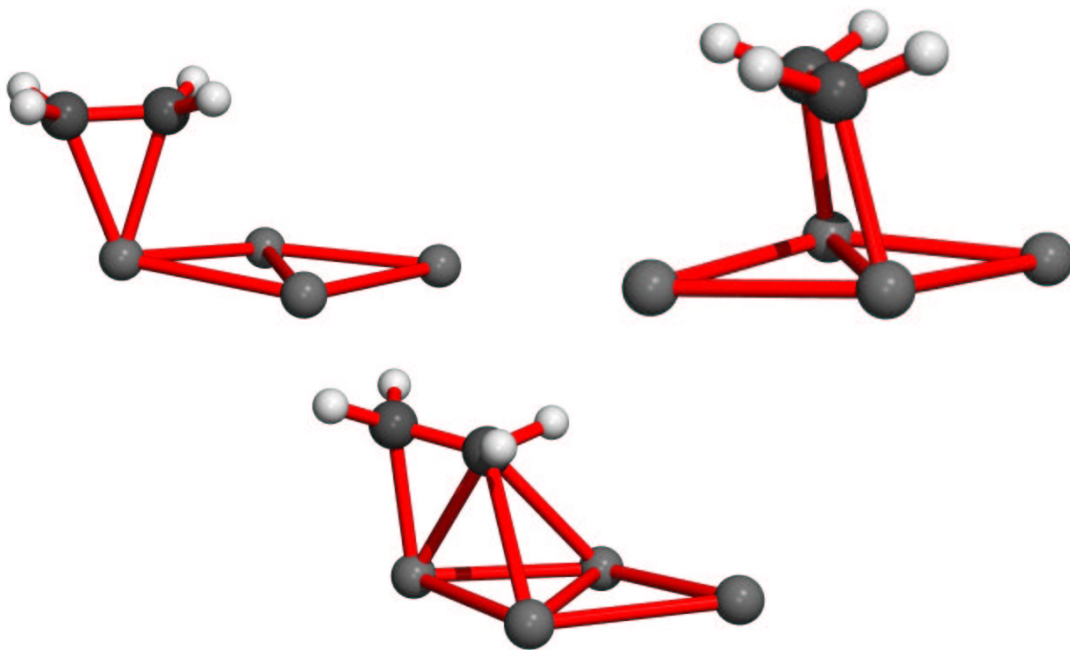
Figure 5.4: Adsorbed ethylene on the π, di-σ and on the asymmetric mode.

§5.2.6   CHCH$_2$

The vinyl group adsorbs in a similar way as the asymmetric ethylidyne; the C–C bond is more inclined, both C atoms interacting with the metal atoms. Two adsorption sites were investigated with the center of mass above either an hcp site or a fcc site. For both sites, the CH group is in a tilted bridge position and the CH$_2$ group is also tilted but atop. Kua and Watwe found a similar geometry for vinyl adsorbed on Pt(111). The adsorption energies are −306 kJ×mol^{-1} for hcp and −293 kJ×mol^{-1} for fcc compared to bare Ru surface and gas phase vinyl. With respect to adsorbed CH and adsorbed CH$_2$, the adsorption energies are +1.3 kJ×mol^{-1} +14.8 kJ×mol^{-1}, respectively (see Figure 5.1, sixth column, the dashed lines).

A C–C bond of 1.43 Å for the hcp site and 1.42 Å for the fcc site describe the geometry of adsorbed vinyl. Like for ethylene the C atoms are closer to sp^3 hybridization than sp^2. The C$_{CH}$–H is activated, the length of the bond being 1.18 Å and 1.14 Å for the hcp site and the fcc site respectively. The C$_{CH_2}$–Ru bond lengths are 2.22 Å for the hcp site and 2.25 Å for the fcc site while the C$_{CH}$–Ru bond lengths are 2.05 and 2.21 Å for the hcp site and 2.06 and 2.34 Å for the fcc site, see Figure 5.5. The main difference with ethylidene is the bonding of the C$_{CH_2}$ group with the surface.
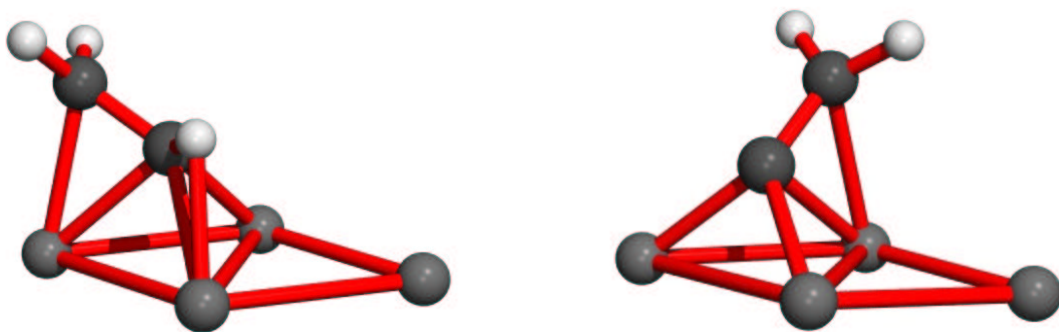
Figure 5.5: Adsorbed vinyl and vinylidene on the hcp site.

§5.2.7   CCH$_2$

Vinylidene is the most stable species (from the C$_2$H$_z$ series) on the Ru(0001) surface. CH$_2$C has a very different adsorption geometry from CH$_3$C. The C atom

is above a three-fold hollow site and CH$_2$ is atop site. The C–C is neither parallel nor perpendicular to the surface, the angle of inclination is about 49°. This geometry is different from the geometry found by Kua and Watwe on Pt(111) with a perpendicular adsorption mode for vinylidene, see Figure 5.6
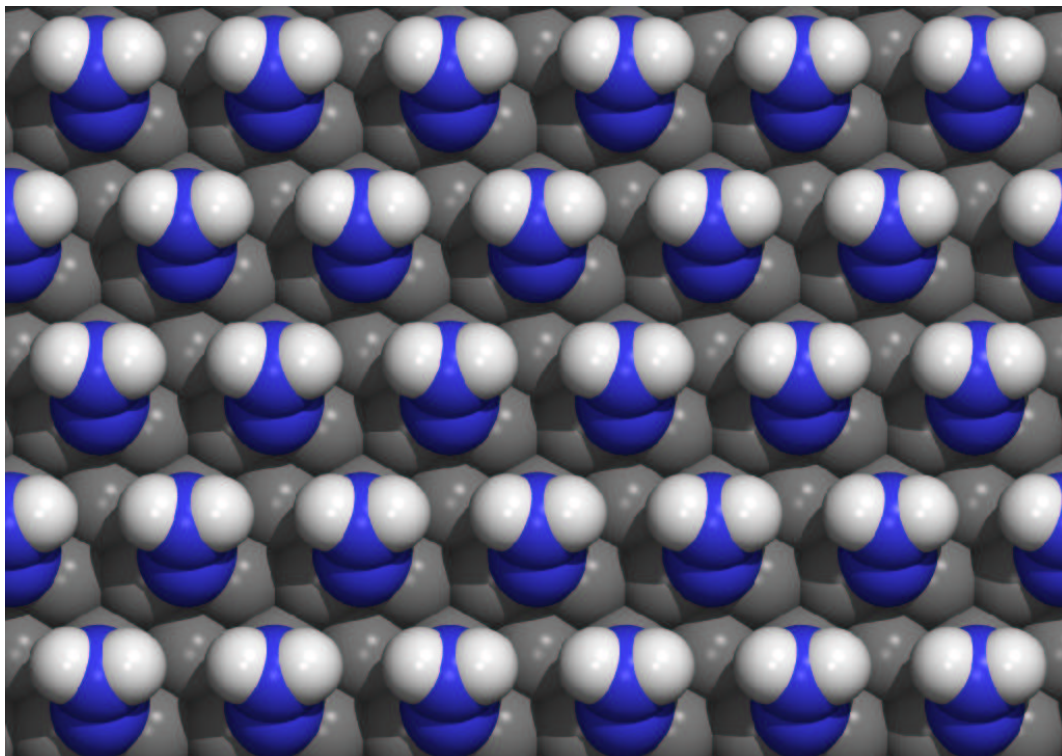
Figure 5.6: Top view of the most stable C$_2$H$_z$ species: CCH$_2$ (vinylidene), adsorbed on the Ru(0001) surface.

With respect to bare metal surface and CCH$_2$ species in gas phase, the adsorption energies are -448 kJ$\times$mol^{-1} for the adsorption on the hcp site and -416 kJ$\times$mol^{-1} for the adsorption on the fcc site. The adsorption energies with respect to adsorbed C and adsorbed CH$_2$ are -83 (hcp) and -51 kJ$\times$mol^{-1} (fcc) (see Figure 5.1, seventh column, the dashed lines).

The C–C bond lengths are 1.40 Å (hcp) and 1.39 Å (fcc), the C–Ru bond lengths are 2.01, 2.03 and 2.11 Å (hcp) and 2.03, 2.02 and 2.15 Å (fcc) while the C$_{CH_2}$–H are 2.29 Å (hcp) and 2.23 Å (fcc). Contrary to the CH$_3$-CH$_z$ (z = 0-2), the adsorbed CH$_2$-CH$_z$ species (z = 0-2) display the two carbon atoms bound to the surface and therefore the C–C bond is parallel or with an angle to the surface inferior to 45°, see

Figure 5.5.

§5.2.8   CHCH

Acetylene adsorbs only with the C–C parallel to the surface. Three adsorption modes are observed: the center of mass is above a bridge site, with one CH group above a fcc site and the other CH group above an hcp site (hcp–fcc); both CH groups are in bridge positions (a sort of tilted di-σ so that the second π orbital is interacting with an other metal atom) and the center of mass is above an hcp site (di–bridge); we were also able to identify an adsorption site with the center of mass atop site (related to π bonding), but this site corresponds to a meta stable situation. The adsorption energies are -241 kJ×mol^{-1} (hcp–fcc), -243 kJ×mol^{-1} (di–bridge) and -106 kJ×mol^{-1} (atop), with respect to bare Ru surface and gas phase acetylene. Compared to two adsorbed CH groups, the adsorption energies are 13 kJ×mol^{-1}, 11 kJ×mol^{-1} and 149 kJ×mol^{-1} respectively (see Figure 5.1, eighth column, the dashed lines).

The C–C bond lengths are 1.42 Å for the hcp–fcc site, 1.39 Å for the bridge–bridge site and 1.30 for the π adsorption mode. The C–H bond lengths are 1.10 Å for hcp–fcc and di–bridge sites while for the top both C–H bond lengths are 1.08 Å. These values slightly differ from the 1.07 Å found for gas phase acetylene and combined with distortions from the linear geometry it points out that the carbons have lost the sp hybridization. The C–Ru bond lengths are 2.16, 2.16, and 2.20 Å for the CH in the hcp site and 2.22, 2.22 and 2.16 Å for the CH in the fcc site. For the bridge–bridge adsorption, each CH has the following C–Ru bond lengths: 2.07, 2.84, and 2.21 Å. The atop adsorption site has 2.08 Å for one CH and 2.07 Å for the other CH. See Figure 5.7 for the hcp–fcc adsorption mode and for the bridge–bridge adsorption mode.

§5.2.9   CCH

The ethynyl radical may adsorb on the Ru(0001) surface with the center of mass above an hcp site, above a fcc site or above atop site. For the hcp site, the final configuration has the C–C bond almost parallel with the Ru surface (14° with the surface) resulting in an hcp–fcc configuration, while the other adsorption sites have the C–C perpendicular with the Ru surface. The adsorption energies are -546 kJ×mol^{-1} (hcp–fcc), -436 kJ×mol^{-1} (fcc) and -383 kJ×mol^{-1} (atop) with respect to gas phase
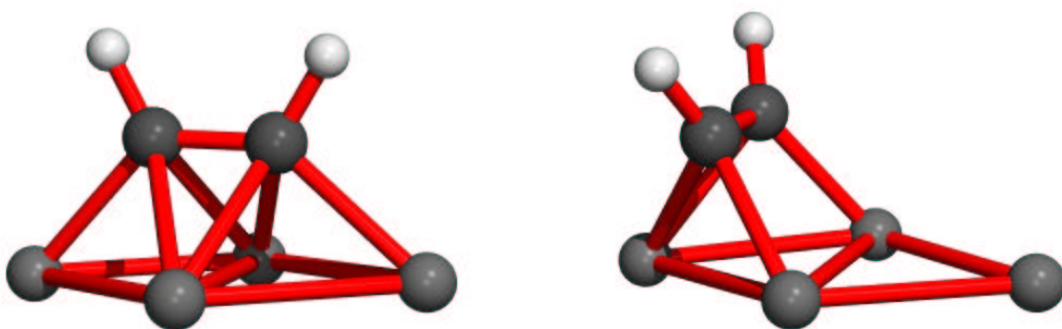
Figure 5.7: Adsorbed acetylene on the hcp–fcc site (tetra-σ) and on the bridge–bridge site (di-σ-π).

CCH and bare Ru surface. The adsorption energies are -20 kJ$\times$mol^{-1}, 89 kJ$\times$mol^{-1} and 143 kJ$\times$mol^{-1} respectively compared to adsorbed C and CH (see Figure 5.1, ninth column, the dashed lines).

The–C bond lengths are 1.38 Å for the hcp–fcc site, 1.25 Å for the fcc and 1.23 Å for the atop site. The C–H bond lengths are 1.09 (hcp–fcc), 1.07 (fcc), and 1.07 Å (atop), if the adsorbate remains linear (C sp) the C–H bond stays at 1.07 Å and close to 1.20 Å for the C–C bond. The C–Ru bond lengths are 1.97, 2.10 and 2.10 Å for the hcp–fcc site, 2.17, 2.18 and 2.18 Å for the fcc site, while for the atop site the C–Ru bond lengths are 1.98 Å. Only the hcp adsorption site has an interaction between the CH and the metal surface. The C$_{CH}$–Ru bond lengths are 2.22, 2.22, and 2.35 Å. This configuration is in between the configuration of adsorbed CCH$_2$ and adsorbed CC, see Figure 5.8.

§5.2.10 CC

Dicarbon can adsorb in two ways, parallel or perpendicular with the surface. Only one adsorption site was found for the perpendicular adsorption with the CC above a fcc site. The adsorption energy is -725 kJ$\times$mol^{-1} with respect to bare metal surface and gas phase CC species and 157 kJ$\times$mol^{-1} with respect to two adsorbed C atoms (see Figure 5.1, tenth column, the dashed lines).

The C–C bond length for this adsorption mode is 1.31 Å and the C–Ru bond lengths are 2.11, 2.10 and 2.11 Å.
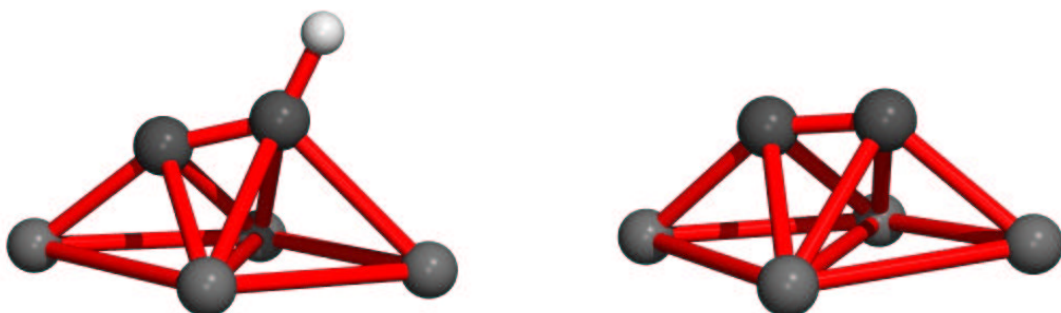
Figure 5.8: Adsorbed CCH on the hcp site and adsorbed dicarbon on the hcp–fcc site.

For parallel C–C to the surface we found that this species can adsorb with both C on bridge sites and the center of mass above an hcp site or with on C above a fcc site and the other C above an hcp site, the center of mass being above a bridge site. The adsorption energies are -644 kJ×mol^{-1}, respectively -725 kJ×mol^{-1} with respect to bare metal surface and gas phase CC species. With respect to two adsorbed C atoms the same adsorption energies are 53 kJ×mol^{-1} and -29 kJ×mol^{-1} respectively (see Figure 5.1, tenth column, the dashed lines).

For the bridge–bridge adsorption mode the C–C bond length is 1.35 Å, while for the hcp–fcc adsorption mode the C–C bond length is 1.36 Å. The C–Ru bond lengths are 1.96, 2.20, and 2.11 Å for both C atoms in the case of the bridge–bridge adsorption mode. For the hcp–fcc adsorption mode the C–Ru bond lengths are 2.04, 2.14 and 2.14 Å for the C sitting in the hcp site and 2.17, 2.17 and 2.06 Å for the C sitting in the fcc site, see Figure 5.8.

§5.3   Coadsorption of CH$_x$ and CH$_y$ species on the Ru(0001) surface, (x, y = 3-0)

We have reported earlier calculations for the interactions between CH$_x$ and H species [1]. In this section, we analyze the interaction between two different CH$_x$ species. This will allow us to calculate the lateral interaction between two species in *all* different configurations [8] as well as to determine the reaction path suitable for

the Fischer Tropsch mechanism of chain growth [9].

§5.3.1   CH$_3$ + CH$_3$

Two methyl groups are difficult to accommodate in a 2 × 2 unit cell (50% coverage). We started the simulations with several initial structures. The converged situation corresponds to a structure where one CH$_3$ is on the fcc site and the other one is in an atop site. In an other local minimum, both CH$_3$ species are in bridge sites. The adsorption energies with respect to two methyl species in the gas phase and bare metal surface are -363 kJ×mol^{-1}, respectively -355 kJ×mol^{-1}. With respect to two adsorbed CH$_3$ species at infinite distance, the adsorption energies are 36 kJ×mol^{-1}, respectively 42 kJ×mol^{-1}. Two close CH$_3$ groups repel each other. For the bridge–bridge situation the adsorption energy is 98 kJ×mol^{-1} with respect to two methyl species in the gas phase and bare metal surface, and 300 kJ×mol^{-1} with respect to two adsorbed CH$_3$ species (see Figure 5.1, first column, the line-dot-line lines). The geometry of those CH$_3$ species is described as follows. The C–H bond lengths are 1.12 Å for all C–H bonds in the case of one CH$_3$ in the three-fold hollow site and one CH$_3$ atop, and 1.09, 1.10 and 1.15 Å for one CH$_3$ and 1.09, 1.10 and 1.14 Å for the other CH$_3$ in the case of bridge–bridge adsorption. The C–Ru bond lengths are 2.28, 2.31, and 2.28 Å for the CH$_3$ in the fcc site, 2.29, 2.29, and 2.29 Å in the hcp site. For the fcc–top adsorption the C$_{methyl-top}$–Ru bond length is 2.16 Å, and for the hcp–top adsorption the C$_{methyl-top}$–Ru bond length is 2.17 Å. For the bridge–bridge adsorption, the C–Ru bond lengths are 2.30 and 2.22 Å for one CH$_3$ and 2.20 and 2.34 Å for the other CH$_3$.

§5.3.2   CH$_3$ + CH$_2$

Optimization of the structures with one CH$_3$ species and one CH$_2$ species on a 2 × 2 unit cell leads to a structure with the CH$_3$ in a tilted atop site, while the adsorbed CH$_2$ remains in a hollow site. In addition, a bridge–bridge configuration is found. The adsorption energies are -541 kJ×mol^{-1} for the CH$_3$ atop and CH$_2$ fcc, -546 kJ×mol^{-1} for the CH$_3$ atop and CH$_2$ hcp, respectively -530 kJ×mol^{-1} for the CH$_3$ bridge and CH$_2$ bridge with respect to gas phase methyl and methylene radical and bare metal surface. With respect to adsorbed CH$_3$ and adsorbed CH$_2$, the same adsorption energies are 67 kJ×mol^{-1}, 62 kJ×mol^{-1} and respectively 79 kJ×mol^{-1} (see Figure 5.1, second column, the line-dot-line lines). The C$_{CH_3}$–H distances are 1.10 Å

for hcp–atop and fcc–atop adsorption while for the bridge–bridge adsorption the distances are 1.10, 1.10, and 1.14 Å. The C$_{CH_2}$–H distances are 1.10 and 1.18 Å for the hcp–atop adsorption, 1.10 and 1.16 Å for the fcc–atop adsorption and 1.10 and 1.10 Å for the bridge–bridge adsorption. The C$_{CH_3}$–Ru bond length is 2.20 Å for hcp–atop adsorption and 2.19 Å for fcc–atop adsorption. The C$_{CH_2}$–Ru bond lengths are 2.10, 2.07, and 2.16 Å for hcp–atop adsorption and 2.08, 2.08 and 2.20 Å for fcc–atop adsorption. The C$_{CH_3}$–Ru bond lengths for the bridge–bridge adsorption are 2.19 and 2.38 Å and the C$_{CH_2}$–Ru bond lengths are 2.06 and 2.12 Å for the same adsorption mode.

§5.3.3   CH$_3$ + CH

The system composed of an adsorbed CH and a CH$_3$ species is very interesting because species with different kind of strong lateral interaction (through the surface and steric repulsion) are mixed. Four cases are discussed. If CH and CH$_3$ are in different kind of sites (CH hcp + CH$_3$ fcc or CH fcc + CH$_3$ hcp), the differences between the initial guess and the optimized structures are minimal. If CH and CH$_3$ are in the same kind of sites (CH hcp + CH$_3$ hcp or CH fcc + CH$_3$ fcc), then a shift of CH$_3$ from the hollow site to the bridge or tilted bridge positions is observed. The adsorption energies are -792 kJ×mol^{-1} for CH hcp + CH$_3$ fcc, -764 kJ×mol^{-1} for CH fcc + CH$_3$ hcp, -798 kJ×mol^{-1} for CH hcp + CH$_3$ bridge and -769 kJ×mol^{-1} for CH fcc + CH$_3$ bridge, with respect to bare Ru surface and CH and methyl in gas phase. The same adsorption energies with respect to adsorbed CH and adsorbed CH$_3$ are 49, 76, 43, and respectively 72 kJ×mol^{-1} (see Figure 5.1, fourth column, the line-dot-line lines). The C$_{CH_3}$–H bond lengths are 1.10 Å for the CH hcp + CH$_3$ fcc, 1.10 Å for the CH fcc + CH$_3$ hcp, 1.10, 1.13, 1.10 Å for CH hcp + CH$_3$ bridge and 1.10, 1.11, 1.10 Å for CH fcc + CH$_3$ bridge. The C$_{CH}$–H bond lengths are 1.10 Å for the CH hcp + CH$_3$ fcc, 1.11 Å for the CH fcc + CH$_3$ hcp, 1.10 Å for CH hcp + CH$_3$ bridge and 1.10 Å for CH fcc + CH$_3$ bridge. The C$_{CH_3}$–Ru distances are 2.39 Å for the CH hcp + CH$_3$ fcc, 2.37 Å for the CH fcc + CH$_3$ hcp, 2.42, 2.20 Å for CH hcp + CH$_3$ bridge and 2.30, 2.32 Å for CH fcc + CH$_3$ bridge. The C$_{CH}$–Ru distances are 2.01 Å for the CH hcp + CH$_3$ fcc, 2.02 Å for the CH fcc + CH$_3$ hcp, 1.99, 2.05, 2.03 Å for CH hcp + CH$_3$ bridge and 1.99, 2.04, 2.03 Å for CH fcc + CH$_3$ bridge, see Figure 5.9.
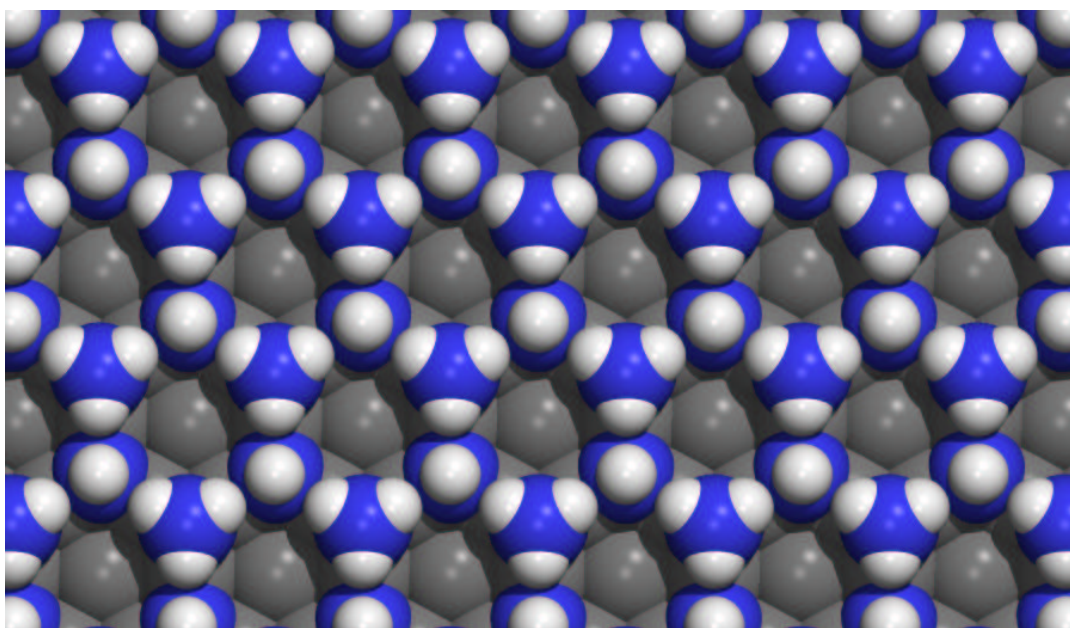
Figure 5.9: Top view of coadsorbed CH with CH$_3$. CH is in hcp three-fold hollow site, while CH$_3$ is in fcc three-fold hollow site.

§5.3.4   CH$_3$ + C

The adsorbed C atom is the only species from the CH$_x$ series that will not push the CH$_3$ out of its hollow site. The adsorption energies are -823 kJ$\times$mol^{-1} for C hcp + CH$_3$ fcc, -818 kJ$\times$mol^{-1} for C hcp + CH$_3$ fcc, -779 kJ$\times$mol^{-1} for C fcc + CH$_3$ fcc and -776 kJ$\times$mol^{-1} for C fcc + CH$_3$ hcp. We calculated also C hcp + CH$_3$ top and this is more stable situation, with a adsorption energies of 835 kJ$\times$mol^{-1}, all with respect to gas phase C, gas phase methyl and bare metal surface. The same adsorption energies with respect to adsorbed C and adsorbed CH$_3$ are 64, 69, 108, 112, and respectively 53 kJ$\times$mol^{-1} (see Figure 5.1, fifth column, the line-dot-line lines). The C–H bond length are 1.10, 1.10, 1.10 Å for C hcp + CH$_3$ fcc, 1.12, 1.10, 1.10 Å for C hcp + CH$_3$ hcp, 1.10, 1.10, 1.09 Å for C hcp + CH$_3$ atop, 1.10, 1.12, 1.10 Å for C fcc + CH$_3$ fcc, 1.10, 1.10, 1.10 Å for C fcc + CH$_3$ hcp. The C$_{CH_3}$–Ru distances are 2.41, 2.41, 2.41 Å for C hcp + CH$_3$ fcc, 2.34, 2.43, 2.54 Å for C hcp + CH$_3$ hcp, 2.17 Å for C hcp + CH$_3$ atop, 2.35, 2.51, 2.35 Å for C fcc + CH$_3$ fcc, 2.42, 2.42, 2.42 Å for C fcc + CH$_3$ hcp. The C$_C$–Ru distances are 1.93, 1.93, 1.93 Å for C hcp + CH$_3$ fcc, 1.88, 1.96, 1.96 Å for C hcp + CH$_3$ hcp, 1.93, 1.95, 1.93 Å for C hcp + CH$_3$ atop, 1.97, 1.87, 1.97 Å for C fcc + CH$_3$ fcc, 1.94, 1.94, 1.94 Å for C

fcc + CH$_3$ hcp.

§5.3.5   CH$_2$ + CH$_2$

Two methylene species in a 2×2 unit cell (50% coverage) can adsorb in three configurations. The adsorption energies with respect to two gas phase methylene groups and the bare metal surface are -798 kJ$\times$mol^{-1} for both methylene in hcp sites, -792 kJ$\times$mol^{-1} for both methylene in fcc sites and -761 kJ$\times$mol^{-1} for the situation when one methylene is in an hcp site and one in a fcc site. The same adsorption energies with respect to two adsorbed CH$_2$ species are 21, 58, and respectively 27 kJ$\times$mol^{-1} (see Figure 5.1, third column, the line-dot-line lines). The C–H bond lengths are 1.10, 1.18 Å for both CH$_2$ from hcp–hcp interaction, 1.10, 1.17 Å for both CH$_2$ from fcc–fcc interaction, 1.12, 1.20 Å for the CH$_2$ in fcc site and 1.10, 1.17 Å for the CH$_2$ in the hcp site for the mix situation. The C–Ru bond lengths are 2.06, 2.06, 2.25 Å for both CH$_2$ from hcp–hcp interaction, 2.06, 2.60o, 2.29 Å for both CH$_2$ from fcc–fcc interaction, 2.15, 1.05, 2.13 Å for the CH$_2$ in fcc site and 2.28, 2.28, 2.08 Å for the CH$_2$ in the hcp site for the mix situation.

§5.3.6   CH$_2$ + CH

CH and CH$_2$ groups can adsorb in all four configurations hcp–hcp, hcp–fcc, fcc–hcp, and fcc–fcc. In all those configurations, adsorbed CH$_2$ is not symmetric. The adsorption energies with respect to CH$_2$ gas phase, CH gas phase and Ru bare surface are 1010 kJ$\times$mol^{-1} for CH hcp + CH$_2$ hcp, 1022 kJ$\times$mol^{-1} for CH hcp + CH$_2$ fcc, 1011 kJ$\times$mol^{-1} for CH fcc + CH$_2$ hcp and 1009 kJ$\times$mol^{-1} for CH fcc + CH$_2$ fcc. With respect to adsorbed CH$_2$ and adsorbed CH are 42, 30, 41, 42 kJ$\times$mol^{-1}, respectively (see Figure 5.1, sixth column, the line-dot-line lines). The C$_{CH_2}$–H distances are 1.10, 1.18 Å for both species in hcp sites, 1.10, 1.15 Å for both species in fcc sites, 1.10, 1.17 Å for CH hcp + CH$_2$ fcc, 1.10, 1.19 Å for CH fcc + CH$_2$ hcp. All the C$_{CH}$–H distances are 1.10 Å. The C$_{CH_2}$–Ru bonds length are 2.14, 2.12, 2.04 Å for both species in hcp sites, 2.07, 2.07, 2.40 Å for both species in fcc sites, 2.28, 2.08, 2.08 Å for CH hcp + CH$_2$ fcc, 2.08, 2.26, 2.08 Å for CH fcc + CH$_2$ hcp. The C$_{CH}$–H bonds length are 2.00, 2.04, 2.01 Å for both species in hcp sites, 2.03, 2.03, 2.02 Å for both species in fcc sites, 2.02, 2.02, 2.07 Å for CH hcp + CH$_2$ fcc, 2.02, 2.02, 2.07 Å for CH fcc +CH$_2$ hcp.

§5.3.7   CH$_2$ + C

C and CH$_2$ species can also adsorb in all four configurations as CH and CH$_2$. The adsorption energies with respect to CH$_2$ gas phase, C gas phase and Ru bare surface are -1055 kJ×mol^{-1} for C hcp + CH$_2$ hcp, -1047 kJ×mol^{-1} for C hcp + CH$_2$ fcc, -1011 kJ×mol^{-1} for C fcc + CH$_2$ hcp and -989 kJ×mol^{-1} for C fcc + CH$_2$ fcc. With respect to adsorbed CH$_2$ and adsorbed C are 42, 51, 86, 109 kJ×mol^{-1}, respectively (see Figure 5.1, seventh column, the line-dot-line lines). The C–H bonds length are 1.10, 1.18 Å for the hcp–hcp combination, 1.10, 1.16 Å for the fcc–fcc, 1.10, 1.10 Å for C hcp + CH$_2$ fcc, 1.10, 1.10 Å for C fcc + CH$_2$ hcp. The C$_{CH_2}$–Ru distances are 2.25, 2.06, 2.06 Å for the hcp–hcp interaction, 2.06, 2.07, 2.31 Å for the fcc–fcc combination, 2.09, 2.09 Å for the C hcp + CH$_2$ fcc (CH$_2$ migrate to bridge), 2.26, 2.21, 2.06 Å for C fcc + CH$_2$ hcp. The other C–Ru bond distances are 1.98, 1.98, 1.88 Å for the hcp–hcp interaction, 1.87, 2.07, 1.94 for the fcc–fcc, 1.99, 1.87, 1.98 Å for C hcp + CH$_2$ fcc, 1.92, 1.97, 1.93 Å for C fcc + CH$_2$ hcp.

§5.3.8   CH + CH

Two CH groups can adsorb in three different ways in three-fold hollow sites in a 2 × 2 structure (50% coverage): hcp–hcp, hcp–fcc, and fcc–fcc. The adsorption energies with respect to two CH gas phase and Ru bare surface are -1261 kJ×mol^{-1} for both CH in hcp site, -1224 kJ×mol^{-1} for both CH in fcc sites and -1250 kJ×mol^{-1} for one CH in hcp site and the other one in fcc site. With respect to two adsorbed CH groups, the same adsorption energies are 23, 60, and 34 kJ×mol^{-1}, respectively (see Figure 5.1, eighth column, the line-dot-line lines). The C–H bond length is 1.10 Å for both CH groups that are adsorbed both on hcp sites, 1.10 Å for both CH groups that are adsorbed both on fcc sites and 1.10 Å for the CH in the hcp site and 1.10 Å for the CH in the fcc site for the mix case. The C–Ru bond lengths are 2.02, 2.03, 2.03 Å for both CH groups that are both adsorbed on hcp sites, 2.03, 2.03, 2.04 Å for both CH groups that are both adsorbed on fcc sites and 2.06, 2.06, 2.06 Å for the CH in hcp site and 2.05, 2.05, 2.05 Å for the CH in fcc site for the mix case.

§5.3.9   CH + C

One CH and one C species behave similar as two CH species. The adsorption energies with respect to CH gas phase, C gas phase and Ru bare surface are -1284 kJ×mol^{-1} for C hcp + CH hcp, -1274 kJ×mol^{-1} for C hcp + CH fcc,

−1244 kJ×mol^{-1} for C fcc + CH hcp and −1229 kJ×mol^{-1} for C fcc + CH fcc. With respect to two adsorbed CH groups, the same adsorption energies are 46, 56, 87, and 101 kJ×mol^{-1}, respectively (see Figure 5.1, ninth column, the line-dot-line lines). The C$_{CH}$–H bond length is 1.10 Å for hcp–hcp, 1.09 Å for fcc–fcc, 1.08 Å for C hcp + CH fcc, and 1.09 Å for C fcc + CH hcp. The C$_{CH}$–Ru bond length are 2.02, 2.02, 2.00 Å for hcp–hcp, 2.06, 2.06, 1.97 Å for fcc–fcc, 2.01, 2.01, 2.01 Å for C hcp + CH fcc, and 2.02, 2.02, 2.02 Å for C fcc + CH hcp. The other C–Ru bonds are 1.96, 1.96, 1.90 Å for hcp–hcp, 1.90, 1.98, 1.98 Å for fcc–fcc, 1.92, 1.92, 1.94 Å for C hcp + CH fcc, and 1.94, 1.94, 1.94 Å for C fcc + CH hcp.

§5.3.10   C + C

Two C atoms can adsorb in three different ways in three-fold hollow sites in a 2×2 structure (50% coverage). The adsorption energies with respect to two C gas phase and Ru bare surface are −1305 kJ×mol^{-1} for both C in hcp site, −1216 kJ×mol^{-1} for both, C in fcc sites and −1264 kJ×mol^{-1} for one C in hcp site and the other one in fcc site. With respect to two adsorbed C groups, the same adsorption energies are 44, 133, and 86 kJ×mol^{-1}, respectively. The distortion of the surface is so important that a first attempt to optimize both C atoms in fcc site gave a shift of the medium layers in order to get both C atoms in hcp sited on Ru(111) surface (fcc structure!). This structure is with 75 kJ×mol^{-1} more stable than the one with both C on fcc sites on Ru(0001) surface (hcp structure) (see Figure 5.1, tenth column, the line-dot-line lines). The C–Ru bond length for hcp–hcp pear are 1.89, 1.96, 1.96 Å for each C atom. For the hcp–fcc we have 1.92, 1.92, 1.92 Å for the C atom sitting in the hcp site and 1.94, 1.94, 1.94 Å for the C atom sitting in the fcc site. Last, for the fcc–fcc situation we have 1.97, 1.91, 1.97 Å for each C atom.

§5.4   Discussion

§5.4.1 2×2 C$_2$H$_z$ on Ru(0001) (z = 6-0)

The most stable adsorbed species of the C$_2$H$_z$ intermediate series is a CCH$_2$ species, which adsorbs above an hcp site with the CH$_2$ group above a metal atom. CCH$_3$ is also stable but has a different geometry: the C–C bond is perpendicular to the surface. CHCH and CCH have a similar stability and similar geometry, with the C–C bond parallel to the surface. The CC dimer is less stable but has a similar

geometry as CHCH.

CHCH$_2$ and CHCH$_3$ have also similar stabilities and similar geometries. The H atom from the CH group is activated because of the presence of the CH$_2$ or CH$_3$ group. Those species can easyly lead to CCH$_2$ and respectively to CCH$_3$.

CH$_2$CH$_3$ is very different compared with the rest of the C$_2$H$_z$ species. Because of the presence of the CH$_3$ group, which has a repulsive interaction with the surface, the two H atoms from the CH$_2$ group are pushed towards the surface. This leads to an instability of the ethyl group in a hollow site or in atop site. The only acceptable site is a bridge site, but also there the adsorption energy is positive compared with gas phase ethane. We expect that this species to be very reactive on the Ru(0001) surface [9].

Except ethane, all other intermediates are stabilized by adsorption. CH$_2$CH$_2$, CCH$_3$, CCH$_2$, CCH, and CC are more stable in the coupled form rather than separately. CHCH$_3$ and CHCH are more stable in the dissociated states, rather than in the coupled form. The other species, CH$_3$CH$_3$, CCH, CH$_2$CH$_3$, CHCH$_2$ have a comparable stability. We expect that the last two to be active in Fischer-Tropsch [9].

Bonding to Ru(0001) is different from Pt(111) where a tetrahedral environment is assured around each C atom. On ruthenium, nearly all intermediates show high coordination with surface atoms.

§5.4.2   CH$_x$ + CH$_y$ on Ru(0001) (x, y = 3-0)

Different CH$_x$ (x = 0-3) species have different lateral interactions. C and CH have a strong lateral interaction through the surface. The CH$_3$ species experience an important direct, short range, steric repulsion. CH$_2$ is somewhere in the middle between these two categories. Lateral interactions between adsorbed C with adsorbed C, adsorbed C with adsorbed CH or adsorbed CH with adsorbed CH are similar and can be in the range 23–58 kJ$\times$mol^{-1} if at least one species is in a stable adsorption site (hcp) or it can be in between 60–133 kJ$\times$mol^{-1} if both are in unfavorable adsorption sites. In all those cases, the adsorbed species share one metal atom on the surface.

CH$_3$ has a small lateral interaction through the surface but a very important steric repulsion at short range. Therefore the systems CH$_3$ + CH$_x$ (x = 1-3) will adapt by displacing the CH$_3$ from the stable three-fold hollow site to the more unfavorable bridge or top sites. This is possible because the CH$_3$ species show a small difference between the adsorption energies of three-fold sites and bridge (17 kJ$\times$mol^{-1}) or atop

(31 kJ×mol^{-1}) sites [1]. The interaction of CH_3 and CH is less repulsive (CH_3 will stop on bridge sites) and the interaction CH_3 + C is even less repulsive, CH_3 will remain in hollow sites.

CH_2 is an important species for the Fischer Tropsch reaction. Its residence time on Ru(0001) is the shortest one [8, 10], so it's importance on Ru(0001) is minimal. Since it adsorbs on the three-fold hollow site the two H atoms are different. The difference can be more or less important if different species are adsorbed in close proximity.

All CH_x species in all relative positions show a repulsive lateral interaction to each other (through the surface or steric repulsion). The smallest lateral repulsion is in the case of two CH_2 species adsorbed in hcp sites (21 kJ×mol^{-1}) or two CH species also in hcp sites (23 kJ×mol^{-1}). The largest lateral repulsion is in the case of C fcc + CH_3 hcp (111 kJ×mol^{-1}), C fcc + CH_3 fcc (107 kJ×mol^{-1}), or C fcc + CH fcc (101 kJ×mol^{-1}).

The lateral interactions can be deduced from Figure 5.1, if one compare the relative position of the black solid line to that of the line-dot-line. The solid line is always under the line-dot-line, so we have only repulsions. We see a small repulsion for the CH_2 + CH_2 and large repulsions for C + CH species.

Because of that repulsive interaction, the geometry of adsorbed CH_x may show distortions compare to the isolated situation, which will induce the repulsion. For instance CH adsorb with a perpendicular C–H bond to the surface. If a methyl is adsorbed nearby, the angle between the CH and the surface become 3.3°.

§5.5 C–C Coupling on Ru(0001) surface

Using the results from the previous sections, computing some TS for C–C coupling reaction we propose two mechanisms for Fischer Tropsch synthesis. See chapter 9.

§5.6 Conclusions

CCH_2 and CCH_3 are the most stable adsorbed species from the C_2H_z (z = 0−6) series despite their different adsorption mode.

CH_2CH_3 is the most reactive and adsorbs on bridge sites because of the repulsion between the methyl group and the surface.

The interaction between adsorbed CH$_x$ and CH$_y$ (x, y = 0-3) is repulsive (through the surface for small x and y, and steric for x or y equal to 3).

The information on the CH$_x$ + CH$_y$ interaction energies together with the relative energies of C$_2$H$_z$ (x, y = 0-3, z = 0-5) give us the possibility to understand the relative stability of C$_2$ species versus the C$_1$ species. We will discuss this more fully elsewhere [9] (see chapter 9).

The CH$_x$ + CH$_y$ interactions give us also information about the dimensions of lateral interaction (energies, distances). Those results have been used to develop a model for calculating the lateral interactions regardless of the positions of two adsorbates [8, 10].

Bibliography

[1] I. M. Ciobîcă, F. Frechard, R. A. van Santen, A. W. Kleyn and J. Hafner, *Chem. Phys. Lett.*, 311, (1999), 185

[2] R. M. Watwe, R. D. Cortight, J. K. Nørskov, J. A. Dumesic, *J. Phys. Chem. B*, 104, (2000), 2299

[3] J. Kua, W. A. Goddard III, *J. Phys. Chem. B*, 102, (1998), 9492

[4] J. Kua, W. A. Goddard III, *J. Phys. Chem. B*, 103, (1999), 2318

[5] R. A. van Santen, *Theoretical heterogeneous catalysis*, World Scientific 1991, 234

[6] J. F. Paul, P. Sautet, *J. Phys. Chem.*, 98, (1994), 10906

[7] I. M. Ciobîcă, F. Frechard, R. A. van Santen, A. W. Kleyn and J. Hafner, *J. Phys. Chem. B*, 104, (2000), 3364.

[8] I. M. Ciobîcă, F. Frechard, C. G. M. Hermse, A. P. J. Jansen and R. A. van Santen, in *Surface Chemistry and Catalysis*, ed. A. F. Carley, P. R. Davies, G. J. Hutchings and M. S. Spencer, Kluwer Academic/Plenum, 2002

[9] I. M. Ciobîcă, G. J. Kramer, M. Neurock, Q. Ge, R. A. van Santen, *J. Phys. Chem. B*, submitted

[10] I. M. Ciobîcă, F. Frechard, A. P. J. Jansen, R. A. van Santen, *Stud. Surf. Sci.*, 133, (2001), 221

Chapter 6

Methane activation on Ru(11$\bar{2}$0)

The thermodynamics of methane decomposition on the ruthenium (11$\bar{2}$0) surface has been investigated with ab initio periodic calculations. All surface intermediates are more stable than the gas phase methane although the last step of the decomposition path: CH → C + H, is highly endothermic. Amongst all of the surface species, CH_2 appears to be the most stable. All of the surface species (CH_x, x = 3-1 and H) adsorb on bridge up sites, while atomic C prefers atop down sites.

The Transition States of the elementary reactions for the dissociation of methane on the ruthenium (11$\bar{2}$0) surface have been investigated with Nudged Elastic Band Method (NEB). The calculated barriers are 49 kJ×mol^{-1} for methane decomposition, 8 kJ×mol^{-1} for methyl decomposition, 52 kJ×mol^{-1} for methylene decomposition respectively. The decomposition of CH_{ads} requires the highest activation energy from the series with 97 kJ×mol^{-1}.

§6.1   Introduction

This chapter presents the thermodynamics of adsorbed CH_x species (x = 0-4) on the ruthenium (11$\bar{2}$0) surface as well as the Transition States for each elementary reaction for CH_x (x = 1-4) decomposition to CH_{x-1} (x = 1-4) and H atom in a similar way that we did before for the ruthenium (0001) surface [1,2], see chapter 4.

We will discuss first the relative stability of each CH_x species on all adsorption sites, then we will discuss the coadsorption with H atom, and finally the Transition States for elementary reactions of CH_x decomposition will be analyzed.

§6.2 CH$_x$ on Ru(11$\bar{2}$0) surface

Adsorbed CH$_4$. Methane is weakly adsorbed. Our experience with Ru(0001) shows that methane is physisorbed with -1 kJ×mol^{-1} for 25.0% coverage and -3 kJ×mol^{-1} for 11.1% coverage. On the (11$\bar{2}$0) surface, the picture is similar, all adsorption modes have a negligible adsorption energy. The shorter metal–H distance is 2.5 Å for the case of adsorbed methane with one H atom pointing down to the surface. All C–H bond length are about 1.1 Å, the methane molecule is not distorted.

Adsorbed CH$_3$. Methyl prefers to adsorb on bridge up position. (See Figure 3.7 for adsorption sites on this surface.) The adsorption energy with respect to gas phase methyl and bare metal surface is -221 kJ×mol^{-1}. The atop up adsorption mode is less stable with 21 kJ×mol^{-1}. This can give us some information about the mobility of methyl species on this particular surface.

All C–H bonds are 1.1 Å, and H–C–H angles are 111° and two times 104° for the stable adsorption mode and three times 109° for the metastable adsorption mode. C–Ru distances are 2.1 Å and 2.3 Å for bridge up adsorption and 2.1 Å for atop up adsorption. Ru–C–Ru angle is 74° and one H atom is at 2.0 Å from a metal atom in the case of the bridge up adsorption mode. The atop up geometry is slightly tilted.

Atop down and bridge down adsorption modes are not stable, during the optimization the atoms move towards the most stable bridge up configuration.

Adsorbed CH$_2$. Methylene also prefers to adsorb on bridge up position. The adsorption energy with respect to gas phase methylene and the bare ruthenium surface is -439 kJ×mol^{-1}. We were not able to identify a stable atop up adsorption mode, since methylene was dissociated to adsorbed CH and adsorbed H. However, we manage to compute a metastable atop down adsorption mode with 19 kJ×mol^{-1} less stable. In addition, methylene seams mobile on this surface.

Among all other species, methylene is the most stable from the CH$_x$ series. This result is different compared with the (0001) surface.

The C–H bonds are 1.1 Å, and H–C–H is 113° for bridge up and 101° for atop down adsorption modes. The C–Ru bond lengths are both 2.1 Å in the case of bridge up configuration and for atop down we have 2.1 Å for the Ru atom on the second layer, 2.1, 2.3 and 2.9 Å for three Ru atoms from the first layer from one row and 2.6 Å for the forth metal atom from the first layer from an other row. This bridge down configuration has the H atoms from adsorbed CH$_2$ close to metal atoms from the first row. The distances are 2.3 Å for one H atom and 2.5 and 2.0 Å respectively

for the other H atom.

Adsorbed CH. Methine prefers too the bridge up configuration for adsorption. With respect to bare ruthenium surface and gas phase, CH the adsorption energy is -624 kJ$\times$mol^{-1}. The atop down, slightly distorted is less stable with 45 kJ$\times$mol^{-1} and next is the tilted atop up adsorption mode with 96 kJ$\times$mol^{-1}. This species has a limited mobility compared with methyl and methylene.

The relative stability of CH is close to the one for CH$_2$, with respect to methane in gas phase. This may be explained by the bridge adsorption site were CH$_x$ species are adsorbed. On the (0001) surface, the adsorbed CH$_2$ species on bridge site is more stable than the adsorbed CH species on bridge site, with respect to methane in gas phase.

The C–H bond lengths are 1.1 Å, C–Ru is twice 1.9 Å for bridge up, 2.1 Å, for Ru$_{down}$–C in atop down adsorption mode, 2.1, 2.0 and 2.6 Å for Ru$_{up}$–C, and 2.9 Å for Ru$_{up}$–C from the other row, respectively. C–Ru distance for atop up adsorption mode is 1.7 Å. Ru–C–Ru for bridge up adsorption is 91°. H–C–Ru angle for atop down is 139° and for atop up is 178°.

Bridge down adsorption mode lead to a distortion of the metal layers.

Adsorbed C. Atomic C behaves a bit different like all CH$_x$. It prefers to adsorb in a tilted atop down configuration (see chapter 3 for a description of the adsorption sitesi for (11$\bar{2}$0) surfaces). With respect to bare metal surface and gas phase atomic carbon, the adsorption energy is -675 kJ$\times$mol^{-1}. The next local minimum is for bridge up adsorption mode, less stable with only 9 kJ$\times$mol^{-1}. It is followed by bridge down with 96 kJ$\times$mol^{-1} less stable and by top up with 126 kJ$\times$mol^{-1}.

The Ru$_{down}$–C distance is 2.0 Å, the Ru$_{up}$–C distances are 2.0, 1.9 and 2.5 Å, respectively for one row and 2.9 Å for the other row in the case of atop down adsorption mode. Bridge up configuration have two distances of 1.9 Å, bridge down has Ru$_{down}$–C bond lengths of 2.1 Å, while Ru$_{up}$–C bond lengths are 1.9 Å. Atop up adsorption mode has a C–Ru bond length of 1.7 Å. Ru–C–Ru angles are 97° for bridge up and for bridge down we have Ru$_{down}$–C–Ru$_{down}$ of 79° and Ru$_{up}$–C–Ru$_{up}$ of 160°.

Adsorbed H. The H atom adsorbs in a bridge up configuration. With respect to H$_2$ molecule in gas phase and the bare Ru surface the adsorption energy is -54 kJ$\times$mol^{-1}. Atop up and atop down are not stable adsorption modes; during the optimization the H atom is moving towards a more stable bridge up geometry. Bridge down is metastable, less stable with 172 kJ$\times$mol^{-1}.

The H–Ru bond lengths are twice 1.8 Å for bridge up and four times 2.0 Å for bridge down. The angles Ru–H–Ru are 99° for bridge up and 83° for Ru atoms in second layer, and 163° for Ru atoms in first layer, respectively, see Figure 3.8

§6.3   Coadsorption of CH$_x$ (x = 0-3) with atomic H

In all those calculations, we considered that H and CH$_x$ (x = 0-3) are adsorbed in bridge up configurations. Other combinations were not tested since we believe that at this coverage other adsorptions are not possible.

CH$_3$ and H. To coadsorb an H atom close to a adsorbed methyl on the Ru(11$\bar{2}$0) surface costs about 23 kJ×mol^{-1}. This is more than in the case of the coadsorption on the Ru(0001) surface. We can explain this by a higher density on the Ru(11$\bar{2}$0) surface and the large volume of the methyl group. The geometry of adsorbed methyl is not changed, the most affected is the H atom, which got now two asymmetric Ru–H bonds of 1.8 and 2.0 Å with the two Ru atoms from the first layer, and also it approaches one atom from the second layer at the distance of 2.0 Å. The distance H–CH$_3$ is 2.8 Å.

CH$_2$ and H. The coadsorption of a H atom with a methylene reduces the adsorption energy with 14 kJ×mol^{-1}. This is similar with the repulsion in the case of coadsorption on the (0001) surface. The geometry of methylene or of H is also not affected by the coadsorption. The distance H–CH$_2$ is 2.3 Å.

CH and H. The lateral interaction between adsorbed CH and adsorbed H is repulsive and about 24 kJ×mol^{-1}. This is more than for CH$_2$ since CH adsorbs stronger. Became of the symmetry constraints the geometries of CH and H do not differ from those adsorbed separately. The distance H–CH is 2.2 Å.

C and H. The lateral interaction between adsorbed C and H is larger than the one for CH, it is 39 kJ×mol^{-1}. Similar to CH and H coadsorption, C and H have a similar geometry like far separate absorptions. The distance H–C is also 2.2 Å.

§6.4   Barriers for the elementary reactions of methane activation on the Ru(11$\bar{2}$0) surface

The energies of the CH$_x$ (x = 3-1) species adsorbed in the most stable site, as well as the Transition States are presented in Figure 6.1. Absolute values relative to

the CH_x in gas phase and the bare metal surface (also optimized) for the most stable adsorption modes are given in Table 6.1.
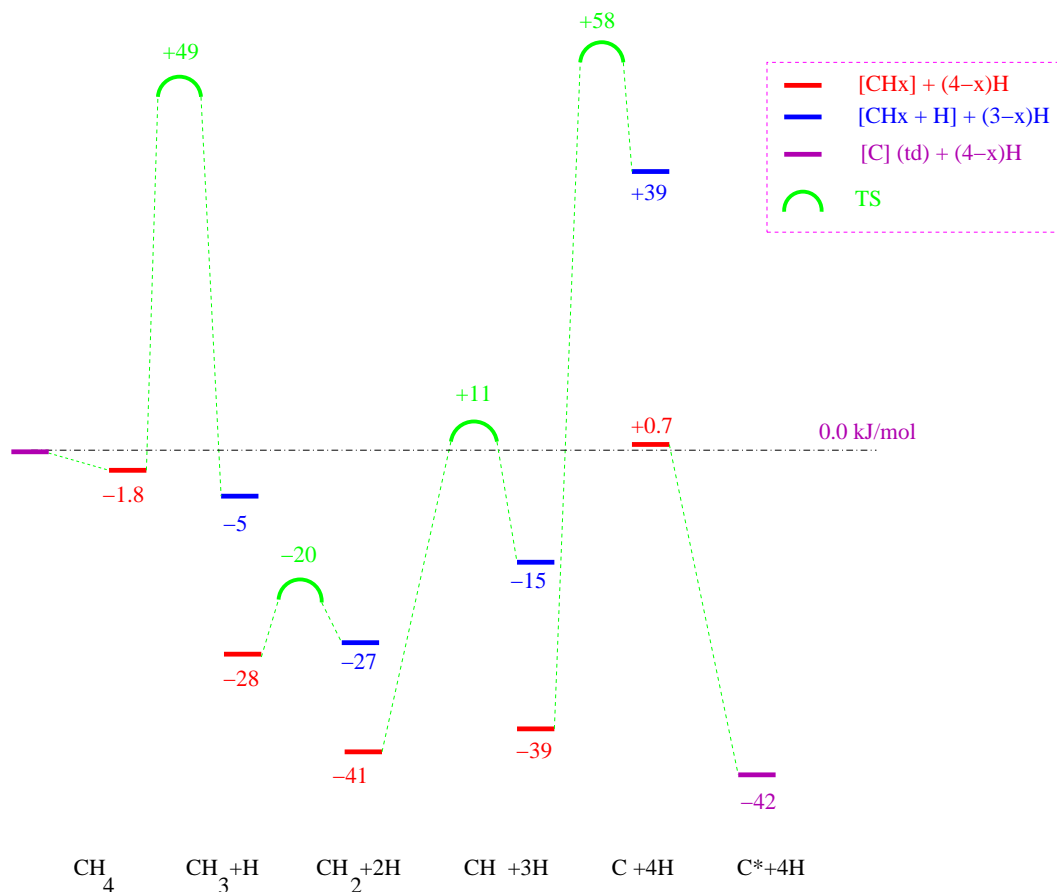
Figure 6.1: Full path for methane activation on the $Ru(11\bar{2}0)$ surface. All species are adsorbed on bridge up sites, except C atom marked with a star, which is adsorbed on a tilted atop down site.

species	CH_3	CH_2	CH	C	H
adsorption site	bu	bu	bu	td	bu
energy $(kJ \times mol^{-1})$	-221.3	-439.2	-624.2	-675.4	-53.9

Table 6.1: Absolute values relative to the CH_x in gas phase and the bare metal surface for the most stable adsorption modes. "bu" is bridge up and "td" is atop down.

CH$_4$ → CH$_3$ + H. The barrier for methane activation on Ru($11\bar{2}0$) we report here is 49 kJ×mol^{-1}. This is smaller than for the Ru(0001) surface. This can be explain by the higher coverage and by the lower coordination for Ru atoms involved in the reaction. The Transition State is a very early one, similar to Ru(0001).

The activated H atom is at 1.5 Å from the C atom. The other H atoms have H–C bond lengths of 1.1 Å. The angles H–C–H are 110°, for the normal H atoms and between 83° and 96° for one H atom activated. The C–Ru distance is 2.2 Å. The Ru–H bond lengths for the activated H atom are 1.9 Å, and 1.8 Å. The Ru–H–Ru is 99°, see Figure 6.2.
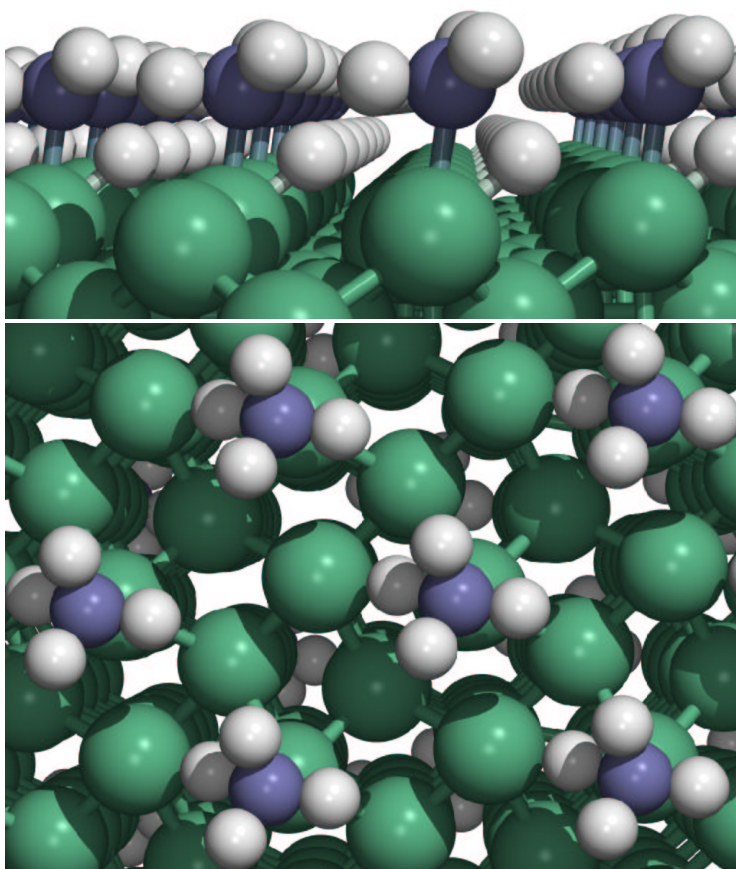
Figure 6.2: TS for methane decomposition on the Ru($11\bar{2}0$) surface.

There are some similarities in between this TS and the same on the close packed surface of ruthenium. Both are with the C atom atop site and with the activated H atom in a nonsymmetrical bridge site.

CH$_3$ → CH$_2$ + H. The activation of methyl is a easy process, similar with activation of methylene on the Ru(0001) surface. The barrier is just 8 kJ×mol^{-1}. The activated H atom is at 1.2 Å from the C atom, while the other C–H bonds are still 1.1 Å. The angle H–C–H between the non-activated H atoms is 111°, while with the activated H atoms they are 101° and 106°. The CH$_3$ group is still in the bridge site with C–Ru bonds of 2.2 Å and 2.3 Å, the Ru–C–Ru angle being 74°. The activated H atom is atop a metal atom at a distance of 2.0 Å. See Figure 6.3.
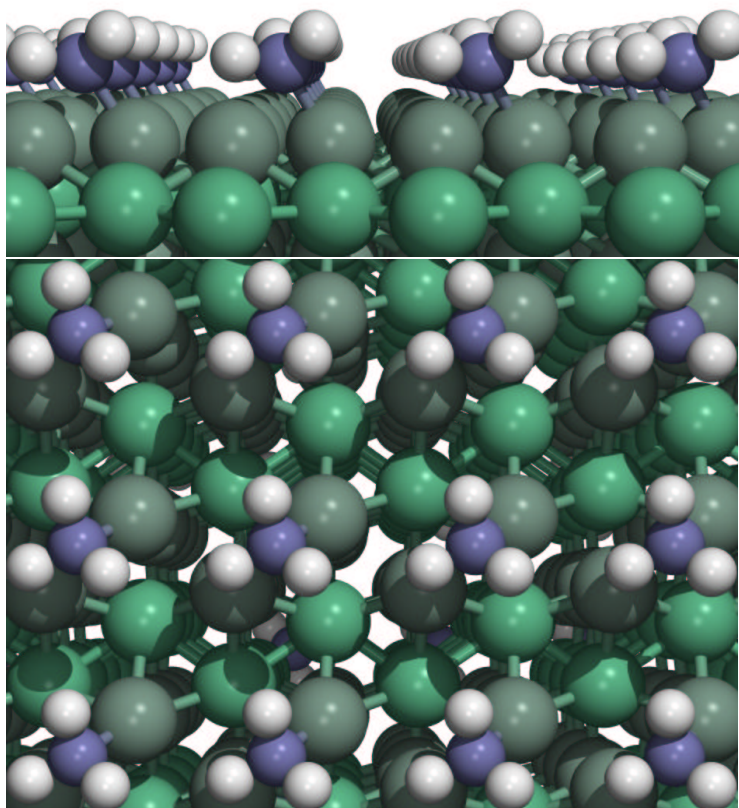
Figure 6.3: TS for methyl decomposition on the Ru(11$\bar{2}$0) surface. Side and top view.

There are certain similarities between this Transition State and the Transition State for methylene decomposition on (0001) surface. Here, by the decomposition of CH$_3$ it results in the most stable species. One H is already activated due to the geometric constraints (one H is atop a metal atom). CH$_2$ on (0001) surface will also give by decomposition the most stable species from that series, one H is also activated due to geometric constraints (one H is atop a metal atom).

CH$_2$ → CH + H. The activation of the most stable intermediates requires 52 kJ×mol^{-1}. The activated H atom is at 1.5 Å from the C atom and it is in a tilted bridge up position at 1.8 Å and 2.1 Å respectively. The remaining CH group is in the initial bridge up configuration, with 2.0 Å and 1.9 Å C–Ru bond lengths (in between Ru–C$_{CH}$ and Ru–C$_{CH_2}$). The angle Ru–C–Ru is 62°, the angle H–C–H is 99°, and the angle Ru–H–Ru for the activated H atom is 87°. See Figure 6.4.
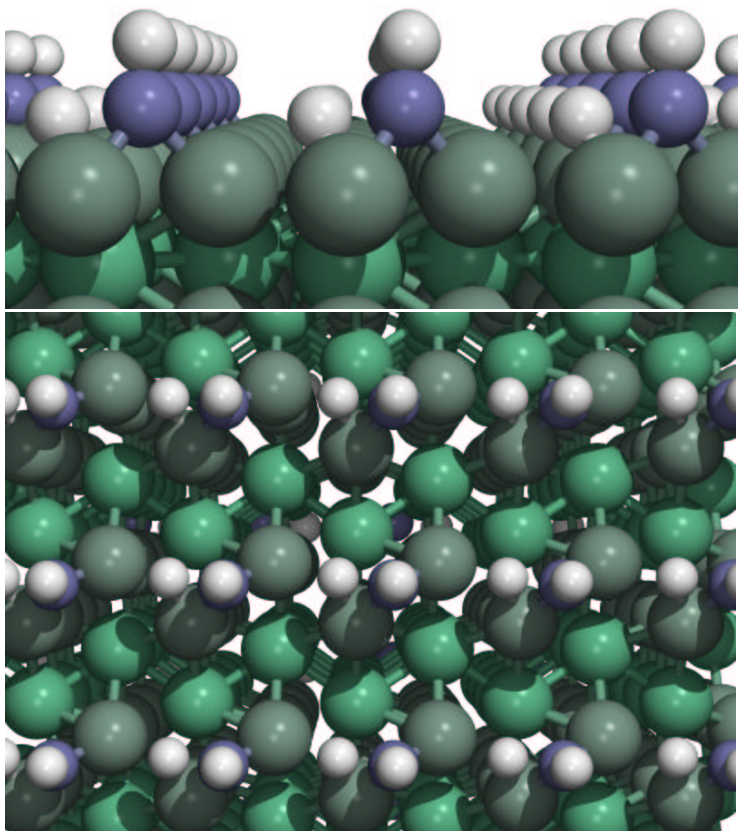
Figure 6.4: TS for methylene decomposition on the Ru(11$\bar{2}$0) surface. Side and top view.

CH → C + H. The activation of CH requires the largest amount of energy from the CH$_x$ series on Ru(11$\bar{2}$0) surface, 97 kJ×mol^{-1}. The activated H atom is also at 1.5 Å from the C atom, the CH is parallel with the surface in this late Transition State. The Ru–H bond lengths are 1.8 Å and 2.0 Å. The Ru–C bond lengths are 1.8 Å and 1.9 Å. The Ru–C–Ru angle is 95° and the Ru–H–Ru angle is 89°. See Figure 6.5.
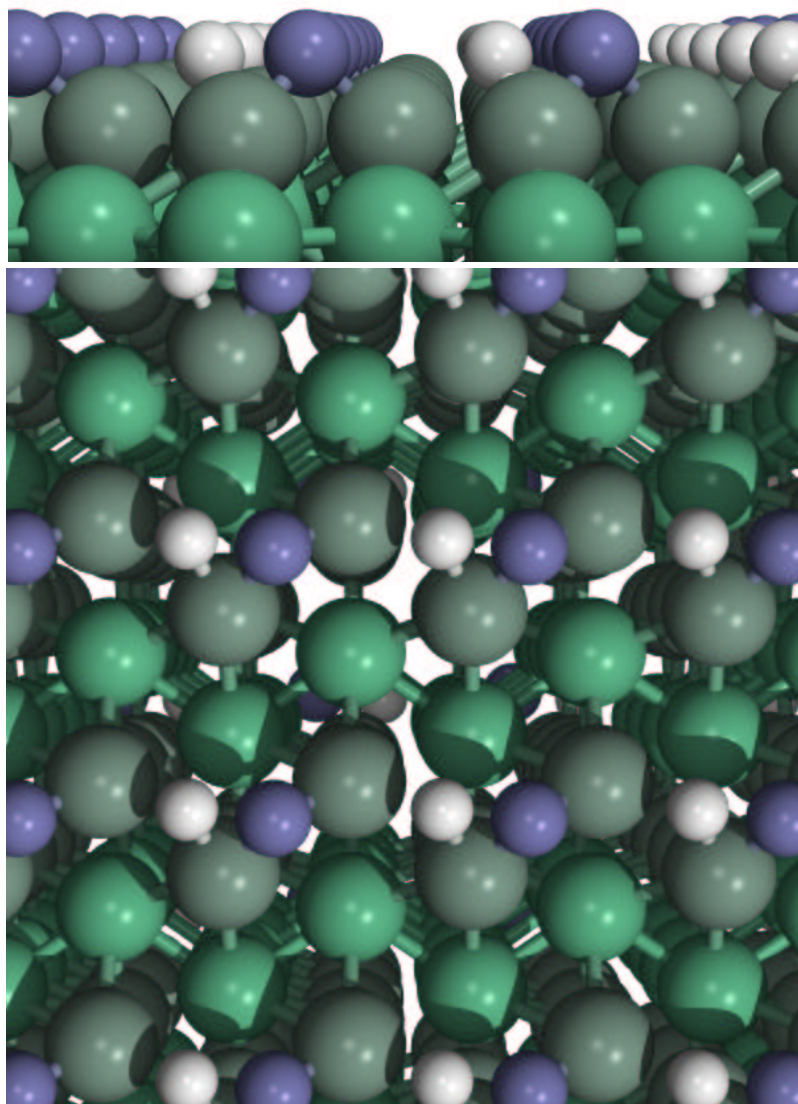
Figure 6.5: TS for methine decomposition on the Ru(11$\bar{2}$0) surface. Side and top view.

§6.5   Conclusions

Adsorbed methyl and adsorbed methylene are mobile on the Ru(11$\bar{2}$0) surface, while CH and C present a limited mobility. All species are more stable on the bridge up adsorption mode, except for adsorbed C, where the tilted top down adsorption mode is with 9 kJ$\times$mol^{-1} more stable. Since those calculations are for 50% coverage,

we expect some important lateral interactions especially for C and CH. Compared to the close packed surface, all species have smaller adsorption energies, and we assume that this is due to the particularity of the surface which has no three-fold sites for adsorption.

Methylene is the most stable species from the adsorbed CH_x series (x = 0-3) on the (11$\bar{2}$0) surface, while on the (0001) surface adsorbed CH was by far the most stable species. The relative stability of adsorbed CH and adsorbed C is not far from the adsorbed CH_2.

H coadsorption with CH_x (x = 0,3) is repulsive. The smallest repulsion is in the case of methylene, which does not have a large volume as methyl and also not a strong adsorption as CH or C.

Transition States for C–H activation on Ru(11$\bar{2}$0) are different from the ones on Ru(0001). Similarities are in the cases CH_4/(0001) with CH_4/(11$\bar{2}$0), CH_2/(0001) with CH_3/(11$\bar{2}$0), and CH/(0001) with CH/(11$\bar{2}$0). The activation of methane and methyl are early Transition States, while the activation of CH is a late Transition State.

The decomposition of methylene and methine has the activated H atom in a bridge site and a C–H distance of 1.5 Å. On the (0001) surface, the decomposition of methyl and methine has the activated H atop a metal atom at the distance of 1.6 Å from the C atom.

Ru(11$\bar{2}$0) is a more open surface compared with the (0001), and more reactive. The CH_x species are strong bonded to the surface, but less than in the case of (0001) surface, due to the lack of three-fold sites, which make the species more reactive.

Bibliography

[1] I. M. Ciobîcă, F. Frechard, R. A. van Santen, A. W. Kleyn and J. Hafner, *Chem. Phys. Lett.*, 311, (1999), 185

[2] I. M. Ciobîcă, F. Frechard, R. A. van Santen, A. W. Kleyn and J. Hafner, *J. Phys. Chem. B*, 104, (2000), 3364

Chapter 7

Carbon monoxide, hydrogen compressed layers and hydrogen–carbon monoxide coadsorption on the Ru surfaces

The interaction of CO with the Ru(0001) surface at several coverages (11.1%, 25.0% and 33.3%) is studied, as well as the interaction of CO with a stepped Ru(0001) surface. Preference for adsorption site (atop versus hcp) is analyzed with DOS diagrams. Hydrogen layers can be densely packed, 1 ML could in fact correspond to more than 100% coverage, where 100% coverage would correspond to 1 addatom for each metal atom on the surface. Calculations are made for 1 ML adsorbed hydrogen up to 300% coverage for 2×2 supercells. The H coadsorption with CO (2×2 (CO + n H), $n = 1, 3, 4$) is discussed for different adsorption sites. The lateral interaction H–CO is repulsive. H_{ads} and CO_{ads} prefer to form islands rather than to form mixed structures. CO is little influenced by coadsorption, except when 1 ML of atomic hydrogen is preadsorbed. H is strongly affected by coadsorption. The H adsorption sites become highly asymmetrically if H and CO share one metal atom. For two coverages (11.1% and 25.0%), computational results on the direct dissociation of CO on the Ru(0001) flat, as well as the stepped surface are presented. Five reaction paths are studied on the flat most compact surface, and other four on the stepped surfaces. For the flat surface, the indirect reaction path for CO dissociation via the insertion

of an H atom, as well as the Boudouard reaction for stepped surfaces are discussed.

§7.1 Introduction

Adsorption of CO to metal surfaces has over the years become the prototype system for molecular chemisorption. A rather simple bonding model has in general been accepted. It is known that on the late transition metals the energetic difference between free and adsorbed CO (the heat of adsorption), is much smaller than the C–O dissociation energy (1084 kJ×mol^{-1} or 11.23 eV [1]).

The adsorption of carbon monoxide and the coadsorption with hydrogen on the close–packed Ru(0001) surface is particularly interesting because of its relevance to the Fischer–Tropsch synthesis and the methanation reaction [2]. While both CO and H$_2$ adsorption on the ruthenium surface has been studied quite extensively over the past decades, only little information is available for the hydrogen carbon monoxide coadsorption system on Ru(0001).

Initially we discuss site preference of CO on different Ruthenium surfaces. On some metals the atop site is preferred, while on some others the hollow site is preferred. Ruthenium is a case where both sites show similar adsorption energies.

In the second part, we are showing results for calculations of a compressed monolayer of H atoms on the Ru(0001) surface. The calculations are in between 25% and 300% coverage.

In the third part, we will show how lateral interactions affect the coadsorbed H atom with CO.

The last part is dealing with CO decomposition on flat and stepped surfaces. CO disproportionation and the indirect route of CO dissociation via H insertion are also presented.

§7.2 Adsorption of carbon monoxide on the flat and the stepped Ru surfaces

The molecular adsorption of CO on the ruthenium surfaces is nonactivated. On the Ru(0001) surface, at 2×2 coverage our calculations give an adsorption energy of -177 kJ×mol^{-1} for the atop site and -176 kJ×mol^{-1} for the hcp hollow site. This agrees well with experimental results [3]. The fcc hollow site gives an adsorption

energy of -169 kJ×mol^{-1} and the bridge site -160 kJ×mol^{-1}, respectively, see Table 7.1. Since all those adsorption energies are very close, the CO molecule is very mobile, and CO diffusion is not activated.

coverage	structure	adsorption site	adsorption energy (kJ×mol^{-1})
25.0%	2×2	atop	-177
25.0%	2×2	hcp	-176
25.0%	2×2	fcc	-169
25.0%	2×2	bridge	-160
25.0%	2×2	atop tilted	*-177
25.0%	2×2	atop tilted	⋆-183
25.0%	2×2	hcp tilted	-176
25.0%	2×2	fcc tilted	atop tilted
25.0%	2×2	bridge tilted	-167
33.3%	$\sqrt{3} \times \sqrt{3}$	atop	-189
33.3%	$\sqrt{3} \times \sqrt{3}$	hcp	-177
33.3%	$\sqrt{3} \times \sqrt{3}$	fcc	-170
33.3%	$\sqrt{3} \times \sqrt{3}$	bridge	-166
11.1%	3×3	atop	-186
11.1%	3×3	hcp	-186
	steps	atop edge	-195
	steps	hcp edge	-195
	steps	hcp bottom	-180

Table 7.1: Adsorption energies for CO on ruthenium surfaces, different sites, different coverages.

* the tilt is versus fcc site.

⋆ the tilt is versus hcp site

Other 2×2 calculations were performed for a CO molecule adsorbed in a tilted geometry. The adsorption energy did not change significantly. For the atop site, the CO molecule was tilted in the direction of a near hcp site or a near fcc site; the adsorption energies are -177 and -183 kJ×mol^{-1}, respectively (0 and 6 kJ×mol^{-1}

more stable than the non tilted ones) for angles of 0.5° and 1.6°, respectively. CO tilted on the hcp site is not stable, the final tilting angle is 0°. By tilting the CO from a fcc site, the molecule is going to the near atop site. The tilted CO on a bridge site gives an adsorption energy of -167 kJ×mol^{-1} (6 kJ×mol^{-1} more stable than the non tilted one) and the tilting angle is 9.0°.

A few calculations for CO adsorption with the O-end pointing to the surface were performed for the fcc and hcp sites. The CO and the surface interaction is repulsive, by fixing the molecule in this position, the adsorption is around $+100$ kJ×mol^{-1} (less stable than separately) and if the separation is allowed the CO molecule will go as far it can go (to the top of the cell) and the adsorption energy is going to zero.

In addition, the parallel adsorption mode was investigated. The CO molecule is not stable parallel with the surface. The final adsorption mode is the CO molecule with the C-end pointing to the surface. A similar orientation dependency has been proposed for NO on Pt(111) by Lahaye et al. [4].

To fully understand the adsorption of CO on this surface, we performed calculations for CO adsorption also at $\sqrt{3}\times\sqrt{3}$ R30° structure (33.3% coverage). In this case the atop site become more stable. The adsorption energy is -189 kJ×mol^{-1} while for the hollow hcp site it remains -177 kJ×mol^{-1}. The other three-fold site, fcc have an adsorption energy for CO of -170 kJ×mol^{-1} and the bridge site -166 kJ×mol^{-1}, see Table 7.1.

The fragile balance for atop/hcp adsorption of CO on Ru(0001) is in favor of the atop site in $\sqrt{3} \times \sqrt{3}$ structure (33.3% coverage). In a 2×2 structure (25.0% coverage), both sites have the same stability. It seems that the lateral interaction of CO atop is more important that the one of CO hcp, since the adsorption energy does not change with the coverage for the hcp site but it change for the atop site.

The C–O bond length is 1.17 Å for the atop site, 1.18 Å for the bridge site and 1.19 Å for the three-fold hollow sites (hcp and fcc) for 2×2, $\sqrt{3} \times \sqrt{3}$ and 3×3 structures, tilted or not. The Ru–C bonds are 1.90 Å for the atop absorptions, 2.05–2.11 Å for the bridge sites and 2.09–2.15 Å for the three-fold hollow sites. The Ru–C–O angle varies between 178 and 180° for atop adsorption mode, 134–142° for bridge and 131–136° for the three-fold hollow sites, respectively. The Ru–C–Ru angles are in between 81 and 82° for bridge sites and in between 76 and 80° for three-fold hollow sites.

Calculations for the 3×3 structure (11.1% coverage) for CO adsorption atop and on hcp sites were performed as well. The adsorption energies are -186 kJ×mol^{-1} for

atop site and for the hcp site.

Steps were also considered. Since Ru is an hcp metal, the steps presented on the Ru(0001) surface are not the same, but two different ones are repeated regularly. The adsorption energy of CO atop at the edge on one of such steps is -195 kJ$\times$mol^{-1}. The adsorption energy of CO hcp at the edge of the step is -195 kJ$\times$mol^{-1}, while at the bottom of the same step is -180 kJ$\times$mol^{-1}. See Figure 7.1. If two CO are adsorbed in hcp site at the step edge and in hcp site at the step bottom, the adsorption energy is -161 kJ$\times$mol^{-1}.
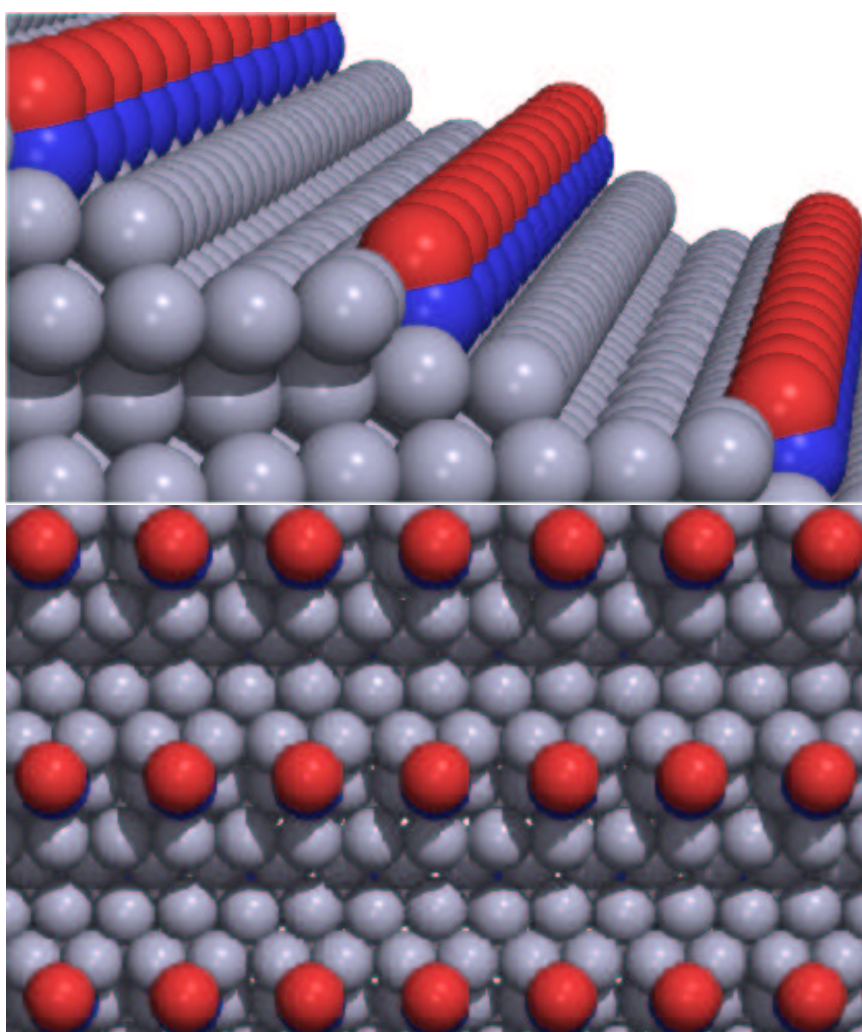
Figure 7.1: CO adsorbed on the bottom of the steps. Top and side view.

The geometry of the CO adsorbed atop on the step edge is not different from the other CO adsorbed atop on flat surfaces, except that the CO molecule is tilted more, the angle with the (0001) terrace is 5°. The geometries of the CO adsorbed hcp on the step edge and the bottom edge, are different from the adsorbed CO on flat surface. The C–O bond lengths are 1.20 Å and 1.30 Å, respectively. The CO adsorbed on the hcp edge has two short C–Ru bonds of 2.08 Å, and a long one C–Ru 2.36 Å, while the other CO have three bonds of 2.08 Å. The angles O–C–Ru are 124° and two times 137° for edge hcp and 156°, and two times 118° for bottom hcp, respectively. The Ru–C–Ru angles are 74, 74, and 83° and 82, 79, and 79°, respectively. The O from the adsorbed CO on bottom hcp is close to the two metal atoms from the step edge, the O–Ru distance is 2.32 Å. When two CO molecules are adsorbed, one on edge hcp and one in bottom hcp, the one is edge hcp is less perturbed, the same C–O and C–Ru are present and the angles O–C–Ru and Ru–C–Ru are similar in within few degree. The other CO, adsorbed on bottom hcp, is more perturbed. The C–O bond length a bit shorter (1.26 Å), the C–Ru bonds are different (2.03, 2.15, 2.15 Å) but the angles O–C–Ru and Ru–C–Ru are the same. The O–Ru from the edge is a bit longer (2.52 Å).

Vibrational frequencies were computed with the AnharmND [5] program for CO in gas phase and CO adsorbed atop site and hcp site in the 2×2 structures. In Table 7.2, the results are presented. Three points were calculated for each side of the parabola and the results were interpolated to calculate the harmonic and anharmonic frequencies. Experimental values are taken from ref. [6].

adsorption	Frequencies in cm^{-1}		
site	harmonic	an-harmonic	experimental
gas phase	2134	2103	2170
atop	1964	1940	1989 [6]
			1990 [7]
hcp	1765	1727	unknown

Table 7.2: Frequencies of CO in the gas phase and adsorbed on Ru(0001) atop and on three-fold hcp hollow site.

We analyzed the Local Density of States (LDOS) for the CO molecules adsorbed on top and hcp sites for 2×2, 3×3, and steps. See Figures 7.2 and 7.3 for the DOS

diagrams for the p_x and p_z orbitals of the C atom from the CO molecule.
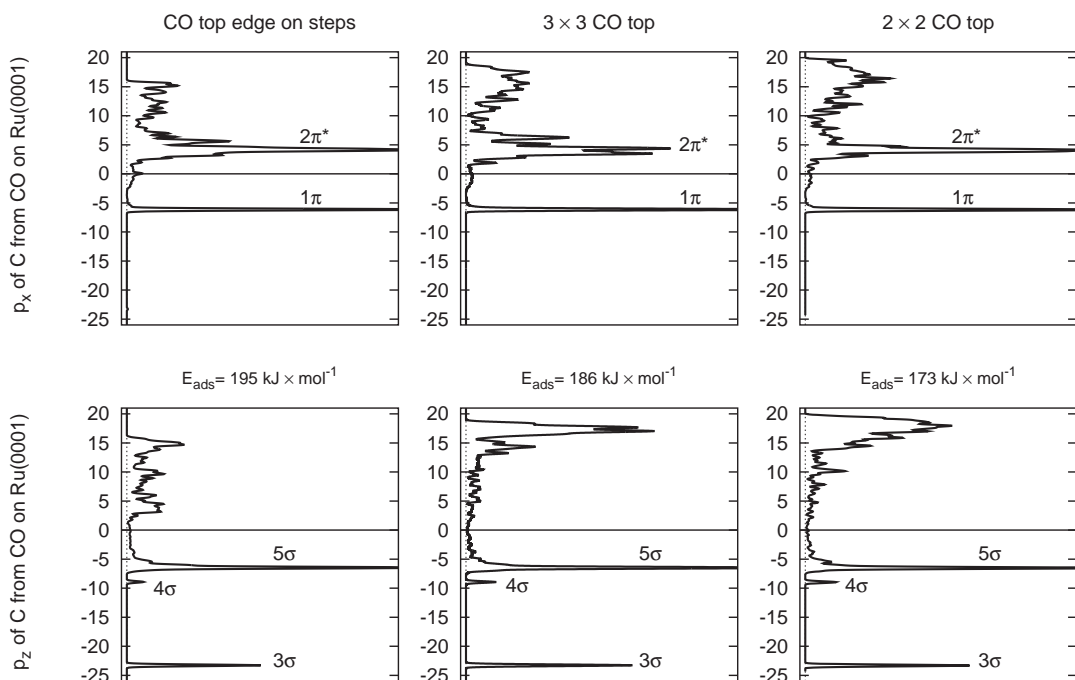
Figure 7.2: DOS diagrams for p_x and p_z orbitals of the C atom from the CO molecule adsorbed atop sites.

Considering the CO adsorbed atop, for the p_x orbital we can see that the $2\pi^*$ is broader and a very small amount is filled (under Fermi level). There is a small difference between the CO adsorbed in 2×2 and 3×3, as well as the CO atop on the step edge.

For the p_z orbital, we can see that the 5σ is similar for the three cases. A common feature for CO adsorbed atop would be that on the step edge, the broadening of the antibonding orbitals is smaller.

Considering the CO adsorbed in the hcp three-fold hollow site, for the p_x orbital we can see that the $2\pi^*$ is also broaden. Compared with the atop adsorption, the $2\pi^*$ is just a little bit higher in energy for the hcp adsorption.

For the p_z orbital we can see that the 5σ is splitted in the case of CO at the step bottom, due to the interaction with more than three metal atoms. Compared with the atop adsorption, the 4σ and 5σ are at the same level but somehow the 3σ
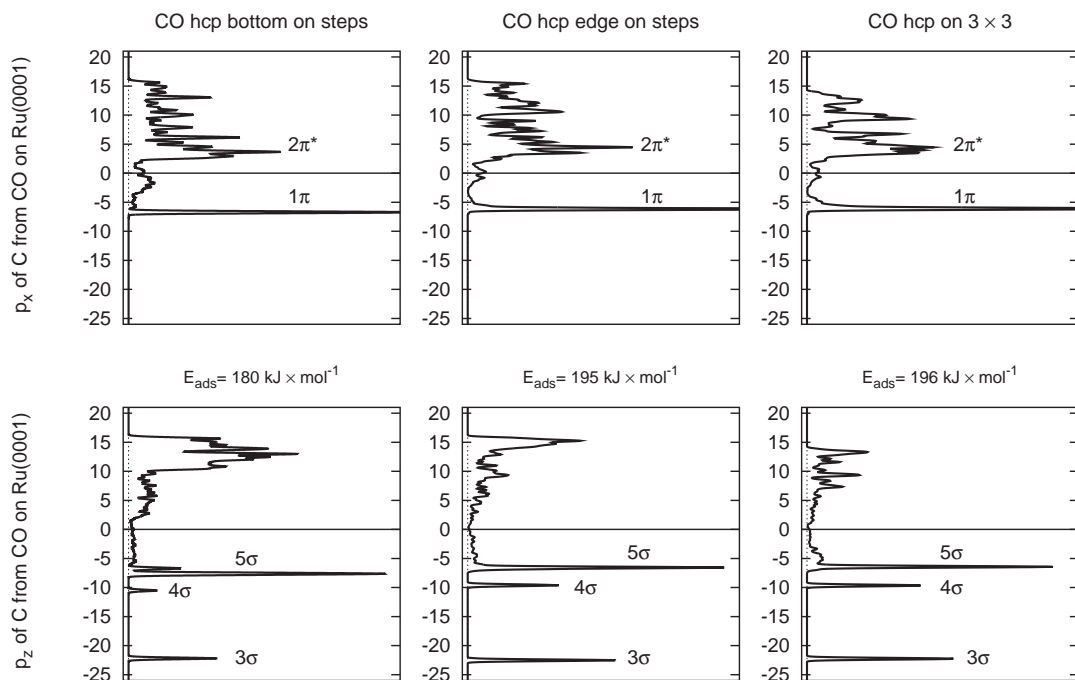
Figure 7.3: DOS diagrams for p_x and p_z orbitals of the C atom from the CO molecule adsorbed hcp sites.

is higher in energy for the hcp adsorption. This could explain the (small) difference in the adsorption energy for atop and hcp adsorption sites.

§7.3 High coverage hydrogen on Ru(0001) surface

The H atom being small, the compression of the adsorbed layer has to be the easiest compared to any other atom. In this section, we will show that, if at lower coverage the adsorption sites are well defined, at higher coverage the H atoms are not sitting on the surface in well-defined sites.

We calculate the adsorption of H atoms in 2×2 unit cells for 25%–300% coverage, in each case for several different structures. The energies of those structures can be seen in Figure 7.4.

For 25% coverage, we calculate the adsorption of H in fcc and hcp three-fold hollow sites, as well as atop and bridge. H subsurface is unstable at this coverage. The fcc
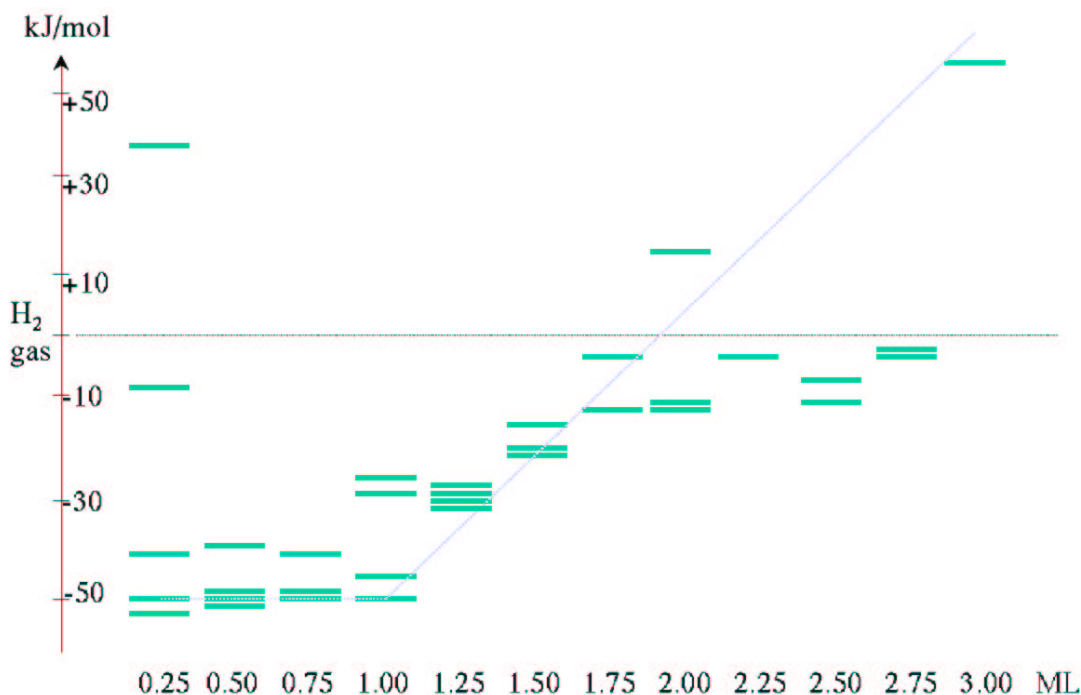
Figure 7.4: Energy diagram (in kJ×mol⁻¹ per H atom relative to $\frac{1}{2}H_2$) for H adsorption on Ru(0001) at several coverages (1 ML = 100% coverage = 4 H atoms per 2×2 unit cell).

site gives an adsorption energy of -53 kJ×mol⁻¹ while the hcp site give 50 kJ×mol⁻¹. The bridge site is less stable, with an adsorption energy of -41 kJ×mol⁻¹ and the atop site is the most unstable one with an adsorption energy of -9 kJ×mol⁻¹. See in Table 7.3 how this will change later on.

For 50%, 75% and 100% coverage, the adsorption of 2, 3 or 4 H atoms in the 2×2 unit cell did not change too much the adsorption energies for the fcc and hcp sites. The lateral interaction at this coverage is still low. For the mixed cases, H fcc and H hcp, when the H atoms share one metal atom (are "far" apart), the adsorption energy is still not affected, and when they share two metal atoms (are "close"), the adsorption energy drops.

The geometries of H atoms adsorbed on the Ru(0001) surface change little up to 100% coverage, except the close adsorption case. The usual Ru–H bond lengths are in between 1.85 and 1.90 Å, for H atoms adsorbed in hollow sites (fcc and hcp). If 2

coverage	sites						adsorption energy	Observations
	f	h	b	t	s	p	$(kJ\times mol^{-1})$	
25%	1	0	0	0	0	0	-53	
	0	1	0	0	0	0	-50	
	0	0	1	0	0	0	-41	
	0	0	0	1	0	0	-9	
	0	0	0	0	1	0	$+37$	Octahedral site
	0	0	0	0	1	0	$+60$	Tetrahedral site 1-3
	0	0	0	0	1	0	$+96$	Tetrahedral site 3-1
50%	2	0	0	0	0	0	-51	
	0	2	0	0	0	0	-48	
	1	1	0	0	0	0	-52	"far"
	1	1	0	0	0	0	-39	"close"
75%	3	0	0	0	0	0	-51	
	0	3	0	0	0	0	-48	
	2	1	0	0	0	0	-42	
	1	2	0	0	0	0	-42	
100%	4	0	0	0	0	0	-51	
	0	4	0	0	0	0	-47	
	3	1	0	0	0	0	-29	
	1	3	0	0	0	0	-26	
125%	4	1	0	0	0	0	-31	
	1	4	0	0	0	0	-29	
	3	0	2	0	0	0	-30	
	0	2	3	0	0	0	-28	

Table 7.3: Adsorption energies for H on Ru(0001) at different coverages. f stands for fcc hollow site, h stands for hcp hollow site, b is bridge site, t is atop site, s is subsurface adsorption site, and p is H_2 molecule in the second layer. For 25% coverages, the subsurface H can sit in an octahedral site (under a fcc hollow site), in a tetrahedral site formed by 3 metal atoms from the first layer and 1 metal atom from the second layer (under an hcp hollow site) or in a tetrahedral site formed by 1 metal atom from the first layer and 3 metal atoms from the second layer (under atop site).

coverage	sites						adsorption energy	Observations
	f	h	b	t	s	p	(kJ×mol^{-1})	
150%	2	2	2	0	0	0	−21	
	1	1	4	0	0	0	−15	
	2	1	2	1	0	0	−20	
	0	0	6	0	0	0	−20	
175%	3	1	3	0	0	0	−5	
	1	3	3	0	0	0	−5	
	3	0	2	2	0	0	−14	
200%	4	4	0	0	0	0	+11	
	4	0	0	4	0	0	−13	
	0	4	0	4	0	0	−14	
225%	1	1	3	4	0	0	−5	
250%	4	0	0	3	1	1	−8	s = octahedral
	1	1	2	2	0	2	−12	
275%	2	1	2	4	0	1	−4	
	1	1	3	4	0	1	−5	
300%	0	0	12	0	0	0	+56	

Table 7.3: (continuation)

H atoms will share two metal atoms on the surface they will be displaced from the center or the hollow site, and the three bonds with the metal will be one shorter, around 1.70–1.76 Å, and two longer, around 1.95–2.05 Å. For the bridge site, the adsorbed H atom will have Ru–H bonds lengths of 1.75–1.80 Å, while the atop site will have Ru–H distances around 1.60 Å.

In Figure 7.5, one can see the difference in between a far adsorption or a close adsorption of two H atoms. For the far adsorption. the H atoms share one metal atom on the surface. The geometries are not affected. For the close adsorption, the H atoms share two metal atoms on the surface. The geometries are affected. The H fcc have a shorter Ru–H distance of 1.81 Å, and two long ones of 1.96 Å. The H hcp have a short distance 1.73 Å, and two long ones of 1.98 Å.

At 100% coverages, the mixed adsorption of H is shown in Figure 7.6. The "Y"

<div align="center">a.   b.</div>
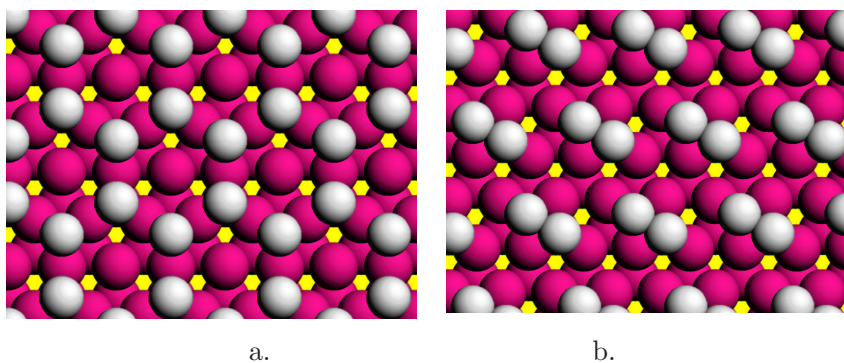
Figure 7.5: H adsorption at 50% coverage: 1 H fcc + 1 H hcp, far (a) and close (b) adsorption (sharing one or two metal atoms on the surface).

like structure formed by an atom in a hollow site and three others in the other kind of hollow site is a structure that we will see also at higher coverages. The H adsorbed in the middle is still symmetric with a Ru–H bond of 1.85 Å. The other three atoms are perturbed, with a short bond around 1.72–1.75 Å and two long ones around 2.03–2.04 Å.

<div align="center">a.   b.</div>
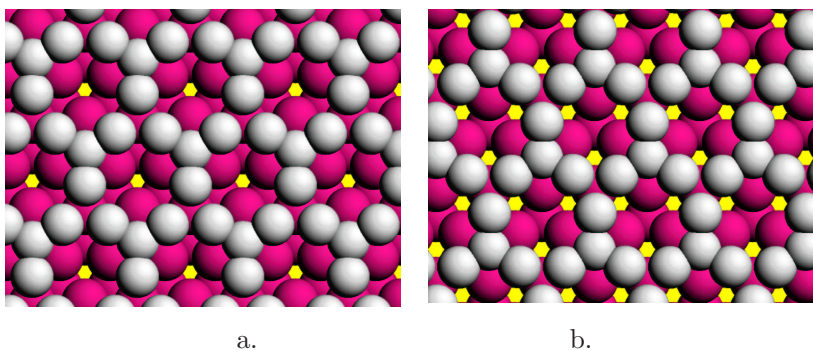
Figure 7.6: H adsorption at 100% coverage: 3 H fcc + 1 H hcp (a), 1 H fcc + 3 H hcp (b).

Going over the classical 1 ML, for 125% coverage, we have to accommodate 5 H atoms in the same unit cell. Jachimowski et al. [8] have shown that 1 ML of H on Ru(0001) can contain up to 142% coverage. Several structures possible are shown in

Figure 7.7. (a) and (b) are similar with the previous "Y" like structure with an extra atom adsorbed in a nearby empty site. (c) and (d) are looking similar with 4 H fcc and 4 H hcp respectively, where one H atom is replaced with a pair of H atoms in bridge sites competing for the hollow site. The H atoms from hollow sites are little affected, with 2 normal Ru–H bonds and a slightly longer one (1.94–2.07 Å). The H atoms from the bridge sites have also normal bonds (for a bridge site) of 1.78 Å. The H_{bridge}–H_{bridge} separation is 1.75 Å.
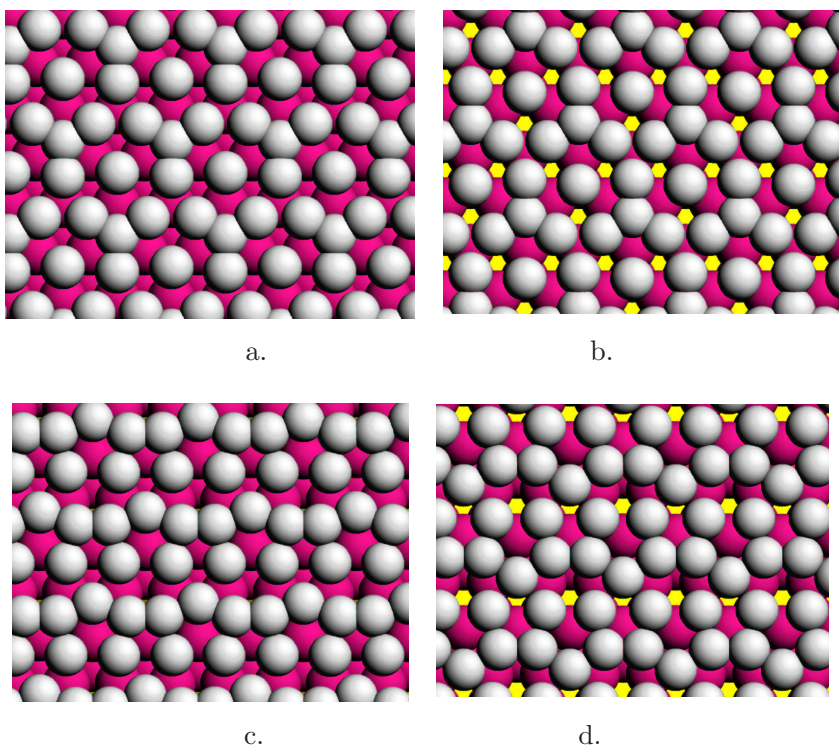
Figure 7.7: H adsorption at 125% coverage: 4 H fcc + 1 H hcp (a), 1 H fcc + 4 H hcp (b), 3 H fcc + 2 H bridge (c) and 3 H hcp + 2 H bridge (d).

At 150% coverage, the bridge site becomes the most populated site. 6 H atoms can sit in the same unit cell. The configuration with 2 H fcc + 2 H hcp + 2 H bridge derived from two situations: 4 H fcc + 2 H hcp and 2 H fcc + 4 H hcp, where two H fcc (hcp) are going to be bridge in a end symmetric situation. For this coverage, still the adsorbed H is more stable than the gas phase one.

In Figure 7.8 four structures for H adsorption at 150% coverage are presented. In (a), the H in fcc and the one in hcp have similar bond lengths of 1.80 Å, and two of 1.90 Å. The H in bridge sites has two bonds in between 1.78–1.80 Å. In (b), the H in hollow sites has a short bond of 1.75–1.77 Å, and 2 long ones of 1.94 Å. The (c) structure is highly asymmetric. All H atoms in hollow sites have a short and two long Ru–H bonds, the H atoms in bridge sites also are slightly distorted. The H atop have bond of 1.61 Å. The (d) structure is more symmetric, with three H atoms competing for the same fcc site and three H atoms competing for the same hcp site. Their H–Ru distances are 1.78–1.80 Å. This situation, of three H bridge atoms around a hollow site (like a "Δ") is to be seen also at higher coverage.

a.

b.

c.

d.
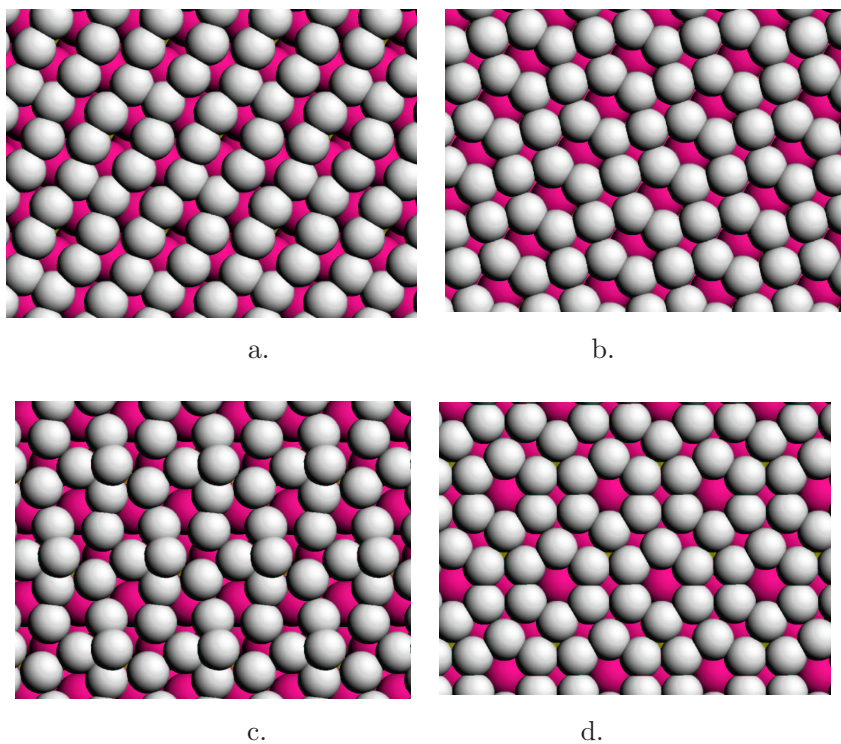
Figure 7.8: H adsorption at 150% coverage: 1 H fcc + 1 H hcp + 4 H bridge (a), 2 H fcc + 2 H hcp + 2 H bridge (b), 2 H fcc + 1 H hcp + 2 H bridge + 1 H atop (c) and 6 H bridge (d).

At 175% coverage, 7 H atoms are accommodated in the unit cell. Two structures

are presented in Figure 7.9. (a) is composed from a "Y" structure and a "Δ". A similar structure (not shown) is obtained simply replacing the fcc site with the hcp one. For the (b) structure, the H atoms in hollow sites have 2 short bonds of 1.77–1.82 Å and a long bond of 2.06–2.10 Å. The H adsorbed in bridge sites has bonds of 1.74–1.81 Å and the H in atop sites has Ru–H bond lengths of 1.62 Å. The H_{fcc}–H_{atop} and H_{atop}–H_{bridge} separations are in between 1.56 and 1.62 Å.

a.   b.
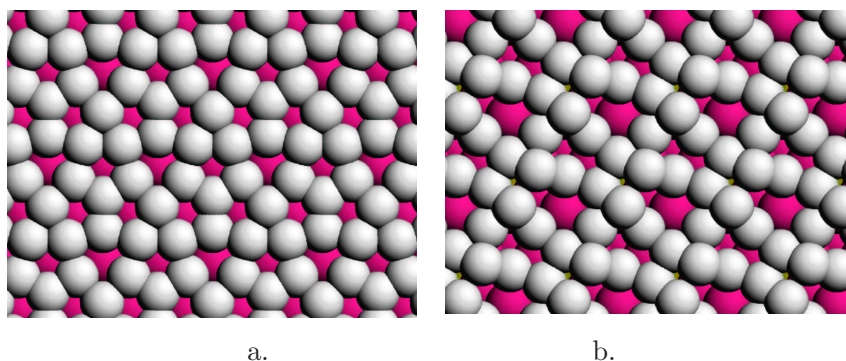
Figure 7.9: H adsorption at 175% coverage: 3 H fcc + 1 H hcp + 3 H bridge (a) and 3 H fcc + 2 H bridge + 2 H atop (b). The 1 H fcc + 3 H hcp + 3 H bridge configuration is similar with the first case.

At 200% coverage, 8 atoms have to stay in the same unit cell. 4 H fcc + 4 H hcp is less stable than the H_2 in gas phase with 11 kJ×mol^{-1}. Nevertheless, if 4 H are going atop then we have a stable situation: 4 H fcc + 4 H atop (-13 kJ×mol^{-1}) or 4 H hcp + 4 H atop (-14 kJ×mol^{-1}).

At 250% coverage, the adsorption energies start to change sign, so the monolayer picture starts to collapse. H_2 molecules start to form in the second monolayer, or H_2 molecules standing with only one H interacting with the surfaces, or subsurface H (in the octahedral site), or a mixture of those situations, in order to lower the energy.

In Figure 7.10 one can see two structures like that. (a) consists of 4 H atoms in fcc sites, 1 H atom in a octahedral subsurface site, 3 H atoms atop and above the other atop site is the H_2 molecule. The subsurface H atom has bonds of 1.97 Å with the Ru atom from the first layer and 1.92 Å with the Ru atoms from the second layer. The H–H bond length in the H_2 molecule is 0.75 Å. The separations between the Ru atom and each of the two H atoms from H_2 are 3.70 and 4.19 Å, the H_2 molecule being tilted. (b) consists in less atoms in the first layer and two H_2 molecules on the

second layer. The H adsorbed in fcc site is slightly disturbed, the other H atoms have typical bond lengths. The H–H in H_2 is 0.75 Å, and the Ru–H_{H_2} distance is 4.16 Å for one molecules and 4.32, 4.60 Å for the other one.

a.   b.
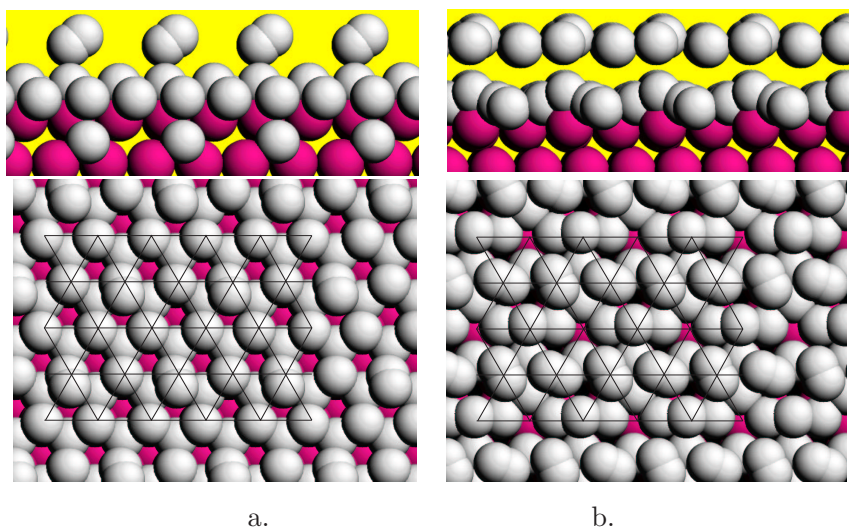
Figure 7.10: H adsorption at 250% coverage: 4 H fcc + 3 H atop + 1 H subsurface + 1 H_2 (a) and 1 H fcc + 2 H hcp + 2 H bridge + 1 H atop + 2 H_2 (b). Top and side view.

The 275% coverage is also characterized by the presence of the second H layer, but this time the H_2 molecules are perpendicular to the surface, see Figure 7.11. For the (a) structure the H–H bond is 0.75 Å, and the Ru–H_{H_2} separation is 3.99 Å. The H_{H_2}–H_{atop} is 2.38 Å. There are 5 H atoms adsorbed atop on only 4 metal atoms! One Ru atom is shared by two H atoms, the Ru–H bond length is 1.92 Å, longer that for the other atop H atoms. The (b) structure is characterized by a Ru–H_{H_2} separation of 3.59 Å, and a H_{H_2}–H_{atop} of 2.04 Å. The rest of the bonds are in the mentioned limits.

In the case of 300% coverage, 1 ML of H atoms, all adsorbed in bridge sites (all bridge sites occupied) is less stable than the H_2 in gas phase with +56 kJ×mol^{-1}!

As we can see from Figure 7.4, the adsorption energy of H atom does not change up to 100% coverage. This is due to the weak lateral interaction of the H atom. Calculations for adsorbed H in $\sqrt{3} \times \sqrt{3}$ and 3×3 structures have been performed, but the adsorption energies and the geometry are similar with the 2×2 case.

a.   b.
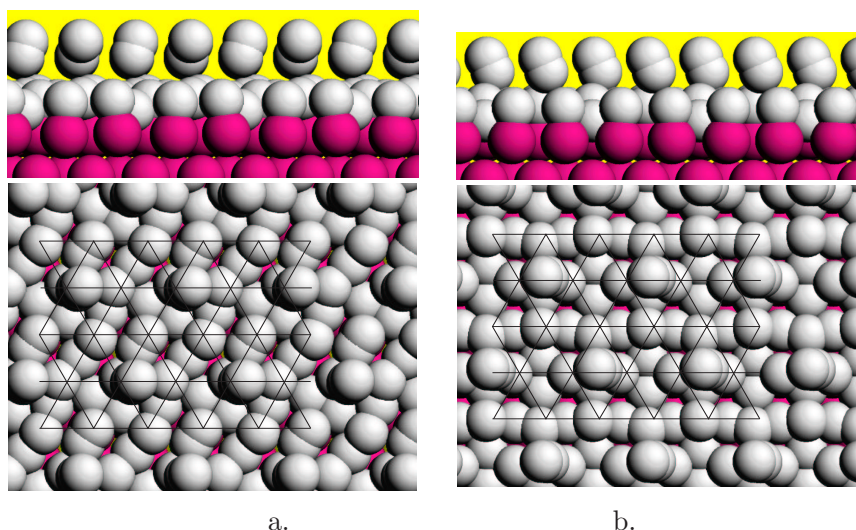
Figure 7.11: H adsorption at 275% coverage: 1 H fcc + 1 H atop + 2 H bridge + 5 H atop + 1 H_2 (a) and 2 H fcc + 1 H hcp + 2 H bridge + 4 H atop + 1 H_2 (b). Top and side view.

For coverages up to 150%, H adsorption is still stable so such configurations should be stable if the compressing of the H layer is made. However, the dissociation of H_2 cannot lead to such structures due to the lack of empty sites for the dissociation reaction.

Up to 200% coverage, the adsorption energies are still under zero, but close to it. Those structures can be stable only at high pressures. For coverages up to 300%, we see a deviation of the linear increase if the adsorption energies due to the formation of the second layer and to subsurface adsorption.

§7.4 Hydrogen–carbon monoxide coadsorption on the Ru(0001) surface

Concerning the H coadsorption we study in a 2×2 unit cell, the interaction of 1 CO molecule with 1, 3 and 4 H atoms, in several different adsorption sites, corresponding to a 25% coverage of CO and 25%, 75% and 100% coverage of H, respectively. See Figure 7.12 for the adsorption energies.

For the interaction of CO with 1 H atom, we consider the cases when CO is
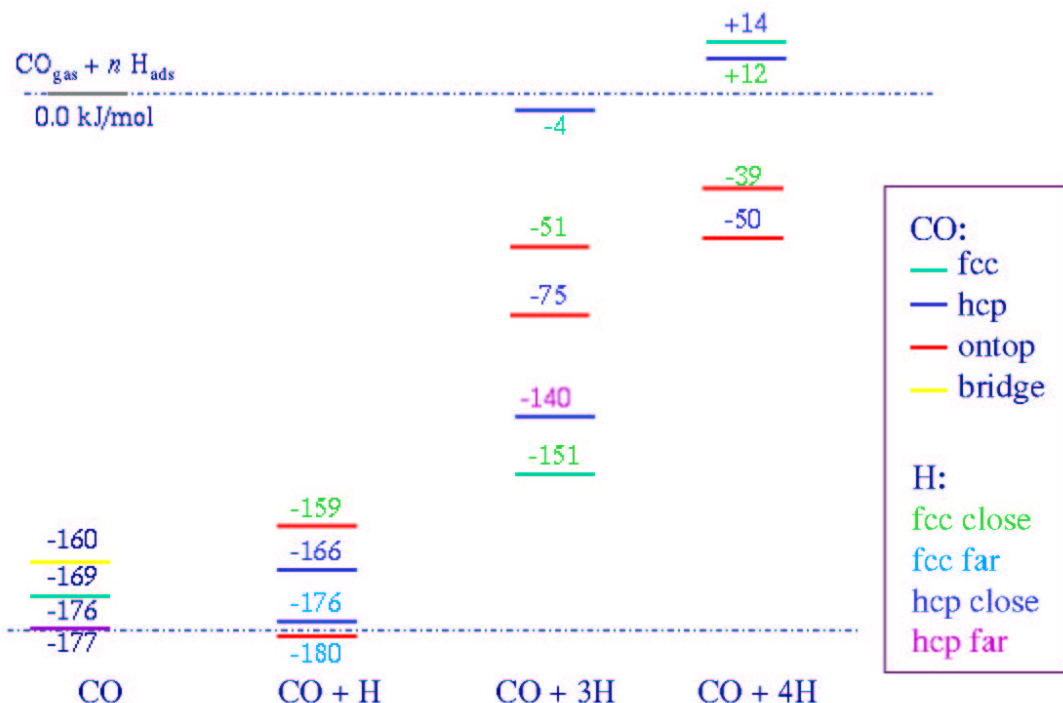
Figure 7.12: Energy diagram (in kJ×mol^{-1}) with respect to H$_2$ and CO in gas phase, for H and CO coadsorption.

adsorbed atop or hcp. For the atop adsorption of CO, the H atom was adsorbed in fcc sites, close to CO (sharing one metal atom) or far (without sharing metal atoms). The CO adsorption energy is -179 kJ×mol^{-1} for the far adsorption and -159 kJ×mol^{-1} for the close adsorption. In this last case, the CO molecule is tilted.

For the CO adsorbed in hcp site we consider three adsorption sites, similar with the CH$_x$ and H coadsorption [9]: an hcp site (where H and CO share one metal atom on the surface), a close fcc site (where the CO and the H share two metal atoms) and a far fcc site (where CO and H share one metal atom and they are opposite). The adsorption energies are -176 kJ×mol^{-1} for the far situation and -166 kJ×mol^{-1} for the same type of site adsorption. The situation where the coadsorbed species were to close, stabilize by the translation of CO to a near top site.

Coadsorption of a CO molecule with 3 H atoms gives a total coverage of 100%. For the CO adsorbed atop, four different adsorption sites were considered for H

adsorption. The first one is with 2 H atoms in close fcc site (one metal atom shared on the surface) and 1 H atom in a far fcc site (no share of metal atoms on the surface). The second is when all three H atoms are in close fcc sites. The next two cases are similar with the first two ones, except that instead of fcc sites, the H atoms are in hcp sites. The adsorption energies are -51 kJ$\times$mol^{-1} for CO atop and 3 H close fcc and -75 kJ$\times$mol^{-1} for CO atop and 3 H close hcp. The other 2 situations evolve in structures with CO adsorbed in the same site as the three H atoms.

For the CO adsorbed hcp, the H atoms can adsorb in the other hcp sites. An other way is in fcc sites, 2 close and 1 far, or 3 close. The adsorption energies are -139 kJ$\times$mol^{-1} for the hcp adsorption of the three H atoms and -4 kJ$\times$mol^{-1} for the close fcc adsorption. The case when 2 H atoms are in a close fcc site and 1 H is in a far fcc site lead to a migration of the CO molecule to the empty fcc site.

For the CO adsorbed fcc, the H atoms where adsorbed on the other fcc site. The adsorption energy is -151 kJ$\times$mol^{-1}.

For the coadsorption of 1 CO molecule and 4 H atoms on a 2×2 unit cell, the total coverage is 125%. This may look strange but evidence that an H monolayer on metal surfaces can be compressed exists, both from experiments [10] and from theory (see previous section). Four cases were considered. CO atop with 4 H in fcc sites, CO atop with 4 H in hcp sites, CO hcp with 4 H in fcc sites and CO fcc with 4 H in hcp sites. The adsorption energy is -38 kJ$\times$mol^{-1}, -51 kJ$\times$mol^{-1}, $+13$ kJ$\times$mol^{-1} and $+14$ kJ$\times$mol^{-1}, respectively. The positive value means that the CO is more stable in the gas phase, does not mean that it is not a local minima.

The C–O bond length is not changed by the H coadsorption. The C–Ru bond lengths are also very little affected by the coadsorption. The O–C–Ru and the Ru–C–Ru angles are more affected, but in general with less than 2–3°. H is the most affected by the coadsorption with CO. The H–Ru bonds lengths are little affected only at low coverage of H (25% CO + 25% H), while at higher coverage of H, the three bonds are no longer equivalent, one is getting shorter than 1.9 Å and the other two are longer than 2.1 Å. The Ru–H–Ru angles are also little affected at lower coverage (less than 5°) and more affected at higher H coverage ($+6$ to -19°).

In order to analyze island formation we calculated for the *CO + 3 H* and *CO + 4 H* systems the following parameters: $x = a - b - c - n * d/2$ and $y = e - b - c + f - b - n * d/2$, where:

- a = energy of CO and n H on Ru(0001)

- b = energy of Ru(0001) slab

- c = energy of CO gas

- d = energy of H_2 gas

- e = energy of CO on Ru(0001)

- f = energy of n H on Ru(0001)

- x = adsorption energy of CO and n H on Ru(0001)

- y = adsorption energy of CO + adsorption energy of n H (all on Ru(0001))

n can be here 3 or 4 (hydrogen atoms). Now, if $|x| < |y|$ we have islands formation and if $|x| > |y|$ we have *no* islands formation. For all the 12 tests, calculations described before we found that islands formation is favorable. The closest situation (11 kJ×mol^{-1} differences between x and y) is for CO fcc + 3 H fcc system. These results, that H and CO prefer to make islands, support the conclusion of White et al. [11] that H and CO form segregated structures.

DOS diagrams [12] (see next section) for the CO and H coadsorption were also studied and the CO ability to strongly adsorb even on a fully covered surface with hydrogen was explained by the fact that the Ru atom where CO will bind is pushed upwards and by doing that the electrons donated by the H atoms, which initially occupied the antibonding d-band regime deplete this. Therefore, Ru is able to form a bond with the CO, at the cost of weakening its bonds with the other Ru atoms.

§7.5   Activated non-dissociative CO chemisorption on the fully hydrogenated Ru(0001) surface

From the first section of this chapter, one can see that the chemisorption of CO on bare Ruthenium surfaces is a non-activated process. The sticking probability reported in the literature [12] is close to 90%. This section is dealing with the activated non–dissociative CO chemisorption on a fully hydrogenated Ru(0001) surface.

The incoming CO, from the gas phase, can be adsorbed on 2 different sites for each of the two fully hydrogen covered Ru(0001) surfaces. Those four situations are displayed in Table 7.4 together with the adsorption energies. The adsorption energies of the CO in the non–occupied three-fold site is less stable compared to the top site.

An important contribution to the difference between the adsorption energy of the CO atop on the two different hydrogenated Ru(0001) surfaces is their relative stability: the surface with H atoms adsorbed in fcc sites is 18 kJ×mol^{-1} (per 4 H atoms) more stable.

system	CO atop (no H)	CO hcp (no H)	CO atop +4 H fcc	CO hcp +4 H fcc	CO atop +4 H hcp	CO fcc +4 H hcp
energy (kJ×mol^{-1})	-177	-176	-38	$+13$	-51	$+14$
C–O (Å)	1.17	1.19	1.16	1.19	1.16	1.19
Ru–C (Å)	1.90	2.15	1.89	2.17	1.87	2.17

Table 7.4: The adsorption energy (in kJ×mol^{-1}) of CO on the Ru(0001) surface saturated with and without hydrogen in different adsorption sites.

If CO is adsorbed atop, the three neighboring H atoms will slightly shift (see Figure 7.13, top). For H adsorbed in the fcc (hcp) site, two Ru–H bonds of 1.83 (1.83) Å and one of 1.87 (1.86) Å are formed. One H will be not affected because of the symmetries, the respective values for the Ru-H bond lengths are 1.89 Å for H fcc and 1.88 Å for H hcp.

In the case that CO is adsorbed in the three-fold hollow sites, three H atoms will undergo a noticeable displacement away from CO (see Figure 7.13, bottom). So, for CO adsorbed hcp (fcc) and 4 H adsorbed fcc (hcp) two Ru–H bonds are 2.22 Å (2.16 Å), one 1.63 Å (1.65 Å) for the three shifted H atoms and 1.89 Å (1.88 Å) for the other H atom. The Table 7.4 shows the bond distances for C–O and C–Ru in those four cases together with the bond distances for CO adsorption on bare Ru surface.

In the case of H coadsorbed fcc, atop adsorption of CO drops the interaction energy considerably (see Table 7.4) to -38 kJ×mol^{-1}. Adsorption of CO on the hcp site becomes weakly repulsive. When H is coadsorbed in the less favorable site hcp, adsorption of CO atop the adsorption energy decreases less with -51 kJ×mol^{-1}. However the total adsorption energy including the 4 H atoms differs only by 11.5 kJ×mol^{-1} with the first case. When H is coadsorbed in hcp sites, CO adsorbed in the fcc site becomes also weakly bound. This state is destabilized compared to the analogous first situation.
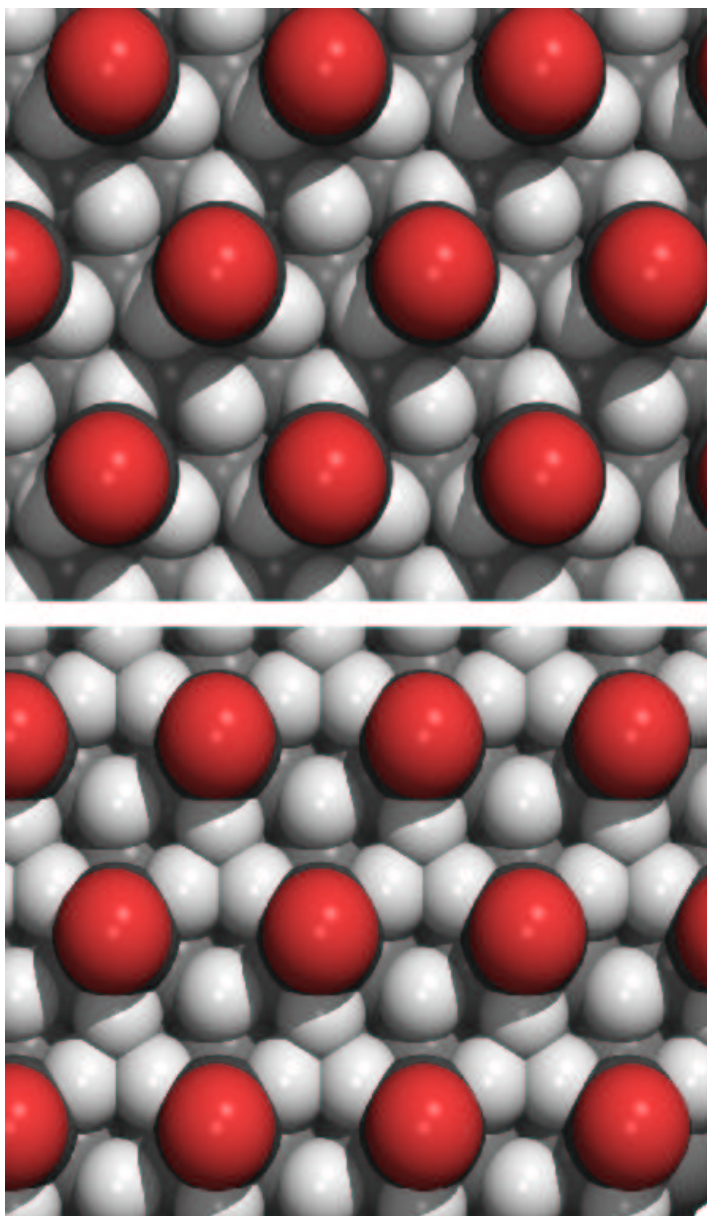
Figure 7.13: The topology of CO adsorbed on a fully hydrogenated surface of Ru(0001). The top part represents CO molecule adsorbed atop site (25% coverage) together with H atoms adsorbed on fcc sites (100% coverage). The bottom part represents the topology of CO molecule adsorbed on the hcp site (25% coverage) together with H atoms adsorbed on fcc sites (100% coverage).

As we will see later, H and CO sharing a metal atom will have repulsive interactions, which are reduced by the H atoms moving away from CO. A reduced steric hindrance is obtained for the CO molecule adsorbed in the top site, the H atoms are pushed toward bridge sites, and while for CO adsorbed in the hcp site the H atoms are displaced toward the less stable atop sites. (The adsorption energy for H atop is -9 kJ×mol^{-1} while for H bridge it is -41 kJ×mol^{-1}.) In addition, when CO is in three-fold sites the H atoms on the surface are more compressed (see Figures 1, top and bottom) as the CO–H distance can only be increased at the cost of significant repulsive interaction between the H atoms.

In conclusion the atop sites are the preferred sites for CO adsorption on the hydrogenated Ru(0001) surface.

For the two most favorable cases on the hydrogen-covered surface, we investigated the reaction path and the origin of the adsorption barrier. On the bare Ruthenium surface, CO adsorption is known to be non-activated [13, 14]. Some points on the potential energy surface were chosen by fixing the distance between the carbon atom and the surface plane (practically the z coordinate of the C atom was not allowed to change). The TS is refined by performing a quasi-Newton optimization of the geometry based on the forces and not on the energy. When needed, extra points are computed on order to get a smoother curve.

Two situations were considered during the adsorption of CO:

- adiabatic reaction, the CO motion is slow enough to allow the metal surface to fully relax,

- non–adiabatic reaction, the CO motion is so fast that the metal atoms cannot relax, the positions of the surface metal atoms are frozen while the H atoms are free.

In all these calculations, CO remains perpendicular with respect to the surface plane and above its adsorption site. For both approaches, a similar barrier around 24 kJ×mol^{-1} is found (see Figure 7.14). The major difference between the two different situations (e.g. the adiabatic and non–adiabatic cases) is that, in the case where the CO approaches slowly, the Ru atom underneath the CO molecule can move upward to initiate the bond. This vertical displacement of the Ru atom is about 0.4 Å for H adsorbed fcc and 0.5 Å for H atom adsorbed hcp in the minimum of the potential energy surface, but the displacement is much larger near the transition state with 0.7 Å for H adsorbed fcc and 0.8 Å for H adsorbed hcp. If the metal atoms

are frozen, the H atoms will be moved away from the Ru atom bound to CO. Long Ru–H distances are 2.15 Å (if H fcc) or 2.18 Å (if H hcp), short Ru–H distances are 1.79 Å (if H fcc) or 1.78 Å (if H hcp) and the normal Ru–H distances are 1.89 Å (if H fcc) or 1.88 Å (if H hcp).

Therefore, even if the heights of the activation barriers are similar for the frozen and relaxed surfaces, the corresponding transition states have rather different geometries. Moreover, the minima of the two interaction potentials are completely different, because of the different model used.

For the *CO atop + 4 H fcc* system the transition state has also been searched with the Nudged Elastic Band method and the same barrier height was found. Two additional points was calculated at 2.63 and 2.75 Å with quasi Newton technique in order to remove the cusp of the curve.

The influence of the C–O bond orientation with respect to the surface normal, has been checked by tilting the CO molecule in the transition state. For each calculation, the z coordinate of the C atom and the x and y coordinates of O are frozen once the molecule is tilted. The differences are rather small for angles between 0° and 35°.

The projected DOS diagrams (see Figure 7.15) for the CO adsorption on the bare and hydrogenated Ru(0001) surfaces bring us the to following conclusions about the quantum chemical basis for activated adsorption and destabilization of CO by the hydrogen.

Firstly, the σ type interactions between the CO 4σ and 5σ with Ru on the clean surface are considered. The downwards shift of 5σ and the broadening of the metal d-band agree with the conventional picture of a bonding occupied 5σ type surface orbital and partially occupied antibonding 5d type orbitals (see Figure 7.15, panels 3, 5, 7).

The π type interactions for the CO 1π and $2\pi^*$ with Ru on the clean surface are significant (see Figure 7.15, panels 5 and 9). The d–band broadening indicates a small bonding component under the Fermi level (ϵ_F). The increased distance between the maximum of the $2\pi^*$ and 1π densities, compared to a free CO molecule, agrees with the antibonding nature of the $2\pi^*$ interaction above ϵ_F. The adsorption of CO on a bare Ru(0001) surface is not activated as two opposite phenomena occur simultaneously: the 5σ–Ru-d$_{(3z^2-r^2)}$ interaction is close to a 4 electrons interaction which should give at the beginning two filled levels, bonding and antibonding, resulting in a repulsion. Only when the interaction is strong enough to push the antibonding level above ϵ_F, the system is stabilized. At the same time, the CO$_{5\sigma}$–Ru-s interaction is
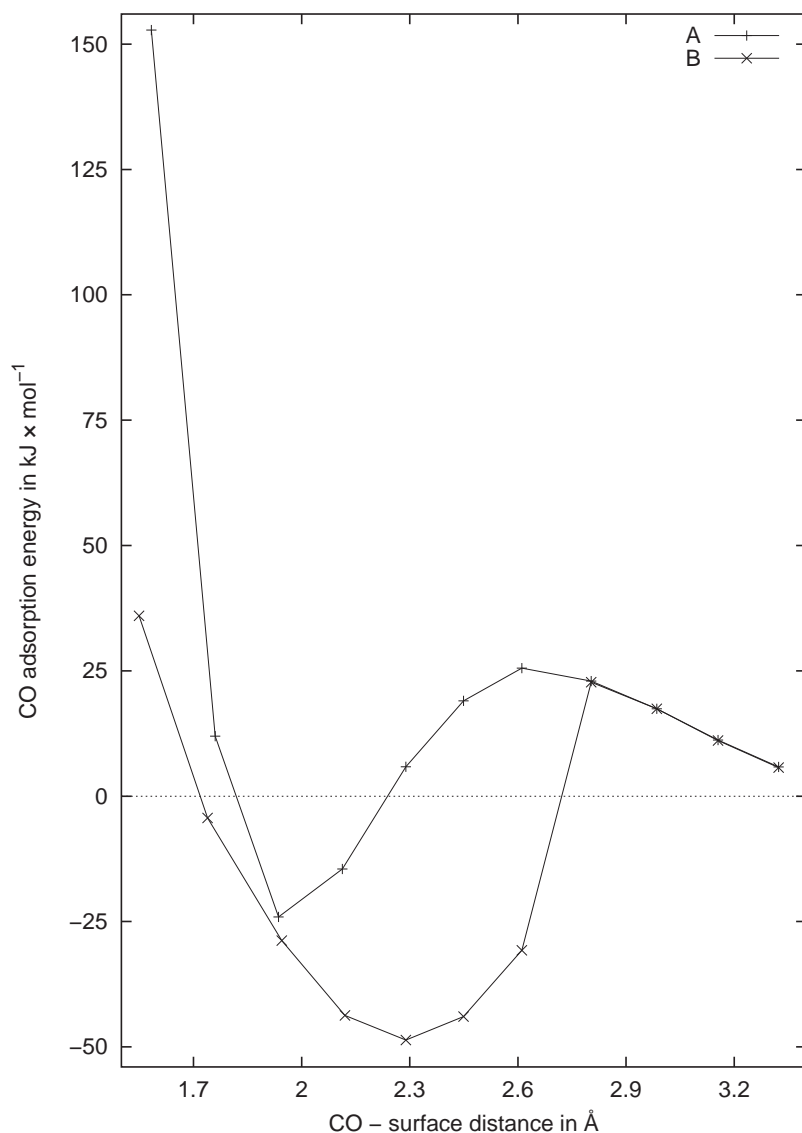
Figure 7.14: The calculated potential energy surface for CO adsorption on 100% hydrogen covered Ru(0001) surface. (A) CO atop + 4H fcc without relaxation of the surface and (B) CO atop + 4H fcc with relaxation of the surface. The y axis is the adsorption energy in kJ×mol^{-1}. The x axis is the distance in Å from the C atom of CO to the surface (e.g. the plane of the Ru atoms which are not relaxing upwards).
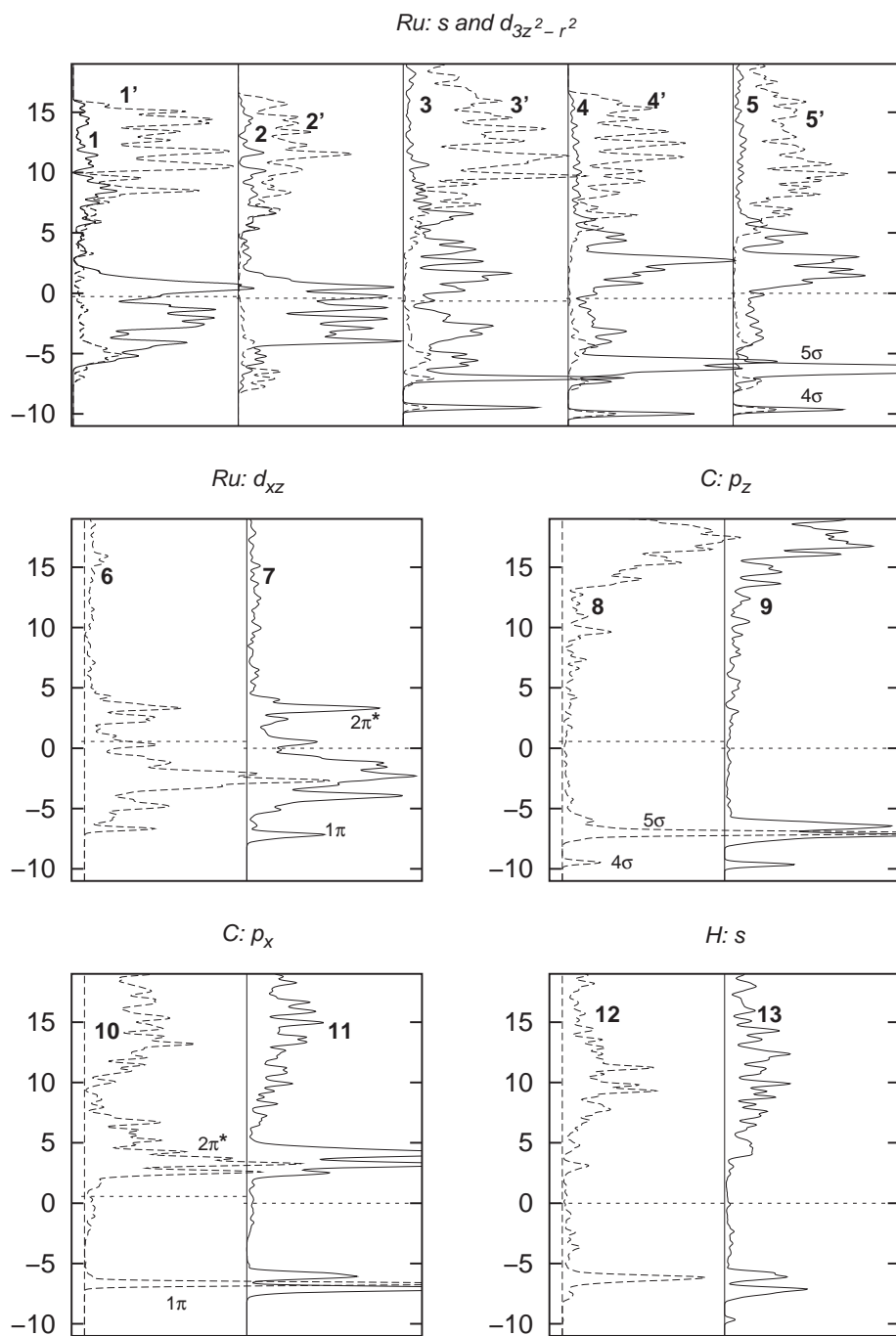
Figure 7.15: The DOS diagrams for s, $d_{3z^2-r^2}$, and d_{xz} atomic orbitals of Ru, p_z and p_x atomic orbitals of C and s atomic orbital of H.

Figure 7.15: (continuation)

(1) – Ru-$d_{3z^2-r^2}$ orbital DOS for the bare Ru(0001) surface.

(1') – Ru-s orbital DOS for the bare Ru(0001) surface.

(2) – Ru-$d_{3z^2-r^2}$ orbital DOS for the Ru atom on hydrogenated surface.

(2') – Ru-s orbital DOS for the Ru atom on hydrogenated surface. (No CO is present.)

(3) – Ru-$d_{3z^2-r^2}$ orbital DOS for the Ru atom where CO molecule is adsorbed.

(3') – Ru-s orbital DOS for the Ru atom where CO molecule is adsorbed.

(4) – Ru-$d_{3z^2-r^2}$ orbital DOS for the Ru atom where CO molecule is adsorbed in presence of 4 H atoms adsorbed. The surface is frozen.

(4') – Ru-s orbital DOS for the Ru atom where CO molecule is adsorbed in presence of H atoms adsorbed in fcc sites. The surface is frozen.

(5) – Ru-$d_{3z^2-r^2}$ orbital DOS for the Ru atom where CO molecule is adsorbed in presence of 4 H atoms adsorbed.

(5') – Ru-s orbital DOS for the Ru atom where CO molecule is adsorbed in presence of H atoms adsorbed in fcc sites.

(6) – Ru-d_{xz} orbital DOS for the Ru atom where CO molecule is adsorbed.

(7) – Ru-d_{xz} orbital DOS for the Ru atom where CO molecule is adsorbed in presence of 4 H atoms adsorbed in fcc sites.

(8) – C_{p_z} orbital DOS for the C atom in CO adsorbed atop.

(9) – C_{p_z} orbital DOS for the C atom in CO adsorbed atop, in presence of H atoms adsorbed in fcc sites. (10) – C_{p_x} orbital DOS for the C atom in CO adsorbed atop.

(11) – C_{p_x} orbital DOS for the C atom in CO adsorbed atop, in presence of H atoms adsorbed in fcc sites.

(12) – H_s orbital DOS for the H atom **far** from CO (the H atom does not share a Ru surface atom with CO).

(13) – H_s orbital DOS for the H atom **close** to CO (the H atom share the Ru surface atom under CO) from CO atop and 4 H fcc.

The y axis is the energy in eV. The x axis is in arbitrary units. Fermi level is at 0.0 eV for the CO + 4 H fcc system. For the other systems the lowest energy level was equalized to that in the CO + 4 H fcc system.

similar to a two electrons interaction (Ru-s almost empty), which is bonding along the whole adsorption path and compensates the barrier arising from the CO-5σ–Ru-

$d_{3z^2-r^2}$ antibonding component. The Ru-p_z behaves like the Ru-s but its influence is smaller.

In the presence of only adsorbed hydrogen, the metal $d_{3z^2-r^2}$ orbital band is narrower. Indeed the bottom of the $d_{3z^2-r^2}$ band is bonding for the Ru atoms and mixed with the s band. Once H is adsorbed, the s band interacts mainly with the H atoms (see Figure 7.15, panel 3, 11, the PDOS 11 is similar to the PDOS for H atoms adsorbed without CO, the only noticeable difference is the absence of the tiny peak around -7.5 eV). The s band is essentially involved in the bond with H and stabilized while the $d_{3z^2-r^2}$ band is destabilized and narrowed. The other components of the d band (not shown) are directly involved in the Ru–H bond and consequently get a peak where is he maximum of the H PDOS.

With H present on the Ru(0001) surface, for adsorbed CO, we see a small effect on the 4σ while it is more important for the 5σ interaction (see Figure 7.15, panels 7, 8). One has to remember that CO attracts the Ru atom, which moves upwards the surface. This is a direct consequence of the Ru–Ru bonds weakening from both CO and H binding. With H and CO co–adsorbed, the middle of the $d_{3z^2-r^2}$ is significantly depleted, compared to only H or CO adsorbed (see Figure 7.15, panels 1, 2, 3 and 4), the $d_{3z^2-r^2}$ band is either part of bonding levels with H and CO or the related antibonding levels above ϵ_F. The effects of the co–adsorption are less pronounced for the other components of the d band (see Figure 7.15, panels 6) as the interactions of the CO π orbitals are weaker.

A very small change is seen for the interaction with the CO $2\pi^*$ orbitals, but a larger difference happens on the interaction with the 1π once H is co–adsorbed. The 1π projected orbital has a clear splitting (see Figure 7.15, panels 9 and 10) due to the combined interactions with s_H and d_{Ru}. This three orbital interaction gives two bonding levels, which appear as a split of 1π orbital and a antibonding level above the Fermi level. The 5σ is also split but because of the coupling via the Ru s– H atoms of the 5σ and 1π orbitals.

In summary two points are of importance:

1. For the bare surface CO adsorbs without a barrier and if 1×1 H is present on the surface, a barrier appears. This is the consequence of the competing s_{Ru}–s_H and s_{Ru}–CO bonds. The interaction s_{Ru} with $CO_{5\sigma}$ is always bonding. If H is present on the surface, this interaction decreases and can not compensate for the repulsions arising from the 4-electron type interaction of CO 4σ with doubly occupied Ru- $d_{3z^2-r^2}$. The barrier is not related to a direct interaction with the

H atoms, the PDOS for the TS (not shown) does not depict any splitting for the H levels. At the TS for CO, only the 5σ is significantly modified compared to the gas phase, the PDOS shows two peaks: the CO $5\sigma-$ Ru-$d_{3z^2-r^2}$ peak slightly stabilized by around 1 eV and 2 eV below a peak which is a mix of the CO 5σ, H s and the other Ru d.

2. The adsorption energy for CO adsorption decreases when H is coadsorbed. This can be understood in terms of bond order conservation. The coordination number of Ru has increased. The Ru atom relaxes upwards because of the Ru–Ru bonds weakening induced by the bonds formed with the H atoms and the CO molecule. For the frozen surface, the weakening of the Ru–H bonds illustrates the competition between CO and H for bonding via the Ru-s orbital.

§7.6 Barriers for CO decomposition on Ru

Since we use NEB to calculate the transition state for CO decomposition, additional calculations were needed (beside the CO adsorption) in order to proceed. We will first focus on the C and O coadsorption system and then to the TS for CO decomposition of flat and stepped Ruthenium surfaces.

Both atomic C and atomic O have a strong adsorption to the Ru(0001) surface. For the C atom, the adsorption energies and geometries were presented before [15]. The atomic oxygen prefers to adsorb also on hcp three-fold hollow sites. The adsorption energies in 2×2 structures, with respect to O_2 in the gas phase and bare metal surfaces is -272 kJ×mol^{-1}. It is followed in relative energy by the fcc three-fold hollow site, bridge and atop sites with adsorption energies of -222, -207 and -122 kJ×mol^{-1}, respectively. The octahedral subsurface site was investigated as well. Subsurface oxygen is not stable, the adsorption energy is $+292$×mol^{-1}. At lower coverage, in a 3×3 structure the adsorption energy for the hcp site is -266×mol^{-1} showing that atomic O has a similar lateral interaction as the CH group, smaller than atomic C.

The Ru–O distances are 2.03 Å for hcp site, 1.99 Å for fcc site, 1.81 Å for bridge site and 1.77 Å for atop site. The octahedral subsurface site has Ru–O bond lengths of 1.88 Å with the Ru atoms from the first layer and 2.02 Å with the Ru atoms from the second layer. All those are for 25.0% coverage. At 11.1% coverage for hcp site the Ru–O distances are 2.02 Å. Atomic O adsorbed on the edge of the steps in an hcp

site have the following Ru–O distances: 2.01, 2.01 and 2.06 Å. Atomic C adsorbed on the edge of the steps, in an hcp site have the following Ru–C distances: 1.96, 1.92 and 1.92 Å.

Three configurations for C and O coadsorption were studied: C hcp + O hcp, C hcp + O fcc and C fcc + O hcp. On the 2×2 structures the adsorption energies, with respect to CO in the gas phase and the bare Ru surface are -77, -47 and -17 kJ$\times$mol^{-1} respectively. The separated adsorption of atomic C and atomic O leads to -150 kJ$\times$mol^{-1}.

In the 3×3 structure only the C hcp + O hcp configuration (the most stable one) was calculated. The adsorption energy is -143 kJ$\times$mol^{-1}. The separated adsorption of atomic C and atomic O leads to -183 kJ$\times$mol^{-1}. The large difference of the adsorption energies for the 2×2 and 3×3 is caused by the important lateral interactions of atomic carbon [16] and atomic oxygen.

For the coadsorption on the Ru steps, we consider four cases: Both C and O adsorbed up the step, both adsorbed down the step, and one up, one down, in all the cases only the hcp sites. The adsorption energies are -110 kJ$\times$mol^{-1} for C hcp up + O hcp up, -99 kJ$\times$mol^{-1} for C hcp up + O hcp down, -24 kJ$\times$mol^{-1} for C hcp down + O hcp down, and -121 kJ$\times$mol^{-1} for C hcp down + O hcp up. The separated adsorption of atomic C and atomic O on steps leads to an adsorption energy of $-163\times$mol^{-1}.

The geometries of coadsorbed atomic C and atomic O follow. In the 2×2 structures, the Ru–C bond lengths are in between 1.91 and 1.97 Å, and Ru–O bond lengths are in between 2.01 and 2.04 Å. In the 3×3 structure the Ru–C bond lengths are 1.91, 1.94 and 1.96 Å, while the Ru–O bond lengths are 1.99, 2.02, 2.07 Å. For the coadsorption on the stepped surface the Ru–C bond lengths are in between 1.92 and 1.98 Å, similar with the bare surface. The Ru–O bond lengths are in between 2.01 and 2.06 Å.

The TS considered are:

1. (2×2) CO hcp $\rightarrow$ C hcp + O hcp

2. (2×2) CO atop $\rightarrow$ C hcp + O hcp

3. (2×2) CO hcp $\rightarrow$ C hcp + O fcc

4. (2×2) CO fcc $\rightarrow$ C fcc + O hcp

5. (3×3) CO hcp $\rightarrow$ C hcp + O hcp

6. (steps) CO hcp up → C hcp up + O hcp up

7. (steps) CO hcp down → C hcp down + O hcp down

8. (steps) CO hcp down → C hcp down + O hcp up

9. (steps) CO hcp up → C hcp up + O hcp down

The TS1 is sometimes called the TS "over the valley", to be distinguish from the one "over the top", in our case that is TS3. In TS1, the CO molecule is tilting and the O atom arrives in an asymmetric bridge position. The barrier for TS1 is 169 kJ×mol^{-1}, see Figure 7.16.
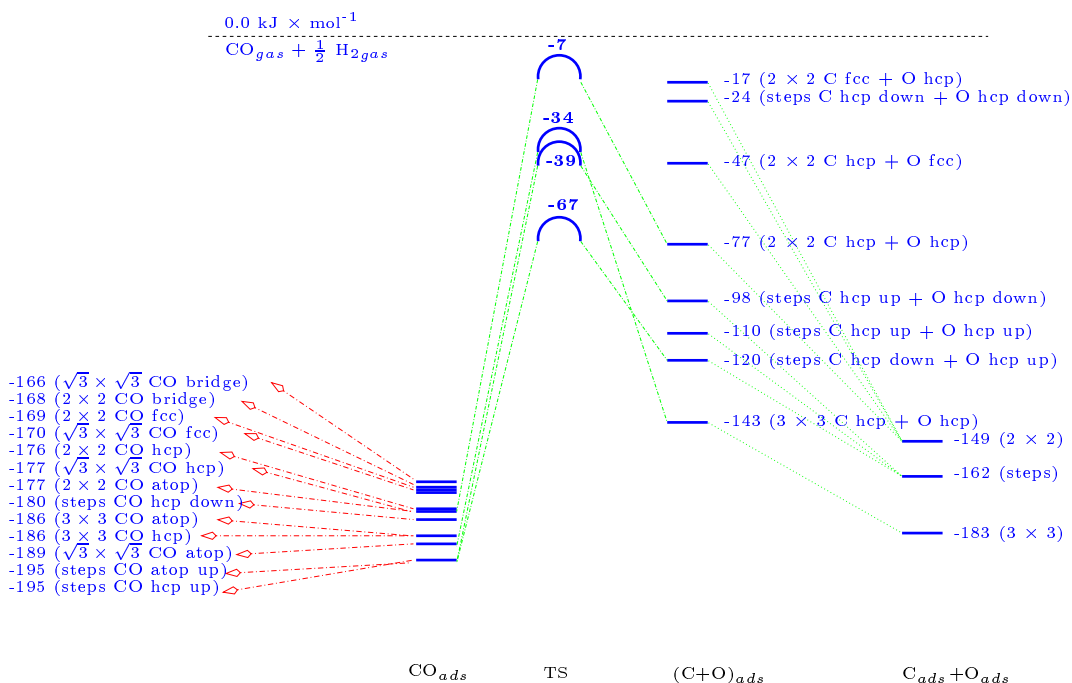
Figure 7.16: CO direct decomposition path. In left are levels for CO adsorption, in right are the levels for C and O coadsorption, sharing or not a metal atom on the surface. TS3 and TS4 are not shown, they are much higher.

Since atop is the preferred adsorption site for CO, we investigated the possibility of a dissociative path starting with CO atop, TS2. The results of the NEB path show that in fact the CO is migrating in a nearby hcp site before the actual dissociation starts.

TS3 is not the favorite dissociation mechanism. Preliminary calculations (without the refinement with quasi Newton algorithm) give a barrier of about 289 kJ×mol^{-1}.

Starting the dissociation with CO in a fcc site, with a mechanism over the top, TS4, will produce an atomic O in an hcp site, more stable than the fcc site. However, this puts the initial CO and the final C in fcc sites, which are less stable. This TS, also in preliminary state show a barrier of about 251 kJ×mol^{-1}.

We have shown before that TS1 is the preferred path for CO dissociation. TS5 is in fact TS1, but at lower coverage, 11.1% instead of 25.0%. The barrier is 152 kJ×mol^{-1}, 17 kJ×mol^{-1} less than in 2×2 structure, see Figure 7.17.
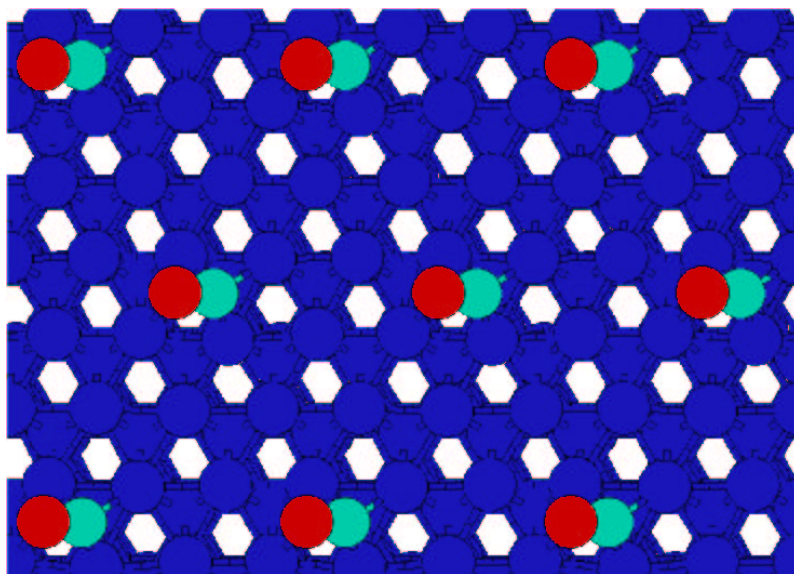
Figure 7.17: TS for CO decomposition on the Ru(0001) flat surface.

For stepped surfaces, TS6 and TS7 are TS1 like, but along the edge or the bottom of the step. The barriers are similar, the influence of the step is not important in those cases.

TS8 is for CO adsorbed at the bottom of the step and the dissociation will occur with the O atom going up, over the step. This reaction path is interesting. Just after the TS, a small minimum is when O atom is in a bridge site formed by two metal atoms at the edge. This adsorption site is more stable than a normal bridge site because of the lower coordination number of the metal atoms at the step. The TS is an early one. Soon after the reaction starts the C and O atoms are not any longer

in contact, they even do not share a metal atom like they would on a terrace. The barrier is 128 kJ×mol^{-1}, see Figure 7.18.
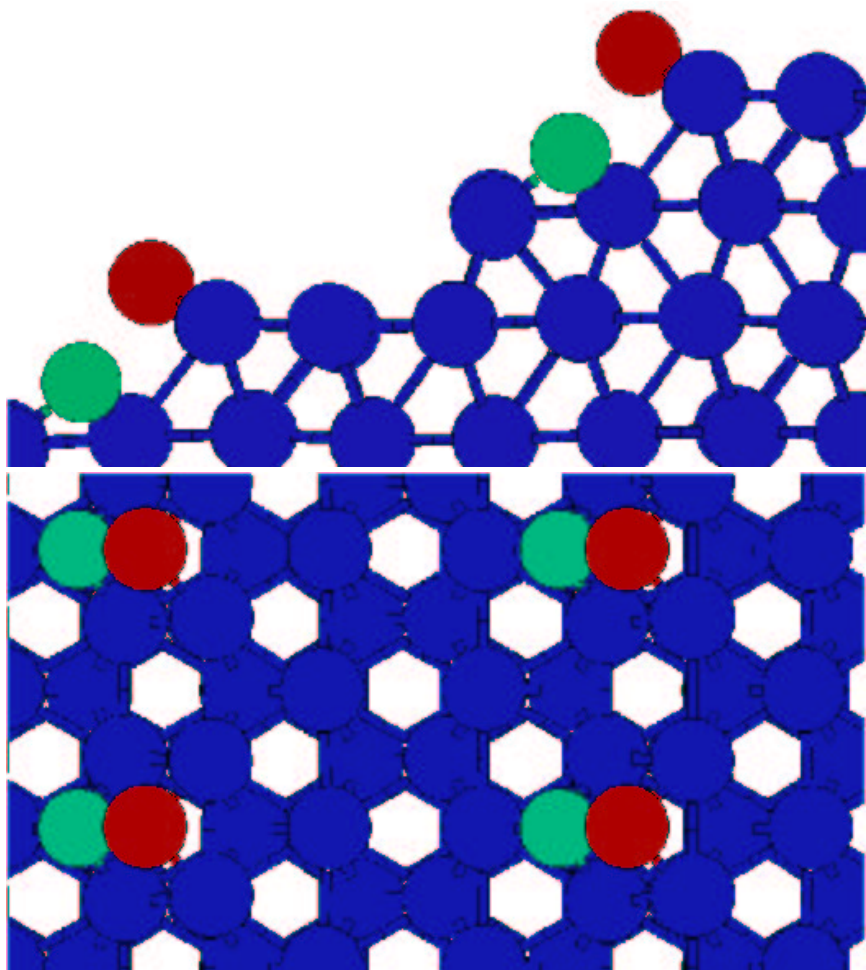
Figure 7.18: TS for CO decomposition on the Ru(0001) stepped surface, side and top view.

TS9 is for CO adsorbed at the edge of the step and the dissociation will occur with the O atom going down, over the step. This mechanism is less probable since there is less change that the O atom will be stabilized in the TS. The barrier is 156 kJ×mol^{-1}, 28 kJ×mol^{-1} more than TS8.

The geometry of TS5 and TS8 follows. The C–Ru bond lengths are 1.97, 2.02, and 2.35 Å for TS5 and 1.97, 1.97 and 1.86 Å for TS8. On the flat surface the C

atom is assisting the O atom in it's movement. The O–Ru bond lengths are 2.18 and 2.40 Å for TS5, and 1.96, and 2.00 Å for TS8. The C–O distances are 1.30 and 2.33 Å for TS5 and TS8 respectively.

§7.7 CO disproportionation on the Ru stepped surface

We also studied the Boudouard reaction (disproportionation of CO) on steps: $2\ CO_{ads} \rightarrow C_{ads} + CO_2$. One CO molecule is adsorbed at the bottom of the step and the other one is adsorbed at the edge of the step. The O atom from the CO molecule sitting at the bottom of the step is moving towards the step, the same way it would do for CO dissociation in TS8. At some point, the interactions with the other CO molecule start to form and an adsorbed nonlinear CO_2 originates, which desorbs in linear configuration. The reaction barrier is 172 kJ×mol^{-1} with respect to two adsorbed CO molecules. This TS was not calculated with NEB, see before (chapter 3).

The geometry of the TS for the Boudouard reaction is now presented. The C atom, which remains at the bottom of the step, has two Ru–C bond lengths of 1.97 Å, and one bond length of 1.88 Å. The other C atom has longer distances: 2.03, 2.82, and 2.84 Å to the metal atoms. The C–O bond lengths are 1.18 Å, and 1.77 Å. The O–Ru bond lengths are 2.05 and 2.02 Å, for the O atom, which is claiming the step edge. The O–C–O angle is 114°, see Figure 7.19.

§7.8 Indirect CO decomposition, via H insertion, on the Ru(0001) surface

In order to understand CO decomposition, specially in a mixture with H_2 (synthesis gas), we investigated the possibility of an insertion of a hydrogen atom in the adsorbed CO molecule, followed by the C–O dissociation.

The CHO radical was adsorbed on an hcp site. The adsorption energy is −124 kJ×mol^{-1} with respect to CO and H_2 gas phase and Ru bare surface. This radical is not very stable, the adsorption energy of CH hcp and O hcp sharing one Ru atom is −190 kJ×mol^{-1}, while the adsorption energy of CO hcp and H fcc sharing one Ru atom is −230 kJ×mol^{-1}.

In Figure 7.20, we can see the energy changes of the reaction path of CO molecule towards dissociation via a hydrogen insertion. The TS for the CHO formation is
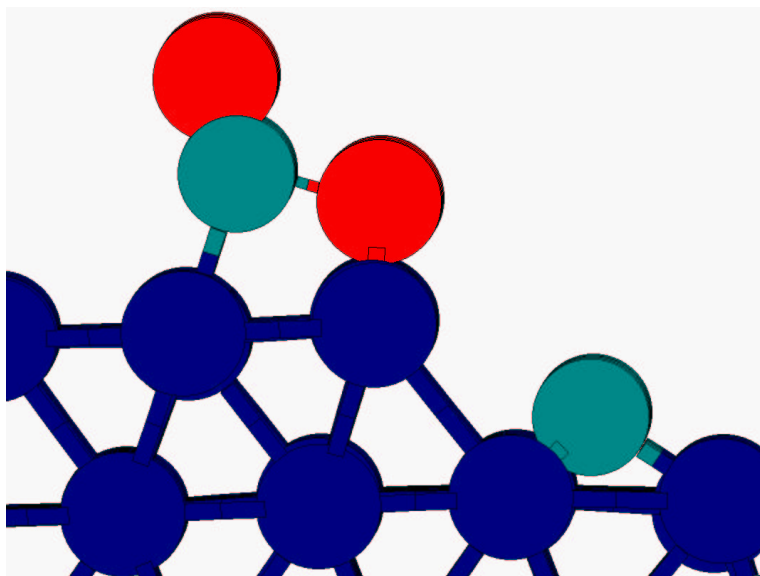
Figure 7.19: TS for CO disproportionation on the Ru(0001) stepped surface.

rather small, just 33 kJ×mol^{-1} above the reaction heat formation. CHO shows a similar stability on Pd(111) [17]. However, the barrier for H addition to CO is only 18 kJ×mol^{-1} above the heat of formation. The TS for the CHO decomposition is about 121 kJ×mol^{-1} with respect to adsorbed CHO. The CH and O formed have to diffuse away from each other and then the CH fragment has to dissociate to form atomic C and atomic H. The overall barrier for the CO dissociation via this mechanism is 228 kJ×mol^{-1}, which is higher than the one involved in TS1.

§7.9   CO decomposition on different transitional metals

Calculations were made for adsorbed atomic C, adsorbed atomic O, adsorbed CO in atop and hcp site for the following surfaces: Fe(0001), Fe(111), Co(0001), Ni(111), Cu(111), Ru(0001), Rh(111), Pd(111), Ag(111), Re(0001), Os(111), Ir(111), Pt(111) and Au(111). In the case of Fe, hcp and fcc structures were computed because bcc is too open and the comparison with the rest of dense packed surfaces was not possible. Fe, Ni and Co surfaces were calculated with spin. For all surfaces a similar model was used: 4 slab layers, 5 vacuum layers, 2×2 structure. In Table 7.5 one can see the adsorption energy of the atomic carbon with respect to the bare metal surface and
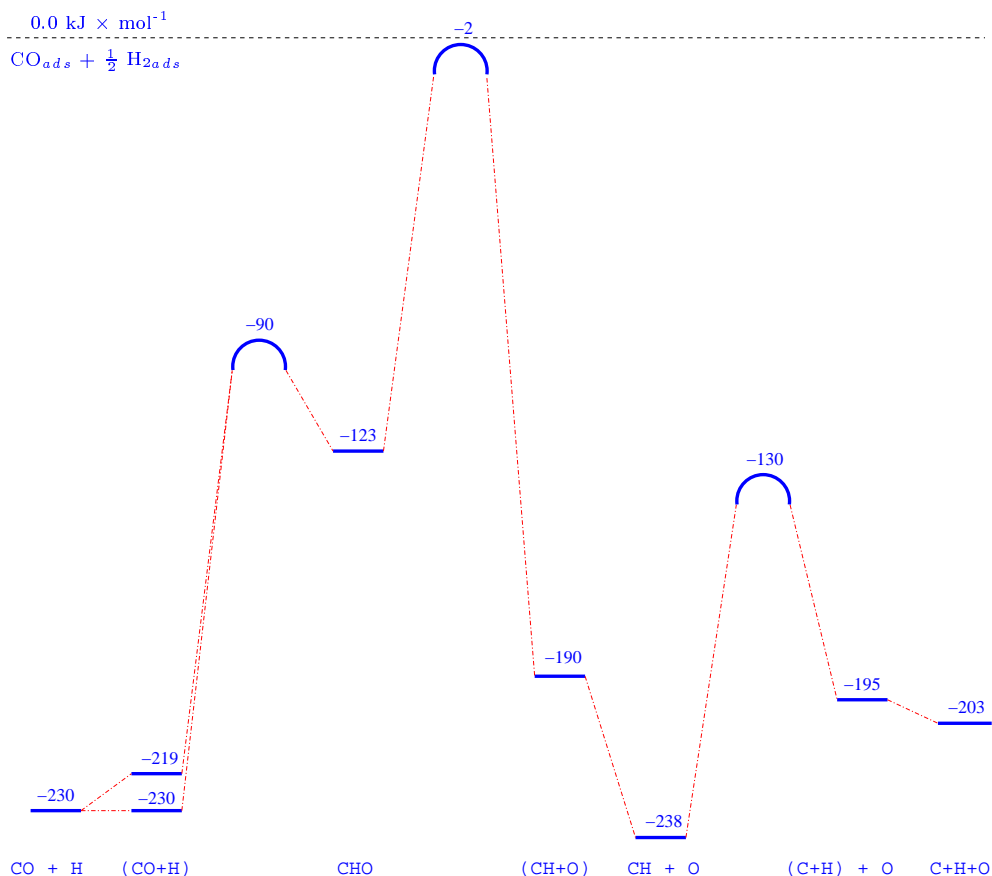
Figure 7.20: CO decomposition path via H insertion. In left is CHO formation from CO and H, and in right is CHO decomposition to CH and O, followed by CH decomposition.

atomic C in the gas phase. In Table 7.6 the adsorption energy of the atomic carbon is presented, with respect to the bare metal surface and atomic O in the gas phase. In Table 7.7 the adsorption energy of the molecular CO is shown with respect to the bare metal surface and CO in the gas phase.

We can see a dependency for C adsorption, the M–C bond strength is decreasing from left to right in the periodic table. For the dependency in the groups, it is less clear.

For the atomic O adsorption the dependency is clearer. The M–O bond strength is decreasing from left to right and from up to down in the periodical table.

	Fe⋆	Co	Ni	Cu
	$-769\ (-695)$	-668	-629	-476
	Ru	Rh	Pd	Ag
	-688	-690	-645	-338
Re	Os	Ir	Pt	Au
-713	-696	-675	-657	-411

Table 7.5: DFT calculated adsorption energies of atomic C on selected noble metals in kJ×mol^{-1}.

⋆ For Fe, hcp, (fcc) structures are calculated, not bcc.

	Fe⋆	Co	Ni	Cu
	$-714\ (-640)$	-550	-496	-429
	Ru	Rh	Pd	Ag
	-557	-469	-382	-321
Re	Os	Ir	Pt	Au
-634	-533	-428	-354	-270

Table 7.6: DFT calculated adsorption energies of atomic O on selected noble metals in kJ×mol^{-1}.

⋆ For Fe, hcp, (fcc) structures are calculated, not bcc.

Molecular CO adsorbed is stronger adsorbed on group VIII[B] and less on I[B] and II[B]. For some metals the atop site is favorable, but for most of them the hollow site seams more stable.

Using the adsorption energies of atomic C and atomic O, as well as the adsorption energies of molecular CO, we calculated an estimated TS barrier for CO decomposition with a Brønsted-Polanyi formula:

$$\Delta TS = 0.5 \times (\Delta R - \Delta P) \tag{7.1}$$

where ΔTS is the change in the TS energy, ΔR is the change in the reactants energy and ΔP is the change in products energy. In Table 7.8, one can see the estimated TS for the CO decomposition on the noble metals.

	Fe⋆	Co	Ni	Cu
	−169 [−115]	−171	−151	−68
	(−179) [(−175)]	(−176)	(−183)	(−85)
	Ru	**Rh**	**Pd**	**Ag**
	−177	−187	−130	−19
	(−176)	(−193)	(−189)	(−18)
Re	**Os**	**Ir**	**Pt**	**Au**
−187	−186	−199	−154	−28
(−154)	(−161)	(−162)	(−168)	(−29)

Table 7.7: DFT calculated adsorption energies of molecular CO atop (hcp) on selected noble metals in kJ×mol⁻¹.

⋆ For Fe, hcp, [fcc] structures are calculated, not bcc.

	Fe⋆	Co	Ni	Cu
	102 (30)	174	224	285
	Ru	**Rh**	**Pd**	**Ag**
	160	212	276	374
Re	**Os**	**Ir**	**Pt**	**Au**
98	161	224	273	369

Table 7.8: Estimated TS for CO decomposition. based on Brønsted-Polanyi relation. Energies are in kJ×mol⁻¹.

⋆ For Fe, hcp, (fcc) structures are calculated, not bcc.

We can see a clear dependency between the CO dissociation barrier and the strength of the M–C bond.

§7.10 Conclusions

CO adsorbs strongly to the closed packed surface of Ru. At lower coverage the atop site is preferred, up to 25%. The lateral interaction of the CO adsorbed atop and CO adsorbed hcp is different, hcp site having the smaller lateral interaction. The adsorption sites located near a step are more favorable with about 20 kJ×mol⁻¹ for

both atop and hcp sites, and with about 10 kJ×mol^{-1} for sites located at the bottom of the steps.

Local Density of States plots are provided for a better understanding of the adsorption energy differences.

The lateral interactions of CO are repulsive above 33.3% coverage, but are attractive at lower coverage.

Hydrogen can form compressed layers on the Ru(0001) surface. Up to 100% coverage, the adsorption energy does not change. Up to 150% coverage, the lateral interaction is still acceptable. After 200% coverage the adsorption energy is going to zero and the second layer of atoms is build.

For the H coadsorption with CO, the lateral interaction are repulsive, H and CO prefer to segregate, rather than to form mixed structures.

At low coverage of H and low coverage of CO, both species can adsorb on the preferred site (CO – atop, H – fcc). However, by increasing the H coverage, the H is forced to populate sites closer to CO molecule and this leads to distortions of the H adsorption site (bond with different lengths H–Ru). CO is little affected by the H coadsorption, unless the H is present at 100% coverage, when the CO will still adsorb on the atop sites with an important decrease of the adsorption energy.

Contrary to the adsorption of CO on a bare Ru(0001) surface, CO adsorption on the Ru(0001) surface completely covered with hydrogen is an activated process and the lowest barrier found, is about 25 kJ×mol^{-1} which could be verified experimentally as well as by DFT calculations. By tilting the CO molecule up to an angle of 35°, the barrier does not change. Experimentally, an additional non–activated reaction channel could be identified, which seems due to CO adsorption at defect sites in the hydrogen overlayer.

When the coverage of adsorbed H is high, there is a strong preference for CO to be adsorbed atop. In this case, the repulsive interactions between adsorbed H and CO are minimized. When CO is adsorbed in a hollow site, its σ levels interact with the same Ru levels as H: the in-phase combination of d and s orbitals, which corresponds to the bottom (bonding between Ru) of the d–s band. With CO atop the competition is reduced to the Ru s band. Also, when CO is hollow, the neighboring hydrogen atoms tend to go to a top site as two of their three bonds are weakened while with CO top only one Ru–H bond is reduced with the H atoms moving to an in–between hollow–bridge site.

Differences in the interaction of CO with the Ru(0001) surface in the absence or

in the presence of H are basically due to the changes in the interaction between 4σ, 5σ molecular orbitals of CO and the $d_{3z^2-r^2}$, s, and p_z orbitals of the Ru atom. If H is present on the surface, the s_{Ru}–$CO_{5\sigma}$ bond gets weaker and the $d_{3z^2-r^2} - 4\sigma$ and 5σ repulsions induce a barrier for the adsorption. As CO and H interact with the lower levels of the d–s band the Ru atom dramatically moves outwards by 0.4 Å, reflecting the strong weakening of the Ru–Ru surface bonds.

The reaction coordinate of CO molecular adsorption on a hydrogenated Ru(0001) surface is dominated by the vertical motion of the metal atom and the need to minimize the CO–H competition for binding to the Ru atoms. This leads to strongly localized interactions.

There is excellent agreement between theory and experiment concerning the supporting data of the mechanism proposed here for the molecular adsorption of CO on hydrogenated Ru(0001) surface.

The reactivity of Ru separates metals, which dissociate CO easily from metals that do not dissociate CO. Our calculations shows that the preferred reaction path is over the valley between the surface atoms. The TS energy is coverage dependent, 17 kJ×mol^{-1} is the difference between the barrier on 2×2 (25.0% coverage) and 3×3 (11.1% coverage).

On steps, the best way to dissociate CO is to adsorb CO at the bottom of the step and the O atom will jump on the next terrace. The barrier for this reaction is 128 kJ×mol^{-1}.

The Boudouard reaction is less probable. The barrier on the steps is higher than for CO dissociation with 44 kJ×mol^{-1}. We expect that on flat surface this difference to be higher.

CHO as intermediate for CO decomposition was also investigated. This indirect route for CO dissociation, which is favorable on Pd [17] is not preferred on Ru. The overall barrier for the indirect path on a flat surface is 59 kJ×mol^{-1} higher than the direct dissociation path on flat surface.

The activation energy for CO dissociation decreases with increasing C–M bond strength.

Bibliography

[1] I. Toyoshima, and G. A. Somorjai, *Catal. Rev. Sci. Eng.*, 19, 105, (1997)

[2] H. N. Storch, N. Golumbic, and R. B. Anderson, *The Fischer-Tropsch and related synthesis*, Whiley New York, 1951.

[3] H. Pfnür, P. Feulner, and D. Menzel, *J. Chem. Phys.*, 79, 4613 (1983).

[4] R. J. W. E. Lahaye, S. Stolte, S. Holloway, and A. W. Kleyn, *J. Chem. Phys.*, 104, (1996), 8301

[5] E. L. Meijer, *Quantum Chemical Computation of Infrared Spectra of Acidic Zeolites*, Ph.D. Thesis, Eindhoven University of Technology, September 2000

[6] P. Jacob, *Phys. Rev. Lett.*, 77, 20, 4229, (1996)

[7] P. Jacob, and B. N. J. Person, *Phys. Rev. Lett.*, 78, 18, 3503, (1997)

[8] T. A. Jachimowski, B. Meng, D. F. Johnson, and W. H. Weinberg, *J. Vac. Sci. Technol. A*, 13, 3, 1564, (1995)

[9] I. M. Ciobîcă, F. Frechard, R. A. van Santen, A. W. Kleyn, and J. Hafner, *J. Phys. Chem. B*, 104, 3364, (2000)

[10] Y. K. Sun, and W. H. Weinberg, *Surf. Sci.*, 214, L246, (1989).

[11] J. M. White, and S. Akhter, *CRC Crit. Rev. Solid State Mater. Sci.*, 14, 130, (1988)

[12] B. Riedmüller, I. M. Ciobîcă, F. Papageorgopoulos, B. Berenbak, R. A. van Santen, and A. W. Kleyn, *J. Chem. Phys.*, 115, (2001), 5244

[13] H. Pfnür, and D. Menzel, *J. Chem. Phys.*, 79, 2400, (1983).

[14] B. Riedmüller, I. M. Ciobîcă, F. Papageorgopoulos, B. Berenbak, R. A. van Santen, and A. W. Kleyn, *Surf. Sci.*, 465, (2000) 347

[15] I. M. Ciobîcă, F. Frechard, R. A. van Santen, A. W. Kleyn, and J. Hafner, *Chem. Phys. Lett.*, 311, 185, (1999).

[16] I. M. Ciobîcă, F. Frechard, A. P. J. Jansen, R. A. van Santen, *Stud. Surf. Sci.*, 133, (2001), 221

[17] M. Neurock, *Topic in Catalysis*, 9, (1999), 135

Chapter 8

Dynamic Monte Carlo for the CH$_X$ species

The determination of Transition States energies and structures has been done with Density Functional Theory. Several calculations are made to determine the lateral interaction of species on the surface. A model to use those results as input in Dynamic Monte Carlo is proposed. Together they form a good tool to help understand the kinetics of heterogeneous catalytic reactions.

§8.1   Introduction

The use of quantum chemical data to simulate overall kinetics of a catalytic reaction will be illustrated using the Eindhoven Dynamic Monte Carlo code. A kinetically model for CH$_4$ decomposition and C hydrogenation on the Ru(0001) surface is proposed.

§8.2   CH$_X$ on Ru(0001)

The activation of methane and methane formation on metal surfaces are catalytically significant reactions. The sequential dehydrogenation of methane is important for CO production and the sequential hydrogenation of carbon are essential parts of the Fisher–Tropsch mechanism. Many theoretical and experimental studies have been conducted for CH$_x$ species adsorbed on transition metal surfaces.

§8.2.1   DFT calculations

The main limitation of DFT is the description of the weak interactions (as van der Waals or hydrogen bonds). The errors due to this limitation are small if the molecules adsorbed are strongly bonded. This is the case of H and CH$_x$, (x = 0, 1, 2, 3) but it is not the case for CH$_4$ [1]. Methane in very weakly adsorbed and DFT calculations show adsorption energies around 0 kJ$\times$mol^{-1}.

Recent calculations for adsorbed CH$_x$ (x = 0-3) species and adsorbed H on Ru(0001) surface have been reported by us [1] for 0.25 ML coverage (see also chapter 4). They show that the three-fold sites are preferred for the adsorption of those species over top or bridge sites. CH$_3$ and H prefer the fcc hollow site (with small difference to the hcp site) and CH$_2$, CH, and C prefer the hcp hollow site for adsorption.

In order to investigate the lateral interaction, calculations for 0.11 ML coverage were done for the same species in their most stable sites. We were able to show that the difference between the adsorption energy of a CH$_x$ species in 2$\times$2 (0.25 ML coverage) and 3$\times$3 (0.11 ML coverage) structure is 10 kJ$\times$mol^{-1} for CH$_3$, 21 kJ$\times$mol^{-1} for CH$_2$, 28 kJ$\times$mol^{-1} for CH and 45 kJ$\times$mol^{-1} for C. Therefore, the idea that the lateral interactions are only significant for species adsorbed on a surface, which share a metal atom, is not true. In the 2$\times$2 structure the three metal atoms, which bind to the adsorbed molecule, have one or two metal atom neighbors on the surface, which accommodate another molecule. In the 3$\times$3 structure, the three metal atoms bound to the adsorbed molecule have no metal atom neighbors on the surface interacting directly to another adsorbate. At least one metal atom not bounded to an admolecule is inserted between the surface metal atoms bound to the adsorbates.

For a pair of identical species (CH$_x$ (x = 0-3), H), calculations were made for the adsorption energies of two species adsorbed on three-fold hollow sites in a 2 $\times$ 2 supercell. They could be on the same kind of site or in a different site. In all the cases, they share one metal atom on the surface. The case when they share two metal atoms was not considered because of the large repulsion [2]. For a pair of different species A and B (CH$_x$ (x = 0-3), H), calculations were made for the adsorption energies for those two species adsorbed on three fold sites in a 2 $\times$ 2 supercell. The species can be on the same kind of site or in different sites, and also they share one metal atom on the surface. The results of these calculations [3] were used to estimate the lateral interactions (see next section).

We also used DFT to calculate the reaction barriers. Previously reported Transition States (TS) [2] were calculated in 2×2 structures, which imply important lateral interaction. New calculations were performed in 3×3 supercells, in order to have the barriers without the lateral interaction. The geometries of the TS found for the 2×2 supercells were the initial guess and the TS were located by minimizing only the forces.

In the case of CH$_3$ $\rightarrow$ CH$_2$ + H reaction, due to the fact that CH$_3$ and CH$_2$ prefer different three-fold hollow sites for adsorption, two different reactions were considered: CH$_{3(hcp)}$ $\rightarrow$ CH$_{2(hcp)}$ + H$_{(fcc)}$ and CH$_{4(fcc)}$ $\rightarrow$ CH$_{2(fcc)}$ + H$_{(hcp)}$ (`fcc` is the three-fold site without a Ru atom below, in the second layer and `hcp` is the three-fold site with a Ru atom below, in the second layer). The barriers were computed for each reaction in 2×2 and 3×3 supercells. For the 2×2 supercell there is no large difference for the activation energy, only 7 kJ×mol^{-1}. With the 3×3 supercell appears a more important decrease for the reaction barrier if the CH$_x$ species are in hcp sites. The difference becomes 14 kJ×mol^{-1} (see Table 4.3).

Since the H atom, CH$_3$ and the CH$_2$ present a small difference for fcc and hcp adsorption energies (respectively 3, 5 and -5 kJ×mol^{-1}) it was difficult to conclude which reaction will have the smaller barrier without performing the calculations.

Lateral interaction

For each A and B pairs from CH$_3$, CH$_2$, CH, C and H we calculated the energy for the following situations: A fcc + B fcc, A fcc + B hcp, A hcp + B hcp, A hcp + B fcc. If A and B are identical then only three different situations occur: fcc + fcc, fcc + hcp and hcp + hcp.

Since the Monte Carlo code used currently handles only lateral interactions in a pairwise additive fashion we correspondingly fitted the lateral interactions from the DFT calculations. It was proposed recently by King et. all [4] that for a coverage of about 0.1 ML the lateral interactions are minimal. Since a 3×3 structure leads to a 0.11 ML coverage, we assume that at larger distance the lateral interactions vanish.

If we draw a circle around a particular site with the radius of **three** times the Ru–Ru bulk distance, there are no less than 60 adsorption sites (only hollow) inside of this circle which, we believe, influence the adsorption energy of the given initial site (see Figure 8.1, 8.2). Those 60 sites are divided into two groups. They are named f or h if they are the same type as the particular site (fcc or hcp) for which the lateral

Figure 8.1: The lateral interactions for an "X" adsorbate in a fcc site. f$_i$ indicates fcc–fcc interactions, and d$_i$ indicates fcc–hcp interactions. With light gray, it is shown the position of an other "X" adsorbate for which the lateral interactions with the original "X" adsorbate are considered negligible.

interactions are calculated. The second group of sites is named d, and it includes the remaining sites, which are of different type compared with the reference site (see Figures 8.1 and 8.2).

We also labeled those sites according to their distance to the center of the circle. Thus we have $6f_1$ sites at the distance of 1 (on the Ru–Ru bulk distance scale), $6f_2$ sites at the distance of $\sqrt{3}$, $6f_3$ sites at the distance of 2 and $12f_4$ sites at the distance of $\sqrt{7}$ if the initial site was a fcc one. Note that they are 2 different f_2 sites. We consider them equal since they are at the same distance to the center of the circle. Concerning the d-sites, we have $3d_1$ sites at the distance of $1/\sqrt{3}$, $3d_2$ sites at the distance of $2/\sqrt{3}$, $6d_3$ sites at the distance of $\sqrt{7}/\sqrt{3}$, $6d_4$ sites at the distance of $\sqrt{13}/\sqrt{3}$, $3d_5$ sites at the distance of $4/\sqrt{3}$, $6d_6$ sites at the distance of $\sqrt{19}/\sqrt{3}$ and $3d_7$ sites at the distance of $5/\sqrt{3}$. The next sites outside the circle are f_5 at the distance of 3, d_8 at the distance of $2\sqrt{7}/\sqrt{3}$, and d_9 at the distance of $\sqrt{31}/\sqrt{3}$.
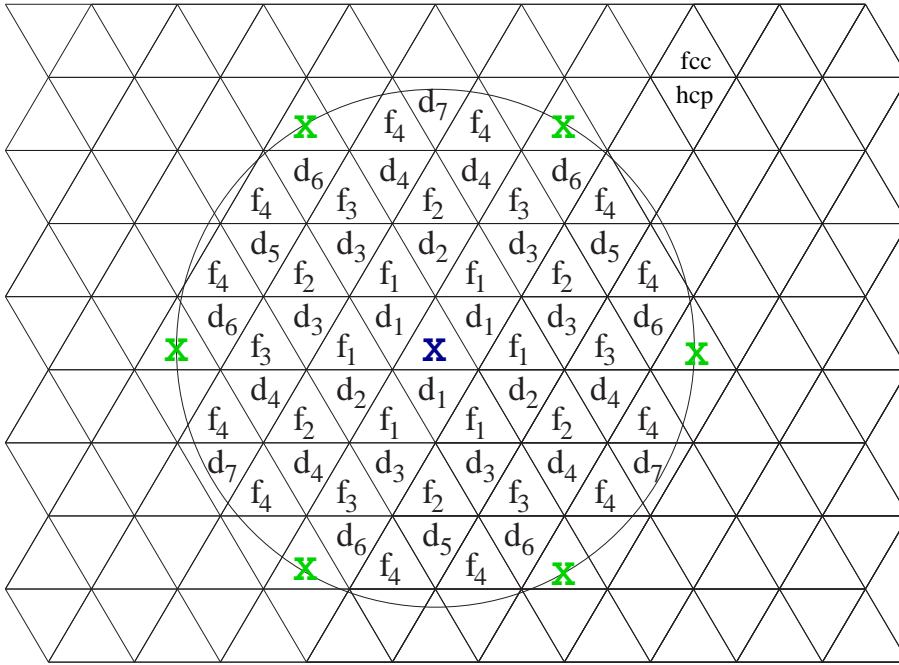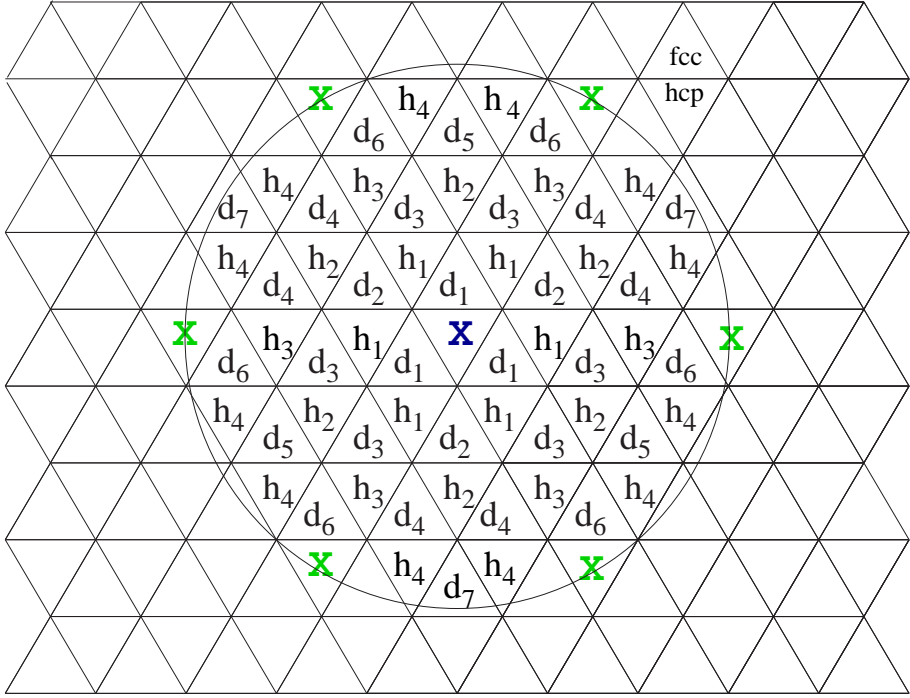
Figure 8.2: The lateral interactions for an "X" adsorbate in an hcp site. h$_i$ indicates hcp–hcp interactions and d$_i$ indicates fcc–hcp interactions.

The resulting equations for the adsorption energies for an A species at different coverages are:

$$
\begin{aligned}
E_{\mathrm{A}fcc}^{(2\times2)} &= E_{fcc}^{\mathrm{A}} + 3\varphi f_3^{\mathrm{A}} \\
E_{\mathrm{A}hcp}^{(2\times2)} &= E_{hcp}^{\mathrm{A}} + 3\varphi h_3^{\mathrm{A}} \\
E_{\mathrm{A}fcc+\mathrm{A}fcc}^{(2\times2)} &= 2E_{fcc}^{\mathrm{A}} + 2\varphi f_1^{\mathrm{A}} + 2\varphi f_2^{\mathrm{A}} + 6\varphi f_3^{\mathrm{A}} + 4\varphi f_4^{\mathrm{A}} \\
E_{\mathrm{A}hcp+\mathrm{A}hcp}^{(2\times2)} &= 2E_{hcp}^{\mathrm{A}} + 2\varphi h_1^{\mathrm{A}} + 2\varphi h_2^{\mathrm{A}} + 6\varphi h_3^{\mathrm{A}} + 4\varphi h_4^{\mathrm{A}} \\
E_{\mathrm{A}fcc+\mathrm{A}hcp}^{(2\times2)} &= E_{fcc}^{\mathrm{A}} + E_{hcp}^{\mathrm{A}} + 3\varphi f_3^{\mathrm{A}} + 3\varphi h_3^{\mathrm{A}} + 3\varphi d_2^{\mathrm{AA}} + 3\varphi d_5^{\mathrm{AA}} \\
E_{\mathrm{A}hcp}^{(3\times3)} &= E_{hcp}^{\mathrm{A}}, \text{ or } E_{\mathrm{A}fcc}^{(3\times3)} = E_{fcc}^{\mathrm{A}}
\end{aligned}
\tag{8.1}
$$

where φ is the change in the adsorption energy due to the lateral interactions between the two sites, f_i^{A}, h_i^{A} and d_i^{AA} reflect the interactions between A fcc – A fcc, A hcp

– A hcp, and A fcc – A hcp respectively (see beginning of section). E^A_{fcc} and E^A_{hcp} are the adsorption energies for the A species on three fold sites *without* any lateral interactions. The first two equations refer to one A species adsorbed on a three-fold site (fcc and hcp) on a 2×2 structure, the next two equations refer to two A species adsorbed on the same three-fold site and the next one refers to 2 A species adsorbed on different three-fold site. The last equation refers to one A species adsorbed on the most stable three-fold site (fcc or hcp) on a 3×3 structure.

If two different species (A and B) are adsorbed together, then the equations become:

$$
\begin{aligned}
E^{(2\times2)}_{\text{A}fcc+\text{B}fcc} &= E^\text{A}_{fcc} + E^\text{B}_{fcc} + 2\varphi f^\text{AB}_1 + 2\varphi f^\text{AB}_2 \\
&\quad + 3\varphi f^\text{AA}_3 + +3\varphi f^\text{BB}_3 + 4\varphi f^\text{AB}_4 \\
E^{(2\times2)}_{\text{A}hcp+\text{B}hcp} &= E^\text{A}_{hcp} + E^\text{B}_{hcp} + 2\varphi h^\text{AB}_1 + 2\varphi h^\text{AB}_2 \\
&\quad + 3\varphi h^\text{AA}_3 + +3\varphi h^\text{BB}_3 + 4\varphi h^\text{AB}_4 \\
E^{(2\times2)}_{\text{A}fcc+\text{B}hcp} &= E^\text{A}_{fcc} + E^\text{B}_{hcp} + 3\varphi f^\text{AA}_3 + 3\varphi h^\text{BB}_3 \\
&\quad + 3\varphi d^\text{AB}_2 + 3\varphi d^\text{AB}_5 \\
E^{(2\times2)}_{\text{A}hcp+\text{B}fcc} &= E^\text{A}_{hcp} + E^\text{B}_{fcc} + 3\varphi h^\text{AA}_3 + 3\varphi f^\text{BB}_3 \\
&\quad + 3\varphi d^\text{BA}_2 + 3\varphi d^\text{BA}_5
\end{aligned}
\tag{8.2}
$$

where φ is the change in the adsorption energy due to the lateral interactions between the two sites, f^AB_i, h^AB_i, d^AB_i and d^BA_i reflect the interaction between A fcc – B fcc, A hcp – B hcp, A fcc – B hcp, and A hcp – B fcc respectively (see beginning of section). E^X_{fcc} and E^X_{hcp}, (X = A, B) are the adsorption energies for the X species on the three fold sites *without* any lateral interaction. The first two equations refer to two species A and B adsorbed on the same three-fold site (fcc and hcp) on a 2×2 structure, the next two equations refer to two species A and B adsorbed on different three-fold sites. The parameters for the interactions of adsorbates of the same species are calculated before and simply used here to calculate the parameters for the interactions of two different species.

The number of lateral interactions is too large to be determined unique with the limited number of calculations available. We therefore tried various functions to describe the variations of the lateral interactions with the distance. The retained function are d=A_d/r^x, f=A_f/r^y and h=A_h/r^z, where d=(d_1, d_2, ..., d_7, d_8, ...),

f=(f_1, f_2, ...) and h=(h_1, h_2, ...). A_d, A_f and A_h are the prefactors, z, x and y are the exponents and r is the distance. The parameters were computed with a least–squares procedure. Attractive terms, like $M/r^\alpha - N/r^\beta$, were also tested but N was always very small, so it was disregarded. The solutions minimize $f_{\geq 4}$, $h_{\geq 4}$ and $d_{\geq 7}$, so they can be neglected.

In a mixed case (A and B) the d term was split in two functions, because the interactions of an A molecule in a fcc site with a B molecule in an hcp site have no reason to be identical to the interactions of the same A molecule in an hcp site with the same B molecule in a fcc site.

In other words if we look at each d_i^{AB}, f_i^{AB} or h_i^{AB} then $d_i^{AB} \neq d_i^{BA}$, $f_i^{AB} = f_i^{BA}$ and $h_i^{AB} = h_i^{BA}$, $\forall$ i and $\forall$ A, B $\in$ {CH$_3$, CH$_2$, CH, C, H}.

The number of lateral interactions being too large, we will not display them. The large values for d_1 in the case of CH$_3$ are to be noted. The size of the volume of the CH$_3$ can explain this. It is not possible for an other species to approach that close. CH$_3$ has 2 kinds of repulsions, through the surface as for all the other CH$_x$ species, but also steric repulsions due to its umbrella shape. CH and C present only lateral interactions through the surface. CH$_2$ is in between, but its repulsions due to steric hindrance are much smaller that for CH$_3$. A typical prefactor for the repulsions through the surface is about 150-200 kJ×mol^{-1} for the f and h functions and around 1000 kJ×mol^{-1} for the d function. The exponent can be in between 2.5 and 3.5. In the case of steric repulsions, the prefactor can go from 100000 kJ×mol^{-1} too much more and the exponent is in between 4.0 and 7.5. The H atom undergoes only small lateral interactions from the very close adsorbates, all the other interactions are negligible.

All the parameters were processed using a Brønsted–Polanyi like formula:

$$\Delta E^{TS} = \frac{1}{2} \times \left(-\Delta E^R + \Delta E^P \right) \tag{8.3}$$

where: ΔE^{TS} is the change in the activation energy, ΔE^R is the change in the energy of the reactants, and ΔE^P is the change in the energy of the products. With this dependency, we can determine the changes in the barrier for each reaction and for each possible configurations. If the decrease of the barrier is larger than its actual value, then the barrier is fixed to zero, in order to avoid negative activation energies.
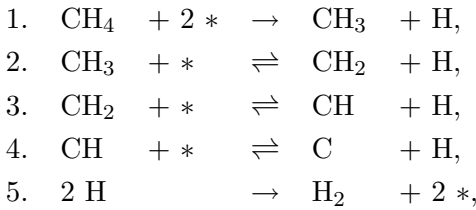
We used Brønsted–Polanyi relation to check the results we have with 2×2 and 3×3 structures. The activation energy changes compare well (see Table 4.2, columns 2 and 3). For CH$_2$ decomposition 1/2 has to be change with 0 and for CH hydrogenation

with 1.

For comparison, Mean Field Approximation (MFA) simulations, Dynamic Monte Carlo (DMC) without lateral interactions and Dynamic Monte Carlo with lateral interaction were performed for the C + 2H$_2$ → CH$_4$ and CH$_4$ → C + 2H$_2$ reactions.

§8.2.2   Mean field

The MFA was carried out with Mathematica [5], by writing the differential equations and solving them at different temperatures. For the elementary reactions steps describing the dehydrogenation of methane to C and H$_2$:

1.   CH$_4$ + 2 *   →   CH$_3$ + H,
2.   CH$_3$ + *   ⇌   CH$_2$ + H,
3.   CH$_2$ + *   ⇌   CH   + H,
4.   CH   + *   ⇌   C   + H,
5.   2 H   →   H$_2$ + 2 *,

the following system of equations can be written:

$$\frac{dc_3}{dt} = k_1 p_1 (c_*[t])^2 + \bar{k}_2 c_2[t] c_H[t] - k_2 c_3[t] c_*[t],$$

$$\frac{dc_2}{dt} = k_2 c_3[t] c_*[t] + \bar{k}_3 c_1[t] c_H[t] - \bar{k}_2 c_2[t] c_H[t] - k_3 c_2[t] c_*[t],$$

$$\frac{dc_1}{dt} = k_3 c_2[t] c_*[t] + \bar{k}_4 c_0[t] c_H[t] - \bar{k}_3 c_1[t] c_H[t] - k_4 c_1[t] c_*[t],$$

$$\frac{dc_0}{dt} = k_4 c_1[t] c_*[t] - \bar{k}_4 c_0[t] c_H[t], \tag{8.4}$$

$$\frac{dc_H}{dt} = k_1 p_1 (c_*[t])^2 + k_2 c_3[t] c[t] + k_3 c_2[t] c_*[t] + k_4 c_1[t] c[t]$$
$$- \bar{k}_2 c_2[t] c_H[t] - \bar{k}_3 c_1[t] c_H[t] - \bar{k}_4 c_0[t] c_H[t] - 2 k_5 (c_H[t])^2,$$

$$\frac{dc_*}{dt} = \bar{k}_2 c_2[t] c_H[t] + \bar{k}_3 c_1[t] c_H[t] + \bar{k}_4 c_0[t] c_H[t] + 2 k_5 (c_H[t])^2$$
$$- 2 k_1 p_1 (c_*[t])^2 - k_2 c_3[t] c_*[t] - k_3 c_2[t] c_*[t] - k_4 c_1[t] c_*[t],$$

where c_H is H coverage, c_3 is CH$_3$ coverage, c_2 is CH$_2$ coverage, c_1 is CH coverage, c_0 is C coverage, c_* is the coverage of empty sites, p_1 is methane partial pressure, k_i is the rate constant for direct reaction i and $\bar{k}_i$ is the rate constant for inverse reaction i. They are the same as the reaction rate constants as in the ME 3.5, except for a geometric factor. In the same way, similar equations for the reactions of hydrogenation of adsorbed C on Ru(0001) surface can be obtained. The simulations

were conducted for several temperatures, several partial pressures for H_2 and CH_4 and different initial coverages of atomic C on Ru(0001).

Figures 8.3, 8.4, show the results at 750 K with Mean Field for methane activation and for 10% carbon hydrogenation on the Ru(0001) surface.
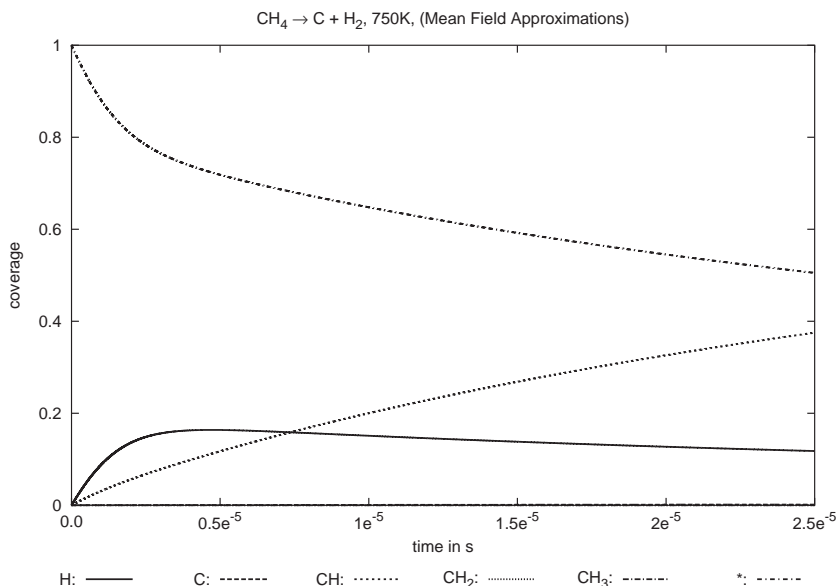
Figure 8.3: MFA results for methane decomposition at 750 K.

§8.2.3 DMC without and with lateral interaction

The DMC simulations were done in two different ways:

- without lateral interactions, using the results for activation energies from the 2×2 calculations; the prefactors were assumed to be 10^{12} for reactions on the surface, (few orders of magnitude) lower if a product is in the gas phase and (few orders of magnitude) larger if a reactant is in the gas phase.

- with lateral interactions, once the values for the lateral interactions had been obtained in the way described in previous section we calculated the changes in barriers using the Brønsted–Polanyi type formula.

The simulations were performed at the following temperatures: 550 K, 650 K, 750 K, and 850 K.
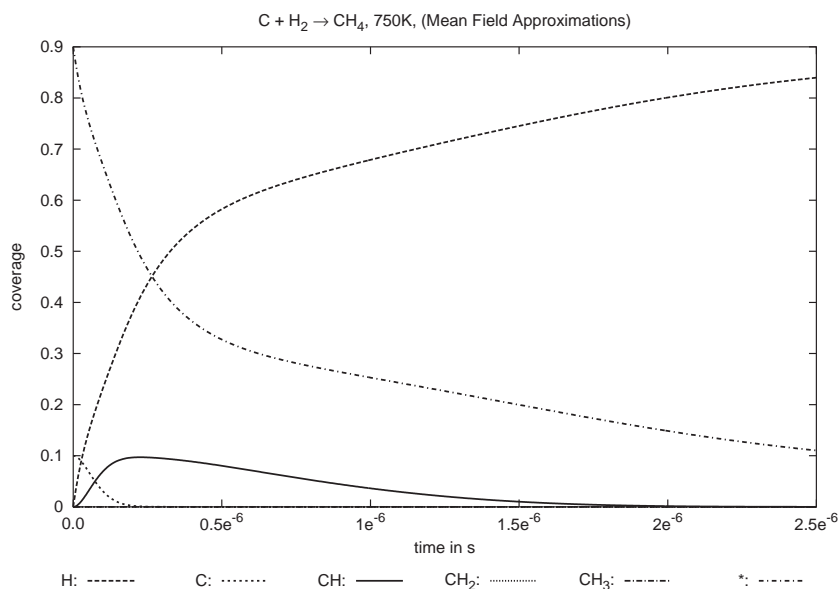
Figure 8.4: MFA results for 0.1 ML C hydrogenation at 750 K.

Figures 8.5, 8.6, 8.7, and 8.8 show the results at 750 K with Dynamic Monte Carlo simulations without and with lateral interactions, for methane activation and for 10% carbon hydrogenation on the Ru(0001) surface.

The results of the simulations for the methane activation process are different depending on the approach considered. MFA and DMC without lateral interactions show exactly the same results. However, DMC with lateral interactions gives a different picture: The reactions are much faster. The effect of the lateral interactions on this reactions is beneficent as the reactant are destabilized by the lateral interactions.

For the carbon hydrogenation, MFA and DMC without lateral interaction shows results, which are slightly different, but the overall trends are identical. The coverage on the surface increases rapidly because of the hydrogen dissociation and therefore the hypothesis on which MFA is based are not anymore valid. DMC with lateral interactions shows again a different reaction as the hydrogenation of carbon is much slower than in the previous cases.

A common feature of all simulations is the absence of the CH$_2$ intermediate. This species is very reactive and its lifetime is extremely short. CH$_3$ has a very similar behavior, with a lifetime a bit enhanced. CH is by far the most abundant species on the surface, as expected from theoretical predictions [1] and in good agreement with
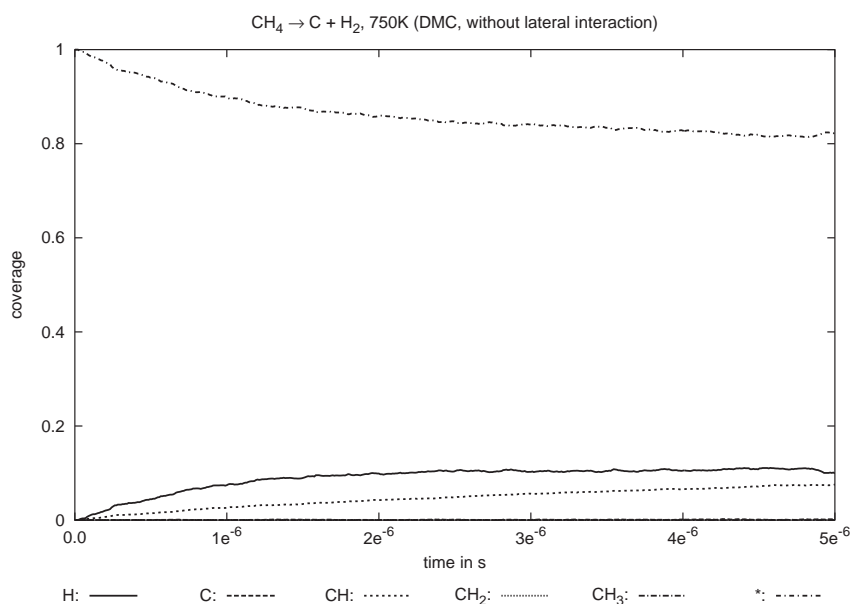
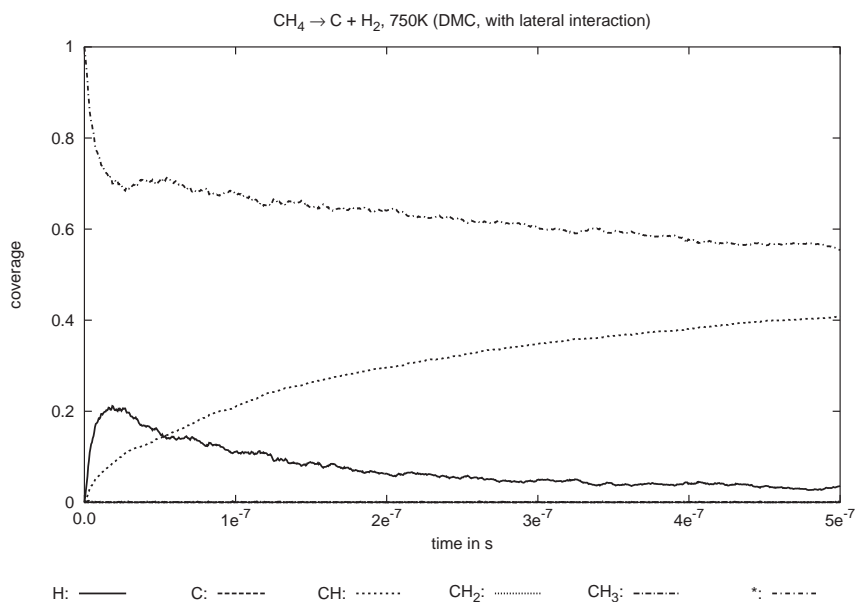Figure 8.5: DMC results for methane decomposition at 750 K without lateral interaction.

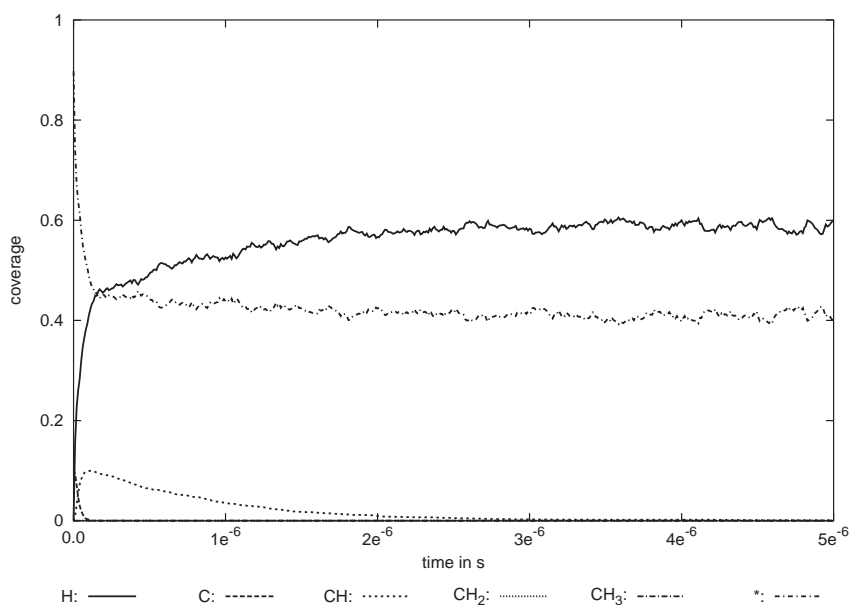Figure 8.6: DMC results for methane decomposition at 750 K with lateral interactions included.

Figure 8.7: DMC results for 0.1 ML C hydrogenation at 750 K without lateral inter-action.
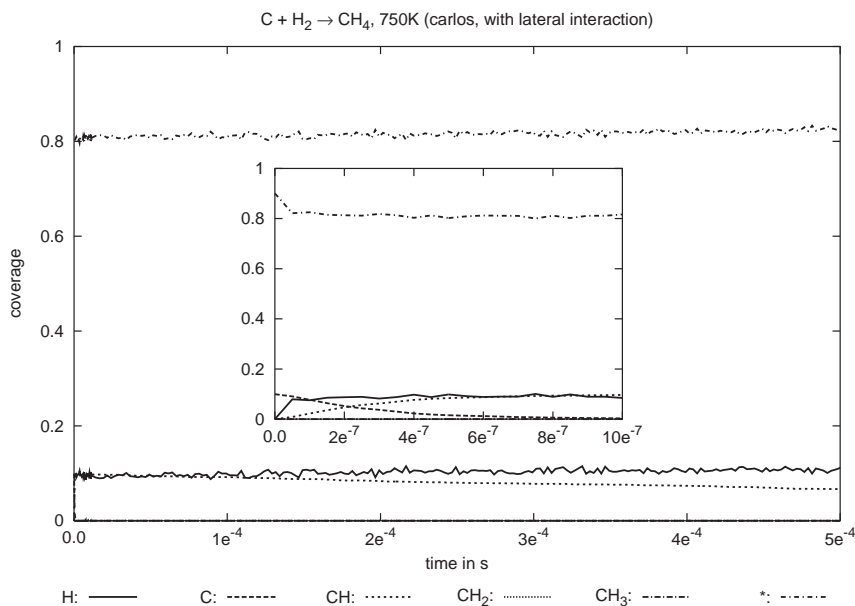

Figure 8.8: DMC results for 0.1 ML C hydrogenation at 750 K with lateral interactions included.

experimental results [6, 7].

The hydrogenation of C to CH and the dehydrogenation of CH to C are the most difficult reactions. The whole system behaves as is the methane decomposes directly to CH followed by the dissociation of CH to C and H.

NO dessorption from Rh(111) was used to test the comparison between the experiments (TPD spectra) and DMC simulations. The agreement is rather good. In the case of CH_x, a direct comparison with experiment is not possible.

§**8.3   Conclusions**

Lateral interactions are primordial as demonstrated by the simulations for two different systems. We successfully developed a model to extract parameters from DFT calculations and used as input in DMC.

Including lateral interaction in DMC slows down hydrogenation of C atom and speed up the decomposition of CH_4 in the system $CH_4 \rightleftharpoons C + 2H_2$. In the case of NO on Rh(111), we have a good agreement with experimental results.

The combination of *ab–initio* calculations for kinetic parameters and DMC simulations allows to get an insight into heterogeneous catalytic reactions at the atomic scale.

Bibliography

[1] I. M. Ciobîcă, F. Frechard, R. A. van Santen, A. W. Kleyn, and J. Hafner, *Chem. Phys. Lett.*, 311, (1999), 185

[2] I. M. Ciobîcă, F. Frechard, R. A. van Santen, A. W. Kleyn, and J. Hafner, *J. Phys. Chem. B*, 104, (2000), 3364

[3] I. M. Ciobîcă, R. A. van Santen, to be published

[4] Q. Ge, R. Kose and D. A. King, *Adv. Catal.*, 45, (2000), 207

[5] *Mathematica 4.0*, Wolfram Research Inc., (1999)

[6] M. -C. Wu and D. W. Goodman *J. Am. Chem. Soc.*, 116, (1994), 1364

[7] M. -C. Wu and D. W. Goodman *Surf. Sci. Lett.*, 306, (1994), L529

Chapter 9

Fischer Tropsch mechanisms on Ru(0001)

Two reaction pathways for Fischer Tropsch synthesis have been computationally analyzed for the Ru(0001) surface, using periodic *ab initio* calculations for 25% coverage. Adsorption energies for the intermediates for the first two catalytic cycles as well as the transition states are reported. Both mechanisms are carbene type mechanisms. It uses adsorbed CH as a building unit, rather than adsorbed CH_2 and growing chains are alkyl like and alkylidene like.

§9.1 Introduction

Fischer Tropsch synthesis is a hot issue and an understanding at molecular scale is very important for such complicated system. Fischer Tropsch synthesis has been intensely studied over the years [1–4]. There are three major reaction mechanisms for the Fischer Tropsch synthesis:

- the carbene mechanism

- the hydroxy-carbene mechanism

- the CO-insertion mechanism

The carbene mechanism consists of adsorbed CH_x as building unit, and adsorbed C_nH_y as chain growth. The hydroxy-carbene mechanism consists of adsorbed H–C–OH as building unit, and C_nH_{2n+1}–C–OH as chain growth. The CO-insertion

mechanism proceeds with the adsorbed CO as building unit (followed by the hydrogenation) and C_nH_y as chain growth. A particular case of the carbene mechanism was proposed by Maitlis [5], where the chain growth has a double bond between the last and the before last atom in the chain: $H_{2n+1}C_n–CH=CH–$.

In this chapter, we study in detail two of the mechanisms for Fischer Tropsch synthesis, which belong to the carbene mechanism category.

§9.2   Results

In a previous chapter (5), we have calculated the relative stability of C_2H_y species on the Ru(0001) surface. In this chapter, two complete reaction cycles are calculated for two plausible mechanisms for chain growth in Fischer Tropsch synthesis.

Since CH_2 is not a stable intermediate [7,8], it cannot be considered as a building unit during chain growth on Ru(0001). Instead, CH was found to be the most stable intermediate in the C_1H_x series. Hence, one needs to include a hydrogenation step in each of the next catalytic cycles.

We consider two different growing chains: an alkylidene, homologues series of CH_2: $CH_3–CH$, etc. (mechanism 1, Figure 9.1) and an alkyl, homologues series of CH_3: $CH_3–CH_2$, etc. (mechanism 2, Figure 9.2).

In the case of alkylidene mechanism 1 in Figure 9.1 we start with an adsorbed R–CH (CH_2 for the first cycle), which reacts with an adsorbed CH. The result is an adsorbed R–CH–CH monoradical (vinyl like), which is adsorbed with the terminal CH in a bridge site and with the before last CH in atop site (the so-called 3-σ adsorption mode). This species can be hydrogenated to form an adsorbed alkene, which could desorbs, or the hydrogenation process can lead to R–CH_2–CH, which is the homologue of the species we start with (has an extra CH_2). The initial species has a choice, besides the coupling with an adsorbed CH, to hydrogenate to adsorbed R–CH_2 and further to the alkane (R–CH_3) or to dehydrogenate to form adsorbed R–C (ethylidyne like), which is one of the most stable species [6]. This mechanism has some similarities with the mechanism proposed by Maitlis [5]. Two key differences are to be noted however. Firstly, the insertion species in this study is adsorbed CH, rather than CH_2. Secondly the growing chain has a structure, which is able to have a double bond at the atom connected at the surface, but because of the high activity of the surface, the last two atoms are connected to the surface, so, the double bond is lost, both C atoms have sp^3 hybridization [6].
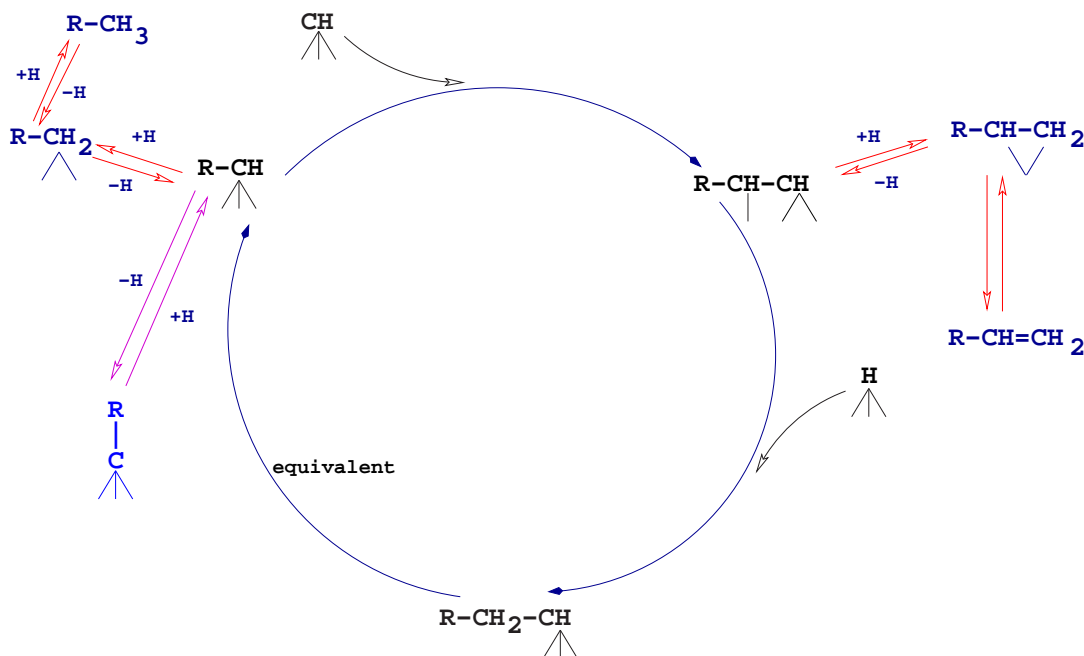
Figure 9.1: Fischer Tropsch, mechanism 1. | indicates atop adsorption, $\wedge$ indicates bridge adsorption, $\mathbb{\wedge}$ indicates three-fold site (fcc or hcp) adsorption and $\vee$ indicates di-σ adsorption mode. The R is H for the first cycle and CH_3 for the second one.

The second (alkyl) mechanism is shown in Figure 9.2. We start with an adsorbed R–CH_2 (CH_3 for the first cycle), which will interact with an adsorbed CH. The result is an adsorbed R–CH_2–CH radical. This species can be hydrogenated to adsorbed R–CH_2–CH_2, which is the homologue of the species we start with, or it can dehydrogenate to form R–CH_2–C (ethylidyne like), which is one of the most stable species [6]. The initial species has a choice, besides the coupling with an adsorbed CH, to hydrogenate to the alkane (R–CH_3). This mechanism is the classical one with one exception: adsorbed CH rather than adsorbed CH_2 is inserted in the growing chain.

It is worthwhile to mention that the two mechanisms share one common intermediate, namely R–CH. Because of this, the growing chain can switch between one mechanism and the other in subsequent growth cycles. In Figure 9.3 we show the adsorption energies of the intermediates and of Transition States, for the first two catalytical cycles in the first mechanism, and in Figure 9.4 we show the same for the second mechanism.
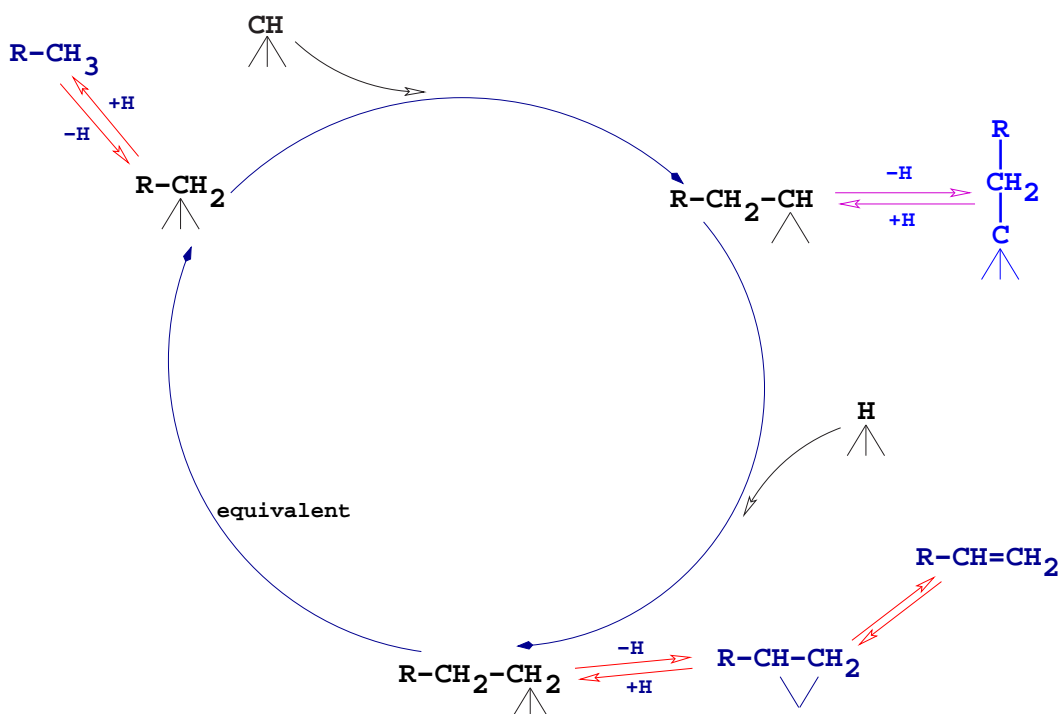
Figure 9.2: Fischer Tropsch, mechanism 2. $|$ indicates atop adsorption, $\bigwedge$ indicates bridge adsorption, $\bigwedge\!\!\!|$ indicates three-fold site (fcc or hcp) adsorption and $\bigvee$ indicates di-σ adsorption mode. The R is H for the first cycle and CH_3 for the second one.

The choice of a common reference energy during the catalytic cycle is not unambiguous, "n CH + n H + H_2" was finally used.

The first transition state in the first mechanism (Figure 9.3) is a coupling of an adsorbed CH_2 with an adsorbed CH to form adsorbed CH_2CH. The barrier is 102 kJ×mol^{-1} with respect to separated adsorbed methylene and methine, and 72×mol^{-1} with respect to close adsorbed methylene and methine. In the TS, the CH group is adsorbed at an hcp site with the C–H tilted in the opposite direction than the incoming CH_2 group.

The second TS is the hydrogenation of vinyl. This process is an easy one. Once the H atom has approached the vinyl (this costs 24 kJ×mol^{-1}), the barrier is only 8 kJ×mol^{-1} to form ethylidene.

The first TS in the second cycle of mechanism 1 is a coupling of adsorbed CH_3–CH with an adsorbed CH to form adsorbed CH_3–CH–CH. The barrier is also important,
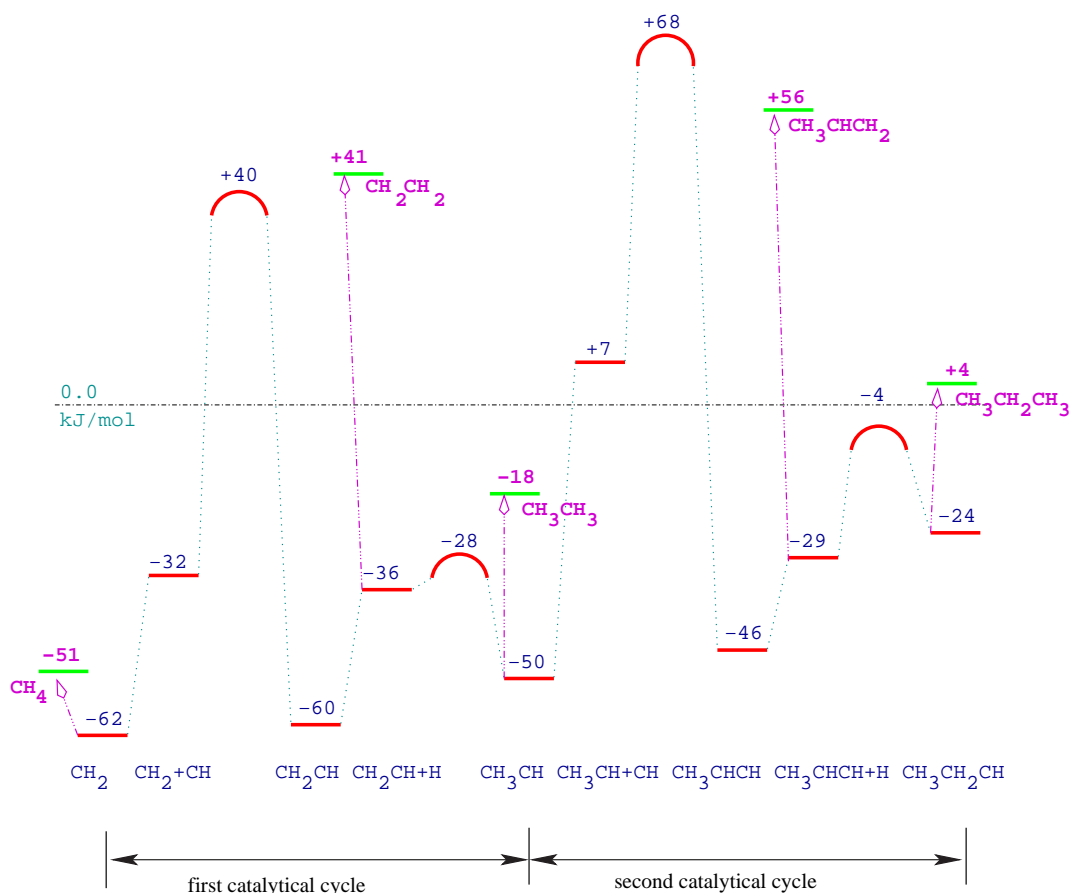
Figure 9.3: Fischer Tropsch, mechanism 1. The first two catalytical cycles, interme-
diates, Transition States, and chain growth termination.

118 kJ×mol^{-1} with respect to separated adsorbed reactants or 61 kJ×mol^{-1} with
respect to reactants adsorbed at neighboring sites.

The second TS in the second cycle is the hydrogenation of adsorbed 1–propenyl
to form propylidene. This reaction has a barrier of 25 kJ×mol^{-1} with respect to the
reactants adsorbed in proximity.

In the second mechanism (Figure 9.4), the first TS is the coupling of methyl with
methylidyne. The barrier is rather small, only 6 kJ×mol^{-1} with respect to adsorbed
CH_3 and adsorbed CH at neighboring sites. This adsorption in proximity is not an
easy process. Both the CH and the CH_3 are tilted to minimize the repulsions. CH_3
has a large repulsion caused by its volume, while the CH has a strong repulsion due
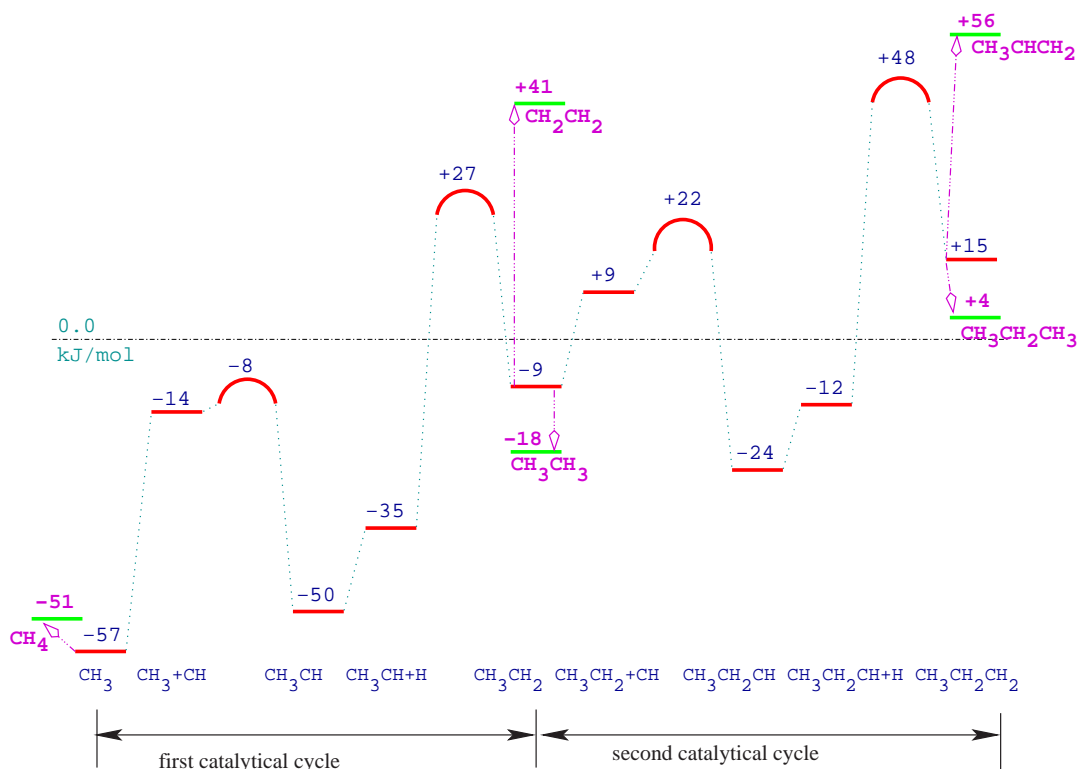
Figure 9.4: Fischer Tropsch, mechanism 2. The first two catalytical cycles, intermediates, Transition States and chain growth termination.

to the strong adsorption (interactions through the metal) [7].

The second TS is for the hydrogenation of ethylidene to form ethyl. The barrier is 77 kJ×mol^{-1} with respect to separated adsorbed species and 62 kJ×mol^{-1} with respect to the adsorbed reactants in proximity.

The second cycle of the second mechanism start with the coupling of ethyl with methylidyne. The barrier is also small, about 22 kJ×mol^{-1}. The last barrier is for the hydrogenation of propylidene to form propyl. This reaction has an activation energy of 72 kJ×mol^{-1} with respect to separately adsorbed species and 60 kJ×mol^{-1} with respect to adsorbed reactants at neighboring sites.

The geometries of the eight transition states are presented next.

The coupling of CH$_2$ and CH and the coupling of CH$_3$CH and CH are similar, in particular their transition state geometries. One H from the CH$_2$ and the H from the CH group in CH$_3$CH are slightly activated with a bond length C–H of 1.14 Å. The

other C–H bonds are 1.10 Å. The C–Ru bond lengths are 2.30 and 2.07 Å, for the CH$_2$ and 2.38 and 2.07 Å, for the CHCH$_3$. The CH group is in an hcp hollow site, and the C–Ru bond length are 2.05, 2.04 and 2.29 Å for the CH, which will couple with CH$_2$, and 2.05, 2.04 and 2.24 Å for the CH, which will couple with CHCH$_3$. The C$_{CH}$–C$_{CH-R}$ is 1.88 Å for R=H and 1.89 Å for R=CH$_3$, see Figure 9.5.

a.

c.

b.

d.
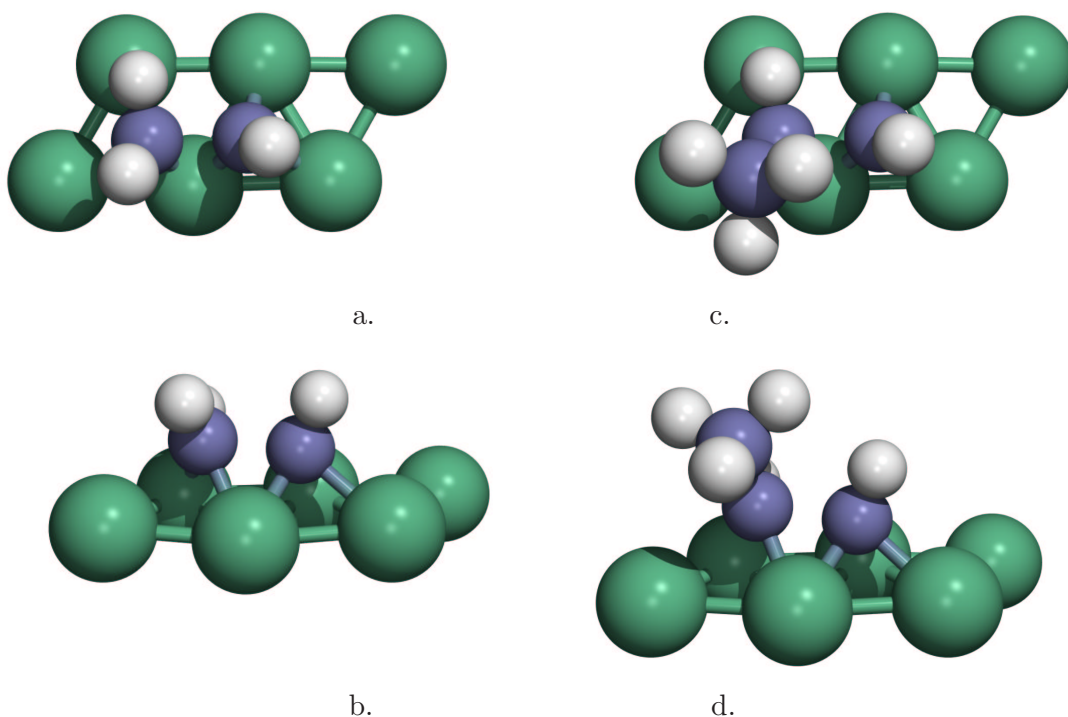
Figure 9.5: Transition States for R–CH coupling with CH, R = H (a, b) and CH$_3$ (c, d). Atop (a, c) and side (b, d) view.

Similarly, the coupling of CH$_3$ and CH closely resembles the coupling of CH$_3$CH$_2$ and CH. All C–H bonds are 1.10 Å. CH$_3$ and CH$_2$CH$_3$ are sitting atop, slightly tilted and CH are sitting in hcp hollow sites. C–Ru bond lengths are 2.21 and 2.27 for CH$_3$ and CH$_2$CH$_3$ respectively, while for CH group they are 1.99, 2.00, and 2.06 Å in both cases. The C$_{CH}$–C$_{CH_2R}$ is 2.60 Å for R=H and 2.66 Å for R=CH$_3$.

The hydrogenation reactions of CH$_2$CH and CH$_3$CHCH have a very early transition states. The geometries of vinyl and 1–propenyl are not very disturbed, and the incoming H is moving over atop at the metal atom where the CH$_2$ or the CH$_3$CH interacts with the surface.

For the hydrogenation of CH_3CH and CH_3CH_2CH, the TS are late. The CH group sitting on the surface have the C–H bond length of 1.17 Å, and the C–Ru bond lengths of 2.14, 2.35 and 2.12 Å. The incoming H has a H–Ru distance of 1.66 Å, characteristic for Ru(0001) C–H bond breaking or making [9]. The C–H bond, which will form after the TS is 1.64 Å for CH_3CH + H and 1.66 Å for CH_3CH_2CH + H, see Figure 9.6.
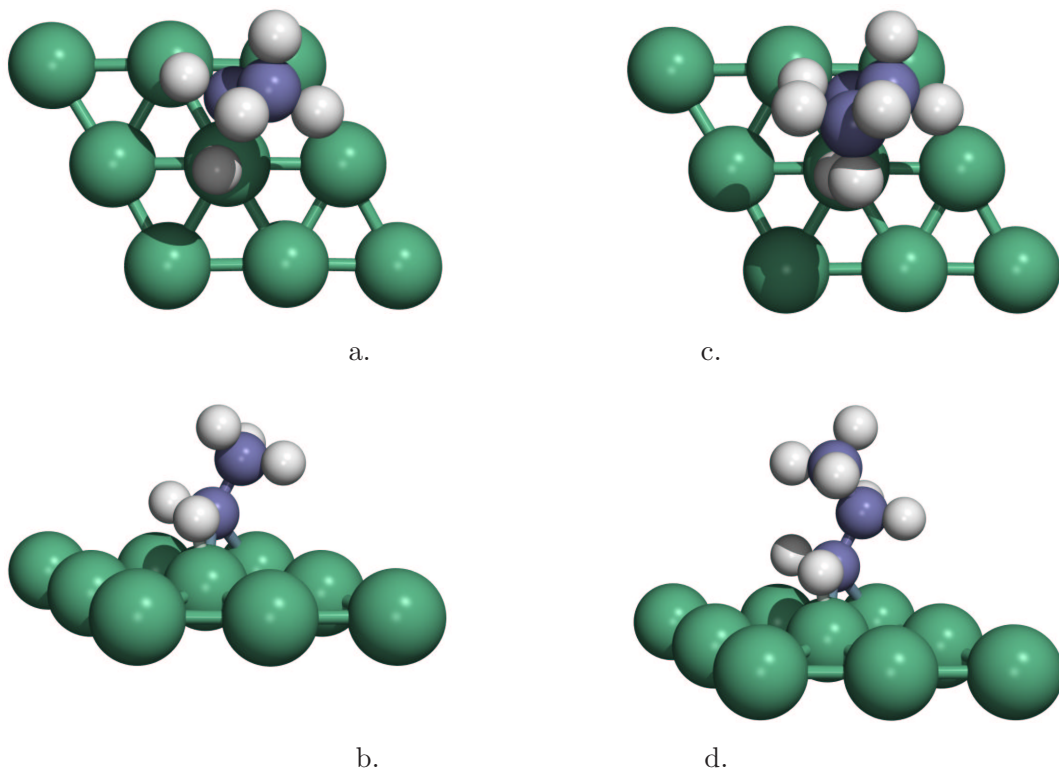
Figure 9.6: Transition States for R–CH_2–CH hydrogenation, R = H (a, b) and CH_3 (c, d). Atop (a, c) and side (b, d) view. The hydrogen atom in shadow in (a) is the one attacking the vinyl group. In (c) the hydrogen atom that is attacking is under one of the hydrogen atoms from CH_3.

Two termination reactions have to be considered, namely the formation of parafines and olefines. In the first mechanism, the olefines can be formed from the vinyl-like intermediates (R–CH–CH) by hydrogenation to the other side. Although this reaction is endothermic, the barrier is low. In the second mechanism, the ole-

fines can be made from alkyls radicals by dehydrogenation (a beta H is lost). This reactions are also endothermic, but the barriers are also small since at least one H atom from the beta carbon is activated.

The parafines can be formed in the first mechanism by a double hydrogenation of the growing chain. If we consider that the barriers for methane formation from CH_2 [9] (≈ 96 kJ$\times$mol^{-1}) are portable to the R–CH, then the barriers for parafines formation R–CH + 2 H $\rightarrow$ R–CH$_3$ are high even through the reactions are slight exothermic. In the second mechanism, the parafines can be made out of alkyls radicals via hydrogenation. High barriers for those reactions are expected (≈ 91 kJ$\times$mol^{-1}).

§**9.3   Conclusion**

We presented two mechanisms for Fischer Tropsch synthesis. Both are considering CH as building block since CH is the most stable species within the CH_x series and hence the most abundant. Each coupling reaction must be followed by a hydrogenation reaction in order to close the catalytic cycle. As "resting states" of the growing chain, we considered an alkyl group (methyl like) and an alkylidene group (methylene like). In both mechanism the CH_{ads} building block have small mobility, while the growing chain has a large mobility on the surface.

In the second mechanisms all species will interact with the surface only with the last C atom, while in the first mechanism some intermediates will bind to the surface with the last two carbon atoms due to the higher unsaturation.

Since the mechanism share a common intermediate (R–CH), they can exchange this species, so a growing chain can use one or the other mechanism for few catalytic cycles. A parallel mechanism is also supported by experimental results.

The hydrogenation of the C_xH_y species occurs in a similar way like for the hydrogenation of CH or CH_2 on Ru(0001). The incoming H atom is in atop position at 1.66 Å from the Ru atom and the H–C bond, which is started, is around 1.6–1.7 Å.

The C–C coupling in the first mechanism has large barriers (more than 100 kJ$\times$mol^{-1} while in the second mechanism those are much smaller.

Going from C_1 species to C_{2+} is different in the two mechanisms presented here. The first mechanism shows a small difference in the reaction heat for a catalytic cycle (the stability of CH_2 and homologues is similar), while the reaction heat for a catalytic cycle in the second mechanism is different for the first catalytic cycle (the stability of CH_3 and homologues is much different due to the fact that CH_3 is

adsorbed in a fcc three fond hollow site, while the homologues R–CH$_2$ are adsorbed in a bridge site). This difference could be responsible for the difference observed in experiments for the first coupling (two C$_1$ species) and the next ones.

The two mechanisms proposed can proceed in parallel. More than that, they share intermediates, so, a hydrocarbonic chain can be formed via few cycles of one mechanism and then few of the other, depending on the local concentrations of H atoms (for hydrogenation) and CH group (for C–C coupling).

Bibliography

[1] R. B. Anderson, *The Fischer Tropsch synthesis*, Academic Press Inc., Orlando, (1984)

[2] J. P. Hindermann, G. J. Hutchings, A. Kiennemann, *Catal. Rev. Sci. Eng.*, 35, (1993), 1

[3] M. E. Dry, *Apl. Catal. A*, 138, (1996), 319

[4] G. P. van der Laan, A. A. C. M. Beenackers, *Catal. Rev. Sci. Eng.*, 41, (1999), 255

[5] P. M. Maitlis, H. C. Long, R. Quyoum, M. L. Turne, Z.-Q. Wang, *Chem. Commun.*, (1996), 1

[6] I. M. Ciobîcă, F. Frechard, R. A. van Santen, Phys. Chem. Chem. Phys., submitted

[7] I. M. Ciobîcă, F. Frechard, A. P. J. Jansen, R. A. van Santen, *Stud. Surf. Sci.*, 133, (2001). 221

[8] I. M. Ciobîcă, F. Frechard, C. G. M. Hermse, A. P. J. Jansen and R. A. van Santen, in *Surface Chemistry and Catalysis*, ed. A. F. Carley, P. R. Davies, G. J. Hutchings and M. S. Spencer, Kluwer Academic/Plenum, 2002

[9] I. M. Ciobîcă, F. Frechard, R. A. van Santen, A. W. Kleyn and J. Hafner, *J. Phys. Chem. B*, 104, (2000), 3364.

Chapter 10

General conclusions

The preferred adsorption sites for H, CH_x (x = 0-3), and C_2H_y (y = 0-5) on Ru(0001) are the three-fold sites (fcc or hcp) with the exception of ethyl. A comparison of the site position energies for an adsorbed species provides an estimate of activation energy for diffusion. These activation energies are of the order of $13-17 \, \mathrm{kJ \times mol^{-1}}$ for monovalent species, $\approx 25 \, \mathrm{kJ \times mol^{-1}}$ for divalent species and $43-57 \, \mathrm{kJ \times mol^{-1}}$ for tri- and multi- valent species. CH is found to be the most stable species of the CH_x series on Ru(0001) in good agreement with the experimental results from Wu and Goodman. CCH_2 and CCH_3 are found to be the most stable species of the C_2H_x series, despite their different adsorption mode.

From the analysis of partial DOS diagrams we can conclude that for the methane decomposition the sp^3 hybrid of C atom and the s orbital of H atom interact mainly with the $d_{3z^2-r^2}$ orbital of the first Ru atom and with the d_{xz}, d_{xy} orbital of the second Ru atom. In all other cases, the main interaction is only in between the σ_{C-H} and the $d_{3z^2-r^2}$ orbital of the Ru atom.

The interaction between adsorbed CH_x and CH_y (x, y = 0-3) is repulsive (through the surface for small x and y, and steric for x or y equal to 3). The information on the $CH_x + CH_y$ interaction energies together with the relative energies of C_2H_z (x, y = 0-3, z = 0-5) give us the possibility to understand the relative stability of C_2 species versus the C_1 species, as well as the dimensions of lateral interaction (energies, distances).

Considering a more open surface, $Ru(11\bar{2}0)$, compared with the close packed surface, all species have smaller adsorption energies, and we assume that this is due to the particularity of the surface which has no three-fold sites for adsorption.

Methylene is the most stable species from the adsorbed CH_x series (x = 0-3) on a $(11\bar{2}0)$ surface.

H coadsorption with CH_x (x = 0-3) is repulsive, the same as on the closed packed surface. Transition States for C–H activation on $Ru(11\bar{2}0)$ are different from the ones on a $Ru(0001)$ surface. Similarities are in the cases $CH_4/(0001)$ with $CH_4/(11\bar{2}0)$, $CH_2/(0001)$ with $CH_3/(11\bar{2}0)$, and $CH/(0001)$ with $CH/(11\bar{2}0)$. The activation of methane and methyl are early Transition States, while the activation of CH is a late Transition State.

$Ru(11\bar{2}0)$ is a more open surface compared with the (0001), and more reactive. The CH_x species are strongly bonded to the surface, but less than in the case of (0001) surface, due to the lack of three-fold sites, which make the species more reactive.

CO adsorbs strongly to the closed packed surface of Ru. At lower coverage the atop site is preferred, up to 25%. The lateral interaction of the CO adsorbed atop and CO adsorbed hcp is different, hcp site having the smaller lateral interaction. The adsorption sites located near a step are more favorable with about 20 kJ×mol^{-1} for both atop and hcp sites, and with about 10 kJ×mol^{-1} for sites located at the bottom of the steps.

Hydrogen can form compressed layers on a $Ru(0001)$ surface. Up to 100% coverage, the adsorption energy does not change. Up to 150% coverage, the lateral interaction is still acceptable. After 200% coverage, the adsorption energy is going to zero and the second layer of atoms is building up.

For the H coadsorption with CO, the lateral interactions are repulsive; H and CO prefer to segregate, rather than to form mixed structures. At low coverage of H and low coverage of CO, both species can adsorb on the preferred site (CO – atop, H – fcc). However, by increasing the H coverage, the H is forced to populate sites closer to CO molecule and this leads to distortions of the H adsorption site (bond with different lengths H–Ru). CO is little affected by the H coadsorption, unless the H is present at 100% coverage, when the CO will still adsorb on the atop sites with an important decrease of the adsorption energy. Contrary to the adsorption of CO on a bare $Ru(0001)$ surface, CO adsorption on the $Ru(0001)$ surface completely covered with hydrogen is an activated process and the lowest barrier found, is about 25 kJ×mol^{-1} which could be verified experimentally as well as by DFT calculations. By tilting the CO molecule up to an angle of 35°, the barrier does not change. Experimentally, an additional non–activated reaction channel could be identified, which seems due to CO adsorption at defect sites in the hydrogen overlayer.

Differences in the interaction of CO with the Ru(0001) surface in the absence or in the presence of H are basically due to the changes in the interaction between 4σ, 5σ molecular orbitals of CO and the $d_{3z^2-r^2}$, s, and p_z orbitals of the Ru atom. If H is present on the surface, the s_{Ru}–$CO_{5\sigma}$ bond gets weaker and the $d_{3z^2-r^2} - 4\sigma$ and 5σ repulsions induce a barrier for the adsorption. As CO and H interact with the lower levels of the d–s band the Ru atom dramatically moves outwards by 0.4 Å, reflecting the strong weakening of the Ru–Ru surface bonds.

On steps, the best way to dissociate CO is to adsorb CO at the bottom of the step and the O atom will jump on the next terrace. The barrier for this reaction is 128 kJ×mol^{-1}.

The Boudouard reaction, as an alternative for the direct CO decomposition, is less probable. The barrier on the steps is higher than for CO dissociation with 44 kJ×mol^{-1}. We expect that on flat surface this difference to be higher.

CHO as intermediate for CO decomposition was also investigated. This indirect route for CO dissociation, which is favorable on Pd, is not preferred on Ru. The overall barrier for the indirect path on a flat surface is 59 kJ×mol^{-1} higher than the direct dissociation path on flat surface.

We successfully developed a model to extract parameters from DFT calculations and used as input in Dynamic Monte Carlo. Including lateral interaction in DMC slows down hydrogenation of C atom and speed up the decomposition of CH_4 in the system $CH_4 \rightleftharpoons C + 2H_2$. The combination of *ab–initio* calculations for kinetic parameters and DMC simulations allows to get an insight into heterogeneous catalytic reactions at the atomic scale.

We presented two mechanisms for Fischer Tropsch synthesis. Both are considering CH as building block since CH is the most stable species within the CH_x series and hence the most abundant. Each coupling reaction must be followed by a hydrogenation reaction in order to close the catalytic cycle. As "resting states" of the growing chain, we considered an alkyl group (methyl like) and an alkylidene group (methylene like). In both mechanism the CH_{ads} building block have small mobility, while the growing chain has a large mobility on the surface.

In the second mechanism all species will interact with the surface only with the last C atom, while in the first mechanism some intermediates will bind to the surface with the last two carbon atoms due to the higher unsaturation.

Since the mechanism share a common intermediate (R–CH), they can exchange this species, so a growing chain can use one or the other mechanism for few catalytic

cycles. A parallel mechanism is also supported by experimental results.

Going from C_1 species to C_{2+} is different in the two mechanisms presented here. The first mechanism shows a small difference in the reaction heat for a catalytic cycle (the stability of CH_2 and homologues is similar), while the reaction heat for a catalytic cycle in the second mechanism is different for the first catalytic cycle (the stability of CH_3 and homologues is much different due to the fact that CH_3 is adsorbed in a fcc three fond hollow site, while the homologues $R–CH_2$ are adsorbed in a bridge site). This difference could be responsible for the difference observed in experiments for the first coupling (two C_1 species) and the next ones.

The two mechanisms proposed can proceed in parallel. More than that, they share intermediates, so, a hydrocarbonic chain can be formed via few cycles of one mechanism and then few of the other, depending on the local concentrations of H atoms (for hydrogenation) and CH group (for C–C coupling).

If we compare our results on ruthenium with similar results on different transitional metal surfaces, we can conclude that for the methanation reaction the stronger the M–C bond is, the more difficult is to hydrogenate.

For Ru(0001), TS for C–C coupling are lower that the TS for methanation, this explain why Fischer Tropsch is happening on ruthenium.

Since CO dissociation can occur on ruthenium, Fischer Tropsch will not proceed via CO insertion mechanisms. We believe that the O atom is removed as water and the C atom is partially hydrogenated and then will enter in the C–C coupling cycle.

Appendix A

How to get Transition States?

§A.1 Methods to get Transition States

There are few methods to get Transition States. Here is a scheme:

- with 1 point
    - a path of slowest ascent
    - normal modes of a local harmonic approximations potential

- use of two points boundary condition

    - "drag" method of the "reaction coordinate"
    - chain of images

We will focus on chain–of–states methods (see Figure A.1). What are needed are the initial state (IS), the final state (FS) and a chain of images describing the path.

§A.2 Examples. What do we need?

Let us consider the following reaction: $CH_2 \rightarrow CH + H$ on the Ru(0001) surface. We would need:

- an optimized structure of reactant (CH_2 on Ru(0001) — IS), see Figure A.2.

- an optimized structure of products (CH + H on Ru(0001) — FS), see Figure A.3. Several coadsorption modes are possible $\rightarrow$ several mechanism possible.
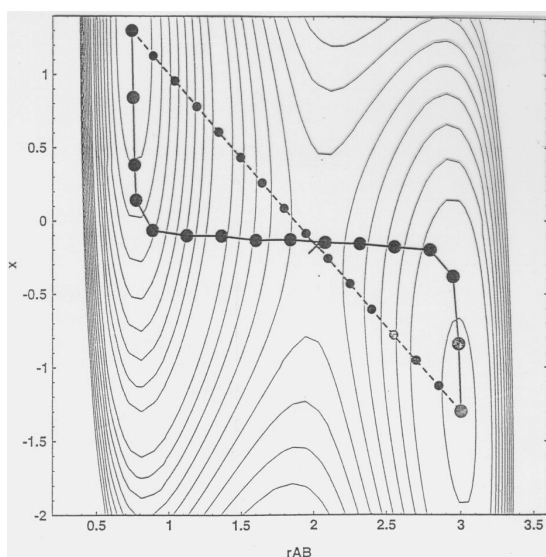
Figure A.1: An example of a chain–of–states method. You can see the interpolated images (small filled circles) and the final images (larger filled circles) describing the reactional path.
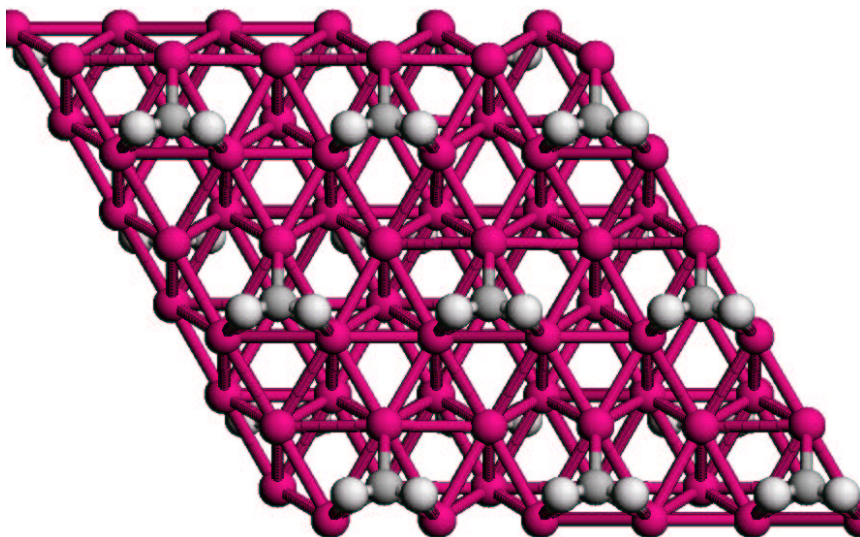
Figure A.2: CH_2 adsorbed in hcp site. The initial state for NEB calculation.

- selecting one mechanism $\rightarrow$ choosing the images (interpolation in hyper-space).
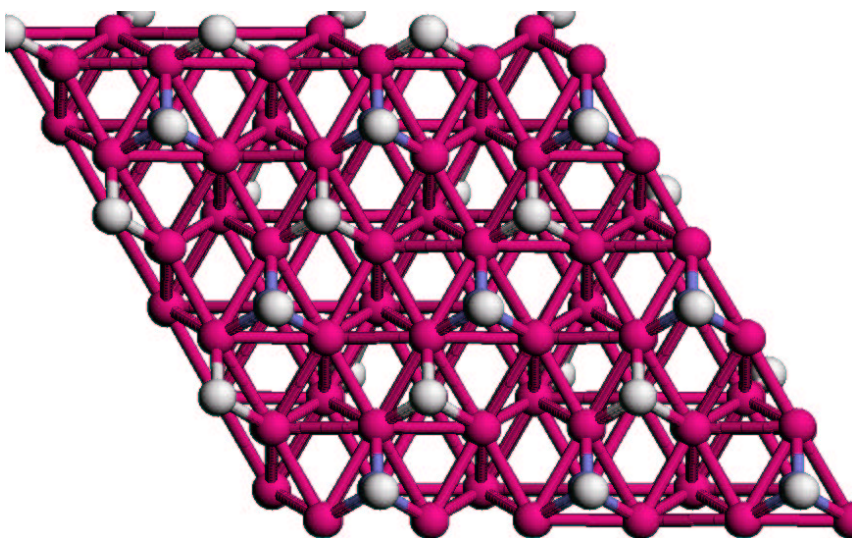
Figure A.3: CH and H coadsorbed on hcp and fcc sites, respectively. The final state for NEB calculation.
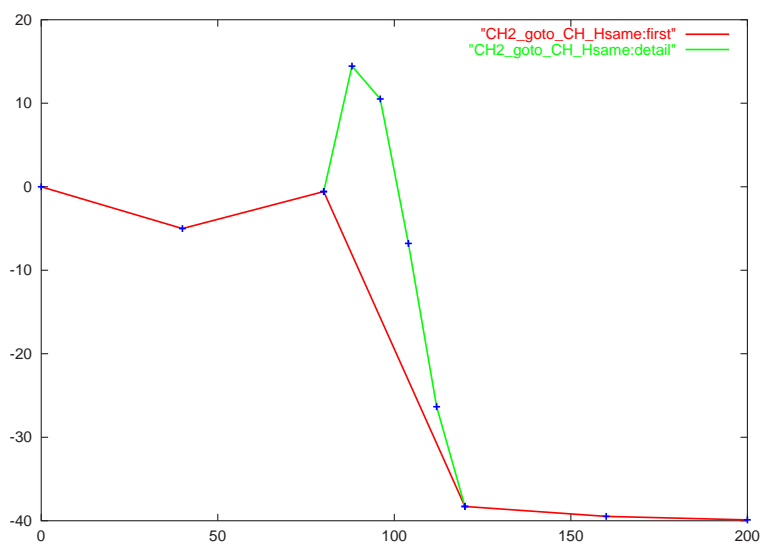
Figure A.4: The reaction path for CH_2 decomposition calculated with NEB.

Calculations will validate or not the proposed mechanism, see Figure A.4. First approach was to consider 4 points in the potential energy hyperspace. Like that, we discover an other minima for the CH_2 (initial state), more stable with less symmetry.

After that, we focus in the middle of the path by choosing images 2 and 3 as initial, respectively final states and we calculated again using 4 images. This time the first image was close enough to the TS in order to use the quasi Newton algorithm.

Summaries

Summary

Fischer Tropsch synthesis is a process that is in focus as an alternative route for the production and transportation of fuels and petrochemical feedstock. There are many chemical reactions involved in this process, but few can be isolated. To initiate the Fischer Tropsch reaction, the initial reaction mixture in different ratios, of CO and H_2 molecules adsorb dissociatively, in order to form atomic species of C, O and H. Those atomic species will recombine in order to form H_2O, CH_4, C_2H_6, C_2H_4, etc. In the recombination process, two aspects are key: hydrogenation and C–C coupling. A good Fischer Tropsch catalyst is characterized by a high rate for C–C coupling and a low rate for hydrogenation. A higher rate for hydrogenation will reduce C–C bond formation and the primary product will be CH_4, as formed for the Ni catalyst. Additionally, if CO dissociation is difficult, CH_3OH can be the primarily product. A too low hydrogenation rate is also not desired, because the hydrocarbon chain then will not be hydrogenated easily and will not desorbs. Too long chains will be formed and reaction will be stopped by product poisoning.

Ruthenium is a metal on which CO dissociation is easier compared to the transition metals at the right side of the periodic table. At the same time the M–C bond is weaker compared with the transitional metals from the left side of the periodic table, where the carbon species cannot be eliminated easily from the surface. These two properties make ruthenium a very good catalyst for Fischer Tropsch synthesis. Unfortunately, the small abundance in nature makes it too expensive for industrial applications at large scale.

The work described in this thesis focuses on the three key aspects mentioned earlier: CO dissociation, C–C coupling and C_xH_y hydrogenation. CO dissociation is the rate limiting step for the overall reaction. Therefore, we investigated defects

(steps) on the surface, in order to understand how the dissociation rate of CO can be enhanced. C–C coupling can take place on the terraces of the metallic surface. The hydrogenation (and/or methanation) was investigated on a close packed surface and on an open surface in order to understand the effect of different surfaces on this process and to find a way to suppress undesired methane formation.

Important for reactions on the surface are the lateral interactions between species adsorbed in close proximity. This effect is discussed in each chapter, but more in detail in the case of the compressed layers of H and interactions with CO.

Dynamic Monte Carlo was used to investigate methanation of CH_x species with the use of Density Functional Theory results. Unfortunately, this could not be applied to the entire Fischer Tropsch process. However, Density Functional Theory results are available and work can be continued to use Density Functional Theory results in order to build a kinetic model with the application of Dynamic Monte Carlo techniques.

Samenvatting

De Fischer-Tropsch-synthese is een proces wat in de schijnwerpers staat als een alternatieve route voor productie en dat transport van brandstoffen en petrochemische basismaterialen. Er zijn veel chemische reacties gemoeid met dit proces, en maar een paar kunnen geïsoleerd worden. Om de Fischer-Tropsch-reactie te initiëren adsorbeert het oorspronkelijk reactiemengsel, bestaande uit verschillende verhoudingen van CO en H_2, al dissociërend om atomair C, O en H te vormen. Deze atomen recombineren om H_2O, CH_4, C_2H_6, C_2H_4 enzovoorts te vormen. Er zijn twee bepalende stappen in het recombinatie proces: hydrogenering en C–C koppeling. Een goede Fischer-Tropsch-katalysator wordt gekarakteriseerd door een hoge C–C koppelingssnelheid en een lage hydrogeneringssnelheid. Een hogere hydrogeneringssnelheid zal C–C bindingsvorming verminderen en het hoofdproduct zal CH_4 zijn, zoals gevormd door de Ni-katalysator. Daarnaast, als CO dissociatie lastig is, kan CH_3OH het hoofdproduct zijn. Een te lage hydrogeneringssnelheid is ook niet gewenst, omdat de koolwaterstofketen dan niet makkelijk hydrogeneert, en niet zal desorberen. Te lange ketens zullen vormen en de reactie zal gestopt worden door productvergiftiging.

Rutheen is een metaal waarop CO dissociatie makkelijker is dan op de overgangsmetalen aan de rechterkant van het periodiek systeem. Tegelijkertijd is de M–C binding zwakker dan die met de overgangsmetalen aan de linkerkant van het periodiek systeem, waar de koolstof verbindingen niet makkelijk van het oppervlak kunnen worden verwijderd. Deze twee eigenschappen maken rutheen een heel goede katalysator voor de Fischer-Tropsch-synthese. Jammer genoeg maakt het geringe voorkomen in de natuur het te duur voor grootschalige industriële toepassingen.

Het werk beschreven in dit proefschrift is gericht op de drie hoofdthema's die hiervoor genoemd zijn: CO dissociatie, C–C koppeling en C_xH_y hydrogenering. CO dissociatie is de snelheidsbepalende stap voor de gehele reactie. Daarom hebben we onderzoek gedaan naar defecten aan het oppervlak (stappen) om te begrijpen hoe de dissociatiesnelheid kan worden verbeterd. C–C koppeling kan plaats hebben op de terrassen van de metaaloppervlakken. De hydrogenering (en/of methanering) is onderzocht op een dichtgepakt en op een meer open oppervlak om het effect van verschillende oppervlakken op dit proces te begrijpen en om een manier te vinden om ongewenste methaanvorming te onderdrukken.

Belangrijk voor de reacties op het oppervlak zijn de laterale interacties tussen moleculen of fragmenten dichtbij elkaar geadsorbeerd. Dit effect wordt behandeld in

elk hoofstuk, maar meer gedetailleerd voor het geval van de gecomprimeerde lagen van H en de interacties met CO.

Dynamische Monte-Carlo met de hulp van dichtheidsfunctionaaltheorieresultaten is gebruikt om de methanering van CH_x verbindingen te onderzoeken. Jammer genoeg kon dit niet worden toegepast op het hele Fischer-Tropsch proces. De dichtheidsfunctionaaltheorieresultaten zijn echter beschikbaar en het werk kan worden voortgezet om dichtheidsfunctionaaltheorieresultaten te gebruiken om een kinetisch model te bouwen onder toepassing van Dynamische Monte-Carlo technieken.

Rezumat

Sinteza Fischer Tropsch este un proces, care începe din ce în ce mai mult să fie considerat ca o alternativă pentru producția și transportul combustibilului și al materiilor prime petroliere. Sînt multe reacții chimice implicate în acest proces, cîteva din ele au putut fi izolate. Pentru a iniția reacția Fischer Tropsch, amestecul de reacție, în diferite proporții, a moleculelor de CO și H_2 este adsorbit disociativ, pentru a forma pe suprafață, speciile: C, O și H. Aceste specii atomice se recombină pentru a forma H_2O, CH_4, C_2H_6, C_2H_4, ș.a.m.d. În procesul de recombinare, două aspecte sînt importante: hidrogenarea și cuplarea a două specii cu atomi de carbon. Un bun catalizator Fischer Tropsch este caracterizat printr-o rată înaltă de cuplare C–C și printr-o rată scăzută de hidrogenare. O rată de reacție mai mare pentru hidrogenare va reduce formarea legăturilor C–C și produsul principal de reacție va fi CH_4, ca în cazul catalizatorului de Ni. În plus, dacă disocierea CO este dificilă, CH_3OH poate fi produsul principal. De asemenea, o rată prea scăzută de hidrogenare nu este dorită, deoarece lanțul hidrocarbonat nu se va hidrogena destul de ușor să poată fi desorbit. Lanțuri hidrocarbonate prea lungi se vor forma în acest caz și reacția va înceta prin otrăvirea cu produs.

Ruteniul este un metal unde disocierea CO este ușoară, comparativ cu metalele tranziționale din dreapta lui, în tabelul periodic. În același timp, legătura M–C este slabă, comparată cu cele ale metalelor tranziționale din partea stîngă a Ru din tabelul periodic, unde speciile de carbon nu pot fi eliminate ușor de pe suprafață. Aceste două proprietăți fac din ruteniu un foarte bun catalizator pentru sinteza Fischer Tropsch. Din nefericire, mica lui abundență în natură îl face prea scump pentru aplicații industriale la scară mare.

Această lucrare urmărește cele trei puncte descrise anterior: disocierea CO, cuplarea C–C și hidrogenarea C_xH_y. Disocierea CO este etapa limitativă a întregii reacții. De aceea am studiat-o pe defecte ale suprafeței pentru a înțelege cum poate fi majorată viteza de reacție. Cuplarea C–C poate avea loc pe suprafața fără defecte a metalului. Hidrogenarea (și/sau metanarea) a fost investigată pe o suprafață densă și pe una mai puțin compactă, pentru a înțelege efectul diferitelor suprafețe asupra acestui proces și de a găsi o modalitate de a elimina formarea nedorită a metanului.

Importante pentru reacțiile pe suprafață sînt interacțiunile laterale între speciile adsorbite în imediata apropiere. Acest efect este discutat în fiecare capitol, mai detaliat pentru stratul compresat de H adsorbit și interacțiunile cu CO.

Monte Carlo Dinamic a fost folosit pentru investigarea metanării speciilor CH_x, folosind rezultatele obținute cu teoria funcțională a densității. Din păcate, aceasta nu a putut fi aplicată întregului proces Fischer Tropsch. Rezultatele obținute cu teoria funcțională a densității sînt disponibile și munca poate fi continuată prin folosirea acestor rezultate pentru a construi un model cinetic pentru aplicarea tehnicii Monte Carlo Dinamic.

Résumé

La synthèse Fischer Tropsch est un procédé qui est considéré comme une alternative de production et de transport des combustibles et matériaux pétrochimiques. De nombreuses réactions chimiques sont impliquées dans ce procédé, mais seulement quelques unes sont isolées et analysées. Pour initier la réaction de Fischer Tropsch, un mélange de CO et H_2, dans des proportions variables, est chimisorbé sur la surface. L'adsorption dissociative conduit à la formation des fragments C, O et H. Ces espèces atomique se recombinent pour former différentes molécules, telles que H_2O, CH_4, C_2H_6, C_2H_4. Dans ce procédé de recombinaison, deux phénomènes sont particulièrement importants : l'hydrogenation et le couplage C–C. Un catalyseur de Fischer Tropsch adéquat se caractérise par une grande vitesse de réaction pour le couplage C–C et par une faible vitesse de réaction d'hydrogenation. Dans le cas d'une importante vitesse de réaction d'hydrogenation, la formation des liaisons C–C est réduite, et le méthane est le principal produit de la réaction. Ceci est observé pour les catalyseurs basés sur le nickel. De plus, si la dissociation du CO est difficile, le methanol peut être le produit principal. Une faible vitesse d'hydrogenation n'est pas pour autant souhaitable. En ce cas, les chaînes hydrocarbonées ne peuvent que très difficilement se désorber de la surface, conduisant à la formation de molécules de molécules de masse croissante. Ceci entraîne à terme l'empoisonement du catalyseur et l'arrêt de la réaction.

Le ruthenium est un métal qui dissocie facilement le monoxide de carbone, en comparaison des élémentes de transition situés à la droite dans la table périodique des éléments. De plus, la liaison carbone–ruthenium est plus faible que celle qui peut être rencontrée pour les métaux situés à la gauche du ruthenium dans la table périodique. Pour ces derniers métaux, les espèces carbonées sont trop stablement chimisorbées sur la surface pour facilement s'en dissocier. Ces deux propriétés font du ruthenium un excellent catalyseur pour la synthèse de Fischer Tropsch. Malheureusement, la faible abondance naturelle de ce métal rend coûteuse les applications à l'échelle industrielle.

Ce mémoire suit les trois points énoncés précédemment. La dissociation du monoxide de carbone, le couplage entre deux espèces carbonées, et l'hydrogenation des molécules hydrocarbonées. La dissociation du monoxide de carbone est l'étape limitante de la réaction. Par cette raison, elle a aussi été analysée dans le cas où des défauts de surface (marches) sont présents. L'effet de ces défauts sur la vitesse

de réaction est quantifié. La réaction de couplage entre deux espèces carbonées est moins sensible à l'état de la surface. L'hydrogenation, et/ou la formation de méthane a été considérée pour les cas de surfaces denses et peu compactes. Ceci permet d'appréhender l'effet des différents types de surface sur le déroulement de la réaction. Des solutions permettant d'éviter la formation du méthane sont proposée.

Les phénomènes d'interactions latérales entre les espèces adsorbées à proximité les unes des autres sont importants afin de permettre la compréhension des réactions sur la surface du catalyseur. Ils seront considérés dans chacun des différent chapitres. Plus de détails seront accordés à ces phénomènes dans le cas des couches compactes d'hydrogene, aussi que dans leur interaction avec le monoxide de carbone.

Des simulations de dynamique utilisant l'algorithme de Monte Carlo ont été réalisées afin d'analyser la méthanation des espèces C_xH_y. Les paramètres de ces simulations ont été déterminées à partir de calculs utilisant la méthode de la théorie de la fonctionnelle densité. Cependant, les simulations de Monte Carlo n'ont pas été étendues à l'ensemble des réactions élémentaires de Fischer Tropsch, bien que les résultats de calculs de chimie quantique soient disponibles pour la construction de modèles cinétique complets de la réaction.

Acknowledgments

First of all, I would like to express my gratitude to my supervisors, Prof. dr. Rutger A. van Santen and Prof. dr. Aart W. Kleyn for the opportunity to work in this research group. We had many work related discussions (and not only), which had an important role in my research and in my scientific development.

I want to thank to all members of the SKA group, especially to theory group members for their support, friendship, welcoming attitude and the time we spend together in different activities.

Many thanks to Prof. dr. Gert-Jan Kramer, my copromotor for many discussions on Fischer Tropsch topic and not only. Many thanks also to Tonek Jansen for the discussions about Dynamic Monte Carlo and for his support as theory group leader. Many thanks as well to Prof. dr. Mathew Neurock for the discussions about calculations on CO decomposition, C–C coupling, and Monte Carlo simulations.

I want to express my gratitude also to Ion Barosan for helping me with the visualizations of some of my results with the AVIS software.

Here is the place to thank also to all my chemistry teachers along the years, who help me to learn this wonderful point of view over the matter, especially to Mrs. Ursan, my first chemistry teacher, Mr. Georghiță, my last chemistry teacher from highschool, Mrs. Hillebrand, my supervisor for the University diploma project.

I would like to thank to Frédéric, Lúis Antônio and Natalia, Xavier Rozanska, Xavier Sayntigny and Valerie, Xavier Cotin, Chrétien, Kirti and Sanjeev, Henk, Maxim, Adil, Francesca and Javier, Nayana, Elena, Paula, Araceli, Ramiro and Rusmely, Marcus, Lucilla, Carlos, Fernando and Pilar, Eric, Robin, Ronald, Roelant, Vili, Paul, Hiroyuki and Mika, Alexei, Willy, Danny, Joost and David for their friendship.

In adition, I would like to thank to Boersma family and to International Neighbor Group for the social events we participated together.

Special thanks go to Lúis Antônio Miguel Marques Barbosa and his wife, Natalia Lebedeva, for the many moments we share, for trips, dinners, Star Trek issues, and for becoming godparents of Ana.

Special thanks to Georgiana Languri, for the time we spend together during my visits at AMOLF, for her friendship and for becoming godmother of Ana.

Specials thanks go to Xavier Rozanska for many discussions concerning NEB and for other moments we spend together; also for keeping my French language alive.

Specials thanks go to Chrétien Hermse for his support with Dutch related administrative papers, but also for many scientifically discussions about lateral interactions and Dynamic Monte Carlo.

Specials thanks go to Frédéric Frechard for the his support, during my PhD thesis research, especially for the beginning.

Many thanks go also to my conationals living in the Netherlands: Ion and Diana Barosan, Bogdan and Carmen Andrei, Laurențiu Păpălău, Sorin Cristescu, Laura Maruster, Georgiana Languri, Florentina Roșca-Prună, Elena Toma, Andreea Gluhoi, Dana Ionescu, as well as my conationals living in Belgium: Adrian and Nicoleta Covaci, for helping me to feel less the homesick of my country.

For the patience, comprehension, love and support I would like to thank to my beloved Sorinela who help me overcome difficult moments, and for my best realization till now: my daughter Ana.

I want to thank to FOM (Stichting voor Fundamenteel Onderzoek der Materie) for supporting my PhD research.

Special thanks to all contributors in the mailing lists where I am also active: rlug and offtopic at lug.ro, debian-user, debian-www and debian-i18n at lists.debian.org, omega at ens.fr, rtfs-project at lists.sourceforge.net, i18n and fonts at XFree86.org, romanians at smartgroups.com, etc.

Special thanks to: Donald Ervin Knuth for TeX (LaTeX 2_ε), Linus Torvalds for Linux (🐧), Ian and Debra Murdock for Debian (🌀).

Curriculum Vitæ

Ionel Mugurel Ciobîcă was born on 24$^{\text{th}}$ of January 1971, in Arbore village, Suceava county, in the North-North-East of Romania — region known also as Bukovina (*Bucovina*). After primary education in the same village, highschool in the capital of the county, and military service during the Romanian "revolution" in 1989, he followed courses at University of Bucharest, Faculty of Chemistry, section of Chemistry, specialization Physical Chemistry. His thesis subject was "A study of Pd clusters with EH method". At University of Provence, Aix-Marseille I, Marseille, France, his master degree diploma title was "A study of water adsorption and decomposition on NaCl(100)" in 1996. In between March 1997 and September 2001 he had a position of PhD student at Eindhoven University of Technology. His PhD thesis title was "The Molecular Basis of the Fischer Tropsch Reaction". Starting with October 2001 he is working for Sasol Technology.

Thesis Statements for
The Molecular Basis of the Fischer Tropsch Reaction

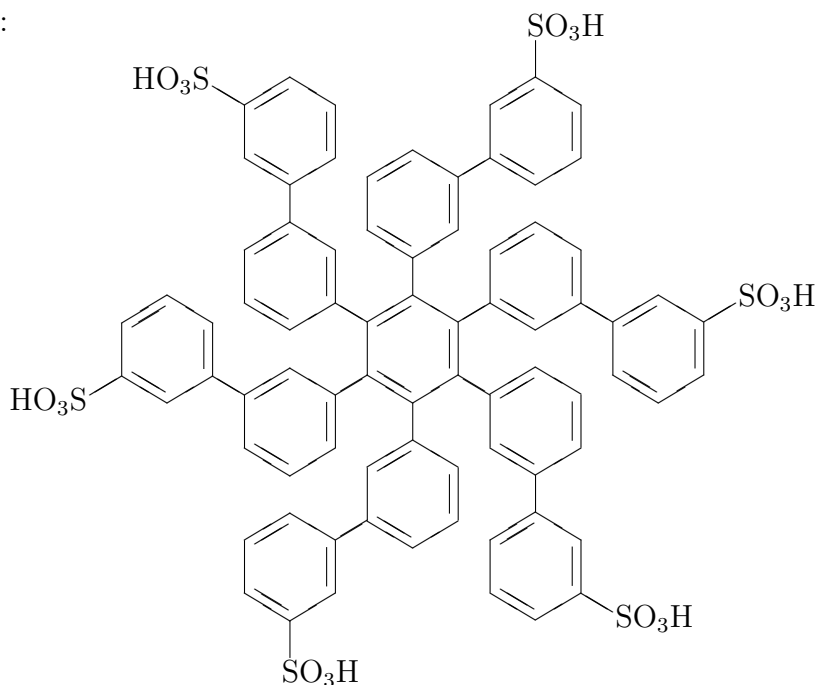Ionel Mugurel Ciobîcă

January 9th, 2002

1. J. Creuze et al. illustrates the role of chemistry in his paper: "Phase transition induced by superficial segregation: the respective role of the size mismatch and of the chemistry" (Surf. Sci. 491, 2001, 1–16). Chemistry is a discipline, is not a phenomena.

2. J. Vogt et. all in the paper "The structure of NaCl(100) and KCl(100) single crystal surfaces: a tensor low energy electron diffraction analysis" (Surf. Sci. 491, 2001, 155–168) claim that "Some of the results are contradictory...". Does this imply that the rest of results agree with all contradictory parts? "A" contradicts with "B" and "C" agrees with both "A" and "B" would lid to "A" don't contradicts with "B", which is a contradiction.

3. R. I. Masel, in his book "Principles of adsorption and reaction on solid surfaces" mentions very often that "since/because HCP is not a primitive Bravais lattice"; this explains the complexity of the HCP structure. This is the reason that one has difficulties to find a book or a paper with informations how to calculate Miller indices for a stepped HCP metal surface. An attempt is made in chapter 3 of this thesis.

4. R. L. Martins starts his paper with: "The catalytic behavior of supported Ru has been found to be unique among the noble metals" (J. Phys. Chem. B, 2001, 105, 10303–10307). Each element is unique otherwise what is the meaning of the Periodic Table of Elements?

5. N. T. Southall and K. A. Dill wrote "Our study certainly has its caveats, as we noted in the original paper." in the article *Response to "Comment on 'The Mechanism of Hydrophobic Solvation Depends on Solute Radius', J. Phys. Chem. B, 2000, 104, 1326"* (J. Phys. Chem. B, 2001, 105, 2082–2083). I wonder whether will be a comment on the response

to comment on the initial paper... Some people likes to make a show out of "Comment on..." and "Response to..."

6. D. -Y. Hwang and A. M. Mebel studied a BeO catalyst for H_2CO formation from H_2 and CO (J. Phys. Chem. A, ASAP, October 2001). There is a need for a new hydrogenation catalyst, in some reactions.

7. A. Frennet proposed that preadsorbed H can activate methane (A. Frennet, Cat. Rev. – Sci. Eng., 1974, 10, 37). An activated CH_5^+ was suggested as intermediate. This proposal is rejected in chapter 4.

8. $\text{\LaTeX}\,2_\varepsilon$ is very convenient for writing papers, reports, presentations, posters, and even complicated chemical structures, thanks to $\text{X}\overset{\frown}{\text{I}}\text{MT}_{\text{E}}\text{X}$ package, by Shinsaku Fujita.
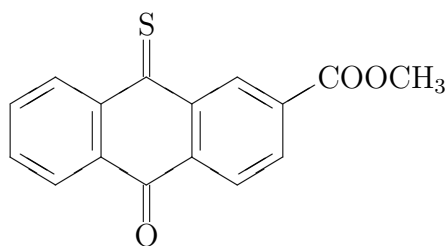
```
\bzdrv{%
1==\bzdrv{4==(yl);2==\bzdrv{5==(yl);1==SO$_3$H}};%
2==\bzdrv{5==(yl);3==\bzdrv{6==(yl);2==SO$_3$H}};%
3==\bzdrv{6==(yl);4==\bzdrv{1==(yl);3==SO$_3$H}};%
4==\bzdrv{1==(yl);5==\bzdrv{2==(yl);4==SO$_3$H}};%
5==\bzdrv{2==(yl);6==\bzdrv{3==(yl);5==HO$_3$S}};%
6==\bzdrv{3==(yl);1==\bzdrv{4==(yl);6==HO$_3$S}}}
```

gives:


```
\hanthracenev[achjop]{{{10}D==O};{{9}D==S};{2==COOCH$_3$}}
```

gives:

9. "A nation is an imagined political community — and imagined as both inherently limited and sovereign. It is imagined because the members of even the smallest nation will never know most of their fellow members, meet them, or even hear of them, yet in the minds of each lives the image of their communion." B. Anderson, *Imagined communities*, p 6. There is a lot of talking about the globalization caused by the Euro. This opinion about "imagined community" of B. Anderson is strange at the first read, but I give him credit for his idea.

10. Romanian language and Dutch language have common words (such as *dop* or *gang*). This is due to colonists, in the XIIth century, from Flandra who settled in Transylvania. Those words are not common with other languages.

11. Romanian alphabet (AĂÂBCDEFGHIÎJKLMNOPRSȘTȚUVXZ – ' , . ; „" « » aăâbcdefghiîjklmnoprsștțuvxz) is a threat to the Dutch National Security. See the Netherlands position represented by Mr. Van Wingen: `http://wwwold.dkuug.dk/JTC1/SC2/WG3/docs/n441.pdf`.

12. Dracula doesn't exists. Dracula was invented by an English writer and made famous by several American movie directors. Any connections between Dracula and Transylvania are pure fictions.

13. A computer is too valuable to waste it by running Microsoft operating systems.

14. Black cherry is the English name of a fruit which is not a cherry. The cherries can be black, but the black cherries ***are not*** black.